

GAIN MECHANISMS, MICROSTRUCTURE LASING,
AND IMAGING OF GaN-BASED
LASING STRUCTURES

By

SERGIY BIDNYK

Diploma in Engineering Physics
Lviv National University
Lviv, Ukraine
1994

Master of Science in Photonics
Oklahoma State University
Stillwater, Oklahoma
1997

Submitted to the Faculty of the
Graduate College of the
Oklahoma State University
in partial fulfillment of
the requirements for
the Degree of
DOCTOR OF PHILOSOPHY
December, 1999

COPYRIGHT

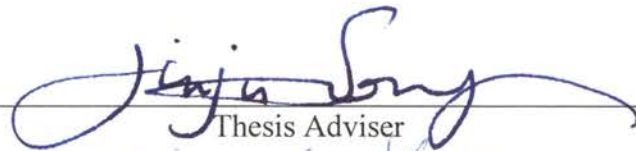
By

Sergiy Bidnyk

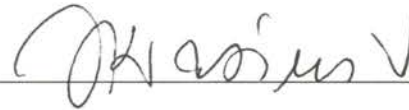
December, 1999

GAIN MECHANISMS, MICROSTRUCTURE LASING,
AND IMAGING OF GaN-BASED
LASING STRUCTURES

Thesis Approved:


Thesis Adviser








Dean of the Graduate College

ACKNOWLEDGEMENTS

I would like to express my sincere appreciation to my advisor, Professor Jin-Joo Song, for the support and guidance she has given me throughout my graduate work. Without her insight in physics and her encouragement, this thesis would not have been possible. I feel fortunate to have started my career under her supervision.

I would also like to extend my sincere gratitude to the members of my thesis committee, Dr. Jerzy Krasinski, Dr. Xin-Cheng Xie, and Dr. David Peakheart, for taking the time to read this thesis and providing valuable comments.

I would like to express my deepest gratitude to Dr. Paul Westhaus for inviting me to come to graduate school at OSU. He has always found the time to answer many of my questions and address all my needs on a day-to-day basis.

I cannot underemphasize the contribution of Professor Yosyp Stakhira at Lviv National University for advising me throughout my undergraduate years. He motivated me to study physics and introduced me to an immense field of semiconductor research.

I would also like to thank Dr. Theodore Schmidt and Dr. Arthur Fischer. The things I learned from them enormously simplified my life and provided me with many shortcuts that made my research efforts much more efficient. I also appreciate the help of and wish the best of luck to all my other groupmates.

I cannot forget a good friendship shared with my partner Brian Little. His remarks have greatly improved this thesis. He has extended my mastering of the English language to limits I did not know existed and tolerated me as his roommate during my graduate years.

I was fortunate enough to meet Terry Wilson who always kept my physique and spirit in excellent shape. I would like to thank Carol Wicksted for her help and care. I appreciate the assistance of Jack Biu Lam in helping me complete the final round of my

experimental work. I would also like to thank my cordial friends for being there for me: Marina Yakolina, Tigran Sarkisyan, Aleksandr Brener, and Sheena Jacob.

And last, but certainly not least, I would like to thank my parents and brother. Though thousands of miles away, they have always been a constant source of support for me. I am always in debt to my parents for their love and deep belief in me.

For my loving parents

Моїм батькам присвячую

PUBLICATIONS AND PRESENTATIONS

The following scientific publications and presentations were generated from the research contained in this thesis:

Books:

- S. Bidnyk, T. J. Schmidt, and J. J. Song, "*Optical Properties of Highly Excited (Al, In) GaN Epilayers and Heterostructures*," Thin Films Handbook: Processing, Characterization and Properties, (Edited by H. S. Nalwa, Academic Press, to be published in 2000).

Refereed scientific publications:

- S. Bidnyk, J. B. Lam, B. D. Little, Y. H. Kwon, J. J. Song, G. E. Bulman, and T. J. Schmidt, "*Mechanism of efficient ultraviolet lasing in GaN/AlGaN separate confinement heterostructures*," Appl. Phys. Lett. (in print).
- Y. H. Cho, T. J. Schmidt, S. Bidnyk, G. H. Gainer, J. J. Song, S. Keller, U. K. Mishra, and S. P. DenBaars, "*Linear and nonlinear optical properties of InGaN/GaN heterostructures*," Phys. Rev. B (in print).
- S. Bidnyk, B. D. Little, J. J. Song, and T. J. Schmidt, "*A technique for evaluating optical confinement in GaN-based lasing structures*," Appl. Phys. Lett. **75** (15), pp. 2163-2165 (1999).
- Y. H. Kwon, G. H. Gainer, S. Bidnyk, Y. H. Cho, J. J. Song, M. Hansen, and S. P. DenBaars, "*Structural and optical characteristics of $In_xGa_{1-x}N$ /GaN multiple quantum wells with different In compositions*," Appl. Phys. Lett. **75** (17), pp. 2545-2547 (1999).
- Y. H. Cho, T. J. Schmidt, A. J. Fischer, S. Bidnyk, G. H. Gainer, J. J. Song, S. Keller, U. K. Mishra, S. P. DenBaars, D.S. Kim, and W. Jhe, "*Effects of carrier localization on the optical characteristics of MOCVD-grown InGaN/GaN heterostructures*," Phys. Stat. Sol. (b) **216** (1) pp. 181-185 (1999).
- S. Bidnyk, T.J. Schmidt, B.D. Little, and J.J. Song, "*Evaluation of optical confinement in GaN-based lasing structures*," Phys. Stat. Sol. (b) **216** (1), pp. 517-520 (1999).

- S. Bidnyk, T. J. Schmidt, B. D. Little, J. J. Song, "*Near-threshold gain mechanisms in GaN thin films in the temperature range of 20-700 K*," Appl. Phys. Lett. **74** (1), pp. 1-3 (1999).
- S. Bidnyk, B. D. Little, T. J. Schmidt, Y. H. Cho, J. Krasinski, J. J. Song, B. Goldenberg, W. G. Perry, M. D. Bremser, and R. F. Davis, "*Stimulated emission in thin GaN films in the temperature range of 300 K to 700 K*," J. Appl. Phys. **85** (3), pp. 1792-1795, (1999).
- T. J. Schmidt, S. Bidnyk, Yong-Hoon Cho, A. J. Fischer, J. J. Song, S. Keller, U. K. Mishra, and S. P. DenBaars, "*Stimulated emission characteristics of InGaN/GaN multiple quantum wells: Excitation length and excitation density dependence*," Appl. Phys. Lett. **73** (25), pp. 3689-3691 (1998).
- S. Bidnyk, B. D. Little, Y. H. Cho, J. Krasinski, J. J. Song, W. Yang, and S. A. McPherson, "*Laser action in GaN pyramids grown on (111) silicon by selective lateral overgrowth*," Appl. Phys. Lett. **73** (16), pp. 2242-2244 (1998).
- S. Bidnyk, T. J. Schmidt, Y. H. Cho, G. H. Gainer, J. J. Song, S. Keller, U. K. Mishra, and S. P. DenBaars, "*High-temperature stimulated emission in optically pumped InGaN/GaN multi-quantum wells*," Appl. Phys. Lett. **72** (13), pp. 1623-1625 (1998).
- S. Bidnyk, T. J. Schmidt, G. H. Park, and J. J. Song, "*Study of surface-emitted stimulated emission in GaN*," Appl. Phys. Lett. **71** (6), pp. 729-731 (1997).
- J. J. Song, A. J. Fischer, T. J. Schmidt, S. Bidnyk, and W. Shan, "*Optical Processes in GaN and its Related Heterostructures*," Nonlinear Optics **18** (2-1), pp. 269-276 (1997).
- W. S. Wong, N. Y. Li, H. K. Dong, F. Deng, S. S. Lau, C. W. Tu, J. Hays, S. Bidnyk, and J. J. Song, "*Growth of GaN by gas-source molecular beam epitaxy by ammonia and by plasma generated nitrogen radicals*," J. Crystal Growth **164**, pp. 159-166 (1996).
- S. Bidnyk, J. B. Lam, B. D. Little, G. H. Gainer, Y. H. Kwon, and J. J. Song, "*Comparative study of near-threshold gain mechanisms in GaN epilayers and GaN/AlGaN separate confinement heterostructures*," SPIE Conf. Proc. **3947** (in print).
- S. Bidnyk, J. B. Lam, B. D. Little, G. H. Gainer, Y. H. Kwon, and J. J. Song, "*Mechanism of efficient ultraviolet lasing in a GaN/AlGaN separate confinement heterostructure*," Mat. Res. Soc. Symp. Proc., **W11.22** (in print).
- Y. H. Kwon, G. H. Gainer, S. Bidnyk, Y. H. Cho, J. J. Song, M Hansen, and S. P. DenBaars, "*Comparison study of structural and optical properties of*

In_xGa_{1-x}N/GaN quantum wells with different In compositions,” Mat. Res. Soc. Symp. Proc., **W12.7** (in print).

- J. J. Song, S. Bidnyk, and T. J. Schmidt, “*Stimulated emission and pump-probe studies of wide-gap nitrides for UV-blue photonic applications,*” (invited), SPIE Conf. Proc. **3896** (in print).
- S. Bidnyk, Y. H. Cho, T. J. Schmidt, G. H. Gainer, J. J. Song, S. Keller, U. K. Mishra, S. P. DenBaars, and W. Jhe, “*Critical issues of localization in the development of InGaN/GaN laser diodes,*” Proc. CLEO/Pacific Rim’99, Technical Digest **2**, 286 (1999).
- Y. H. Cho, W. Jhe, T. J. Schmidt, S. Bidnyk, G. H. Gainer, and J. J. Song, “*Optical Characteristics of Group III-Nitride Quantum Structures,*” Proc. 3rd Korea-China Joint Workshop on Advanced Materials, (invited) 351 (1999).
- S. Bidnyk, T.J. Schmidt, B.D. Little, and J.J. Song, “*Optical confinement and gain mechanisms in GaN-based lasing structures,*” 3rd Int. Conf. Nitride Semicond. Proc., We P092 (1999).
- Y.H. Cho, T.J. Schmidt, A.J. Fischer, S. Bidnyk, G.H. Gainer, J.J. Song, S. Keller, U.K. Mishra, S. P. DenBaars, D.S. Kim, and W. Jhe, “*Effects of carrier localization on the optical characteristics of MOCVD-grown InGaN/GaN heterostructures,*” 3rd Int. Conf. Nitride Semicond. Proc., We P093 (1999).
- T.J. Schmidt, S. Bidnyk, Y.H. Cho, G.H. Gainer, and J.J. Song, “*Nonlinear optical spectroscopy of highly excited InGaN/GaN multiple quantum well blue laser structures,*” 1999 CLEO Technical Digest Series, CTuU4, pp. 202-203 (1999).
- S. Bidnyk, T.J. Schmidt, B.D. Little, J. Krasinski, and J.J. Song, “*Novel technique for evaluation of optical confinement in semiconductor laser structures through spatially and spectrally resolved emission spectra,*” 1999 CLEO Technical Digest Series, CTuK52, 145 (1999).
- S. Bidnyk, T. J. Schmidt, B. D. Little, J. J. Song, “*Study of near-threshold gain mechanisms in MOCVD-grown (In, Al) GaN epilayers and heterostructures,*” Mat. Res. Soc. Symp. Proc **572**, pp. 439-444 (1999).
- B. D. Little, S. Bidnyk, T. J. Schmidt, J. B. Lam, Y. H. Kwon, J. J. Song, S. Keller, U. K. Mishra, and S. P. DenBaars, W. Yang, “*Comparative study of emission from highly excited (In, Al) GaN thin films and heterostructures,*” Mat. Res. Soc. Symp. Proc **572**, pp. 351-355 (1999).
- S. Bidnyk, T. J. Schmidt, B. D. Little, J. Krasinski, J. J. Song, S. Keller, and S. P. DenBaars, “*Comparative study of near-threshold stimulated emission mechanisms*

in GaN epilayers and InGaN/GaN multiquantum wells," SPIE Conf. Proc. **3625**, pp. 68-77 (1999).

- T. J. Schmidt, Y. H. Cho, S. Bidnyk, J. J. Song, S. Keller, U. K. Mishra, and S. P. DenBaars, "*Nonlinear optical spectroscopy of band tail states in highly excited InGaN,*" SPIE Conf. Proc. **3625**, pp. 57-67 (1999).
- S. Bidnyk, B. D. Little, Y. H. Cho, J. Krasinski, J. J. Song, W. Yang, S. A. McPherson, "*Laser action in optically pumped GaN pyramids grown on (111) silicon by selective lateral overgrowth,*" MRS Internet J. Nitride Semicond. Res. **4S1**, G6.48 (1999).
- T. J. Schmidt, S. Bidnyk, Y. H. Cho, A. J. Fischer, J. J. Song, S. Keller, U. K. Mishra, and S. P. DenBaars "*Amplification path length dependence studies of stimulated emission from optically pumped InGaN/GaN multiple quantum wells,*" MRS Internet J. Nitride Semicond. Res. **4S1**, G6.54 (1999).
- Y. H. Cho, T. J. Schmidt, S. Bidnyk, J. J. Song, S. Keller, U. K. Mishra, and S. P. DenBaars, "*Influence of Si-doping on carrier localization of MOCVD-grown InGaN/GaN multiple quantum wells,*" MRS Internet J. Nitride Semicond. Res. **4S1**, G6.44 (1999).
- S. Bidnyk, B. D. Little, Yong Hoon Cho, J. Krasinski, J. J. Song, W. Yang, S. A. McPherson, "*Laser action in optically pumped GaN pyramids grown on (111) silicon by selective lateral overgrowth,*" MRS Res. Soc. Symp. **537**, G6.48 (1998)
- T. J. Schmidt, S. Bidnyk, Yong-Hoon Cho, A. J. Fischer, J. J. Song, S. Keller, U. K. Mishra, and S. P. DenBaars, "*Amplification path length dependence studies of stimulated emission from optically pumped InGaN/GaN multiple quantum wells,*" Mat. Res. Soc. Symp. **537**, G6.54 (1998).
- Y. H. Cho, T. J. Schmidt, S. Bidnyk, J. J. Song, S. Keller, U. K. Mishra, and S. P. DenBaars, "*Influence of Si-doping on carrier localization of MOCVD-grown InGaN/GaN multiple quantum wells,*" Mat. Res. Soc. Symp. **537**, G6.44 (1998).
- S. Bidnyk, Y. H. Cho, T. J. Schmidt, J. J. Song, S. Keller, U. K. Mishra, and S. P. DenBaars, "*Study of stimulated emission in InGaN/GaN multi-quantum wells in the temperature range of 175 K to 575 K,*" Mat. Res. Soc. Symp. Proc. **512**, pp. 199-204 (1998).
- S. Bidnyk, Y. H. Cho, T. J. Schmidt, J. J. Song, S. Keller, U. K. Mishra, and S. P. DenBaars, "*Characterization of InGaN/GaN lasing structures for high temperature device applications,*" 1998 CLEO Technical Digest Series **6**, CWD2, pp. 223-224 (1998).

- S. Bidnyk, B. D. Little, T. J. Schmidt, J. Krasinski, and Jin-Joo Song, "*High-temperature stimulated emission studies of MOCVD-grown GaN films*," SPIE Conf. Proc. **3419**, pp. 35-43 (1998).

Scientific Conference Presentations:

- S. Bidnyk, J. B. Lam, B. D. Little, G. H. Gainer, Y. H. Kwon, and J. J. Song, "*Comparative study of near-threshold gain mechanisms in GaN epilayers and GaN/AlGaIn separate confinement heterostructures*," SPIE Photonics West, **3947-24**, San Jose, CA (January 23-28, 2000).
- S. Bidnyk, J. B. Lam, B. D. Little, G. H. Gainer, Y. H. Kwon, and J. J. Song, "*Mechanism of efficient ultraviolet lasing in a GaN/AlGaIn separate confinement heterostructure*," MRS Fall Meeting, **W11.22**, 130 (November 29-December 3, 1999).
- Y. H. Kwon, G. H. Gainer, S. Bidnyk, Y. H. Cho, J. J. Song, M Hansen, and S. P. DenBaars, "*Comparison study of structural and optical properties of $In_xGa_{1-x}N/GaN$ quantum wells with different In compositions*," MRS Fall Meeting, **W12.7**, 134 (November 29-December 3, 1999).
- Y. H. Cho, S. K. Eah, S. C. Hohng, D. S. Kim, W. Jhe, T. J. Schmidt, S. Bidnyk, G. H. Gainer, and J. J. Song, "*Optical emission characteristics of GaAs and GaN based materials using near-field and far-field optics*," (invited) Korea Physics Society Fall Meeting, **I-05**, (October 15-16, 1999).
- S. Bidnyk, Y. H. Cho, T. J. Schmidt, G. H. Gainer, J. J. Song, S. Keller, U. K. Mishra, and S. P. DenBaars, "*Critical issues of localization in the development of InGaIn/GaN laser diodes*," CLEO/Pacific Rim '99, **WP3**, 39, Seoul, Korea (August 30 – September 3, 1999).
- Y. H. Cho, W. Jhe, T. J. Schmidt, S. Bidnyk, G. H. Gainer, and J. J. Song, "*Optical Characteristics of Group III-Nitride Quantum Structures*," The 3rd Korea-China Joint Workshop on Advanced Materials, (invited), 351, Cheju, Korea (August 23 - 27, 1999).
- S. Bidnyk, T.J. Schmidt, B.D. Little, and J.J. Song, "*Optical confinement and gain mechanisms in GaN-based lasing structures*," 3rd Int. Conf. Nitride Semicond., **We P092**, 127, Montpellier, France (July 5-9, 1999).
- Y.H. Cho, T.J. Schmidt, A.J. Fischer, S. Bidnyk, G.H. Gainer, J.J. Song, S. Keller, U.K. Mishra, S. P. DenBaars, D.S. Kim, and W. Jhe, "*Effects of carrier localization on the optical characteristics of MOCVD-grown InGaIn/GaN heterostructures*," 3rd Int. Conf. Nitride Semicond., **We P093**, pp. 127-128, Montpellier, France (July 5-9, 1999).

- T.J. Schmidt, S. Bidnyk, Y.H. Cho, G.H. Gainer, and J.J. Song, "*Nonlinear optical spectroscopy of highly excited InGaN/GaN multiple quantum well blue laser structures*," CLEO/QELS '99, **CTuU4**, pp. 202-203, Baltimore, MD (May 23-28, 1999).
- S. Bidnyk, T.J. Schmidt, B.D. Little, J. Krasinski, and J.J. Song, "*Novel technique for evaluation of optical confinement in semiconductor laser structures through spatially and spectrally resolved emission spectra*," CLEO/QELS '99, **CTuK52**, 145, Baltimore, MD (May 23-28, 1999).
- S. Bidnyk, T. J. Schmidt, B. D. Little, J. J. Song, "*Study of near-threshold gain mechanisms in MOCVD-grown (In, Al)GaN epilayers and heterostructures*," MRS Spring Meeting, **Y5.37**, 382, San Francisco, CA (April 5-9, 1999).
- B. D. Little, T. J. Schmidt, S. Bidnyk, J. J. Song, S. Keller, U. K. Mishra, and S. P. DenBaars, "*Comparative study of emission from highly excited InGaN, GaN, and AlGaN thin films*," MRS Spring Meeting, **Y7.4**, 388, San Francisco, CA (April 5-9, 1999).
- S. Bidnyk, T. J. Schmidt, J. J. Song, "*Novel technique for evaluation of optical confinement in (In, Al) GaN heterostructures through spatially and spectrally resolved edge-emitted stimulated emission*," APS Centennial Meeting, **LC22 10**, 685, Atlanta, GA (March 20-26, 1999).
- B. D. Little, T. J. Schmidt, S. Bidnyk, Y. H. Cho, G. H. Park, J. J. Song, W. Yang, "*Excitation wavelength dependence of stimulated emission from AlGaN epilayers*," APS Centennial Meeting, **LC22 8**, 685, Atlanta, GA (March 20-26, 1999).
- S. Bidnyk, T. J. Schmidt, J. J. Song, "*Comparative study of near-threshold stimulated emission mechanisms in GaN, InGaN and InGaN/GaN multiquantum wells*," SPIE Photonics West, **3625-8**, San Jose, CA (January 25-29, 1999).
- T. J. Schmidt, Y. H. Cho, S. Bidnyk, J. J. Song, S. Keller, U. K. Mishra, and S. P. DenBaars, "*Nonlinear optical spectroscopy of band tail states in highly excited InGaN*," SPIE Photonics West, **3625-7**, San Jose, CA (January 25-29, 1999).
- S. Bidnyk, B. Little, Y. H. Cho, J. Krasinski, J. J. Song, W. Yang, S. A. McPherson, "*Laser action in optically pumped GaN pyramids grown on (111) silicon by selective lateral overgrowth*," MRS Fall Meeting, **G6.48**, 160, Boston, MA (November 30 - December 4, 1998).
- T. J. Schmidt, S. Bidnyk, Y. H. Cho, A. J. Fischer, J. J. Song, S. Keller, U. K. Mishra, and S. P. DenBaars, "*Amplification path length dependence studies of stimulated emission from optically pumped InGaN/GaN multiple quantum wells*," MRS Fall Meeting, **G6.54**, 161, Boston, MA (November 30 - December 4, 1998).

- Y. H. Cho, T. J. Schmidt, S. Bidnyk, J. J. Song, S. Keller, U. K. Mishra, and S. P. DenBaars, "*Influence of Si-doping on carrier localization of MOCVD-grown InGaN/GaN multiple quantum wells*," MRS Fall Meeting, **G6.44**, 159, Boston, MA (November 30 - December 4, 1998).
- S. Bidnyk, T. J. Schmidt, J. J. Song, S. Keller, U. K. Mishra, S. P. DenBaars, "*Stimulated emission studies of the group III nitrides over the temperature range 10 K to 700 K*," OSA/ILS-XIV Annual Meeting, **ThQQ5**, 144, Baltimore, MD (October 4-9, 1998).
- J. J. Song, S. Bidnyk, T. J. Schmidt, Y. H. Cho, S. Keller, S. P. DenBaars and W. Yang, "*Stimulated emission studies of MOCVD-grown GaN and InGaN structures*," 5th Wide Bandgap Semiconductor Workshop, St. Louis (4-7 August 1998).
- Y. H. Cho, T. J. Schmidt, S. Bidnyk, G. H. Gainer, J. J. Song, S. Keller, S. P. DenBaars, "*Optical characterization of GaN, InGaN, and InGaN/GaN multiple quantum wells grown by metalorganic chemical vapor deposition*," 5th Wide Bandgap Semiconductor Workshop, St. Louis, MO (4-7 August 1998).
- S. Bidnyk, C. K. Choi, T. J. Schmidt, J. Krasinski, and J. J. Song, "*High-Temperature Stimulated emission studies of MOCVD-grown GaN films*," SPIE Asia Pacific Symposium on Optoelectronics, **3419-06**, pp. 35-43, Taipei, Taiwan (July 9-11, 1998).
- S. Bidnyk, Y. H. Cho, T. J. Schmidt, and J. J. Song, S. Keller, U. K. Mishra, and S. P. DenBaars, "*Characterization of InGaN/GaN lasing structures for high temperature device applications*," CLEO/IQEC '98, **CWD2**, pp. 223-224, San Francisco, CA (May 3-8, 1998).
- S. Bidnyk, Y. H. Cho, T. J. Schmidt, J. J. Song, S. Keller, U. K. Mishra, and S. P. DenBaars, "*High-temperature stimulated emission in optically pumped InGaN/GaN multi-quantum wells*," MRS Spring Meeting, **F4.11**, 113, San Francisco, CA (April 13-17, 1998).
- S. Bidnyk, C. K. Choi, T. J. Schmidt, J. S. Krasinski, and J. J. Song, "*Study of stimulated emission in GaN thin films in the temperature range of 20 K to 700 K*," APS March Meeting, **A18.08**, 24, Los Angeles, CA (March 16-20, 1998).
- W. Shan, T. J. Schmidt, S. Bidnyk, A. J. Fischer, B. D. Little, and J. J. Song, "*Optical processes in GaN and related heterostructures*," Fourth Wide Band Gap and Nitride Workshop, St. Louis, MO (March 11-14, 1997).

- J. J. Song, A. J. Fischer, T. J. Schmidt, S. Bidnyk, and W. Shan, "*Optical processes in GaN and its related heterostructures*," Int. Symposium of Quantum Structures for Photonic Applications, Sendai, Japan (March 6-8, 1997).
- S. Bidnyk, "*Theoretical aspects of translation symmetry breakdown in semiconductor structures*," 40th Anniversary Physical Society Conference, 64, Lviv, Ukraine (May 27 - 28, 1993).

TABLE OF CONTENTS

Chapter	Page
I. INTRODUCTION	1
Economic Projections and Applications of Group-III Nitrides	1
Past and Future in Short-Wavelength Laser Diode Development	7
Organization of This Thesis	12
II. GENERAL OPTICAL PROPERTIES OF THE GROUP-III NITRIDES	14
Physical Properties and Band Structure of the Group-III Nitrides	14
Photoluminescence	18
Strain Considerations	21
Absorption	23
Reflection and Photorefectance	26
Pump-Probe Experiments on GaN and InGaN Thin Films	29
Ultrafast Carrier Dynamics	33
III. GAIN MECHANISMS IN SEMICONDUCTORS	37
Introduction to Gain Mechanisms in Semiconductors	37
Exciton-LO-Phonon Recombination	42
Exciton-Exciton Recombination	50
Exciton-Electron and Exciton-Hole Collisions	56
Stimulated Emission From an Electron-Hole Plasma	62
IV. OPTICAL PROPERTIES OF GaN-BASED LASING MEDIUMS AT HIGH TEMPERATURES	67
High-Temperature Stimulated Emission and Damage Mechanisms in GaN Epilayers	67
Stimulated Emission in InGaN/GaN Multi-Quantum Wells at Elevated Temperatures	82
V. GAIN MECHANISMS IN GaN-BASED LASING STRUCTURES	93
Origin of Stimulated Emission in GaN Epilayers	94

Chapter	Page
Mechanism of Efficient Ultraviolet Lasing in GaN/AlGaN Separate Confinement Heterostructures	107
Critical Issues of Localization in InGaN-Based Lasing Structures	122
Gain Mechanism in AlGaN Epilayers	133
 VI. MICROSTRUCTURE LASING	 139
Origin of Surface-Emitted Stimulated Emission in GaN Epilayers.....	139
Effects of Microcracks on the Lasing Characteristics of GaN-Based Structures	148
Ring-Cavity Lasing in Laterally Overgrown GaN Pyramids	154
 VII. IMAGING TECHNIQUES FOR WIDE-BAND-GAP SEMICONDUCTORS	 167
Transverse Lasing Modes in GaN-Based Lasing Structures	167
Novel Technique for Evaluating Optical Confinement in GaN-Based Lasing Structures	173
 VIII. SUMMARY	 185
 BIBLIOGRAPHY	 188
 APPENDICES	 197
APPENDIX A — DETERMINATION OF GAIN THROUGH THE VARIABLE STRIPE METHOD.....	198
APPENDIX B — EXTRACTION OF GAIN FROM SPONTANEOUS EMISSION SPECTRA	205
APPENDIX C — PUMP-PROBE EXPERIMENTAL CONFIGURATIONS	212

LIST OF TABLES

Table	Page
I. Technical characteristics of state-of-the-art InGaN LEDs.....	3
II. Early reports on GaN-based laser diodes arranged in chronological order.	8
III. Fundamental properties of GaN, AlN, and InN.....	16
IV. Results of a least squares linear fit of the energy positions of spontaneous and stimulated emission peaks as a function of temperature for GaN thin films (for temperatures above 300 K).....	71
V. Si doping concentrations in GaN barriers and stimulated emission threshold densities at room temperature for InGaN/GaN MQW samples as measured by SIMS.....	84

LIST OF FIGURES

Figure	Page
1. Market for compound semiconductors.....	2
2. LED market.....	2
3. Market for laser diodes.....	4
4. Room temperature lasing in AlGaIn/GaN VCSEL structure.....	10
5. Structure and symmetries of the lowest conduction band and the uppermost valence bands in wurtzite GaN.....	17
6. Near-band-edge exciton luminescence spectra as a function of temperature taken from a 7.2- μm -thick GaN epilayer. The inset shows the spectrum of the same film over a wider range of photon energies taken at 10 K.....	20
7. The measured transition energies of various free excitons versus the energy position of <i>A</i> -exciton.....	22
8. Absorption spectra of a 0.38- μm -thick GaN epilayer in the vicinity of the fundamental band-gap.....	24
9. Absorption spectra of a 0.44- μm -thick $\text{Al}_{0.17}\text{Ga}_{0.83}\text{N}$ epilayer in the vicinity of the fundamental band-gap.....	25
10. Comparison of conventional reflectance (top) and photoreflectance (bottom) spectra taken from a 7.2- μm -thick GaN/sapphire sample at 10 K.....	27
11. Photoreflectance spectrum of a GaN epilayer grown on SiC.....	28
12. Nanosecond nondegenerate optical pump-probe absorption spectra of a 0.38- μm -thick GaN thin film at 10 K.....	31
13. 10 K nanosecond nondegenerate optical pump-probe absorption spectra from an InGaIn thin film as a function of above-gap optical excitation.....	32

Figure	Page
14. 10 K absorption spectra for a 0.38- μm -thick epilayer of GaN grown on sapphire as function of pump fluence.	34
15. Absorption spectra as a function of time delay for a pump fluence of 750 $\mu\text{J}/\text{cm}^2$ showing the ultrafast near-zero delay dynamics.	35
16. Absorption as a function of time delay for the three wavelengths denoted by arrows in Figure 15.	36
17. Schematic drawing of the various gain mechanisms in a semiconductor such as exciton-exciton, exciton-hole, exciton-electron, and exciton-phonon recombination.	41
18. Recombination of an exciton by emission of an LO-phonon.	46
19. Maximum gain frequency Δ_{max} as a function of temperature.	47
20. Threshold current density j_{th} for a 50 keV electron beam with $\eta = 1.5\%$ versus temperature.	48
21. Stimulated emission spectrum of CdS at 77 K.	49
22. Emission spectra of GaN at 1.8 K as a function of optical excitation density. .	52
23. Dispersion curves of the excitonic polariton, showing the exciton-exciton interaction.	53
24. Shift of the P emission line versus the intensity of UV photons at 4.2 K in CdS.	54
25. Calculated gain spectra of the exciton-exciton scattering in CdS for different temperatures.	55
26. Recombination of excitons through (a) exciton-electron and (b) exciton-hole collisions.	59
27. Calculated gain spectra for the exciton-electron scattering process in CdS.	60
28. Theoretical shapes of the spontaneous and gain curves corresponding to the exciton-electron interaction.	61
29. Formation of gain from an electron-hole plasma.	65
30. Gain spectra of GaAs at two different pump intensities.	66

Figure	Page
31. Perpendicular side views of the heater assembly.	74
32. Pumping configuration for (a) edge-emitted stimulated emission and (b) surface-emitted spontaneous emission.	75
33. Emission spectra at 700 K from a GaN film grown on a sapphire substrate. ...	76
34. Dependence of integrated emission intensity on the pump density for a GaN film at 700 K.	77
35. Stimulated emission threshold as a function of temperature for GaN thin films grown on sapphire and SiC.	78
36. Energy positions of stimulated and spontaneous emission as a function of temperature for GaN thin films grown on sapphire and SiC.	79
37. Temperature “tuning” of the stimulated emission peak wavelength position...	80
38. A microscope image of burn spots on the surface of a GaN film.	81
39. The energy diagram and sample structure of InGaN/GaN MQWs.	87
40. Spectra taken at pump powers slightly above the stimulated emission threshold for samples with GaN barriers doped with silicon.	88
41. Emission spectra for an InGaN/GaN MQW sample with a Si concentration of $2 \times 10^{18} \text{ cm}^{-3}$ in the barriers at (a) 200 K, (b) 300 K, and (c) 450 K.	89
42. Stimulated emission from a moderately doped (Si concentration of $2 \times 10^{18} \text{ cm}^{-3}$ in the barriers) InGaN/GaN multi-quantum well sample at room temperature.	90
43. Temperature dependence of the stimulated emission threshold in the temperature range of 175-575 K for the InGaN/GaN MQW sample.	91
44. Integrated intensity of InGaN/GaN MQW emission as a function of pump density for different temperatures.	92
45. Typical emission spectra from a 4.2- μm -thick GaN epilayer at room temperature for different pumping densities. The inset shows the dependence of the integrated emission intensity on the excitation power.	100
46. Stimulated emission threshold as a function of temperature for GaN thin films grown on SiC in the temperature range of 20 to 300 K.	101

Figure	Page
47. Stimulated emission threshold as a function of temperature for GaN thin films grown on SiC and sapphire in the temperature range of 20 to 700 K. .	102
48. Reflectance spectra at different pump densities at 10 K.	103
49. The absolute energy positions of the spontaneous and SE peaks for GaN thin films grown on SiC and sapphire.....	104
50. Energy difference (ΔE) between spontaneous and SE peaks as a function of temperature for GaN thin films grown on SiC and sapphire.	105
51. Energy difference (ΔE) between spontaneous and SE peaks as a function of excitation density at 100 K.	106
52. Lasing and low-density PL spectra from a GaN/AlGaN SCH taken at (a) 30 K and (b) 300 K.	113
53. Temperature dependent spontaneous emission spectra.....	114
54. Temperature dependence of threshold pump densities for a 4.2- μm -thick GaN epilayer and GaN/AlGaN SCH.	115
55. Lasing modes obtained from two different microcavities.....	116
56. Temperature dependent data obtained from a single microcavity.	117
57. Temperature dependence of low density PL peak positions and lasing modes in a GaN/AlGaN SCH.	118
58. Energy position of lasing modes relative to spontaneous emission from the GaN active region in the SCH and the energy difference between spontaneous and SE peaks in 4.2- μm -thick GaN epilayer.....	119
59. PLE and PL spectra from a GaN/AlGaN SCH taken at 10 K.	120
60. Time-resolved photoluminescence intensity of the three peaks depicted in Figure 53 under picosecond optical excitation at 10 K.....	121
61. Photoluminescence, photoluminescence excitation, and time-resolved photoluminescence from (a) an InGaN/GaN multi-quantum well and (b) an InGaN epilayer at 10 K.	126

Figure	Page
62. Evolution of emission spectra from below to above the stimulated emission threshold from (a) an InGaN/GaN multi-quantum well and (b) an InGaN epilayer.....	127
63. Photoluminescence, stimulated emission, PLE, and modal gain spectra taken at 10 K from (a) an InGaN MQW and (b) an InGaN epilayer.	128
64. Modal gain spectra of (a) an InGaN/GaN multi-quantum well and (b) an InGaN epilayer as a function of above-gap optical excitation density.	129
65. Differential absorption spectra, $\Delta\alpha(I_{exc}) = \alpha(I_{exc}) - \alpha(0)$ at (a) 10 K and (b) room temperature as a function of the optical excitation density for the InGaN epilayer.....	130
66. 10 K nanosecond non-degenerate pump-probe experimental results for (a) an InGaN/GaN multi-quantum well and (b) an InGaN epilayer showing absorption bleaching of band tail states with increasing excitation density. .	131
67. Stimulated emission peak position as a function of excitation photon energy for the InGaN/GaN MQW.	132
68. Photoluminescence spectra as a function of excitation pump density near the stimulated emission threshold for the $Al_{0.17}Ga_{0.83}N$ sample at 30 K. The inset shows the same spectra at room temperature.	136
69. Spontaneous and stimulated emission energy peak positions as functions of temperature for the $Al_{0.17}Ga_{0.83}N$ sample. The inset shows the energy difference between the two peaks.	137
70. The stimulated emission threshold as a function of temperature for the $Al_{0.17}Ga_{0.83}N$ sample. Solid dots are the experimental data.	138
71. Schematic diagram of the backscattering geometry experimental setup.	144
72. Emission spectra in the backscattering geometry from a 7.2- μ m-thick GaN epilayer as a function of the distance from a defect.....	145
73. Stimulated emission intensity versus position relative to the sample edges for GaN samples of thickness (a) 7.2 μ m and (b) 0.8 μ m.	146
74. Crack on the surface of a 4.2- μ m-thick GaN epilayer grown on sapphire.....	147
75. Stimulated emission from a GaN sample grown on SiC at room temperature.	150

Figure	Page
76. A picture of the sample surface of the GaN/AlGaN separate confinement heterostructure after cleaving.....	151
77. Lasing and spontaneous emission in the GaN/AlGaN separate confinement heterostructure at room temperature.	152
78. Optical pumping geometry. The high finesse emission exits the sample at a large angle ($\phi \sim 18^\circ$).	153
79. SEM image of GaN pyramids with a 15- μm -wide hexagonal base, grown on a (111) Si substrate by selective lateral overgrowth.	160
80. Experimental geometry. The pyramids were individually pumped, imaged, and spectrally analyzed through a high-magnification telescope system.	161
81. Emission spectra of a 15- μm -wide GaN pyramid under different levels of optical pumping above and below the lasing threshold at room temperature.	162
82. Peak intensity as a function of excitation density.	163
83. Lasing modes in a 15- μm -wide GaN pyramid.	164
84. Emission spectra of a 15- μm -wide GaN pyramid under different levels of optical pumping above and below the lasing threshold at room temperature.	165
85. Multi-mode laser action in (a) 15- μm -wide and (b) 5- μm -wide pyramids.	166
86. Near-field pattern of InGaN MQW laser diodes at output powers of (a) 70 mW and (b) 100 mW under room temperature cw operation.	170
87. Images of the beam propagation from (a) near-field to (b) 20 μm from the sample taken from an InGaN/GaN MQW sample at room temperature under pulsed excitation.	171
88. Computer simulation of TEM_{01} using Hermite-Gaussian solutions.	172
89. Experimental configuration. A microscope assembly (NA=0.9) was used to project the image of the sample onto the spectrometer slits.	178
90. Spatially resolved emission spectra from a 7.2- μm -thick GaN epilayer at excitation densities above the SE threshold.....	179

Figure	Page
91. Cross sections of the 3-D plot shown in Figure 90 taken at (a) substantially above the GaN epilayer, (b) slightly above the epilayer, (c) in line with the epilayer, and (d) slightly below the epilayer.....	180
92. Formation of an interference pattern in a GaN epilayer.....	181
93. Edge emission from GaN epilayers with different thicknesses.....	182
94. Spatially resolved emission spectra from a GaN/AlGaN SCH at excitation densities above the lasing threshold.....	183
95. Mechanism of optical confinement and leak in a GaN/AlGaN separate confinement heterostructure.....	184
A-1. Pumping configuration for the variable stripe gain experiment.....	202
A-2. Ideal output intensity characteristics for different values of d in the variable stripe experiment.....	203
A-3. Dependence of emission intensity on excitation length for a 1.9- μm -thick GaN epilayer grown on a -sapphire	204
B-1. (a) Spontaneous emission $L(h\nu, \Delta E_F)$. (b) Gain spectra $g(h\nu, \Delta E_F)$ calculated from the spontaneous emission.....	211
C-1. Relative spectral width of the beams in pump-probe experiments.	215
C-2. Experimental set-up for the two-beam transmission and reflection spectroscopy.....	216

CHAPTER I

INTRODUCTION

There is currently a tremendous amount of research activity in the area of nitride semiconductor compounds, which is expected to generate a plethora of novel applications for the electronics industry in the years to come. This activity has been sparked by the realization of high-brightness ultraviolet (UV), blue, green, and amber light emitting diodes as well as UV-blue laser diodes. In the next decade, group-III nitrides are expected to be an essential part of many devices around us including traffic lights, full-color information displays, long-lived light bulbs, DVD players, laser printers, underwater and satellite-to-satellite communication devices, and solar blind photodetectors. With much research still in progress, myriads of applications for this new material system have not even been thought of yet. This monograph will focus on the optical properties of the group-III nitrides with an emphasis on future applications. In this chapter, we evaluate the potential market for group-III nitrides, describe different applications, give a historical perspective on the subject, and talk about the organization of this thesis.

Economical Projections and Applications of Group-III Nitrides

We shall begin with an economical analysis of the semiconductor market. Silicon technology has been around for several decades and nowadays represents a tremendous market of \$150 billion. In 1997 the total market for compound semiconductors (the group-III nitrides belong to this category) was \$5.7 billion. Optoelectronics is one of the

most common applications for compound semiconductors. How much of this market could GaN potentially capture in the future?

To answer this question we should look at the distribution of applications within the compound semiconductor market, which is given in Figure 1. Light emitting diodes (LEDs), laser diodes (LDs), and analog devices constitute 77% of the compound semiconductor market. In the year 2002 the total market for compound semiconductors is estimated to increase and reach values as high as \$9 billion a year, but the distribution is expected to remain the same.

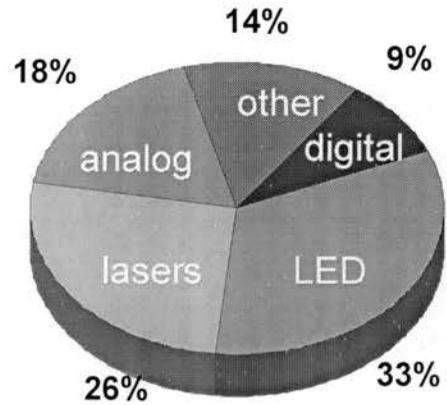


Figure 1. Market for compound semiconductors. From Ref. [1].

Let's examine the LED market in greater detail. In 1998 the total market for LEDs was 33% of the total market for compound semiconductors (see Figure 1) and was valued at approximately \$2.5 billion. We can further divide this market into categories according to the emission wavelength (or color), as depicted in Figure 2. Most LEDs are AlGaAs- or AlGaInP-based and are used for infrared applications, such as optical switches, position measurement devices, optical encoders, and fluid level indicators. The market for blue, green, and yellow InGaN LEDs is still emerging and represents a relatively small market share. Currently, only a handful of high-tech companies possess the capability to produce InGaN-based LEDs in substantial quantities. Among the biggest suppliers are Nichia Corporation (Japan) with shipments of over 30 million units/month, Cree Research Inc. (USA) producing 20 million units/month, and Hewlett Packard (USA) delivering approximately 10 million units/month. Among smaller suppliers are EMCORE (USA), Toyoda Gosei (Japan), Infineon Technologies (Germany), and Samsung (Korea).

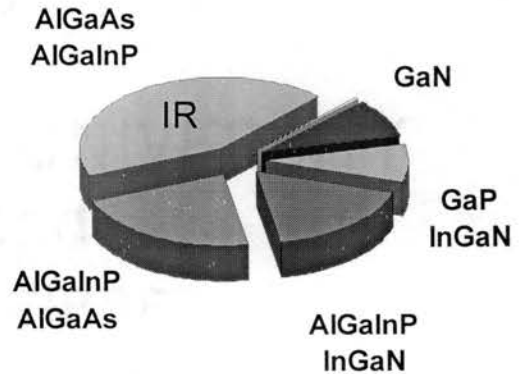


Figure 2. LED market. From Ref. [1].

The current price of a blue LED varies from company to company within the range of \$0.25 - \$1.00 apiece, which is rather expensive compared to AlInGaP LEDs. However, the cost of InGaN LEDs is not considered to be an intrinsic problem. With an actual production increase of 30-50% a year, the price of these LEDs is expected to drop to \$0.10-\$0.50 apiece in 2 to 3 years. We note that the cost of packaging InGaN LEDs is about the same as for any other LED. Our research group has confirmed that high optical quality GaN structures can also be grown on Si substrates.² By further developing this technology, the processing cost will drop substantially due to larger wafer area and the possibility for a back-side contact (currently nitride-based LEDs require both contacts to be on the light emitting side of the sample due to the insulating nature of the sapphire substrate). Recently developed white LEDs are 10 times more efficient, last a thousand times longer, and have an emission spectrum closer to that of the sun than the spectrum of a regular incandescent bulb. The cost of a white LED array (with a power equivalent to that of an electric bulb), however, remains relatively high at about \$30 and will probably not allow wide-scale use of the product for quite some time.

It has been predicted that full-color displays and traffic lights will utilize a considerable part of all nitride LEDs produced.³ Table I summarizes several technical characteristics of state-of-the-art InGaN LEDs of different colors. For the purpose of comparison we also present typical values for amber AlInGaP LEDs. Current blue and green InGaN-based LEDs already have a higher external quantum efficiency and output power compared to AlInGaP-based amber LEDs. In fact, GaN-based LEDs are predicted

	InGaN (blue)	InGaN (green)	InGaN (amber)	AlInGaP (amber)
Wavelength (nm)	470	525	595	595
FWHM (nm)	30	35	50	17
Efficiency (lumen/W)	5	30	35	86
Power (mW)	6	5	1.5	4.5
External Quantum Efficiency (%)	12	12	5	11

Table I. Technical characteristics of state-of-the-art InGaN LEDs. Typical values for AlInGaP LEDs are also given for comparison. From Ref. [1].

to prevail in the market for visible spectrum emitters. Perhaps the only exception is in the long-wavelength range (amber-red), where the efficiency of GaN-based LEDs drops dramatically.

The market for LDs is only slightly smaller than that for LEDs. It is also one of the fastest growing markets in the US. In 1999 the total market for LDs was \$2.15 billion. Most LDs are used in storage (\$1

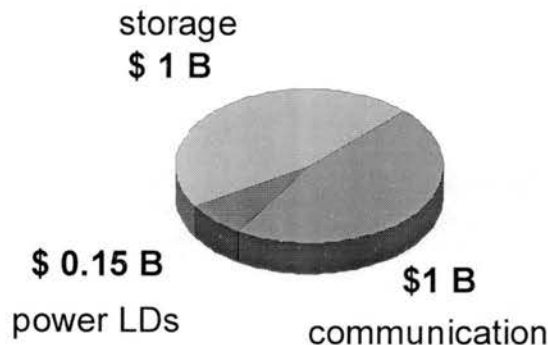


Figure 3. Market for laser diodes.

billion) and communication (\$1 billion) as illustrated in Figure 3. We note that the minimum spot size a laser can be focused to is proportional to the wavelength of the laser light. Due to the shorter emission wavelength of GaN-based lasers, storage and high-resolution printing are natural choices for GaN LD applications.

The annual market in the world for printing is rather large (\$100 billion). The historical trend in this field is to move to higher resolution and speed. In order to lower production costs, shorter wavelength and higher power laser diodes are necessary. There are some limitations, however, as to how short the wavelength needs to be. The organic photoreceptors used in printers should be sensitive to the laser wavelengths and the optics should not be very expensive. A compromise is found somewhere around 400 nm. It has been estimated that through the utilization of a 5 mW InGaN-based laser with a high quality beam profile, it would be possible to achieve printing speeds of up to 60 pages a minute.

In 1999 more than 300 million lasers were used for optical storage devices. By utilizing InGaN-based lasers it will be possible to improve the resolution and increase the storage capacities of optical disks. Currently, DVD/HD technology is being developed utilizing InGaN LDs with an emission wavelength of 410 nm. This will allow the laser beam to be focused to a spot approximately 0.24 μm in diameter. By utilizing both sides of the optical disks, their capacity will increase to 30 GB. In order to read information from DVD/HD disks, a minimum laser output power of 5 mW (cw) is required. For

recording information the output power should be at least 50 mW (pulsed). Current state-of-the-art nitride laser diodes meet these requirements.

Communication devices are dominated by InP and GaAs lasers emitting in the wavelength range of 1.0-1.5 μm (some preliminary research to fabricate nitride-based LDs in this wavelength range has been done on GaInNAs). The desired spectral range of these lasers is dictated by the dispersion properties of optical fibers. Recently, there has been a lot of effort dedicated to the development of rare-earth-ion-doped GaN optical-fiber amplifiers and fiber lasers.⁴ The advantage of GaN over smaller gap semiconductors and glasses include greater chemical stability, efficient carrier generation (by exciting the rare-earth ions), and physical stability over a wide temperature range. GaN also has a high level of optical activity even under conditions of high defect density, which would quench emission in other smaller-gap III-V and in most II-VI compounds. It is unlikely, though, that GaN-based devices will win a significant portion of the communication market in the near future. Finally, the high-power LD market for industry and medical applications has traditionally utilized InGaAsP/GaInP and AlGaAs/GaAs lasing structures. GaN-based LDs are expected to significantly contribute to this market once the development of high-power LDs is completed.

The large band-gap of AlGaIn alloys (3.4-6.2 eV at room temperature) has prompted researchers to develop solar-blind devices for UV detection. Sunlight in the spectral range of 250 to 300 nm is filtered out by ozone located 15 km above the surface of the earth. Thus any source of UV radiation within the atmosphere can be easily seen by a solar-blind detector even on a sunny day. This would allow for effective military applications, such as the tracking of missiles and warplanes. A recently developed GaN-based linear array of UV detectors⁵ has an order of magnitude improvement in size, weight, and power consumption in comparison to photomultiplier tubes and microchannel plates now used to detect UV light. The UV photodetectors could also be used to detect UV light in hot environments and to detect UV emissions from flames. State-of-the-art nitride-based UV photodetectors have a remarkably good selectivity with a ratio of UV to visible responsivity exceeding eight orders of magnitude.⁶ In 1999 the market for UV detectors was rather small but it is expected to grow to as much as \$100 million a year.

In 1997 our research group was the first to report the optical properties of GaN epilayers and InGaN multi-quantum wells at temperatures as high as 400°C under intense optical excitation.^{7,8} We observed stimulated emission and a low temperature sensitivity of the stimulated emission threshold over a large temperature range. This result suggested that GaN-based structures are excellent candidates for high-temperature optoelectronic devices. The market for high-temperature devices is estimated to be \$400 million in 1999, but it has the potential to grow to as large as \$12 billion. The reason why this market remains small stems from the lack of semiconductors capable of high-temperature operation. Nitride devices are expected to revolutionize this field and find many applications in the automotive and aerospace industries.

The general increase in the worldwide communications market in recent years has resulted in a very fast rate of annual growth. In 1999 the number of cellular phones in use exceeded 400 million and continues to grow at a rate of 30% a year. The market for satellite communication is also growing at a rate of 25% a year and about 100 new satellites are launched every year. The market for radio frequency (RF) semiconductors for satellite communication was estimated to be \$200 million in 1998. The total market for RF semiconductors in 1999 was \$4.5 billion. It has been overwhelmingly dominated by Si and GaAs, leaving less than 1% to other semiconductors. However, there are two newcomers to this market: SiC and GaN. The latter emerges for frequencies in the tens of GHz and RF powers up to 100 W. The combination of these two parameters leaves GaN as the only candidate for many military applications (Si devices are not operable at frequencies above 1 GHz and GaAs devices fail at RF powers exceeding 10 W). State-of-the-art field effect and heterojunction bipolar transistors based on GaN have already been shown to possess superior characteristics and are expected to extend the capabilities of RF electronics in the near future.

There are many other applications for group-III nitrides utilizing photovoltaic and photoconductive properties that were not included in the current discussion. However, the majority of these applications are presently unrealized.

Past and Future in Short-Wavelength Laser Diode Development

Having described some of the applications of the group-III nitrides, we should now give a brief historical background on how this research originated and to where it will be directed in the future. By far the most anticipated event in nitride research has been the invention of the 'blue laser diode.' The first observation of optically pumped lasing in GaN was made by Dingle *et al.*⁹ in the early 1970s using needle-like GaN single crystals at a temperature of 2 K, but it took almost a quarter of a century before the first current injection lasing was observed. It all began with work done by Akasaki and Amano in 1989, who developed p-type doping and were first to report the observation of room temperature coherent emission in an InGaN/GaN quantum well structure using pulsed current injection.^{10,11} Their device consisted of a 7.5-nm-thick InGaN active layer, GaN waveguide layers, and AlGaN cladding layers. In December 1995, the fabrication of LDs using group-III nitrides was announced for the first time by Nakamura *et al.*¹² at Nichia Chemical, Inc. The active lasing medium was composed of InGaN multi-quantum wells and the threshold current density was 4 kA/cm² under pulsed operation at room temperature. Since then, the performance of Nichia InGaN LDs has steadily improved, and the lifetime of LDs under cw conditions at room temperature has recently exceeded 10,000 hours making them suitable for commercial applications. Inspired by this discovery, several industrial research laboratories and university research groups have also succeeded in the fabrication of InGaN/GaN/AlGaN-based blue LDs operating at room temperature. Table II summarizes the early reports on GaN-based LDs in chronological order. Nowadays, almost all major multinational electronics companies and many universities and research laboratories are involved in continuing studies and optimization of group-III nitrides for device applications. In spite of the substantial progress made, there are many issues that merit further study.

# QWs	Current type	Temp. (K)	J_{th} (kA/cm ²)	Wavelength (nm)	Ref.	Company/ University
26	pulsed	RT	4.0	417	12	Nichia
20	pulsed	RT	9.6	416	13	Nichia
20	pulsed	RT	8.0	410	14	Nichia
10	pulsed	RT	13.0	419	15	Nichia
7	pulsed	RT	4.6	406	16	Nichia
1	pulsed	RT	2.9	376	17	Meijo
3	cw	233 K	8.7	411	18	Nichia
25	pulsed	RT	50	417.5	19	Toshiba
3	cw	RT	9.0	409	20	Nichia
3	cw	RT	7.0	400	21	Nichia
4	cw	20-70°C	3.6	406	22	Nichia
4	cw	RT	7.3	399-401	23	Nichia
4	cw	RT	3.6	405-407	24	Nichia
8	pulsed	RT	48	402.8	25	Cree
	cw	RT	11	404-435	26	Cree
4	cw	RT	4	396-397	27	Nichia
10	pulsed	RT	12.7	420	28	UCSB
5	pulsed	RT	12	405-425	29	Fujitsu
5	pulsed	RT	9.5	417.5	30	Sony
	cw	20-60°C	1.5	390-440	31	Nichia
	pulsed	RT	10.6	412-417	32	Toshiba
	pulsed	RT	15	410-420	33	UCSB
10	pulsed	RT	25	419-432	34	Xerox
5	pulsed	RT	8.5-14	395-408	35	SDL
4	cw	RT	7.0	393.3	36	Nichia

Table II. Early reports on GaN-based laser diodes arranged in chronological order.

Even the best GaN-based LDs have huge densities of dislocations, predominantly threading between the substrate and the surface. Whereas it appears that they have no effect whatever on the efficiency of light emission, there is great concern that these defects limit the lifetime of the LDs. This great number of dislocations arises due to the lack of lattice-matched substrates. GaN growth onto a variety of substrates has been investigated. The most common substrate is sapphire which is cheap, but the lattice mismatch with GaN is rather high (16%). GaN can be grown on 6H-SiC, however the high cost of SiC wafers has not allowed the widespread use of this material. GaN growth has also been performed on spinel (MgAl_2O_4) substrates. None of these substrates, however, have resulted in the growth of high crystalline quality GaN epilayers (when compared to other technologically important semiconductors such as GaAs and Si).

A substantial decrease in dislocation density was observed in regions of lateral epitaxial overgrowth (LEO) compared to regions of conventional vertical growth. LEO occurs when GaN is grown from a mask pattern. Under optimized conditions, lateral to vertical growth rate ratios of up to 5 can be achieved. The LEO technique has resulted in a four to five order of magnitude reduction in dislocation density. This observation triggered research on similar experimental techniques to improve the crystalline quality of GaN epilayers, such as selective area growth and pendeo-epitaxy. These techniques allow the growth of high-quality GaN epilayers independent of the type of substrate. In order to facilitate the incorporation of GaN optoelectronic devices into Si-based electronics, there have been many successful attempts to grow GaN on Si substrates by LEO. Yet there is still much to be done in this field to optimize the growth parameters and reduce the cost of processing.

GaN-based LDs also face strong competition from an alternative technique for blue laser light generation. By utilizing a traditional high-power infrared distributed Bragg reflector laser (850 nm) combined with a LiNbO_3 doubling crystal, it is possible to generate high beam-quality laser emission at 425 nm with powers as high as 15 mW. The laser emission generated in this manner has low noise and is naturally well-suited for use in applications requiring precise mechanical alignment. It is likely that the first DVD/HD recorders will be made utilizing this blue light generation technique. However, InGaN/GaN LDs are more compact and considerably cheaper to produce. The optical

parameters of these LDs are already satisfactory for reading information from optical disks. The ratio of performance to cost favors GaN-based lasers in comparison to lasers utilizing the second harmonic generation technique.

With the realization of edge-emitting InGaN-based lasers, the next milestone for group-III nitrides is the development of a vertical cavity surface emitting laser (VCSEL). The output beam from the state-of-the-art edge-emitting "blue laser" is highly divergent due to diffraction from the narrow aperture formed by the edge of the active layer. Furthermore, the edge-emitting laser cannot be used to fabricate or to access the light from two-dimensional arrays. These arrays can be used to create very large bandwidth (several THz) data links, while each individual device is only required to maintain a relatively low modulation rate (50-100 GHz). A two dimensional array of VCSELs could also dramatically reduce the read-out time in dense optical memory systems.

Our research group successfully achieved laser action at room temperature in InGaN/GaN multi-quantum well based VCSELs, as shown in Figure 4. To avoid lattice temperature heating effects due to large excitation density, the experiment was performed in "single shot" mode: the obtained spectra are the result of a single 6-ns-long pulse. While optimization of the structure is still necessary, we clearly demonstrated the feasibility of fabricating a nitride-based VCSEL. Currently, many research group are pursuing the development of current-injection VCSELs. It might take several years before the first applications utilizing a blue vertical cavity surface-emitting laser emerge.

Finally, the nitride research community is putting a lot of effort into the

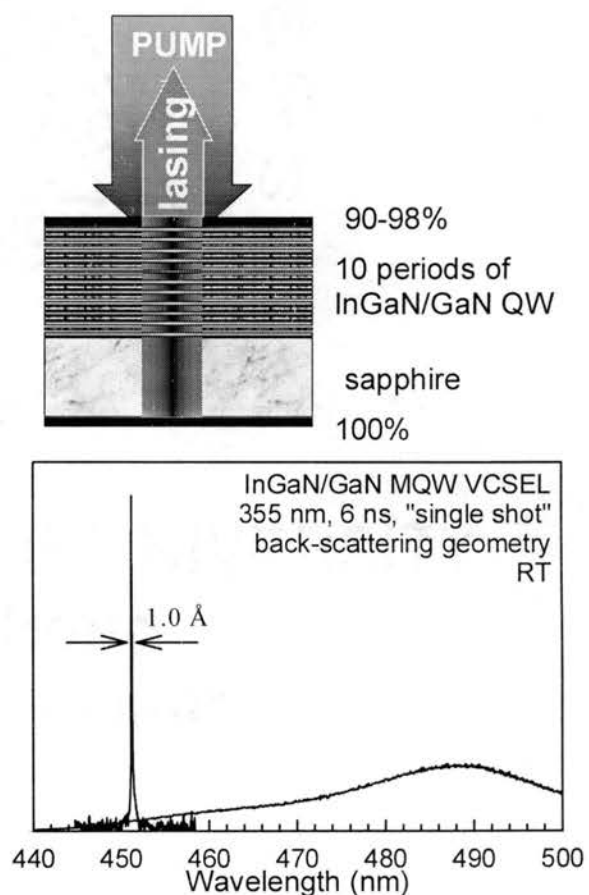


Figure 4. Room temperature lasing in AlGaN/GaN VCSEL structure.

realization of even shorter emission wavelength LDs for near- and deep-UV applications. It might be more challenging to manufacture LDs emitting photons with energies exceeding the GaN band-gap of 3.5 eV. In principle, these LDs could be realized by utilizing AlGaN compounds, but at this time it would be difficult to predict all the technological hurdles associated with short-wavelength LD development. The first step in this direction was taken by scientists at NTT's Basic Research Laboratory who fabricated a UV LED (346 nm) based on an $\text{Al}_{0.08}\text{Ga}_{0.92}\text{N}/\text{Al}_{0.12}\text{Ga}_{0.88}\text{N}$ multi-quantum well structure.³⁷

Many aspects of the group-III nitrides have not been explored yet. This material system is very subtle from the viewpoints of optical characterization, growth, and device processing. Numerous exciting research studies are in progress on the group-III nitrides, and many more are yet to be done.

Organization of This Thesis

This monograph describes some of the contributions to the research of group-III nitrides done by the author. The thesis is organized in the following way. Chapter II deals with fundamental optical properties of GaN and its alloys. These include band structure, photoluminescence, pressure-dependent measurements, absorption, reflection, photo-reflectance, pump-probe studies, and ultrafast phenomena.

Chapter III gives a review of the general optical properties of semiconductors under high levels of optical excitation. It emphasizes the different gain mechanisms that occur in the presence of strong Coulomb interactions and are pertinent to the group-III nitrides.

In Chapter IV we describe the optical characterization of GaN epilayers and InGaN/GaN multi-quantum wells at temperatures as high as 700 K. The studies in this chapter include both high and low excitation density regimes. Damage mechanisms in GaN are also described in this chapter.

In Chapter V we present a comprehensive picture of gain mechanisms in GaN, InGaN, and AlGaN epilayers as well as in InGaN/GaN multi-quantum wells and GaN/AlGaN separate confinement heterostructures. Conclusions are drawn based on numerous experiments performed in different time scales (from cw to picosecond). This chapter also summarizes temperature-dependent studies as well as studies related to various excitation power/wavelength conditions.

Chapter VI describes the research that has been done to study stimulated emission and lasing properties of GaN in the presence of self- and intentionally-formed microcavities, scattering defects, and dislocations.

Chapter VII discusses issues related to the near- and far-field stimulated emission patterns of GaN-based lasing structures and describes a novel experimental technique for evaluating optical confinement in wide-band-gap semiconductors.

Finally, the appendices give details on the experimental techniques used to determine optical gain, such as the variable stripe method (Appendix A) and the pump-probe technique (Appendix C). The procedure used to extract gain values from spontaneous and stimulated emission spectra is given in Appendix B.

CHAPTER II

GENERAL OPTICAL PROPERTIES OF THE GROUP-III NITRIDES

The group-III nitrides have many interesting optical properties associated with excitons, impurities, optical nonlinearities, and stimulated emission. In this chapter we discuss the general optical properties of GaN and its related alloys through a variety of experimental techniques such as photoluminescence, absorption, reflection, photo-reflectance, pump-probe, and others. We cover different time scales using a variety of excitation sources, from continuous wave to femtosecond pulses. Excitonic recombination and the effects of strain are also included in this chapter.

Physical Properties and Band Structure of the Group-III Nitrides

All optical processes in semiconductors are related to their band structure. GaN crystallizes in either the cubic (zincblende), hexagonal (wurtzite), or rock salt structure. The wurtzite structure is by far the most common and will be the subject of our discussion. In GaN, AlN, and InN a hexagonal unit cell contains six atoms of each type. It can be represented by two interpenetrating hexagonal close-packed sublattices, one of each type of atom, offset along the c -axis by $5/8$ of the cell height ($5c/8$). Table III summarizes some of the fundamental physical properties of GaN, AlN, and InN.

The conduction band minimum of wurtzite GaN has Γ_7 -symmetry with a quantum number of $J_z = 1/2$. The maximum of the conduction band is also located at the Γ -point, resulting in a direct fundamental band-gap. Crystal-field and spin-orbit coupling

splits the top of the valence band in GaN into three different sub-bands, denoted by A , B , and C . The A -band has Γ_9 -symmetry, while B and C have Γ_7 -symmetry. The structure and symmetries of the bands are shown in Figure 5.

At low excitation densities, free excitons (a bound state of an electron and hole) represent the lowest energy intrinsic excitation of electrons and holes in pure materials. For materials where the electron and hole are very tightly bound, the excitons are referred to as Frenkel excitons. Another type of exciton is a Wannier-Mott exciton, or simply a Wannier exciton. They are characterized as having relatively weak exciton binding energies so that the electron and hole are separated from each other by a comparatively large distance in the crystal. For GaN, excitons are well described by the Wannier formalism and for the rest of this monograph the term exciton will refer to a Wannier-Mott exciton.

Excitons associated with the Γ_9^v valence band (A -band), the upper Γ_7^v valence band (B -band), and the lower Γ_7^v valence band (C -band) are often referred to as A -, B -, and C -excitons. The ternary compounds InGaN and AlGaN typically do not exhibit excitonic features at room temperature. This is because these alloys contain high levels of compositional fluctuations and defects. Recent experimental results on higher quality AlGaN epilayers have shown that at low temperatures, AlGaN has an excitonic resonance observable by absorption measurements (see page 23). Once the quality of these ternary compounds is improved, we expect to see excitonic features in these materials over a wide temperature range. In this chapter we will mostly concentrate on the optical properties of GaN.

		GaN	AlN	InN
Band-gap	E_g	3.39 eV (300 K)	6.2 eV (300 K)	1.89 eV (300 K)
		3.50 eV (1.6 K)	6.28 eV (5 K)	
Temperature coefficient	dE_g/dT	-6.0×10^{-4} eV/K		-1.8×10^{-4} eV/K
Pressure coefficient	dE_g/dP	4.2×10^{-3} eV/kbar		
Lattice constants	a	3.189 Å	3.112 Å	3.548 Å
	c	5.185 Å	4.982 Å	
Thermal expansion	$\Delta a/a$	5.59×10^{-6} K ⁻¹	4.2×10^{-6} K ⁻¹	
	$\Delta c/c$	3.17×10^{-6} K ⁻¹	5.3×10^{-6} K ⁻¹	
Thermal conductivity	k	1.3 W/cm K	2 W/cm K	
Index of refraction	n	2.33 (1 eV)	2.15 (3 eV)	2.80 - 3.05
		2.67 (3.38 eV)		
Dielectric constants	ϵ_0	10	8.5±0.2	15.3
	ϵ_∞	5.5	4.68-4.84	

Table III. Fundamental properties of GaN, AlN, and InN. Adapted from Ref. [38].

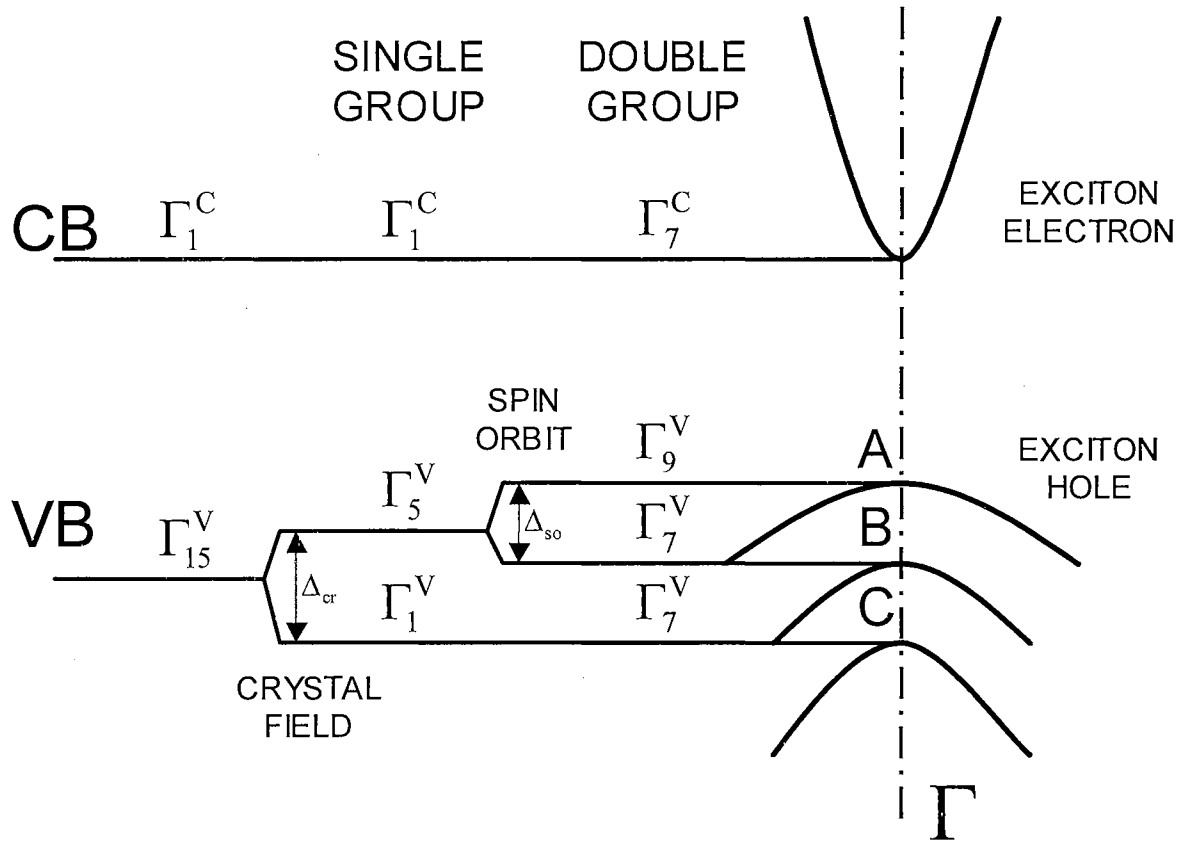


Figure 5. Structure and symmetries of the lowest conduction band and the uppermost valence bands in wurtzite GaN at the Γ -point ($k \approx 0$). Adapted from Ref. [39].

Photoluminescence

At low temperatures, near-band-edge luminescence spectra observed from most GaN samples are dominated by strong, sharp emission lines resulting from the radiative recombination of free and bound excitons, as shown in Figure 6. In addition to near-band-edge exciton emission, nominally undoped GaN samples often exhibit a series of emission structures in the energy range of approximately 2.95-3.27 eV, and a broad emission band in the yellow spectral region with a peak position around 2.2 eV, as shown in the inset of Figure 6. The intensity of these low emission bands relative to that of the exciton emissions vary from sample to sample depending on the crystal quality. These two additional bands result from radiative recombination from impurity levels within the GaN band-gap.

The free exciton state of GaN can be described by the Wannier-Mott approximation, where the electrons and holes are treated as nearly independently interacting through their Coulomb fields. The Coulomb interaction reduces the total energy of the bound state relative to that of the unrelated free carrier states by an amount corresponding to the exciton binding energy E_b . Free excitons exist in a series of excited states similar to the excited states of a hydrogen-like atomic system. Optical transitions can occur from discrete states below the band-gap E_g at the exciton energies:

$$E = E_g - \frac{E_b}{n^2}. \quad (1-1)$$

Bound exciton states involve both an exciton and an impurity. Excitons can be bound to neutral or ionized donors and acceptors. The energy of the photon produced through the annihilation of an exciton is:

$$h\nu = E_g - E_b - E_{BX}, \quad (1-2)$$

where E_{BX} is the exciton localization energy. In the Haynes approximation $E_{BX} \approx 0.1E_i$, where E_i is the impurity binding energy.

Figure 6 shows that in GaN the bound exciton dominates the luminescence spectrum at low temperatures. Since as-grown GaN is always n-type, bound excitons are expected to be bound to neutral donors. However, their intensity decreases with increasing temperature due to thermal dissociation and becomes unresolvable for temperatures exceeding 100 K. Free excitons were found to dominate the photoluminescence spectra at temperatures exceeding 40 K. At temperatures exceeding 200 K, excitons broaden and eventually band to band recombination of free carriers dominates the photoluminescence spectra.

By changing the composition of In and Al in InGaN and AlGaN alloys, it is possible to tailor the band-gap anywhere between 1.9 and 6.2 eV. The photoluminescence spectra of (Al, In) GaN alloys usually exhibit broad features and an abnormal temperature behavior of the emission peak position, possibly due to fluctuations in alloy composition.

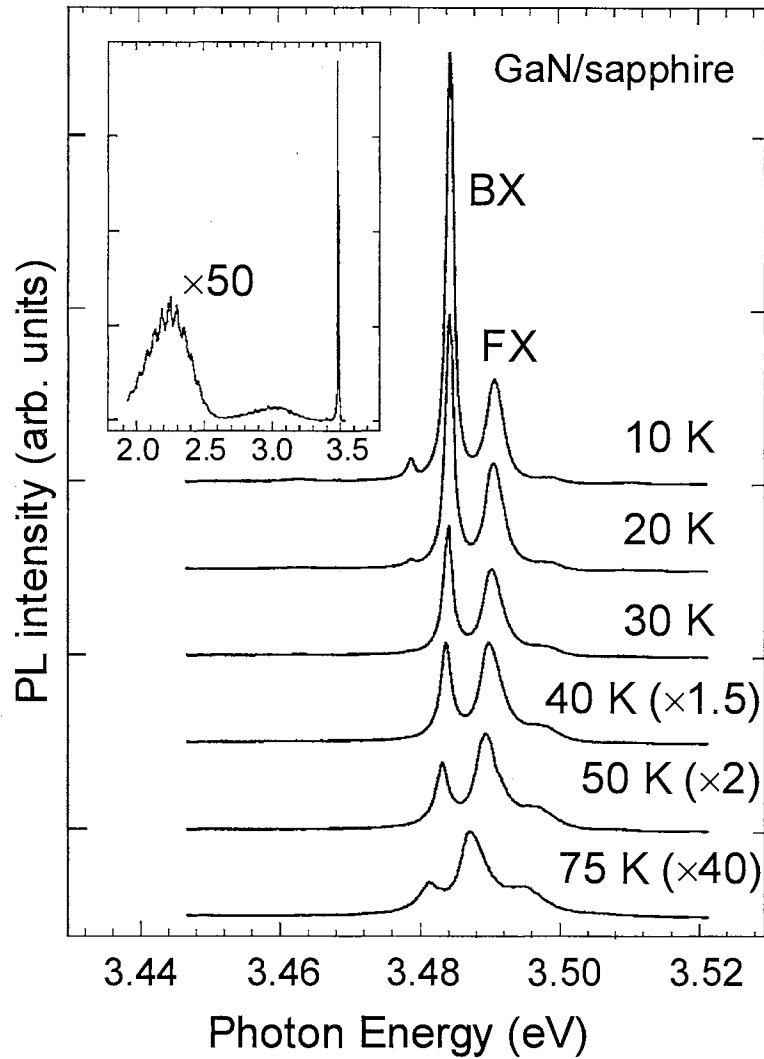


Figure 6. Near-band-edge exciton luminescence spectra as a function of temperature taken from a 7.2- μm -thick GaN epilayer. The inset shows the spectrum of the same film over a wider range of photon energies taken at 10 K. From Ref. [39].

Strain Considerations

Due to the lattice mismatch and difference in thermal expansion coefficients between GaN epilayers and substrates, one has to take into account the effects of residual strain when considering the excitonic energy transitions. Some degree of strain relaxation occurs through the formation of a large density of dislocations, however the residual strain has a relatively strong influence on the optical properties of the sample. It is difficult to separate the effects of strain caused by lattice parameter mismatch from those involving thermal-expansion mismatch to exactly determine their influence on the optical properties of GaN epilayers. We note, however, that the overall effect of residual strain generated in GaN on sapphire is compressive, which results in an increased band-gap, while the stress induced in GaN on SiC is tensile, which leads to a decrease in the measured exciton transition energies. The energy positions of the exciton resonances associated with *A*-, *B*-, and *C*-exciton transitions are also sample dependent.

The effects of strain become obvious when the lattice parameters of GaN are compared to those of virtually strain-free bulk GaN. In general, the introduction of strain changes the lattice parameters and generates variations in the electronic band structure. Figure 7 shows an example of the fit of experimentally observed exciton transition energies versus the *A*-exciton transition energy, which gives an estimate of the coefficients of crystal-field splitting for the Γ_9 and Γ_7 orbital states and describes the spin-orbit coupling (see Figure 5).⁴⁰ The numerical values of these band-structure parameters can be used to make estimates of the deformation potentials of GaN.

At this time, however, there is no quantitative agreement between different research groups on what the precise values of hydrostatic deformation potentials are, which prompts further research in this field.

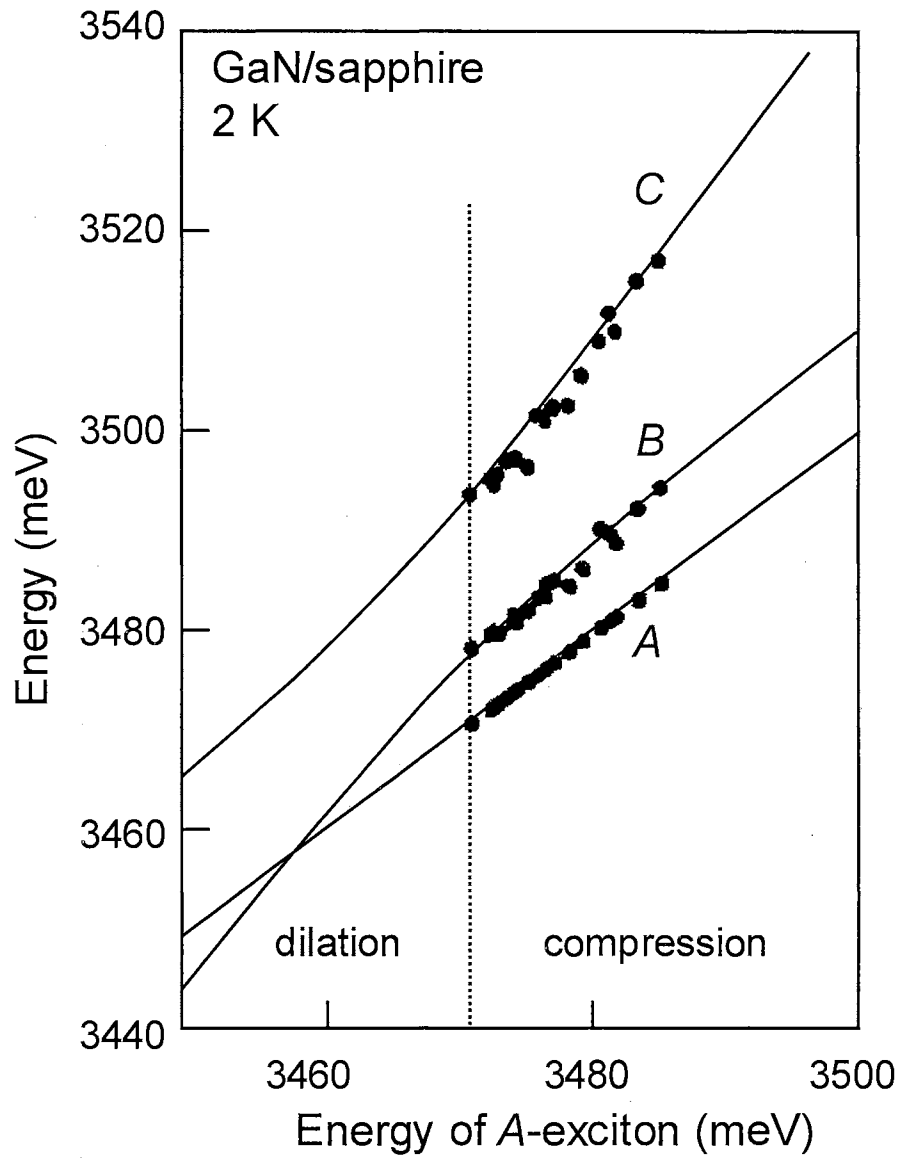


Figure 7. The measured transition energies of various free excitons versus the energy position of *A*-exciton. The solid lines are fits to the data. Adapted from Ref. [40].

Absorption

In high quality GaN epilayers, low temperature absorption spectra are usually dominated by sharp excitonic resonances, as shown in Figure 8. Since the concentration of impurities in these samples is relatively small, bound excitons are not expected to contribute significantly to band-edge absorption. At 10 K, we can clearly observe three different absorption features associated with *A*-, *B*-, and *C*-excitons. From theory, the *C*-exciton transition is only allowed for $E||c$, thus its intensity is significantly reduced in the transmission configuration (where $E\perp c$). However, if the pumping configuration is modified, an increase in the *C*-exciton absorption is expected.⁴¹

Figure 8 also shows changes in absorption over the temperature range of 10 K to 450 K. An excitonic resonance is clearly observed in the 300 K absorption data. In fact, excitonic resonances were observed at least a hundred degrees above room temperature. The absorption spectrum at each temperature was fit to a double-Lorentzian functional form. The energy position of the *A*-exciton was found to be well approximated by the Varshni equation:

$$E(T) = E(0) - \frac{\alpha T^2}{\beta + T}, \quad (1-3)$$

with $\alpha = 11.8 \times 10^{-4}$ eV/K and $\beta = 1414$ K.

Similar experiments were performed on InGaN and AlGaN epilayers. The InGaN epilayers usually exhibit a very wide absorption edge (several hundred meV) and have no excitonic features in absorption. Excitons have been observed in AlGaN epilayers at low temperatures, as shown in Figure 9. The excitonic feature disappears for temperatures above 150 K. The difficulties in observing excitons in InGaN and AlGaN epilayers could be related to material quality. We further note that the abnormal temperature behavior of the band-gap in these alloys cannot be adequately fit by the Varshni equation.

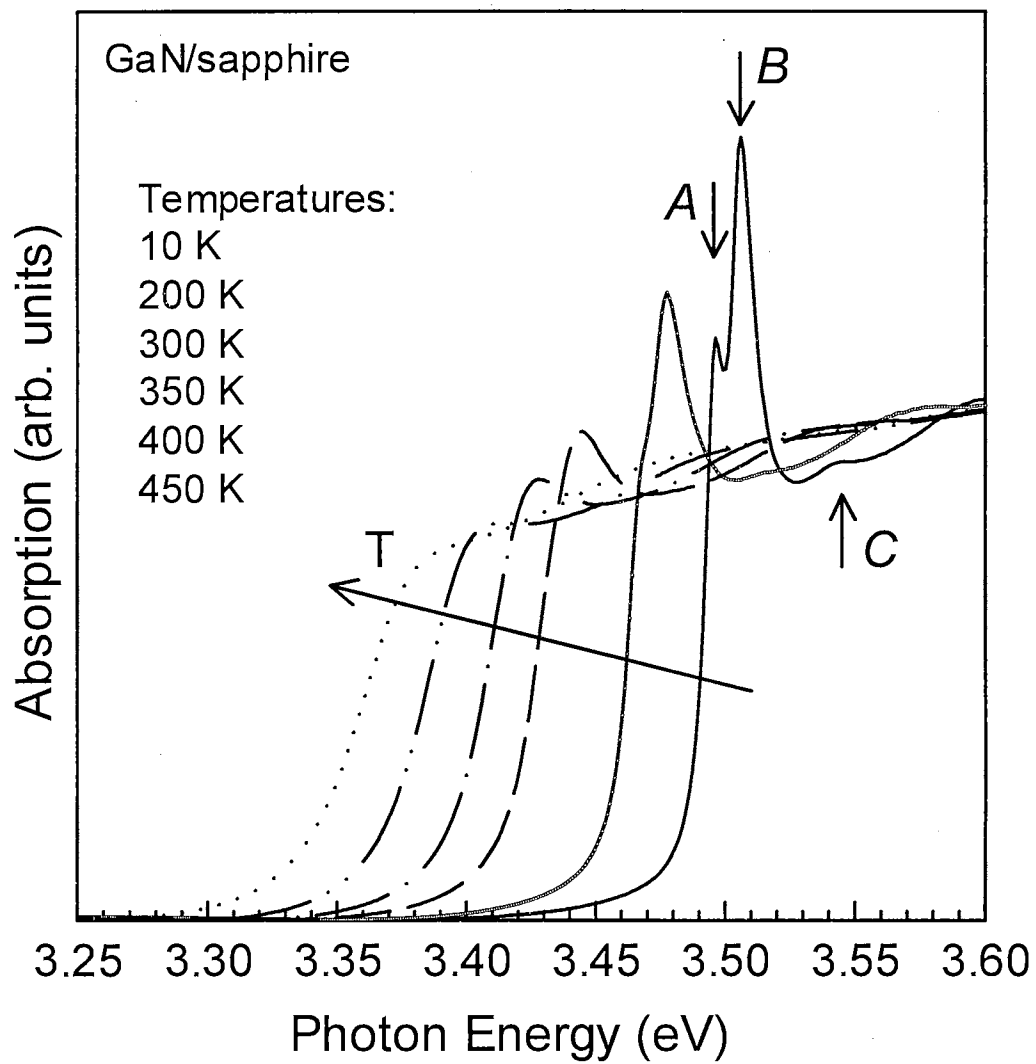


Figure 8. Absorption spectra of a 0.38- μm -thick GaN epilayer in the vicinity of the fundamental band-gap. At 10 K excitonic features associated with the *A*-, *B*-, and *C*- excitons are observed. Adapted from Ref. [39].

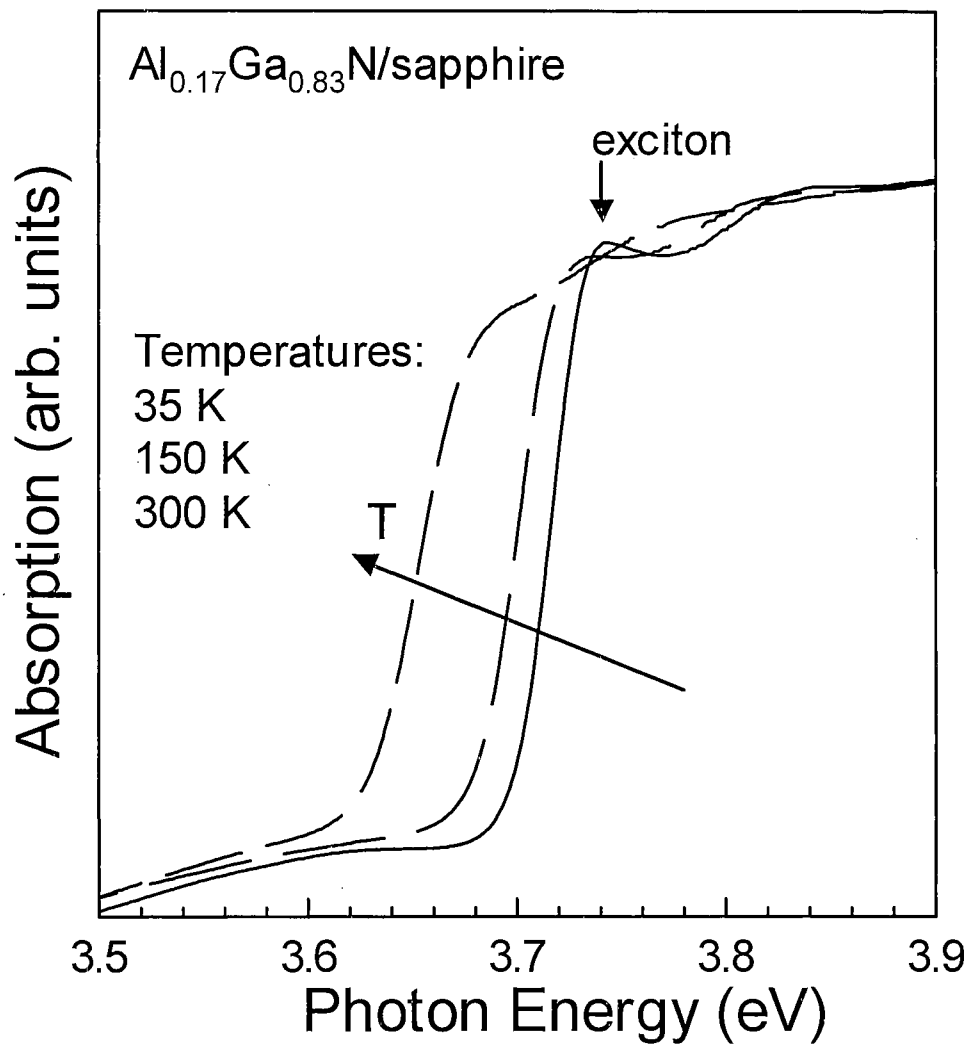


Figure 9. Absorption spectra of a 0.44-μm-thick Al_{0.17}Ga_{0.83}N epilayer in the vicinity of the fundamental band-gap. At low temperatures a weak excitonic feature is observed. Adapted from Ref. [42].

Reflection and Photoreflectance

Recent results obtained from reflectance and photoreflectance measurements have clearly demonstrated the signatures of transitions related to the *A*-, *B*-, and *C*-excitons, as well as the fundamental band-to-band ($\Gamma_9^V - \Gamma_7^V$) transition.³⁹ The unambiguous observation of these transitions allows a precise determination of their energy positions and the binding energy of excitons (using the hydrogenic model described by Eq. 1-1). Figure 10 shows reflection and photoreflectance spectra from a GaN/sapphire sample at 10 K. As can be seen in the figure, photoreflectance is capable of detecting weak signals and contains more spectral features than the reflectance spectrum. This makes it easy to positively identify the nature of the transition.

Such identifications permit a direct estimate of the binding energy for the *A*- and *B*-excitons from the separation between the $n = 1$ and $n = 2$ states for excitons, assuming that the hydrogenic model based on the effective mass approximation is applicable. A binding energy of $E_x = 21$ meV for the *A*- and *B*-excitons was obtained.⁴³ GaN samples grown on SiC exhibit stronger *C*-exciton resonances compared to those grown on sapphire in photoreflectance spectra (see Figure 11) and were used to obtain the binding energy of the *C*-exciton. The best theoretical fit of the experimental data yielded a value for the binding energy of the *C*-exciton to be 23 meV.

Even though strong resonances associated with the formation of excitons could often be observed near the band-edge of GaN by various spectroscopic methods, we found that the photoreflectance technique is the most reliable in determining exciton binding energies.

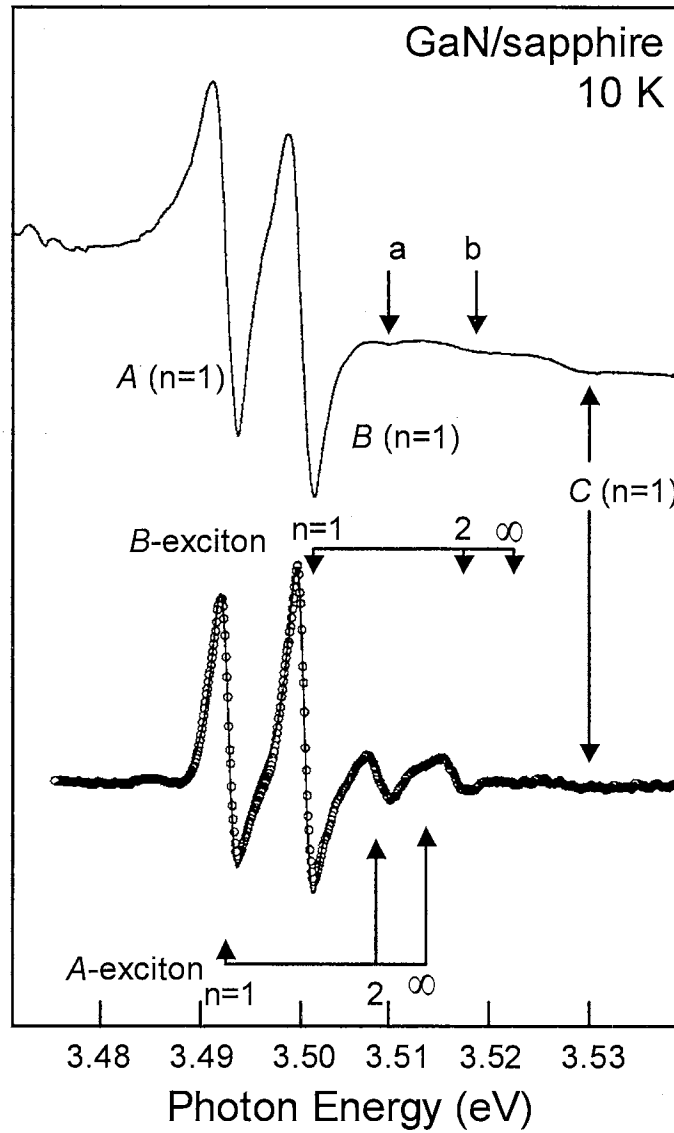


Figure 10. Comparison of conventional reflectance (top) and photoreflectance (bottom) spectra taken from a 7.2- μm -thick GaN/sapphire sample at 10 K. Open circles are experimental data and solid lines represent the best result of the least squares fit to the photoreflectance data. Adapted from Ref. [39].

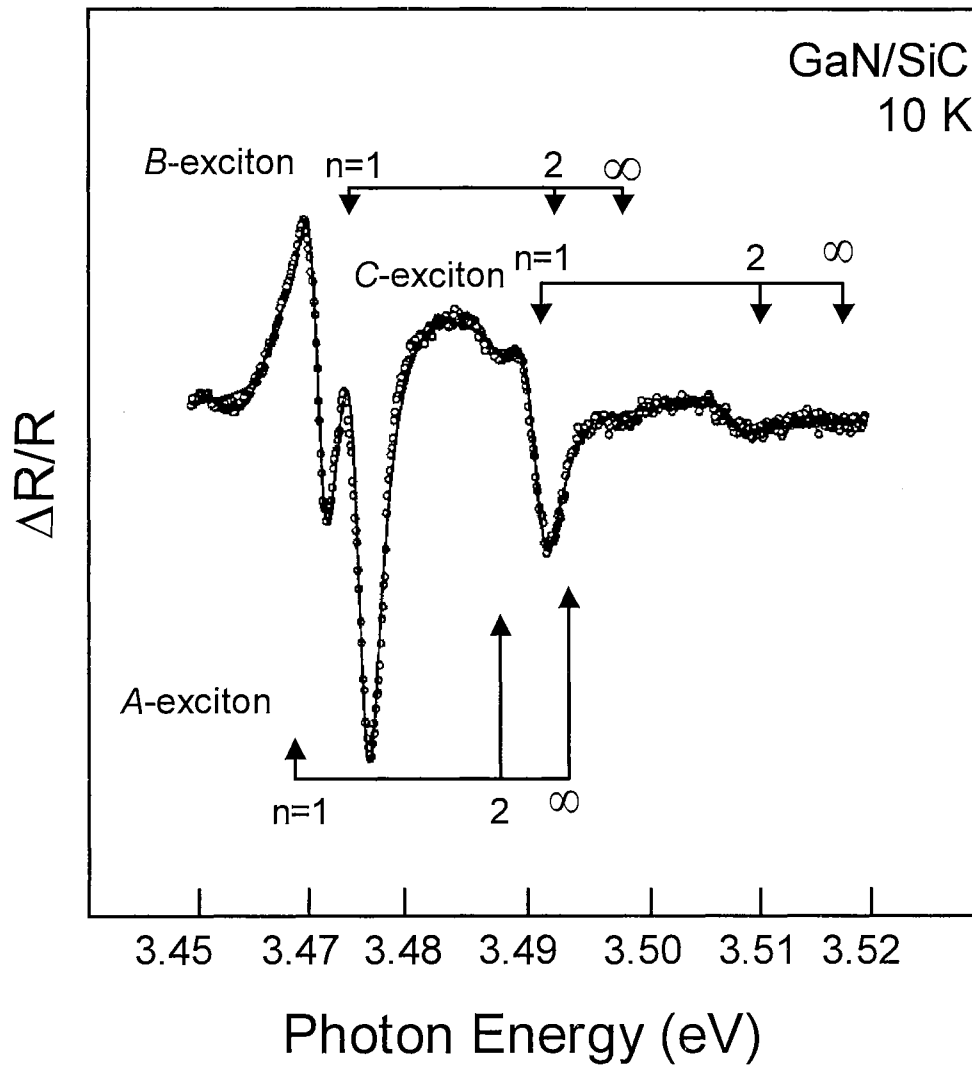


Figure 11. Photoreflectance spectrum of a GaN epilayer grown on SiC. The sample exhibits strong transition signals associated with the C-exciton. From Ref. [39].

Pump-Probe Experiments on GaN and InGaN Thin Films

Nanosecond nondegenerate optical pump-probe absorption experiments on GaN and InGaN epilayers have been performed in transmission geometry. The details of the experimental setup and pumping configurations are given in Appendix C.

Figure 12 shows 10 K absorption spectra near the fundamental absorption edge of a 0.38- μm -thick GaN sample at different pump power densities I_{exc} . At low temperature, strong, well resolved features are observed in the absorption spectrum for $I_{exc} = 0$, corresponding to the *A*- and *B*- free exciton transitions. The unpumped absorption spectrum agrees very well with cw absorption values for the same sample (see Figure 8). As I_{exc} is increased, the exciton resonances decrease and saturate due to screening by free carriers. At pump power densities of $I_{exc} \approx 3 \text{ MW/cm}^2$ they are no longer observable in the absorption spectra. The measured induced transparency and induced absorption were found to exceed $4 \times 10^4 \text{ cm}^{-1}$. The below-gap induced absorption was found to reach a maximum several nanoseconds after the pump pulse, slowly returning to zero over approximately the next 100 ns.⁴⁴ Similar results were obtained from room temperature experiments. We note that the amount of lattice heating generated by the nanosecond pump beam is significantly less than that required to account for the observed band-gap shift.⁴⁵ We believe the discrepancy lies in the inferior crystalline quality of the GaN epitaxial film, where the multitude of crystalline defects and deep levels contribute to the observed below-gap induced absorption.^{46,68}

Figure 13 shows the results of nanosecond nondegenerate optical pump-probe experiments performed on a 0.1- μm -thick $\text{In}_{0.18}\text{Ga}_{0.82}\text{N}$ layer. The absorption edge of the layer is considerably broader than that of the GaN film due to the inhomogeneous incorporation of indium. With increasing I_{exc} , absorption bleaching of the tail states is clearly observed. This bleaching covers the entire spectral range of the absorption tail. We note that, contrary to GaN epilayers, no induced absorption was observed in the

below-gap region of the InGaN layers. Instead, clear features attributed to net optical gain were observed in the below-gap region of the bleaching spectra.^{47,48} The results suggest that the high stimulated emission threshold of GaN relative to InGaN originates from induced absorption in the below-gap region of GaN with increasing carrier concentration, an effect absent in InGaN.

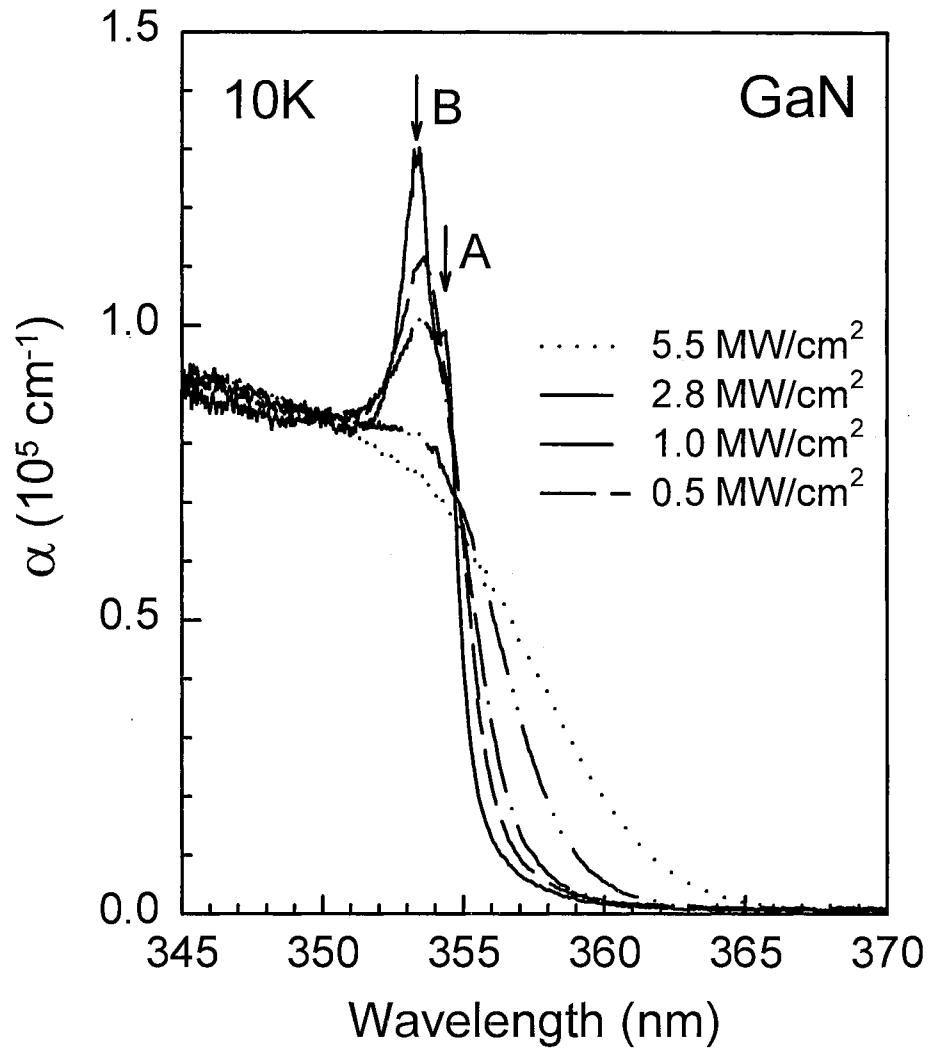


Figure 12. Nanosecond nondegenerate optical pump-probe absorption spectra of a 0.38- μm -thick GaN thin film at 10 K. The *A*- and *B*- exciton transitions are clearly seen in the unpumped spectrum. With increasing optical excitation, induced transparency in the excitonic region was observed. From Ref. [49].

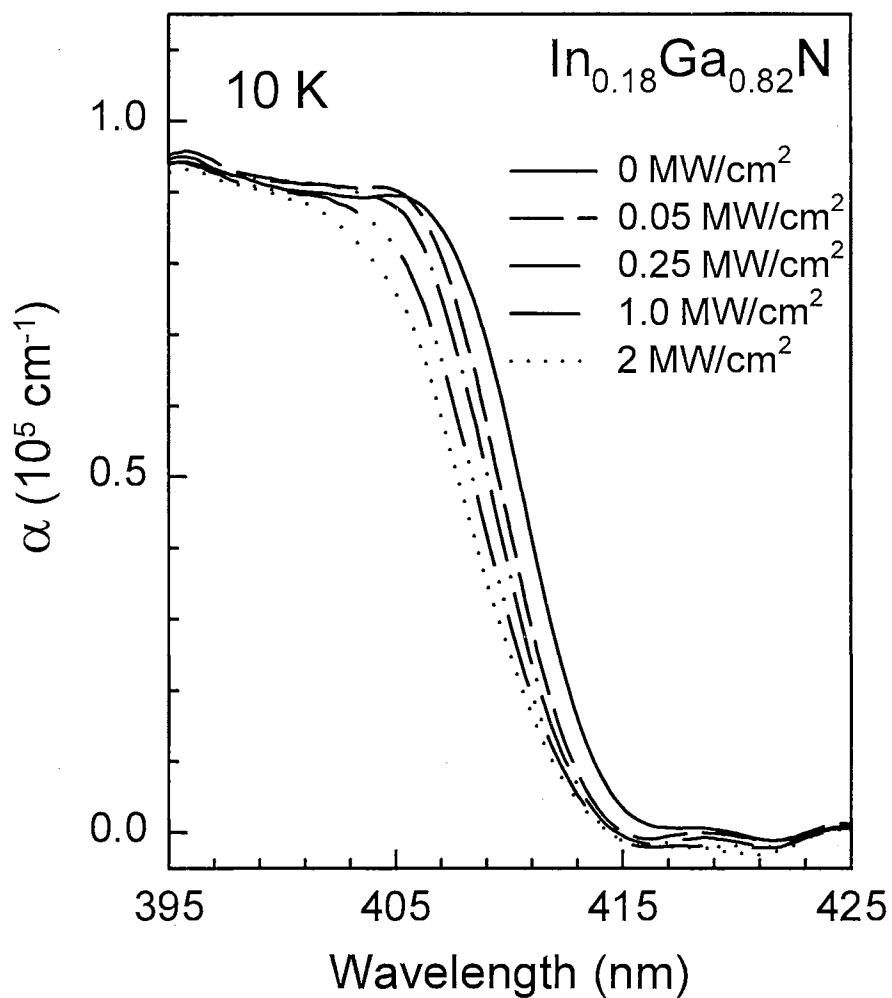


Figure 13. 10 K nanosecond nondegenerate optical pump-probe absorption spectra from an InGaN thin film as a function of above-gap optical excitation. Clear bleaching of these band tail states is observed with increasing excitation, whereas below-gap induced absorption is completely absent. From Ref. [49].

Ultrafast Carrier Dynamics

Femtosecond pump-probe measurements were performed on GaN epilayers to study carrier dynamics in the band-edge region. The experimental setup is similar to the one described in Appendix C. Figure 14 shows absorption spectra for a 0.38- μm -thick epilayer of GaN grown on sapphire at 10 K as a function of pump fluence. Excitonic absorption was found to begin saturating at a pump fluence of 20 $\mu\text{J}/\text{cm}^2$, which corresponds to an estimated carrier density of $1 \times 10^{18} \text{ cm}^{-3}$.

We can deduce additional information if we introduce an optical delay between the pump and probe beams. Figure 15 shows absorption spectra as a function of time delay for a pump fluence of 750 $\mu\text{J}/\text{cm}^2$. At zero delay between pump and probe, induced absorption is observed below the unpumped band-gap due to ultrafast band-gap renormalization. After 375 fs, a large induced transparency at around 356.5 nm is observed just below the excitonic resonance which is due to a transient electron-hole plasma. After 1 ps, the absorption has partially recovered to a level associated with excitonic phase-space filling. The absorption then recovers with a characteristic time of ~ 20 ps, a value which increases with increasing excitation density.

Figure 16 shows absorption as a function of time delay for the three wavelengths denoted with arrows in Figure 15. We note that the induced absorption below the band-gap at zero delay is followed by an induced transparency which reaches a maximum value at 400 fs. Understanding ultrafast phenomena in GaN is important not only from a theoretical standpoint but also for fast optical switch applications.

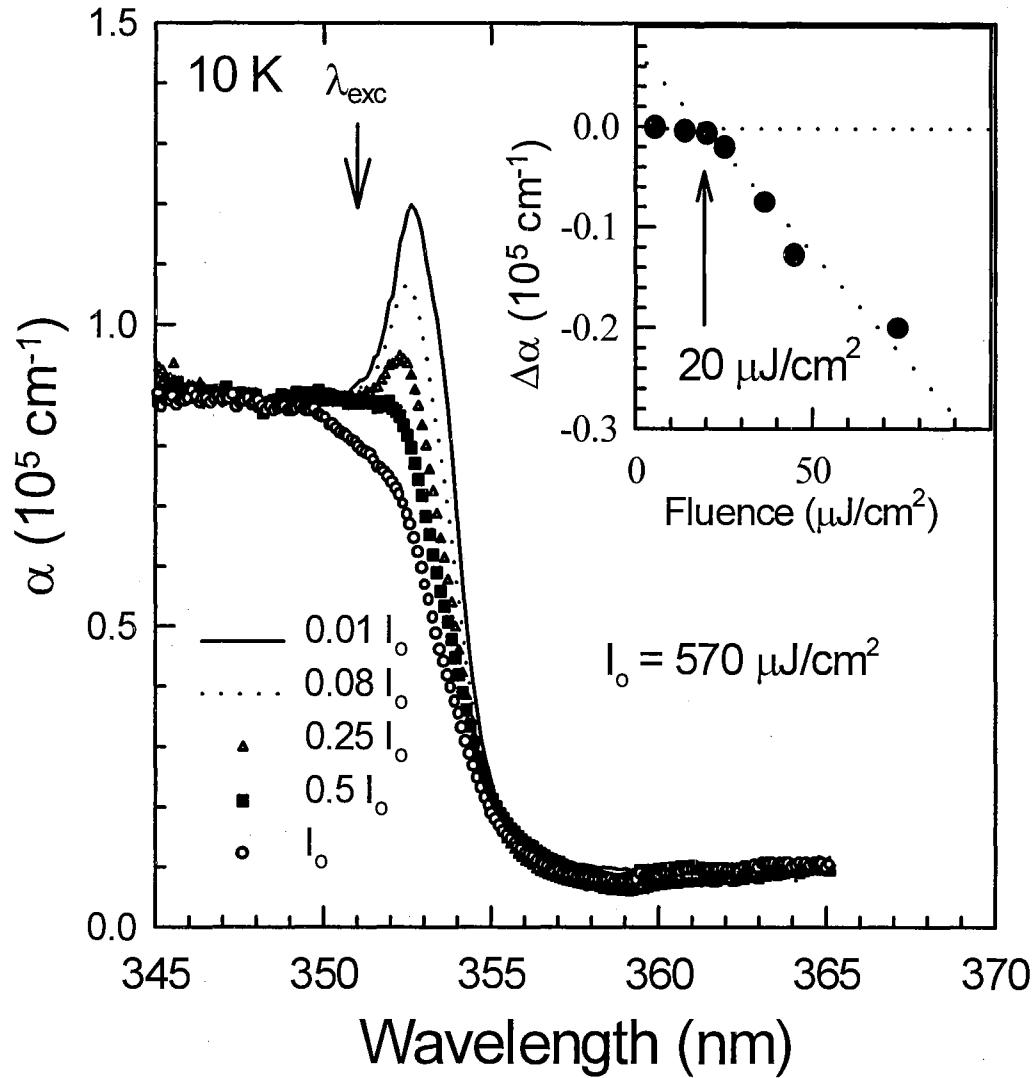


Figure 14. 10 K absorption spectra for a 0.38- μm -thick epilayer of GaN grown on sapphire as function of pump fluence. The inset shows the near-band-edge change in absorption as a function of fluence. From Ref. [50].

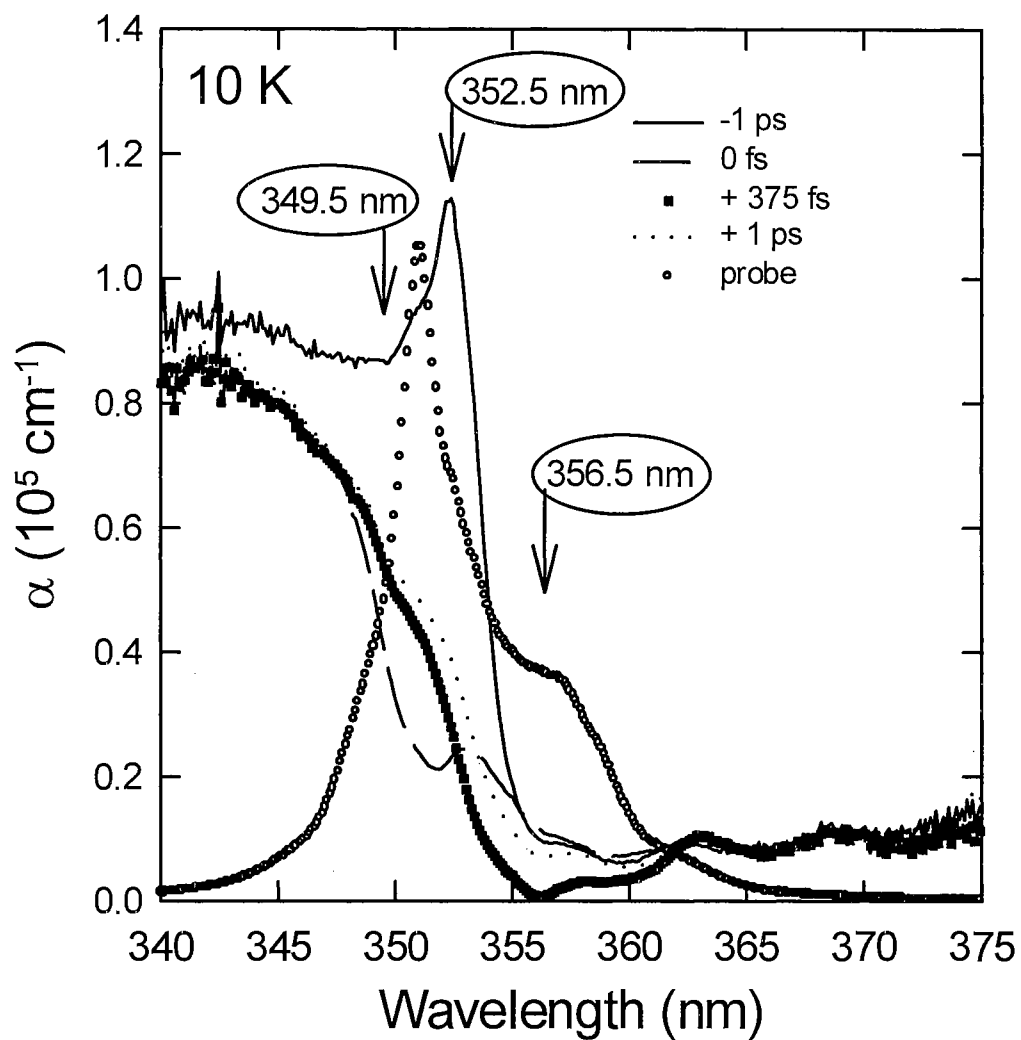


Figure 15. Absorption spectra as a function of time delay for a pump fluence of $750 \mu\text{J}/\text{cm}^2$ showing the ultrafast near-zero delay dynamics. Note the induced transparency at 356.5 nm. From Ref. [50].

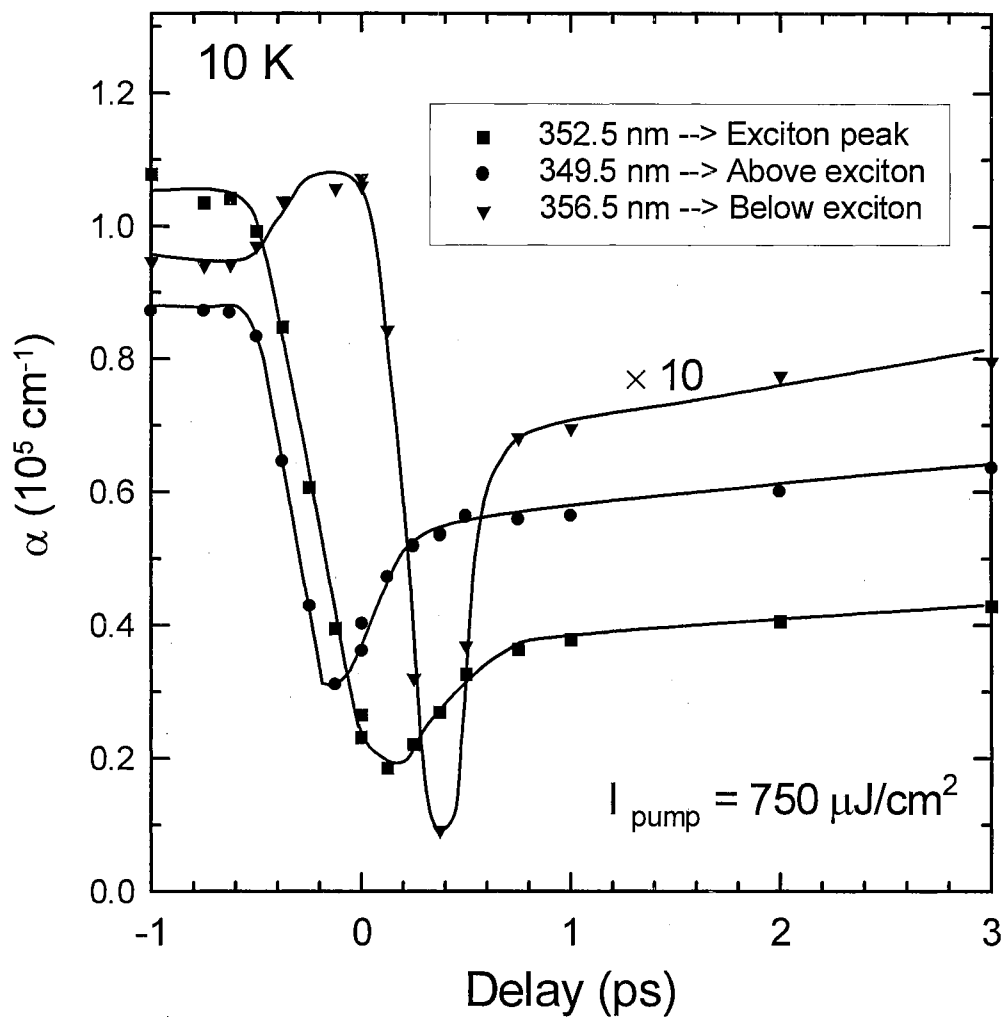


Figure 16. Absorption as a function of time delay for the three wavelengths denoted by arrows in Figure 15. Note the induced absorption below the band-gap at zero delay followed by induced transparency which reaches a maximum at 400 fs. The solid lines are guides for the eye. From Ref. [50].

CHAPTER III

GAIN MECHANISMS IN SEMICONDUCTORS

In the past three decades, semiconductor laser technology has advanced considerably. The structure of modern lasers has become more complex with the advent of surface-emitting semiconductor lasers, strained layer quantum-well lasers, high-power laser arrays, and many more. Nowadays, we have a variety of semiconductor lasers covering a wide wavelength range from hundreds of nanometers to several microns. However, all laser devices require the presence of an optical medium which provides gain. In order to make progress towards the production of these devices, a thorough understanding of gain mechanisms and gain spectra is required. In this chapter we review optical gain mechanisms in semiconductors including exciton-phonon, exciton-exciton, exciton-electron, exciton-hole, and electron-hole plasma, all of which are pertinent to the group-III nitrides. A brief theoretical description and supporting experimental data are also given.

Introduction to Gain Mechanisms in Semiconductors

We will begin with the introduction of basic recombination mechanisms as well as definitions of gain in semiconductors. We should mention, though, that many characteristics of semiconductor lasers are related to both positive gain and negative gain (optical absorption loss).

In order to characterize the optical properties of semiconductor materials one usually considers four basic electronic mechanisms:

- spontaneous recombination (photon emission)
- stimulated generation (photon absorption)
- stimulated recombination (coherent photon emission)
- nonradiative recombination

Optical gain is directly related to stimulated recombination. When a photon perturbs the system and stimulates the recombination of an electron and hole, a new photon is created which is in phase with the stimulating photon. This is the positive gain mechanism that is absolutely necessary for lasers to operate.

The optical gain $g(\omega)$ can be defined by any one of three equivalent equations, each of which determines the rate of stimulated recombination or stimulated emission:⁵¹

- Spectral density equation:

$$\frac{d}{dt} \left(\frac{dN}{d\omega} \right) = \frac{c}{\eta_r} g(\omega) \frac{dN}{d\omega}, \quad (3-1)$$

where $\frac{c}{\eta_r}$ is the group velocity of light in a semiconductor and $\frac{dN}{d\omega}$ is the spectral

density of photons per unit volume with frequency ω ($\frac{dN}{d\omega} = \frac{N_\omega}{W_0}$, where W_0 is the unit

volume in 6-D phase space).

- Volume density equation:

$$\frac{dN}{dt} = \frac{c}{\eta_r} g(\omega) N, \quad (3-2)$$

where $N = \left(\frac{dN}{d\omega} \right) \Delta\omega \Delta\psi$ is the volume density of photons lying in the solid angle $\Delta\psi$

and $I = \frac{c}{\eta_r} N$ is the flux of photons with frequencies in the range ω to $\omega + \Delta\omega$ in the

solid angle $\Delta\psi$.

- Path amplification equation:

$$\frac{dI}{dZ} = g(\omega) I, \quad (3-3)$$

where Z is a coordinate in the direction of photon flux propagation and I is the flux intensity.

In order to calculate gain one has to assume a certain model for a semiconductor. However, there are no direct experiments to measure the band structure, density of states function, matrix elements, or other characteristics. Therefore, one has to derive a formula for $g(\omega)$ by making some assumptions about the characteristics mentioned above and then compare them with experimental curves for $g(\omega)$ in order to reach conclusions about the validity of the hypothesis.

One of the most important parameters directly related to gain is the lasing threshold. As the injected carrier density or optical pumping increases, so does the optical gain. However, the steady-state gain in a laser operating above threshold must be equal to its threshold value. If the gain were higher than the threshold value g_{th} , then the field amplitude would continue to increase without any limit, which is impossible in the steady state. Once the pumping intensity reaches its threshold value the gain does not change:

$$g(I > I_{th}) = g_{th}. \quad (3-4)$$

There are many gain mechanisms, both free-carrier and excitonic, which might cause lasing in semiconductors. The pumping of a semiconductor sample can be done by intense incoherent or coherent light from a pulsed or cw lamp or laser. Alternatively, we can electrically inject carriers. In any event, let us assume that the properties of atoms permit selective excitation only from a lower level into certain selected upper levels. We are not interested in the nature of the pumping and, in fact, it does not influence the stimulated recombination parameters as long as we assume quasi-equilibrium conditions. What is important is the nature of the inversion created in the semiconductor which results in different gain mechanisms.

The four major gain mechanisms for strongly excited direct band-gap semiconductors can be classified as follows:^{52,53}

- exciton-phonon recombination
- exciton-exciton recombination
- exciton-electron (hole) recombination
- electron-hole plasma recombination.

Figure 17 gives a schematic representation of these different gain mechanisms. In exciton-electron recombination the exciton loses energy and momentum to a free electron and recombines at or near $k=0$. A similar process happens in exciton-hole recombination, however in this case the exciton interacts with a hole. Exciton-exciton recombination occurs when two excitons in the $n=1$ hydrogen-like energy level scatter, promoting one exciton to the $n=2$ level while the other exciton recombines at an energy lower than the $n=1$ level by the energy difference between $n=1$ and $n=2$. Sometimes an exciton loses energy and momentum to a longitudinal optical (LO) phonon and again recombines at or near $k=0$. In this case we are dealing with exciton-LO-phonon recombination. Finally, we can have stimulated emission from an ionized electron-hole plasma (not pictured), where the gain is due to the recombination of free carriers.

An interesting observation is that some semiconductors have different gain mechanisms at different temperatures or even different excitation powers. For example, Benoit à la Guillaume *et al.*⁵⁴ showed that at least three different mechanisms can lead to lasing in CdS. The first, which corresponds to low gain, is due to the annihilation of a free exciton with the emission of a photon and an LO-phonon. The second, yielding medium gain, is due to exciton-exciton interaction. The third, which results in high gain, involves exciton-electron interaction.

To distinguish and classify these different gain mechanisms, scientists consider various factors such as the energy position of stimulated emission peaks, the shape of the peaks, the thresholds of stimulated emission at different temperatures, and the excitonic structure of the materials. The following sections treat the four major optical gain mechanisms in semiconductor materials in more detail. Several recombination mechanisms will not be considered in this chapter, since they have not been observed in the group-III nitrides. These are the radiative decay of excitonic molecules,⁵³ electron-hole scattering,⁵⁵ and Bose-condensation of exciton molecules.⁵⁶ We will also limit our discussion to systems which can be considered to be time-independent. In the case of pulsed laser excitation, we assume that the length of the pulse is much longer than the typical carrier recombination time, *i.e.* the system is always in quasi-equilibrium.

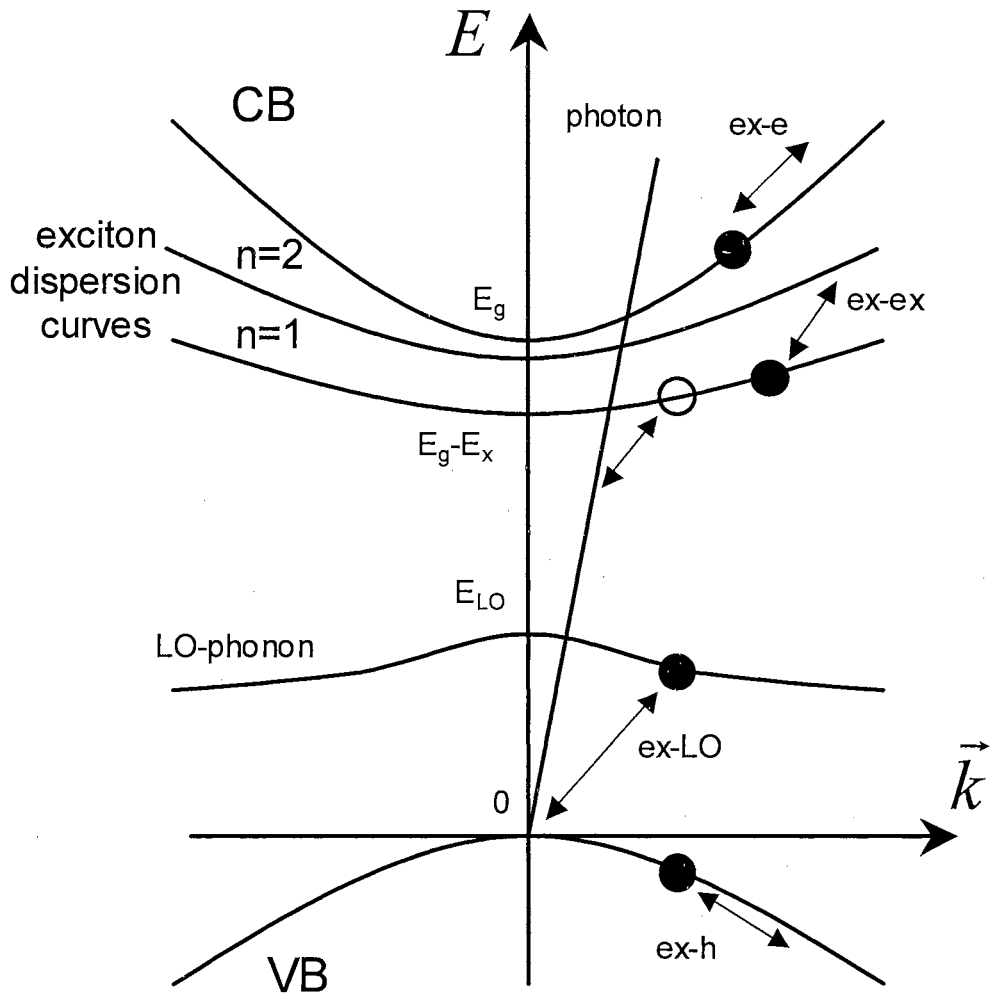


Figure 17. Schematic drawing of the various gain mechanisms in a semiconductor such as exciton-exciton, exciton-hole, exciton-electron, and exciton-phonon recombination.

Exciton-LO-Phonon Recombination

In 1962, Thomas and Hopfield⁵⁷ reported that in II-VI compounds, the recombination of electrons and holes via excitonic states is more favorable than the band-to-band transitions which happen in pure III-V compounds. Since the system of an exciton coupled to a photon is equivalent to two coupled oscillators, direct exciton recombination cannot be used to establish lasing. It is necessary to have a third field to obtain positive gain in II-VI compounds. At low temperatures one can observe a process in which a polariton (a hybrid state of an exciton and a photon) is scattered from the exciton-like part to the photon-like part of the dispersion curve by the emission of a longitudinal optical (LO) phonon as shown in Figure 18. This process is called exciton-LO-phonon recombination and has been observed to lead to gain in CdS, CdSe, and ZnO, especially when large crystal volumes were pumped homogeneously by two-photon excitation. Under these conditions, exciton-LO-phonon recombination dominated the luminescence spectra up to the highest excitation powers.

Haug⁵⁸ developed a theory for the A_1 -LO (A_1 denotes the free A -exciton line) recombination channel. He showed that the threshold for the A_1 -LO transition increases very strongly with temperature mainly because of the increase in the number of thermal phonons, which enable the absorption process. It is possible that in a given crystal, lasing from the A_1 -LO line will compete with lasing from bound exciton recombination at low temperature and free exciton recombination at high temperature.

To calculate the laser parameters for the A_1 -LO recombination process, Haug used two major assumptions:

- the intraband scattering processes of the excitons which contribute to a thermal equilibrium distribution are so fast that the excitons are always in a thermal equilibrium, *i.e.* we have the case of full dynamical homogenization
- the lifetime of the optical phonons is so short that their population is always equal to the thermal value

Both assumptions are reasonable as long as we do not pump the sample far above threshold, where one needs to take into account the finite relaxation times for both processes.

Numerical analysis determines the frequency Δ_{\max} for which the gain function has its maximum value from the following equation:

$$\frac{dG(\Delta_{\max})}{d\Delta_{\max}} = 0. \quad (3-5)$$

Figure 19 shows the maximum gain frequency Δ_{\max} vs. temperature.

The threshold pump rate P_{th} was calculated to be equal to:

$$P_{th} = \frac{2k - B\Delta_{\max}^{3/2} n_0^{a,th}}{A \left(\frac{\Delta_{\max}}{kT} \right)^{3/2} \exp\left(-\frac{\Delta_{\max}}{kT} \right)}, \quad (3-6)$$

where $n_0^{a,th}$ is the thermal number of quanta and A and B are fitting parameters (for CdS it was estimated that $A = 1.7 \times 10^{-7}$ and $B = 1.55 \times 10^{35} \text{ erg}^{-3/2} \text{ sec}^{-1}$). Figure 20 gives a plot of the threshold pump rate vs. temperature in CdS according to Eq. 3-6.

Note that the threshold rises very fast in the high-temperature region. One can therefore expect that at high temperatures other recombination mechanisms will have a lower threshold than the LO-phonon-assisted transition.

On the basis of the work described in Ref. [59] it is possible to conclude that even materials showing laser emission from bound excitons at low temperatures can show laser emission from the LO-phonon-assisted decay of free excitons at higher temperatures where a larger fraction of the bound excitons are thermally ionized.

At low temperatures, a positive gain is possible because the number of LO-phonons present is very small. All that is necessary for the buildup of laser oscillation is to achieve sufficient gain to overcome the bulk and end losses of the cavity. Packard *et al.*⁵⁹ calculated that to overcome losses of 100 cm^{-1} , a carrier density of about 10^{18} cm^{-3} is required at 77 K. These values are readily achievable with either optical or electrical pumping.

Figure 21 shows the stimulated emission spectrum from a high-purity CdS crystal at 77 K excited by a pulsed electron beam. Laser emission occurs at the center of the

dominant peak in the spectrum for this crystal. By comparison with the luminescence data of Gross *et al.*⁶⁰ it is reasonable to suggest that the origin of this peak is the decay of a free exciton accompanied by the emission of a photon and an LO-phonon.

It should be pointed out that the dispersion of optical phonons will not affect the width of the luminescence line due to one-phonon processes: this width will be determined mainly by the exciton kinetic energy. The resonance line of exciton luminescence should be narrow, since only excitons having a zero wave vector and hence zero kinetic energy radiate within it.

The spectral intensity distribution in a one-phonon exciton-luminescence line can be found from the following consideration. The intensity $I_{m=1}(k)$ of radiation from excitons having the wave vector k with the emission of a phonon is proportional to the number of excitons having this wave vector, $dN(k)/N$, and the probability $W_1(k)$ of interaction of an exciton with a phonon having the wavevector k :

$$I_{m=1}(k) \propto \frac{dN(k)}{N} W_1(k) \propto K^2 \exp\left(-\frac{E_{kin}}{kT}\right) dK W_1(k). \quad (3-7)$$

Since the contribution of phonons to the line width is small, the line shape for a one-phonon process may be found by calculating the intensity $I_{m=1}(E)$ of radiation from excitons with a given kinetic energy E . From the dispersion relation $E_{kin} = \hbar^2 k^2 / 2m$, one can derive from Eq. 3-7 an expression for the shape of the emission line from a one-phonon process:

$$I_{m=1}(E) \propto E^{1/2} \exp\left(-\frac{E_{kin}}{kT}\right) dE W_1(k) \propto E^{1/2} \exp\left(-\frac{E_{kin}}{kT}\right) \varphi(E) dE, \quad (3-8)$$

where $\varphi(E)$ is the factor by which the shape of the one-phonon line differs from a Maxwellian lineshape. The similarity in the asymmetry of the spontaneous emission shown in Figure 21 to that described by Eq. 3-8 lends additional support to the fact that we observe the phonon-assisted decay of free excitons.

In GaN the LO-phonon energy has been estimated to be approximately 92 meV. Even though many orders of LO-phonon resonances (phonon replicas) have been observed below the band-gap in photoluminescence experiments and above the band-gap in photoluminescence excitation experiments, we found that in high-quality GaN

epilayers the exciton-LO-phonon recombination does not dominate the gain spectrum at any temperature. However, in some samples with inferior crystalline quality (particular those with polycrystalline morphology) the stimulated emission peak tends to originate at the same energy position as the exciton-LO-phonon resonance.

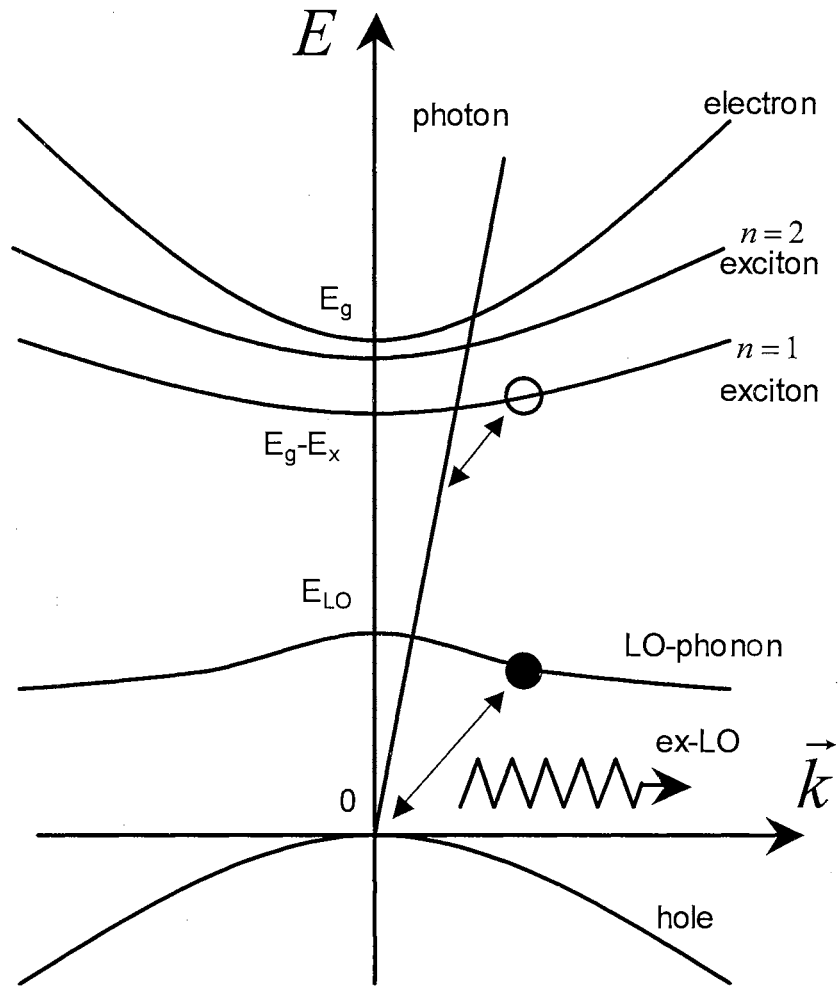


Figure 18. Recombination of an exciton by emission of an LO-phonon.

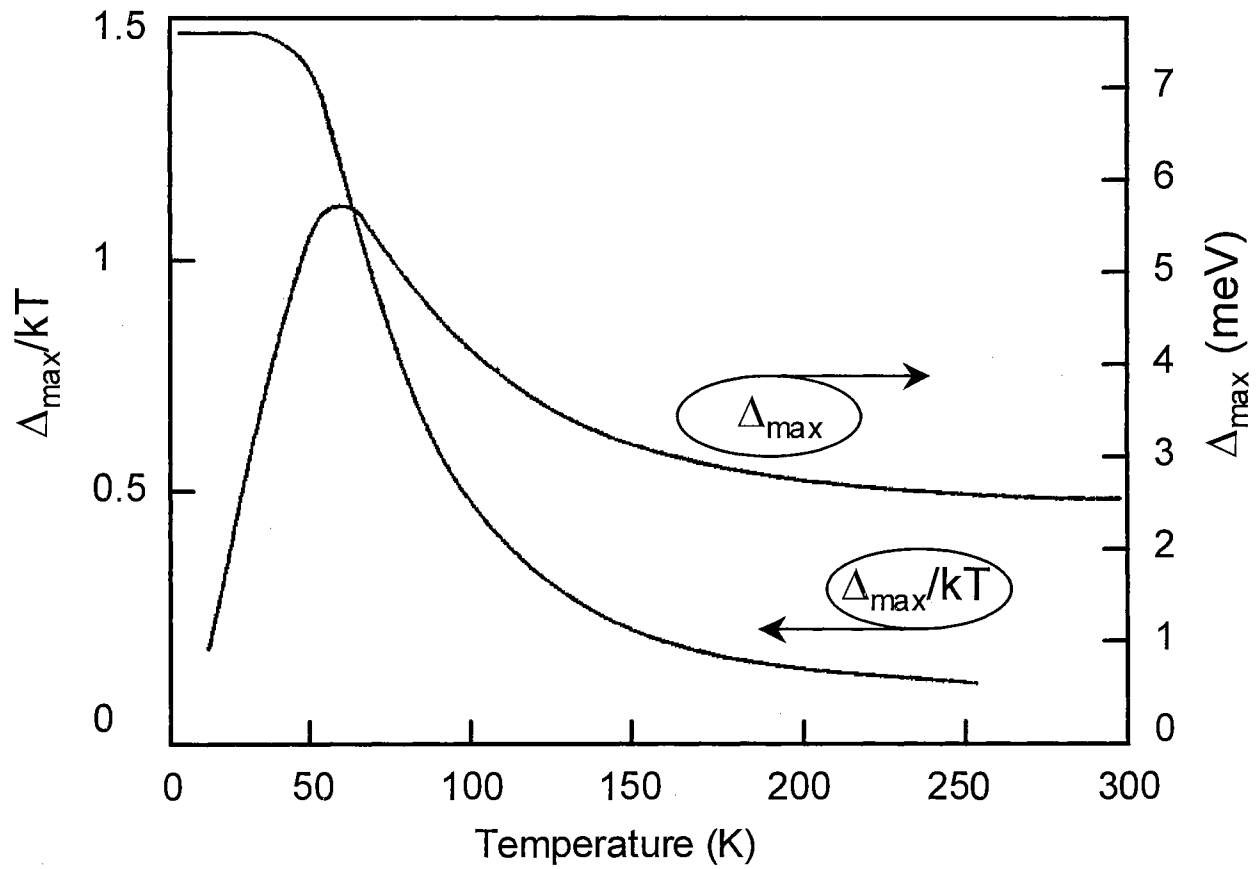


Figure 19. Maximum gain frequency Δ_{\max} as a function of temperature. From Ref. [58].

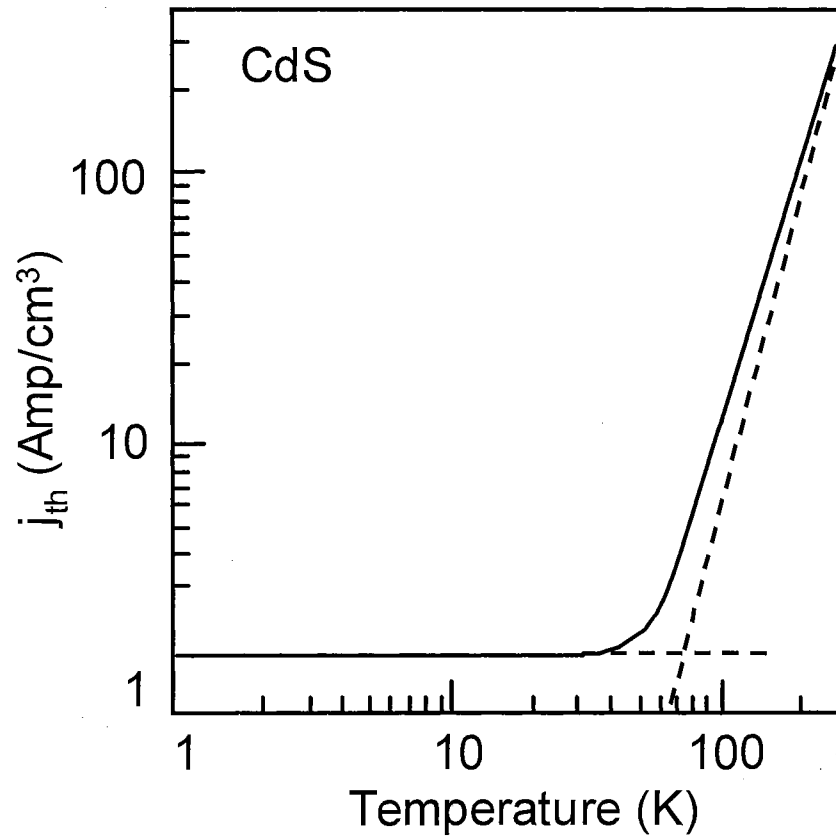


Figure 20. Threshold current density j_{th} for a 50 keV electron beam with $\eta = 1.5\%$ versus temperature. From Ref. [58].

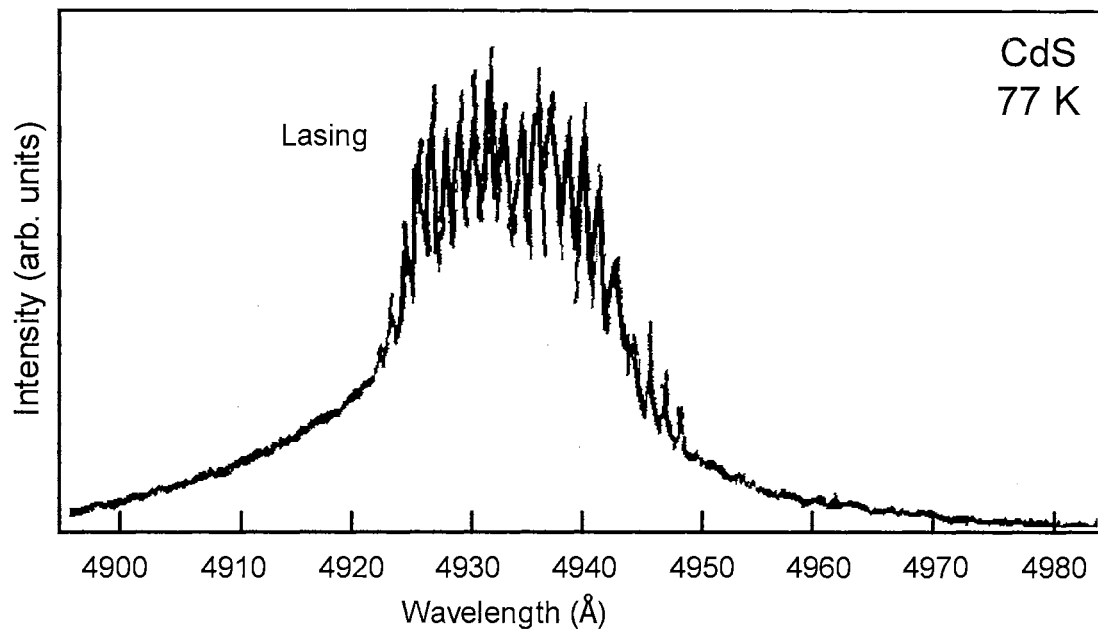


Figure 21. Lasing spectrum of CdS at 77 K occurring at a wavelength appropriate for the decay of a free exciton with the simultaneous emission of one LO-phonon. From Ref. [59].

Exciton-Exciton Recombination

In the group-III nitrides, the exciton binding energy is relatively large (see page 26). This results in the exciton being stable not only at increased temperatures but also under high optical excitation conditions. Excitons in GaN epilayers represent a strong type of Coulomb interaction that introduces new remarkable features into the gain profile spectra.

Figure 22 shows a low temperature spectrum of highly excited GaN with different excitonic lines, taken from Ref. [61]. The emission lines were interpreted as an inelastic interaction between two excitons.

To explain the appearance of the excitonic-scattering emission lines (also called *P*-lines), Klingshirn⁶² suggested the following process: during the exciton-exciton collision one of the excitons scatters into an excited excitonic state, while the other one scatters into a photon-like state as shown in Figure 23.

According to Levy and Grun⁵³ this process has the following energy balance:

$$h\nu = E_g - 2E_x - E_{e,h}^c, \quad (3-9)$$

where $h\nu$ is the energy of the emitted photon and $E_{e,h}^c$ is the kinetic energy of the unbound electron-hole pair created during the collision (here P_∞ is considered; the P_2 -line follows by analogy). We neglect the excitonic kinetic energy. At low excitation intensities one can consider the bands to be empty. The unbound pairs created during the process have a very small kinetic energy $E_{e,h}^c \approx 0$. However, as the excitation density increases, the bottoms of the bands become filled. Thus the unbound pairs created in the process of exciton-exciton collision must have higher energies, and the kinetic energy $E_{e,h}^c$ can no longer be neglected:

$$h\Delta\nu = -E_{e,h}^c. \quad (3-10)$$

Assuming that we have elliptical bands with only one extremum each, the band-filling effect gives a line shift equal to:

$$\hbar\Delta\nu = \left[\frac{1}{m_e^*} + \frac{1}{m_h^*} \right] \frac{\hbar^2}{8} \left(\frac{3}{8\pi} \right)^{2/3} n^{2/3}, \quad (3-11)$$

where m_e^* and m_h^* are the electron and hole effective masses, and n is the number of free carriers per unit volume. The experimental data for CdS at 4.2 K and the fit to Eq. 3-11 are shown in Figure 24.

To calculate the exciton-exciton gain, Haug and Koch⁶³ made the following assumptions:

- the intraband scattering rates are very fast processes, so the excitons are always in a thermal equilibrium distribution within their bands
- the exciton systems are nondegenerate, so we can use a Boltzmann distribution for all electronic excitations

Calculated gain spectra of the exciton-exciton scattering in CdS for different temperatures are shown in Figure 25. The curves are obtained by a numerical integration of momentum. The exciton-exciton process gives rise to a rather symmetric gain spectrum with a flat transition from gain to absorption. With increasing temperature the maximum of the gain shifts to lower energies.

Besides CdS, exciton-exciton scattering has also been observed in ZnSe, CdSe, and ZnO. Later in Chapter V we will show that exciton-exciton collisions result in strong gain in GaN epilayers at temperatures below 150 K and in GaN/AlGaN separate confinement heterostructures up to room temperature.

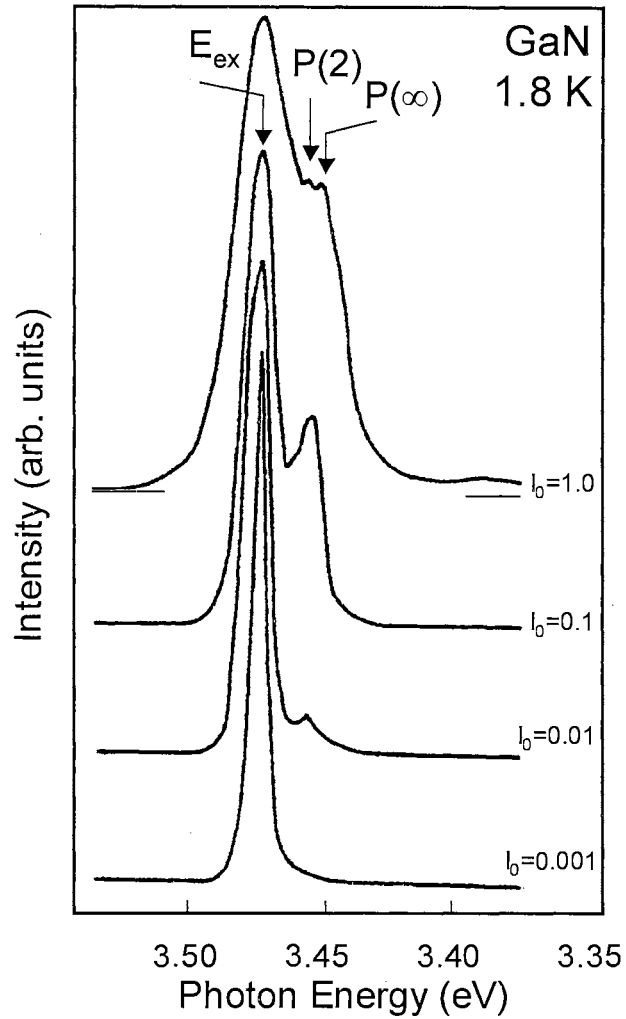


Figure 22. Emission spectra of GaN at 1.8 K as a function of optical excitation density. I_0 corresponds to an excitation power of approximately 2.5 MW/cm^2 . New emission lines attributed to inelastic scattering of excitons into the $n=2$ and $n=\infty$ excited states appear with increasing optical excitation. From Ref. [61].

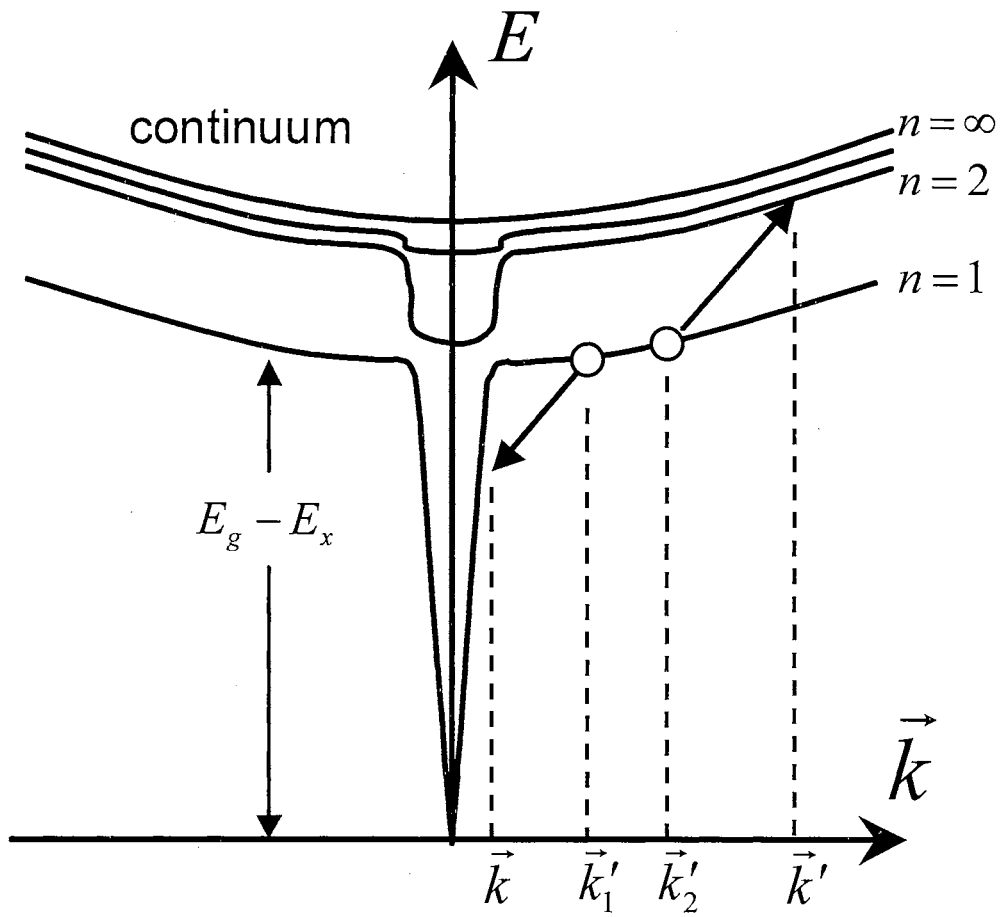


Figure 23. Dispersion curves of the excitonic polariton, showing the exciton-exciton interaction. Adapted from Ref. [62].

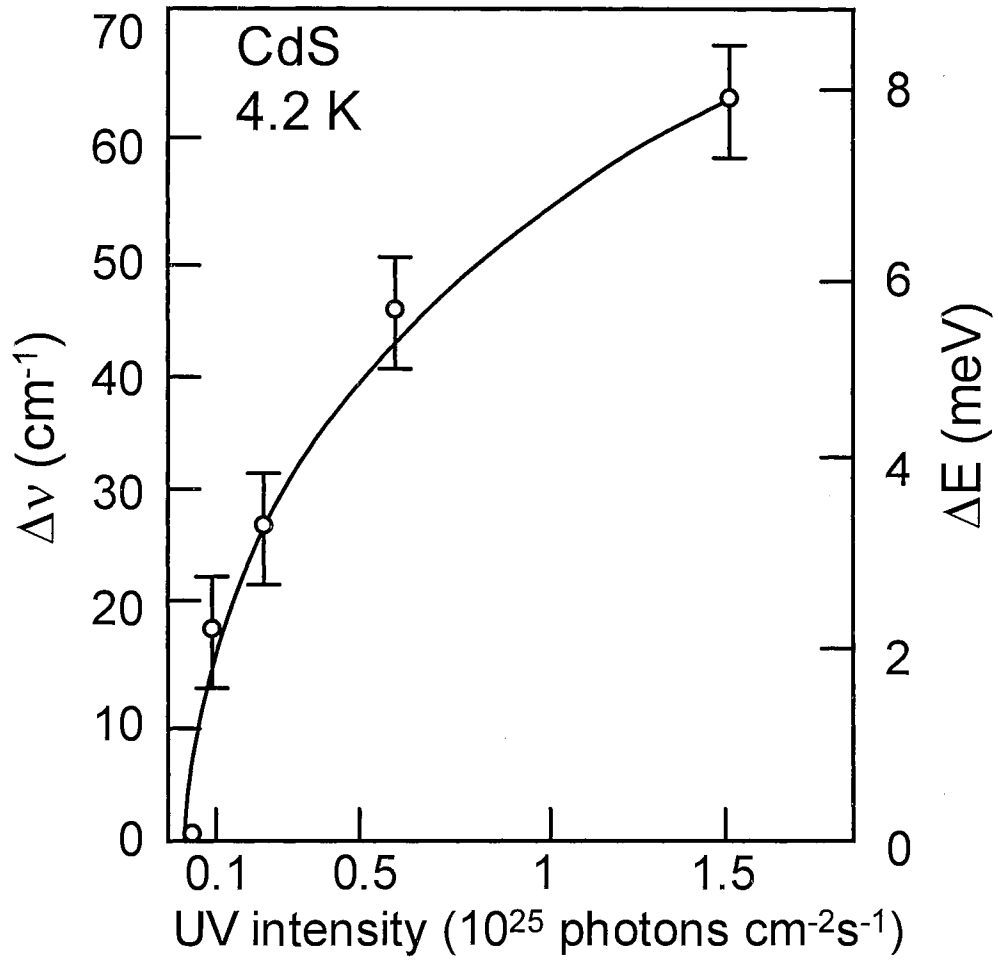


Figure 24. Shift of the *P* emission line versus the intensity of UV photons at 4.2 K in CdS. From Ref. [53].

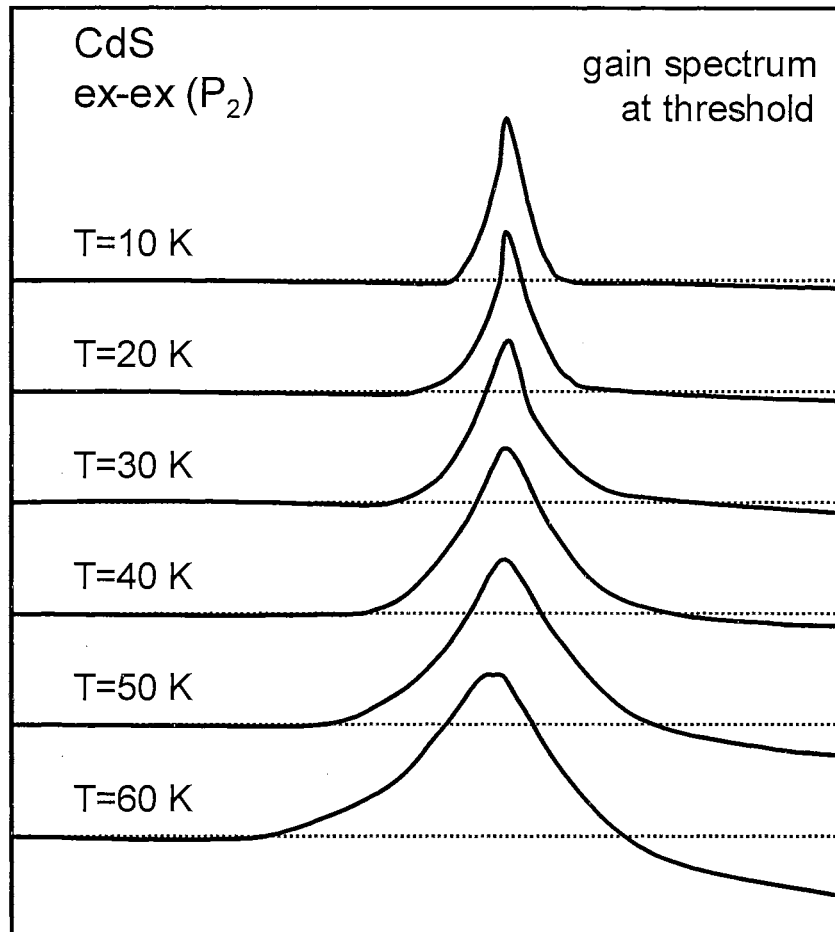


Figure 25. Calculated gain spectra of the exciton-exciton scattering in CdS for different temperatures, including the transition to the $n = 2$ exciton states only (P_2 -emission). From Ref. [63].

Exciton-Electron and Exciton-Hole Collisions

As temperature and excitation intensity increase, stimulated emission occurs due to a process which is somewhat similar to exciton-exciton recombination, but with one significant difference: the exciton interacts with an available electron or hole scattering the carrier to higher energy states, as shown in Figure 26. Usually the effective mass of the electron is considerably smaller than that of the hole (the valence band is flatter), therefore the thermal population of the final states is smaller for an electron than for a hole.⁶⁴ This is the reason why the exciton-electron recombination process in pure semiconductors is more important than the exciton-hole process. However, when we have a p-doped material, there is a possibility that exciton-hole recombination may play a dominant role. Almost everything derived for exciton-electron collisions holds true for exciton-hole collisions with the simple substitution of the hole effective mass for the electron effective mass.

The energy balance equation is given by the following:⁵³

$$E_x + E_e^i = h\nu + E_e^f, \quad (3-12)$$

where E_x is the exciton binding energy, E_e^i and E_e^f are the energies of the electron before and after the collision, and $h\nu$ is the energy of the emitted photon. Eq. 3-12 can also be written in the following form:

$$E_g - E_x + \frac{h^2 K^2}{2 M_x} + E_g + \frac{h^2 k_i^2}{2 m_e^*} = h\nu + E_g + \frac{h^2 k_f^2}{2 m_e^*}. \quad (3-13)$$

Usually, the effective mass of the electron is much smaller than the effective mass of the hole ($m_e^* \ll m_h^*$). Thus, we can neglect the electron mass compared to the exciton mass M_x . In addition, the exciton momentum K is much larger than the electron momentum k_i . Therefore, we can simplify Eq. 3-13 as follows:

$$h\nu = E_g - E_x - \frac{h^2 M_x}{2 m_e^*} \frac{K^2}{M_x}. \quad (3-14)$$

The intensity of the emission line is proportional to the product of the density of exciton states and the thermal distribution of excitons:

$$I(h\nu) \propto E^{1/2} \exp\left(-\frac{E}{k_B T}\right), \quad (3-15)$$

where E is the exciton kinetic energy. The maximum value of $I(h\nu)$ occurs when $E = \frac{1}{2} k_B T$. Substitution of this into Eq. 3-14 yields the emission band peak position:

$$h\nu = E_g - E_x - \frac{\hbar^2}{2} \frac{M_x}{m_e} k_B T. \quad (3-16)$$

We expect to have a linear temperature shift for the exciton-electron emission band. Indeed, this shift was observed by Bille *et al.*⁶⁵ for an emission line in CdS.

To calculate the exciton-electron and exciton-hole gain, H. Haug and S. Koch⁶³ made some assumptions which are almost the same as for the case of exciton-exciton recombination:

- the intraband scattering rates are very fast, so the electrons and holes are always in a thermal equilibrium distribution within their bands
- the electron and hole systems are nondegenerate, so we can use a Boltzmann distribution for all electronic excitations

Using these assumptions the authors performed a numeric evaluation of the momentum integrals and obtained the gain curves shown in Figure 27. The exciton-electron gain spectra have a characteristic asymmetry due to the steep transition from gain to absorption on the high energy side. With increasing temperature the maximum value of the gain shifts to lower energies faster than the band-edge.

The shape of the gain curve and the position of its maximum depend explicitly on the density of excitons n_{ex} . Benoit à la Guillaume *et al.*⁵⁴ showed that the variation of the gain amplitude is large and proportional to the electron density n_{el} . Their theoretical calculation of optical gain is shown in Figure 28. The gain curves A' and B' correspond to the spontaneous emission curves A and B . The maximum of the gain curve moves rapidly towards lower energy as T increases and also as n_{ex} decreases. This shift can reach values as high as 100 meV in CdS at exciton and electron temperatures below

77 K. Dynamic gain effects correspond to a small variation of the slope of the low-energy tail during the pulse and to a large shift of the maximum of the gain curve.

Thus, it is likely that exciton-electron (hole) interaction plays a significant role in the group-III nitrides at moderate excitation densities. This type of interaction can be best observed under short pulse excitation conditions. The temporal dynamics of gain in GaN is currently being investigated on both femtosecond and picosecond scales.

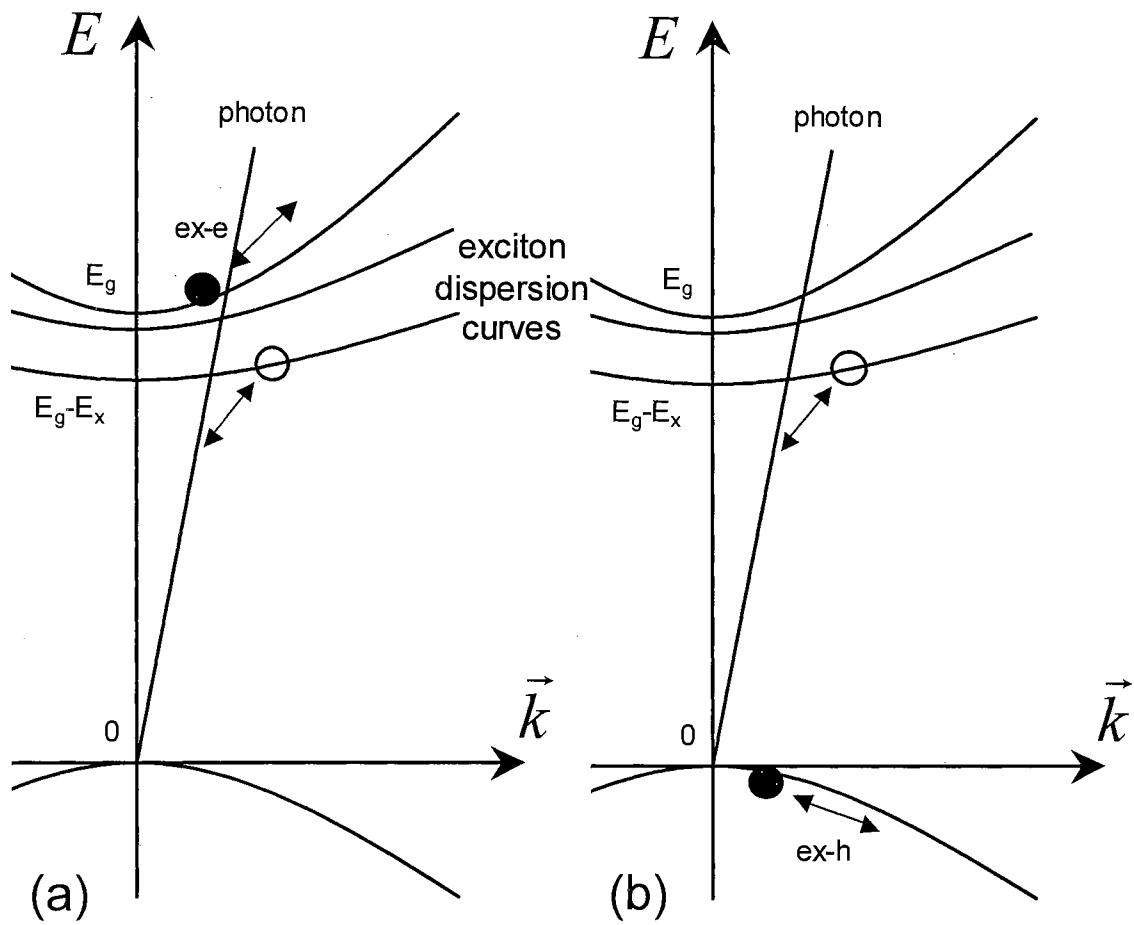


Figure 26. Recombination of excitons through (a) exciton-electron and (b) exciton-hole collisions.

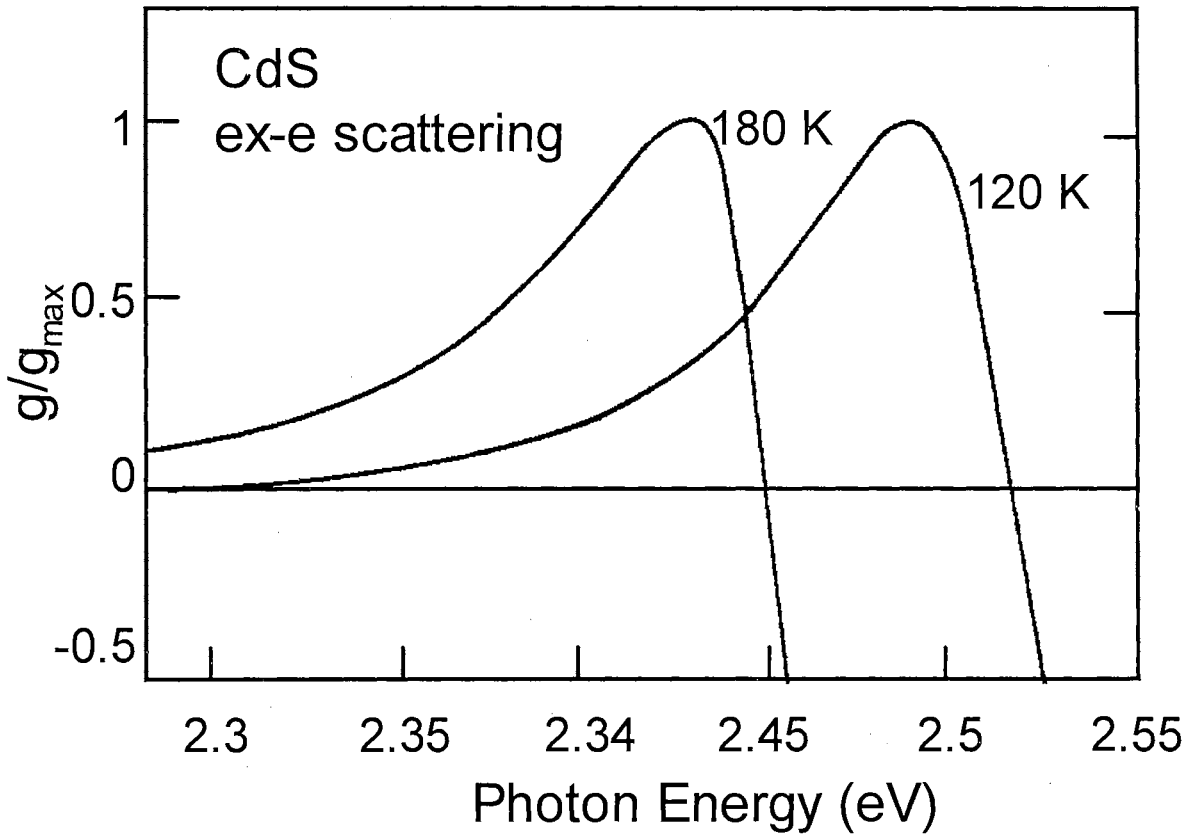


Figure 27. Calculated gain spectra for the exciton-electron scattering process in CdS. From Ref. [63].

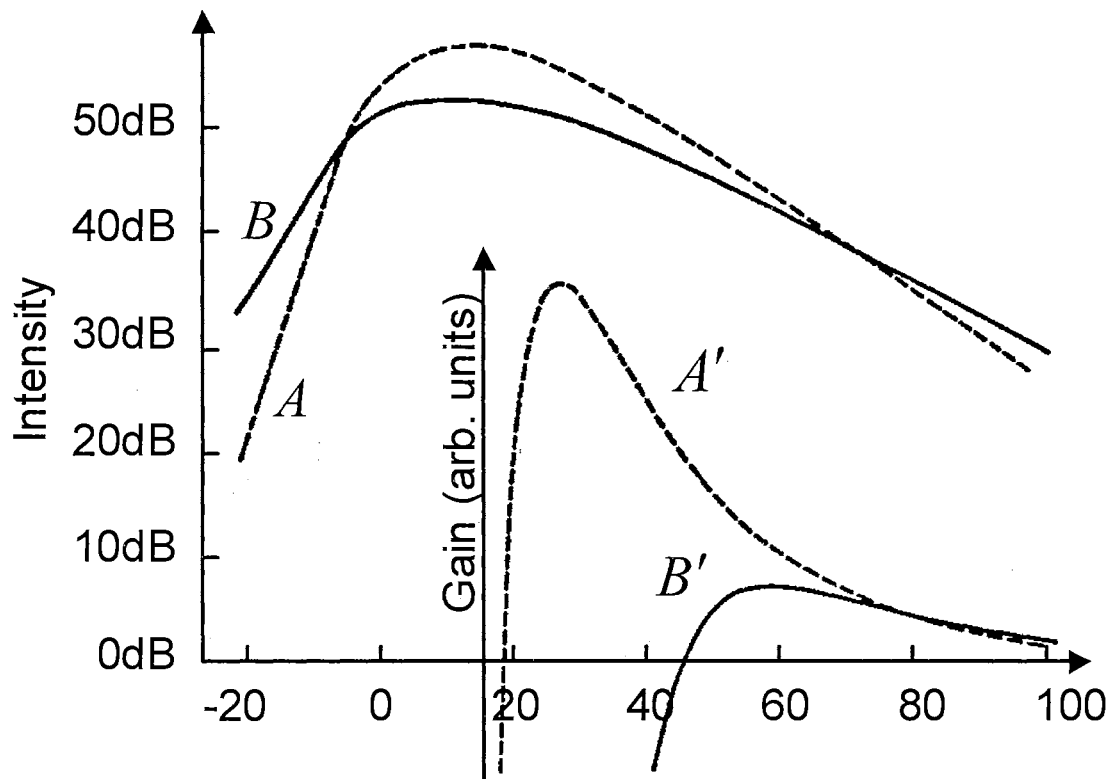


Figure 28. Theoretical shapes of the spontaneous and gain curves corresponding to the exciton-electron interaction. Gain curves A' and B' correspond to the spontaneous emission curves A and B . From Ref. [54].

Stimulated Emission From an Electron-Hole Plasma

As the density of electrical or optical excitation is increased, the density of electron-hole pairs becomes so high that bound states such as excitons are no longer stable and quickly dissociate. The dissociation of excitons is due to the screening of the attractive Coulombic force between the electrons and holes due to the presence of a high density of free carriers. The electron-hole pairs can then form a collective state, described as an electron-hole plasma. Transition from excitons to an electron-hole plasma is often called the Mott transition.

A rough estimate of the density at which the Mott transition occurs can be given by the following argument. If the screening length becomes comparable to the Bohr radius of the exciton, any state bound by Coulombic force can no longer exist. Mathematically it can be written as:

$$a_0 \approx k_D = \left(\frac{\epsilon_0 k_B T_p}{8\pi n e^2} \right)^{1/2}, \quad (3-17)$$

where a_0 is the exciton Bohr radius in the ground state, k_D is the inverse Debye-Hückel screening length, $k_B T_p$ is the thermal plasma energy, and n is the density of free carriers. From Eq. 3-17 we can estimate the density of free carriers at which the Mott transition occurs:

$$n = \frac{\epsilon_0 k_B T_p}{8\pi e^2} \left(\frac{1}{a_0} \right)^2. \quad (3-18)$$

An electron-hole plasma creates an inversion of filled conduction-band states with respect to empty valence-band states resulting in large optical gain in a direct-gap semiconductor. When an electron-hole plasma is present, luminescence studies become unreliable because the resultant amplification of the luminescence can cause considerable distortion of the recombination spectra. To establish the distribution of excited states in the crystal one should examine the gain spectra.

The gain linewidth is equal to the sum of the carrier Fermi energies. At higher temperatures, thermal excitation of the Fermi system modifies the distribution of carriers which results in a shift of the high-energy edge of the gain spectrum to lower energy. However, the gain linewidth still represents the sum of the carrier Fermi energies.⁶⁶

The chemical potential at any temperature is given by:

$$\mu(n, T) = E'_g + E_F^e + E_F^h, \quad (3-19)$$

where E_F^e and E_F^h are the carrier Fermi energies.

The presence of large number of free carrier tends to screen the crystal potential and reduce the band-gap. Optical gain is present at energies between the reduced band-gap E'_g and the chemical potential:

$$E'_g < h\nu < E'_g + E_F^e + E_F^h. \quad (3-20)$$

The mechanism of optical gain formation is graphically shown in Figure 29. We note that, for energies above the chemical potential, band-to-band absorption is expected:

$$h\nu > E'_g + E_F^e + E_F^h. \quad (3-21)$$

Hildebrand *et al.*⁶⁷ determined the Fermi energies for the electrons (E_F^e) and holes (E_F^h) from the following formula:

$$n = p = \left(\frac{m_d^{e,h} kT}{2\pi\hbar^2} \right)^{3/2} f_{1/2}^{e,h} \left(\frac{E_F^{e,h}}{kT} \right), \quad (3-22)$$

where $f_{1/2}^{e,h} \left(\frac{E_F^{e,h}}{kT} \right)$ is given by:

$$f_{1/2}^{e,h} \left(\frac{E_F^{e,h}}{kT} \right) = \frac{2}{\sqrt{\pi}} \int_0^{\infty} \frac{\sqrt{x} dx}{\exp \left(x - \frac{E_F^{e,h}}{kT} \right) + 1}. \quad (3-23)$$

Using Eq. 3-20 together with Eq. 3-22 and Eq. 3-23 one can extract the gain bandwidth.

Only a combination of different techniques – luminescence, gain measurements, transmission, and excitation spectroscopy – allows an accurate determination of the optical properties of the electron-hole plasma.

The electron-hole plasma gain mechanism has been extensively studied in GaAs and InP. Gain spectra of GaAs for different pump intensities at 2 K are shown in Figure 30.

Note that the position of the gain maximum in GaAs (1.511 eV) is nearly independent of the pump level. This is the case only if the density and the temperature stay constant when the pump intensity is changed.⁶⁷ There could be a balance between the effects of increasing density and a corresponding increase in temperature.

The critical pump level for the creation of an electron-hole plasma varies greatly in different material structures. An electron-hole plasma usually results in large values of gain (150-200 cm^{-1} in InP, 500-600 cm^{-1} in GaAs). We found that an electron-hole plasma is the dominant gain mechanism in GaN epilayers at temperatures above 150 K (see Chapter V) and can result in gain values as large as 500 cm^{-1} (see page 149).

There are many ways to extract gain spectra from a semiconductor. The appendices give details on the experimental techniques used to determine optical gain. Appendix A describes the variable stripe method, which is one of the most commonly used techniques. The procedure used to extract the gain values from spontaneous emission spectra is given in Appendix B. Finally, the pump-probe technique is described in Appendix C.

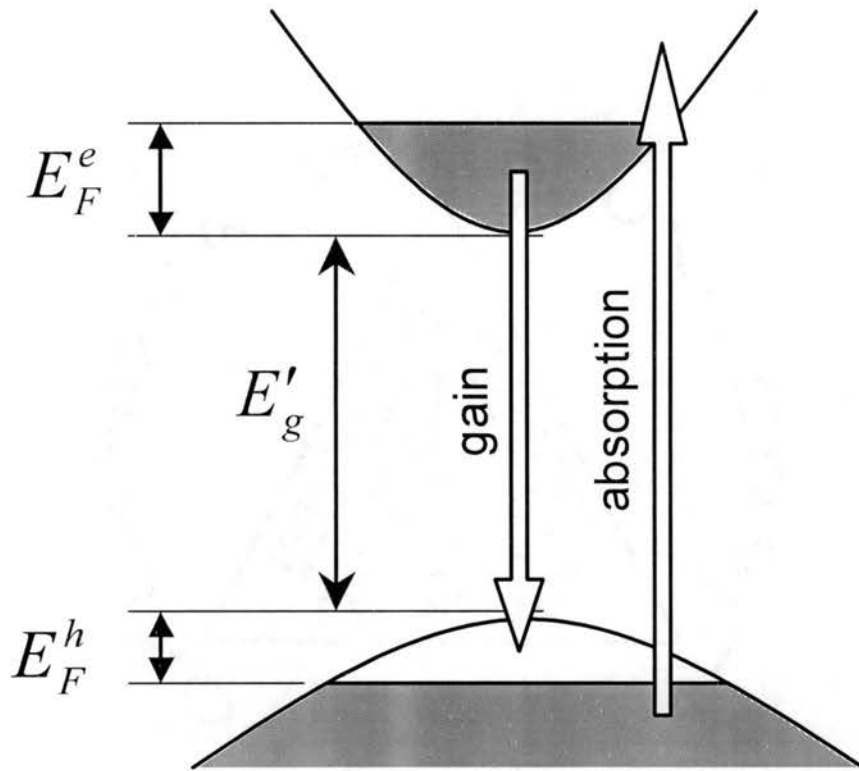


Figure 29. Formation of gain from an electron-hole plasma. E'_g is the reduced band-gap. E_F^e and E_F^h are the electron and hole Fermi energies.

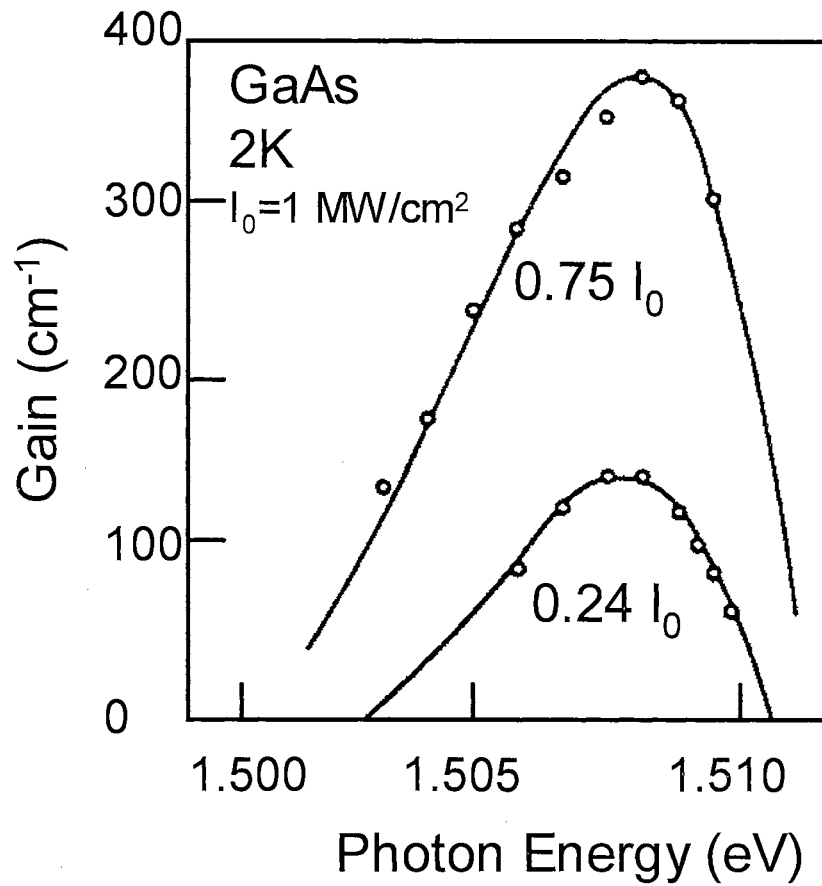


Figure 30. Gain spectra of GaAs at two different pump intensities. An electron-hole plasma is the dominant gain mechanism in GaAs at high levels of optical pumping. From Ref. [67].

CHAPTER IV

OPTICAL PROPERTIES OF GaN-BASED LASING MEDIUMS AT HIGH TEMPERATURES

New industrial and military applications require semiconductor devices that operate at high temperatures. Examples include the *in situ* monitoring of internal combustion engines for the automobile industry, electronics for ultrahigh-speed aircraft capable of withstanding large temperature variations, and electrical components for high power electronic devices. It is likely that a myriad of potential applications have not even been thought of due to the unavailability of sturdy semiconductor-based optoelectronic systems. GaN-based structures are believed to have the prospect of drastically advancing many current technologies by cutting costs and improving the performance of systems for wide-temperature applications. This chapter describes the contributions of our research group to the optical studies of GaN-based lasing mediums at high temperatures.

High-Temperature Stimulated Emission and Damage Mechanisms in GaN Epilayers

Many cryostat systems designed for use in studying the optical properties of semiconductors from room temperature down to below 10 K are commercially available, but at the time this manuscript was written there were only a few examples of systems which allow high temperature operation. In order to perform optical experiments at highly elevated temperatures, we designed, built, and tested a cryostat for use at temperatures up to at least 600°C.

The high-temperature cryostat system was designed in such a way that heat leakage from the sample was significantly reduced. To achieve this, several steps were taken: (i) the whole system was kept under a vacuum to minimize convective heat losses (this provides the additional advantage of both the metal and the sample being protected from corrosive oxidation at very high temperatures); (ii) the hot finger was thermally isolated from the rest of the cryostat by ceramic studs to prohibit conductive heat transfer; and (iii) a radiation shield around the hot finger minimized radiation losses. To heat the samples, we used a high power cartridge-style heater embedded in a hot finger. This can be seen in Figure 31, which gives side views of the heater assembly. The cryostat comprises the vacuum chamber, windows, cartridge heater, thermocouple, hot finger, and sample mount. The control system is composed of a temperature controller, power connections, and a solenoid valve for the purge. The cryostat and control system have quick disconnects for the thermocouple wire, the heater cable, and the gas purge lines, which run between the two units. All the components of the control system are mounted in an encasement complete with protective fuses, on/off switches, etc. The flexibility of the system is expected to greatly aid in other experiments that might become envisioned in the future.

This high-temperature cryostat system was used to study stimulated emission in GaN at elevated temperatures. We note that stimulated emission and laser action in GaN and related heterostructures at temperatures up to 300 K have been extensively studied in the literature (see Ref. [39], for example). Many scientists realized that the high efficiency of GaN-based LEDs has not been compromised in spite of an extremely high density of structural defects.⁶⁸ At the same time, GaN films were shown to possess a low temperature sensitivity of the lasing threshold near room temperature.⁶⁹ This suggested further research was needed to explore the optical properties and suitability of GaN-based structures for high temperature optoelectronic devices as well as to study the effects of sample quality on the performance of these devices. Some preliminary above room temperature stimulated emission experiments on GaN epilayers grown on sapphire and SiC^{69,70} as well as a theoretical prediction of the temperature sensitivity⁷¹ have been published, but, to our knowledge, there have been no reported studies on stimulated emission or lasing in GaN beyond 450 K.

Our group was first to achieve stimulated emission in high quality thin GaN films grown on sapphire and SiC substrates at temperatures as high as 700 K. The temperature dependence of the energy positions for spontaneous and stimulated emission peaks was established and empirical equations were given. The temperature sensitivity of the stimulated emission threshold was measured, from which a characteristic temperature was derived. We showed that GaN has an extremely low temperature sensitivity compared to other semiconductors. Based on the observed unique properties of stimulated emission in GaN thin films at high temperatures we suggested some possible device applications.

The GaN samples used in this study were all nominally undoped epitaxial films grown on (0001) sapphire and 6H-SiC substrates by metalorganic chemical vapor deposition. Thin AlN buffers were deposited on the substrates at 775°C. The GaN layers were deposited at 1040°C on the AlN buffers. These conditions typically result in high quality single-crystal GaN layers.^{72,73} The thickness of the layers ranged from 0.8 to 7.2 μm. Photoluminescence, absorption, reflection, and photoluminescence excitation spectra for these samples have been described previously (see Chapter II and Ref. [74]).

In this study two different pumping configurations were applied. For high-temperature stimulated emission work the samples were mounted on a copper heat sink attached to the custom-built wide temperature range cryostat/heater system described previously. The third harmonic (355 nm) of an injection-seeded Nd:YAG laser with a pulse width of 6 ns and a repetition rate of 30 Hz was used as the pumping source. The laser beam was focused into a line on the sample surface using a cylindrical lens. The laser light intensity was continuously attenuated using a variable neutral density filter. The sample emission was collected from the sample edge, as shown in Figure 32(a).

To study spontaneous emission we used a frequency doubled cw Ar⁺ laser (244 nm, 40 mW) as an excitation source. In order to avoid a spectral distortion of the spontaneous emission due to re-absorption, the laser beam was focused into an 80-μm-diameter spot on the sample surface and the spontaneous emission was collected from a direction near normal to the sample surface, as depicted in Figure 32(b).

In the first configuration the signal from the sample was dispersed by a Spex 1-m spectrometer and recorded with a side-mounted optical multi-channel analyzer. In the

second configuration we used a double-grating Spex 1403 spectrometer with a side-mounted photomultiplier tube.

Stimulated emission was observed at temperatures as high as 700 K for thin GaN films grown on SiC and sapphire substrates. The emission spectra at 700 K for different excitation powers near the stimulated emission threshold are shown in Figure 33 for the GaN sample grown on sapphire. At excitation powers below the stimulated emission threshold only broad reabsorbed spontaneous emission is present. As the pumping density increases and crosses the stimulated emission threshold, a significant spectral narrowing occurs and the peak intensity starts to increase superlinearly as shown in Figure 34, clearly indicating the onset of stimulated emission. The full width at half maximum of the stimulated emission peaks for both samples is only 5 nm at 700 K. We note that the maximum of the stimulated emission peak at 700 K is located at approximately 412 nm, which is in the same wavelength range as the lasing from InGaN/GaN multi-quantum wells at room temperature reported in Ref. [22]. The polarization ratio TE:TM for the stimulated emission peak was measured to be greater than 20:1. We estimated the stimulated emission threshold values at 700 K to be 6.4 and 5.6 MW/cm² for GaN films grown on sapphire and SiC, respectively.

The temperature dependence of the stimulated emission threshold for the two different samples is shown in Figure 35. GaN epilayers grown on sapphire (solid circles) and SiC (open triangles) exhibited similar stimulated emission threshold trends and roughly followed an exponential dependence. The stimulated emission threshold for the sample grown on SiC was measured to be 0.57 MW/cm² at room temperature, 1.7 MW/cm² at 500 K, and 5.6 MW/cm² at 700 K. The solid lines in Figure 35 represent the results of the best least-squares fit of the experimental data to the empirical equation for the temperature dependence of the stimulated emission threshold:

$$I_{th}(T) = I_0 \exp\left(\frac{T}{T_0}\right). \quad (4-1)$$

The characteristic temperature T_0 was estimated to be 172 K and 173 K over the temperature range of 300 K to 700 K for the GaN epilayers grown on sapphire and SiC, respectively, indicating the very low temperature sensitivity of the stimulated emission threshold. These obtained values of characteristic temperature are considerably larger

than the near room temperature values reported for other material systems,^{75,76} where small values of T_0 were found to be detrimental to above room temperature laser operation. Such a remarkably low temperature sensitivity of the stimulated emission threshold in GaN epilayers suggests GaN-based lasing mediums are well suited to high temperature applications.⁸

Figure 36 depicts the energy position of the spontaneous and stimulated emission peaks for a 7.2- μm -thick GaN film grown on sapphire (solid circles) and a 3.7- μm -thick GaN film on SiC (open triangles) versus temperature. We note that the energy position of the spontaneous emission peak was measured at very low excitation power in order to avoid any effects associated with band-gap renormalization and/or band filling. The position of the stimulated emission peak was measured at a pump density slightly above the stimulated emission threshold value at each temperature. For temperatures above 300 K the energy positions of the stimulated and spontaneous emission peaks are well approximated by a linear fit (solid lines). The results of this fit are summarized in Table IV. For our samples, the behavior of the spontaneous and stimulated emission energy positions at elevated temperatures in GaN epilayers was found to be independent of the substrate. A small difference in the absolute energy position of spontaneous and stimulated emission peaks (and, subsequently, in the coefficients presented in Table IV) can be explained by the different values of residual strain for GaN thin films grown on sapphire and SiC substrates.⁷⁴ The formulas presented in Table IV constitute empirical values for the energy position of spontaneous and stimulated emission peaks for GaN thin

Sample	Spontaneous Emission (eV)	Stimulated Emission (eV)
3.7 μm GaN/SiC	$3.56-5.17 \times 10^{-4} \times T$	$3.56-8.15 \times 10^{-4} \times T$
7.2 μm GaN/sapphire	$3.58-5.35 \times 10^{-4} \times T$	$3.58-8.20 \times 10^{-4} \times T$

Table IV. Results of a least squares linear fit of the energy positions of spontaneous and stimulated emission peaks as a function of temperature for GaN thin films (for temperatures above 300 K). The small difference in coefficients is most likely due to different residual strain in the GaN epilayers grown on sapphire and SiC substrates.

films in the temperature range of 300 K to 700 K.

Chow *et al.*⁷⁷ reported a many-body calculation of gain spectra in GaN and concluded that at room temperature the excitonic absorption decreases in amplitude with increasing carrier density and disappears with the appearance of gain. They predicted that the gain peak at high densities is shifted toward lower energies from the exciton resonance by several tens of meV. In this work we experimentally confirmed the large energy separation between the spontaneous and stimulated emission peaks (it gradually increases from 90 meV at room temperature to approximately 200 meV at 700K). Both this large energy difference and the relatively high values of stimulated emission thresholds in this temperature range effectively eliminate exciton-related effects from the consideration of stimulated emission mechanisms. We therefore conclude that free carrier recombination or an electron-hole plasma is the dominant stimulated emission mechanism in GaN thin films for temperatures above 300 K. We note that our conclusions about the origin of stimulated emission in the temperature range studied are consistent with those reported by Amano *et al.*⁷⁸

The broadening of the stimulated emission peak was found to be considerably smaller than the temperature-induced shift in energy position, as shown in Figure 37. Raising the temperature from 300 K to 700 K allows a "tuning" of the stimulated emission peak energy from the near-UV spectral region to blue (a range of more than 40 nm). We did not observe any degradation of the GaN epilayers in spite of the very high pumping densities required to reach the stimulated emission threshold at temperatures exceeding 700 K.⁷⁹ This unique property of stimulated emission in GaN thin films might result in new types of optoelectronic devices utilizing this temperature tuning. The low temperature sensitivity of the stimulated emission threshold over such a large temperature range could potentially lead to the development of laser diodes operating hundreds of degrees above room temperature.

In the current work, the maximum temperature at which stimulated emission in GaN could be observed was directly related to the density of line defects (or cracks) on the sample surface. The stimulated emission threshold was previously shown (Figure 35) to exponentially increase with temperature. This requires higher levels of optical pumping to reach the stimulated emission threshold. When pump densities on the order of

10 MW/cm² are reached, the sample surface starts rapidly deteriorating. A microscope image of burn spots on the surface of a GaN film is shown in Figure 38. We noticed that, in spite of the uniform density of the excitation beam, most of the burn spots tend to originate at linear defects, such as cracks, in the vicinity of the sample edge. If we assume a single pass amplification (the sample facets were not specially prepared), the sample emission is amplified when the photon flux propagates along the longest path, *i.e.* the stimulated emission intensity is strongest near the sample edges and weakest in the middle of the sample. This explains the fact that most of the burn spots were found near the sample edges. Also, we note that the burn spots always propagate towards the middle of the sample in the direction opposite to the amplification direction of the stimulated emission flux, as shown in Figure 38. We conclude that the GaN epilayer quality becomes a strong limiting factor for stimulated emission in bulk GaN at high temperatures.

In order to explain the burning mechanism in GaN epilayers, it is important to understand the effect of defects on stimulated emission. Under strong optical excitation the defect spots dissipate a significant amount of heat that eventually leads to surface burning. In fact, once we exceed the damage threshold pumping density, unpolarized surface emitted stimulated emission is observed to increase and the burn spots tend to originate from linear surface defects, such as cracks. Therefore, surface quality is a strong limiting factor for the observation of stimulated emission at high temperatures. The high density of defects in GaN is associated with the film-substrate lattice mismatch and thermal expansion coefficient mismatch. Even though significant progress in improving the epilayer quality has been made,⁸⁰ a high density of structural defects might always be present in GaN-based working devices. The effects of surface defects on optical gain measurements are described in more detail in Chapter VI.

Side Views

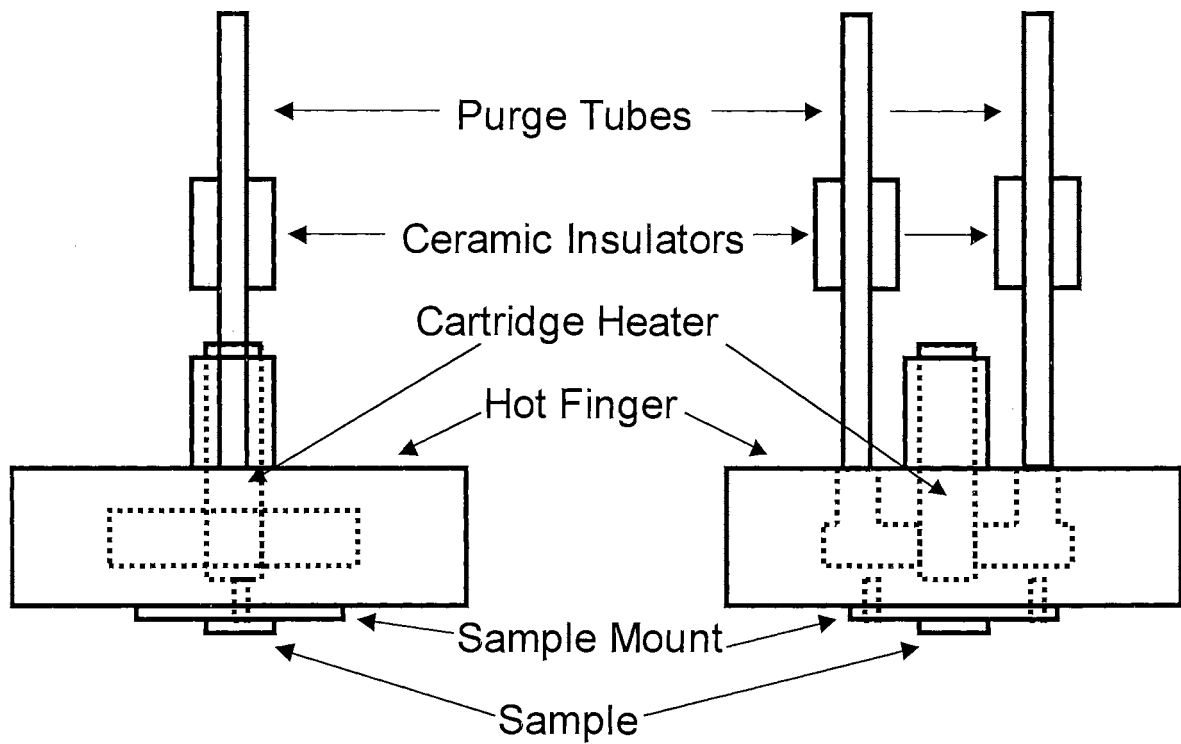


Figure 31. Perpendicular side views of the heater assembly. The area in dotted lines intersecting the cartridge heater is the purge cavity. Adapted from Ref. [81].

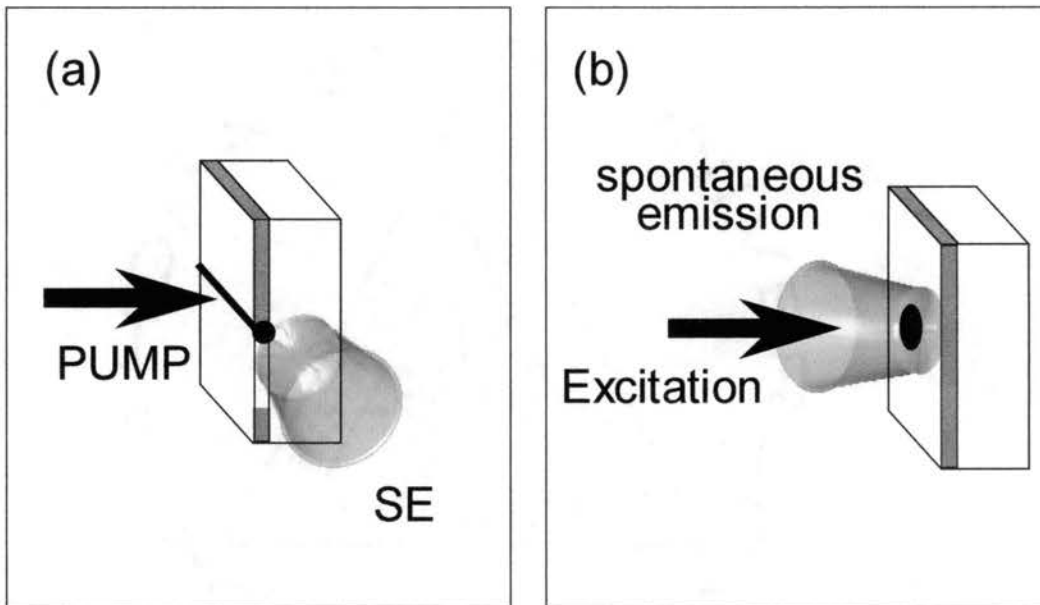


Figure 32. Pumping configuration for (a) edge-emitted stimulated emission and (b) surface-emitted spontaneous emission.

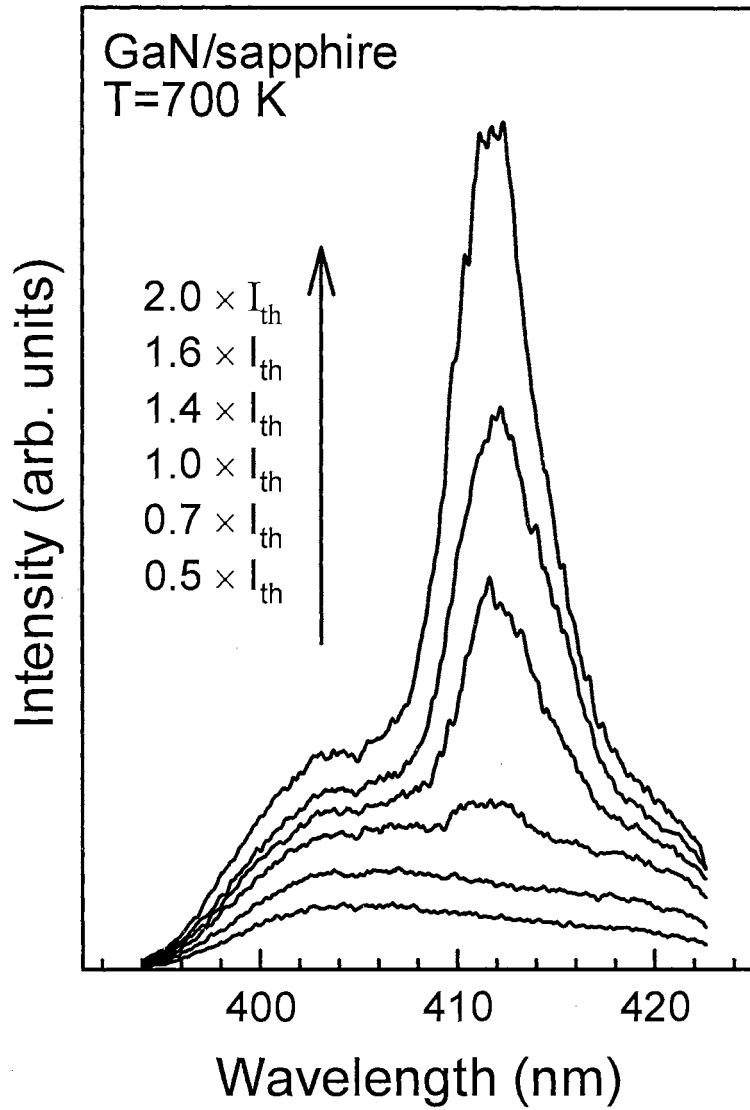


Figure 33. Emission spectra at 700 K from a GaN film grown on a sapphire substrate. The full width at half maximum of the stimulated emission peak is only 5 nm at 700 K.

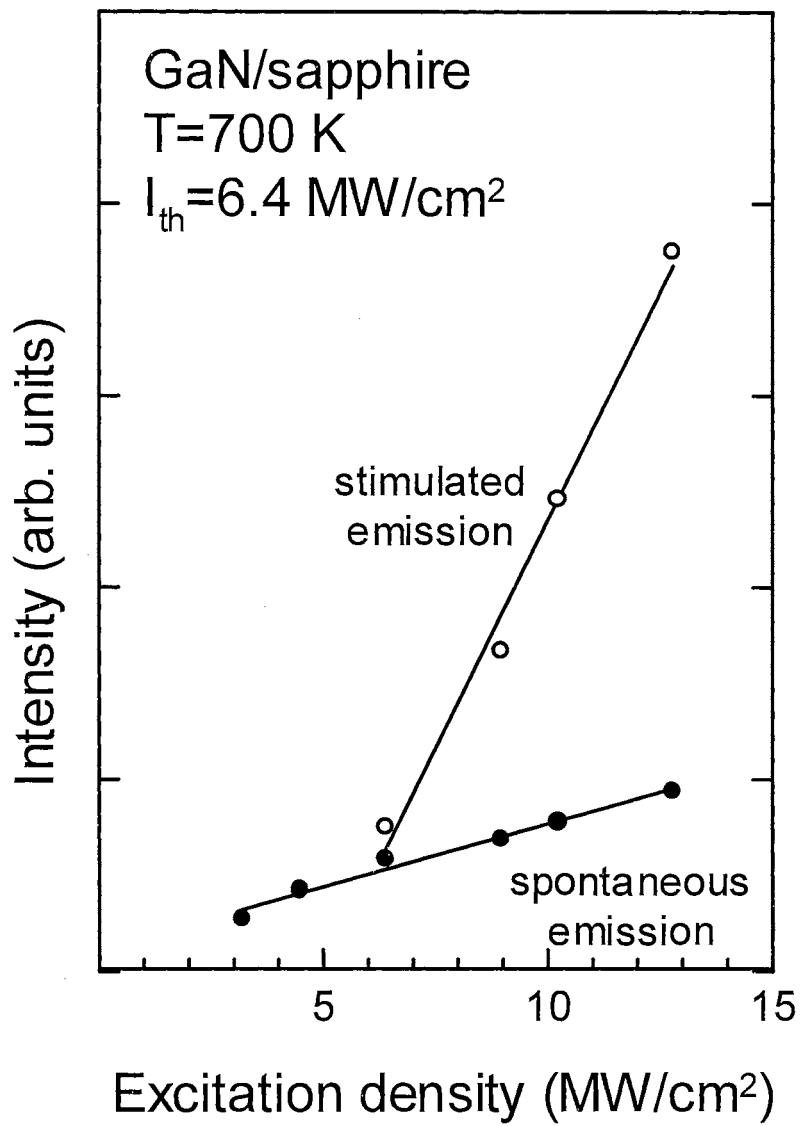


Figure 34. Dependence of integrated emission intensity on the pump density for a GaN film at 700 K.

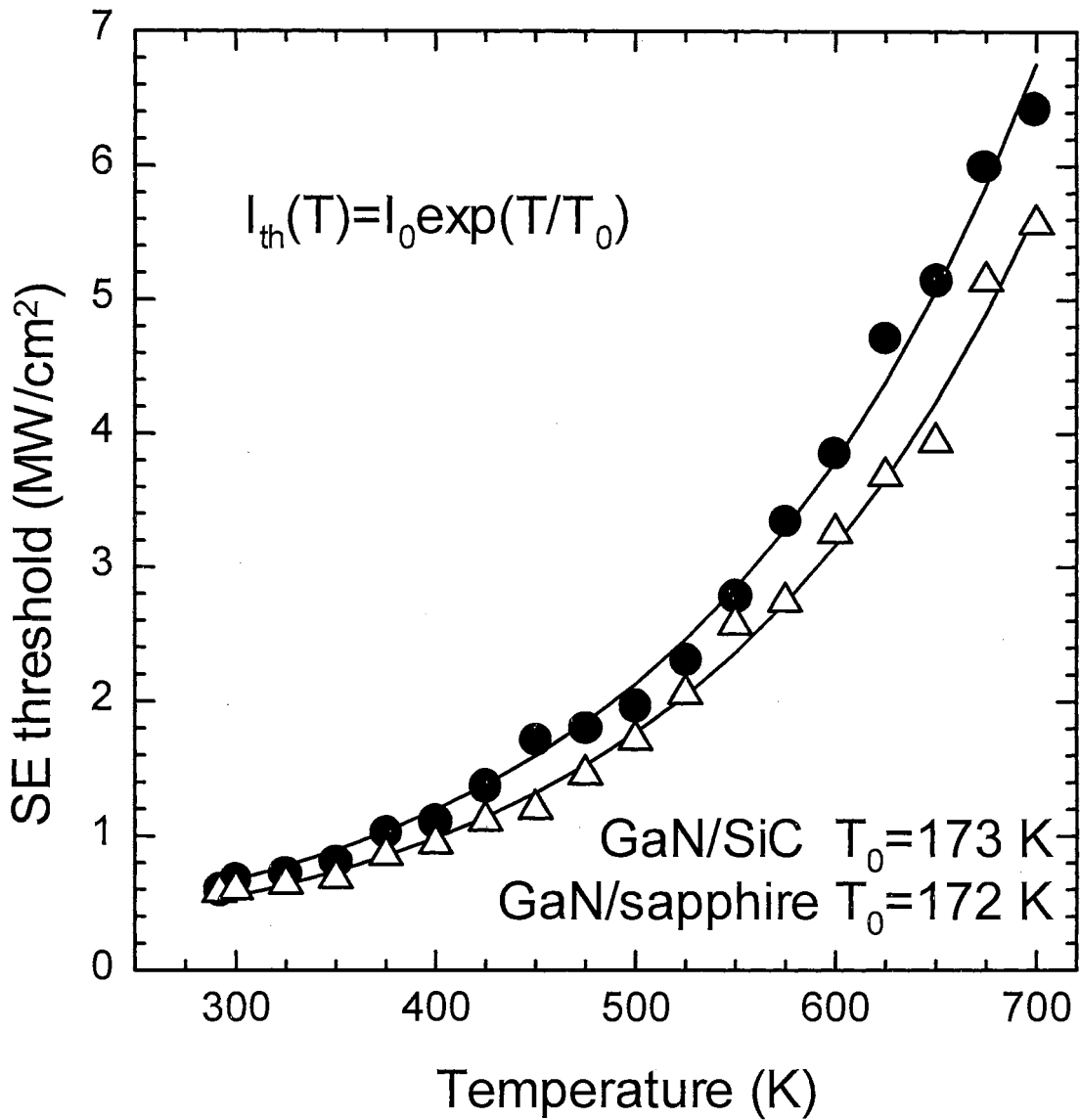


Figure 35. Stimulated emission threshold as a function of temperature for GaN thin films grown on sapphire (solid circles) and SiC (open triangles). The solid lines represent the best least-squares fit to the experimental data. Characteristic temperatures of 172 and 173 K were obtained for samples grown on sapphire and SiC, respectively.

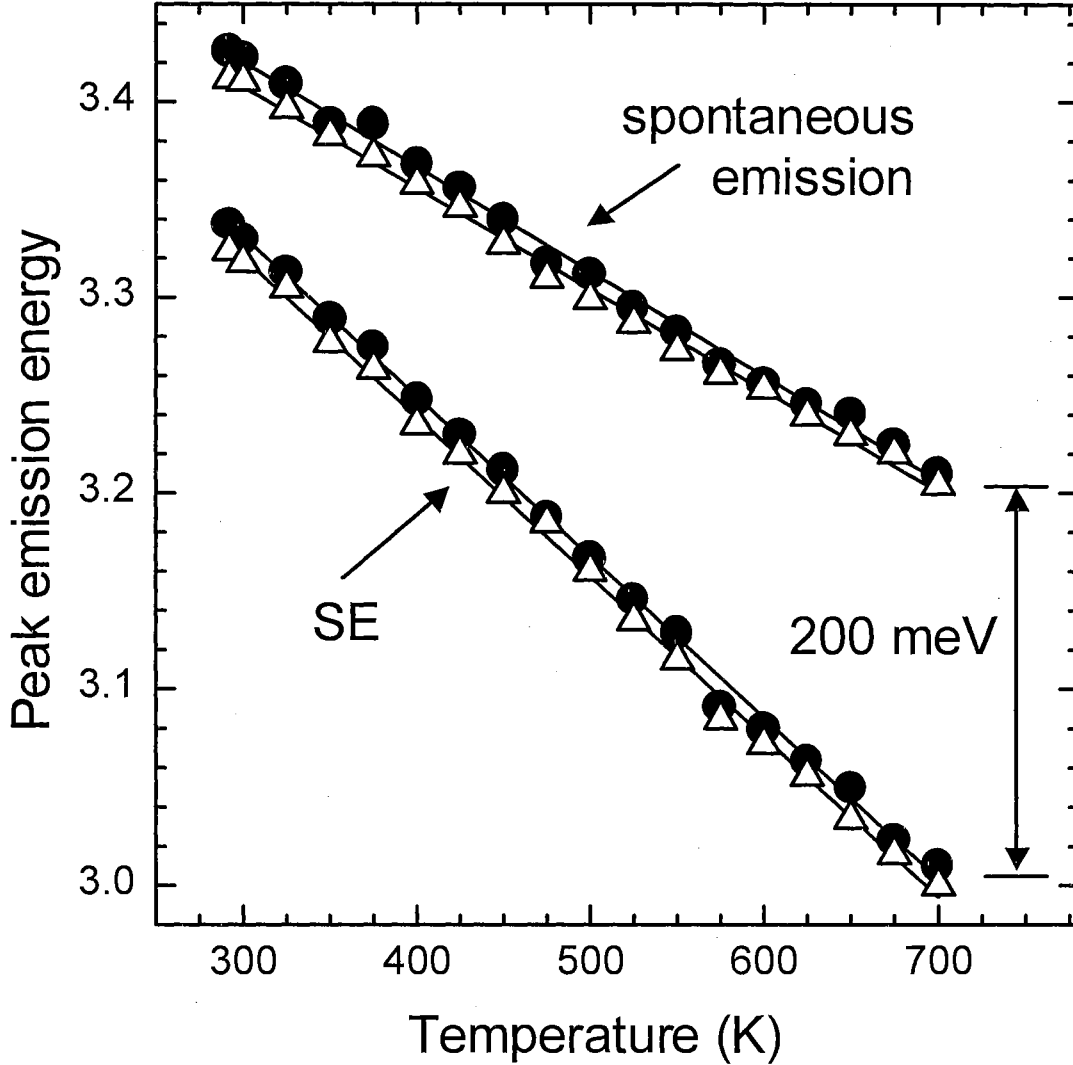


Figure 36. Energy positions of stimulated and spontaneous emission as a function of temperature for GaN thin films grown on sapphire (solid circles) and SiC (open triangles). The solid lines represent a linear fit to the experimental data. The results of the fit are summarized in Table IV. The energy separation between the peaks gradually increases from 90 meV at room temperature to 200 meV at 700 K, indicating that an electron-hole plasma is responsible for the stimulated emission mechanism in this temperature range.

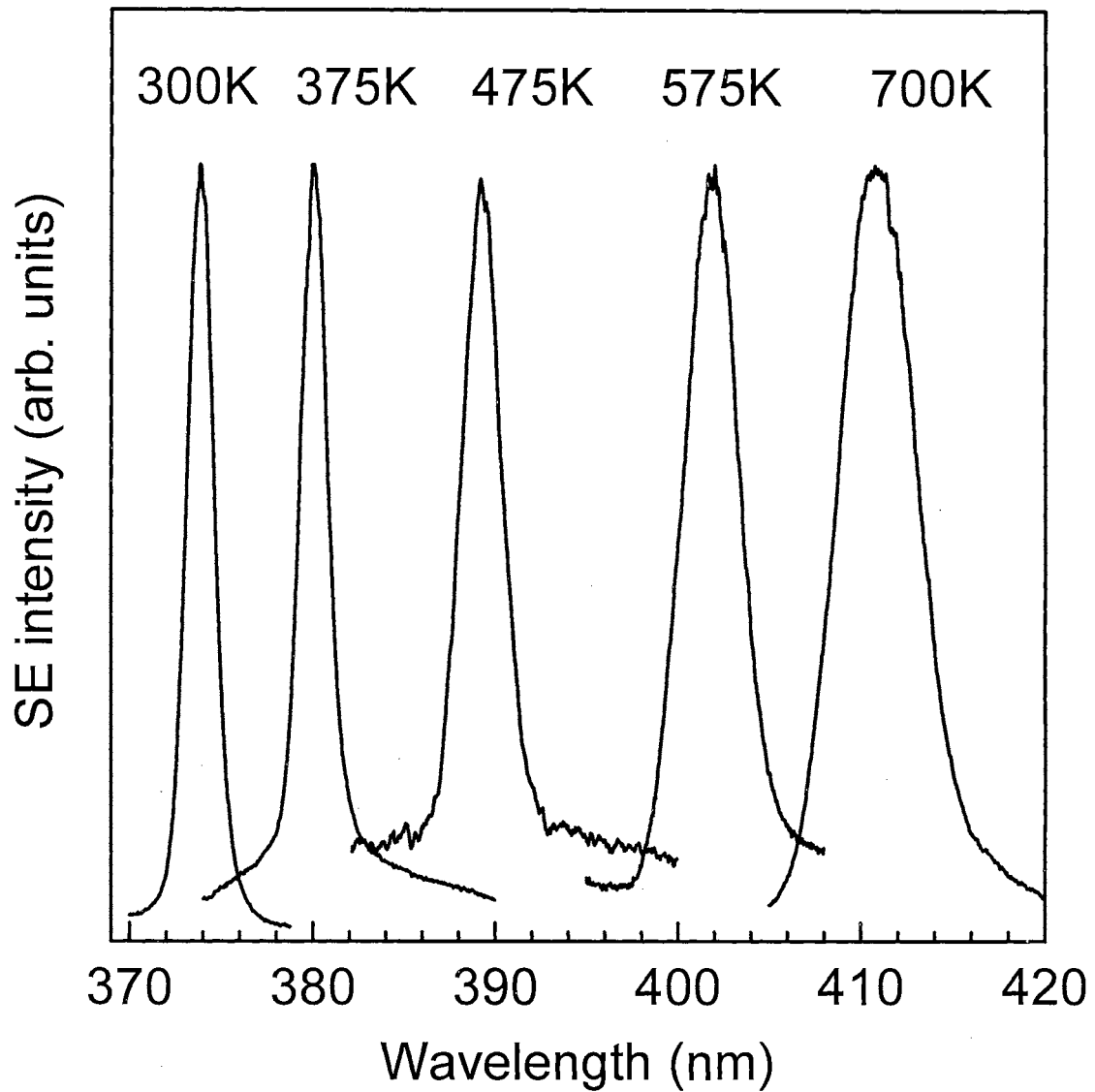


Figure 37. Temperature “tuning” of the stimulated emission peak wavelength position. The broadening of the stimulated emission peak is considerably less than its shift in energy as the temperature is raised from 300 to 700 K for a GaN epilayer grown on SiC.

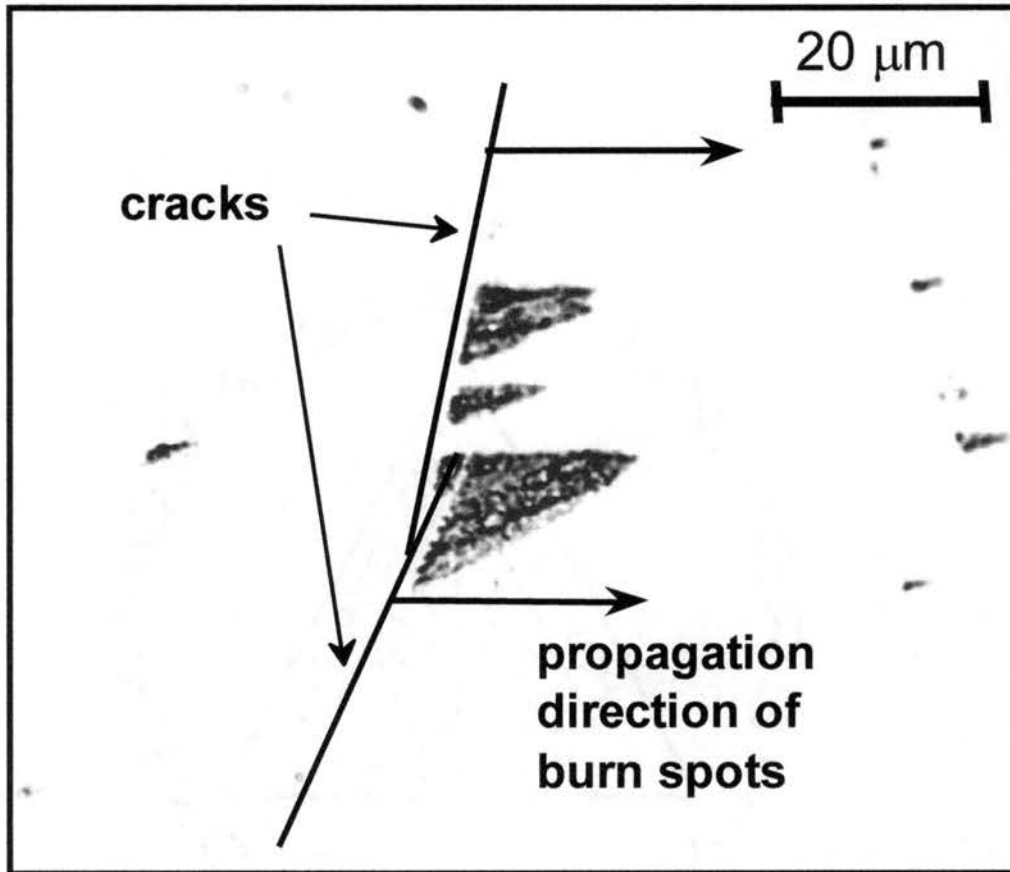


Figure 38. A microscope image of burn spots on the surface of a GaN film. Burn spots tend to originate at linear defects such as cracks near a sample edge and propagate towards the middle of the sample. Surface defects are shown to be a strong limiting factor for high-temperature stimulated emission in thin GaN films.

Stimulated Emission in InGaN/GaN Multi-Quantum Wells at Elevated Temperatures

The low temperature sensitivity of the lasing threshold in ridge-geometry InGaN multi-quantum well (MQW) structures near room temperature⁸² in comparison to structures based on other materials, as well as the previously described success in the demonstration of high-temperature stimulated emission in GaN epilayers prompted further research to explore the possibilities of high temperature applications for III-V nitride MQW wells. To our knowledge, there have been no reported studies on stimulated emission or lasing in InGaN/GaN/AlGaIn-based heterostructures at temperatures above 80°C. In this section, we describe the results of an experimental study on stimulated emission in optically pumped InGaN/GaN MQW samples in the temperature range of 175-575 K. Narrow stimulated emission peaks with a full-width at half maximum of approximately 1 Å were observed throughout this temperature range. The stimulated emission threshold density was plotted as a function of temperature, and a characteristic temperature of 162 K has been derived. We also discuss the effects of Si doping on the luminescence intensity and stimulated emission threshold density of InGaN/GaN MQWs. Also, we examined the dependence of the integrated emission intensity on pumping density for different temperatures. Finally, we suggest possibilities for the development of InGaN/GaN MQW-based optoelectronic devices capable of high temperature operation.

The InGaN/GaN MQW samples used in this work were grown on a 1.8- μm -thick GaN base layer by metalorganic chemical vapor deposition (MOCVD) using trimethylgallium (TMGa), trimethylindium (TMIn), trimethylaluminum (TMAI), and ammonia precursors. Disilane was used as the n-type dopant. The GaN base layer was deposited on a (0001) sapphire substrate at a temperature of 1050°C.⁸³ The temperature was reduced to 790°C for the growth of the MQW region.⁸⁴ The TMGa and TMIn flows during InGaN well and GaN barrier growth were 5 $\mu\text{mol}/\text{min}$ and 14 $\mu\text{mol}/\text{min}$, respectively. The disilane flow was varied between 0 and 2 nmol/min . The ammonia flow

was held constant at 0.35 mol/min. The GaN barriers were doped with Si at a concentration range of 1×10^{17} to 3×10^{19} cm^{-3} for the different samples studied. The MQWs were capped with a 100 nm $\text{Al}_{0.07}\text{Ga}_{0.93}\text{N}$ layer grown at 1040 °C.⁸⁵ The number of periods in the MQW samples was 12. The nominal well and barrier layer thicknesses were 30 and 45 Å, respectively. The energy diagram and sample structure of InGaN/GaN MQWs used in this work is shown in Figure 39. In order to evaluate the interface quality and structural parameters such as the average In composition in the MQW and the period of the superlattice, the samples were analyzed with a 4-crystal high-resolution x-ray diffractometer (HRXRD) using $\text{Cu } K\alpha_1$ radiation. The angular distances between the satellite superlattice diffraction peaks and GaN (0002) reflections were obtained by ω -2 θ scans. The spectra clearly showed higher-order satellite peaks indicating high interface quality and good layer uniformity.

The samples were mounted on a copper heat sink attached to a wide temperature range cryostat/heater system. This study was performed in the side-pumping geometry, where edge emission from the samples was collected into a Spex 1-m spectrometer and recorded by an optical multi-channel analyzer (details on pumping configurations are given on page 69).

The effects of Si doping on the optical properties of bulk GaN,^{86,87} InGaN/GaN MQWs,^{85,88} and GaN/AlGaIn⁸⁹ MQWs have been studied by many authors. We performed optical pumping on InGaN/GaN MQW samples with different Si doping. Typical spectra obtained at pump densities slightly above the stimulated emission threshold are depicted in Figure 40. All samples exhibited bright emission in the blue region of the electromagnetic spectrum. We observed that only moderate concentrations of Si increased the luminescence intensity and reduced the stimulated emission threshold pump density in InGaN/GaN MQWs. Table V summarizes the Si concentrations as measured by secondary ion mass spectroscopy (SIMS) and the stimulated emission threshold densities at room temperature for the samples studied in this work. The maximum luminescence intensity and lowest stimulated emission threshold ($I_{th} = 55 \text{ kW/cm}^2$ at room temperature) were observed for the sample with a Si concentration of $2 \times 10^{18} \text{ cm}^{-3}$ in the barrier layer. This threshold is 12 times lower than

that of a high quality nominally undoped single-crystal GaN film measured under the same experimental conditions.

Si concentration in GaN barriers (cm^{-3}) as measured by SIMS	Stimulated emission threshold density at room temperature (kW/cm^2)
$<1 \times 10^{17}$ (undoped)	58
1×10^{18}	58
2×10^{18}	55
1×10^{19}	92
3×10^{19}	165

Table V. Si doping concentrations in GaN barriers and stimulated emission threshold densities at room temperature for InGaN/GaN MQW samples as measured by SIMS.

Figure 41 shows the emission spectra for the InGaN/GaN MQW sample with a Si concentration of $2 \times 10^{18} \text{ cm}^{-3}$ for various temperatures and excitation powers. Dotted lines represent the broad spontaneous emission spectra taken at pump densities approximately half that of the stimulated emission threshold for each temperature. Spontaneous emission in InGaN MQWs has recently been attributed to the recombination of excitons localized at certain potential minima in the quantum well.^{90,91} However, a more detailed discussion of the stimulated emission mechanisms will follow in Chapter V. As we raise the excitation power density above the stimulated emission threshold, a considerable spectral narrowing occurs (solid lines in Figure 41). The emission spectra are comprised of many narrow peaks of less than 1 Å full width at half maximum (FWHM), which is on the order of our instrumental resolution. The major effect of the temperature change from 200 K [Figure 41(a)] to 450 K [Figure 41(c)] was a shift of the spontaneous emission and stimulated emission peaks toward lower energy. There was no noticeable broadening of the stimulated emission peaks when the temperature was varied over a range of 400 K.

The emission coming from the sample was found to be strongly dependent on the pumping and collecting configurations. It was possible to align the sample in such a way

that even at room temperature only one narrow stimulated emission peak could be observed. An example of such a spectrum is shown in Figure 42. The full width at half maximum of the peak (1 \AA) was resolved only in the second order of a 1200 groove/mm grating in the 1-m spectrometer.

The temperature dependence of the stimulated emission threshold is shown in Figure 43 (solid dots). Stimulated emission was observed throughout the entire temperature range studied, from 175 K to 575 K. The stimulated emission threshold was measured to be $\sim 25 \text{ kW/cm}^2$ at 175 K, $\sim 55 \text{ kW/cm}^2$ at 300 K, and $\sim 300 \text{ kW/cm}^2$ at 575 K, and roughly followed an exponential dependence. It is likely that such low stimulated emission threshold values are due to a large localization of carriers in MQWs. The solid line in Figure 43 represents the best result of a least-squares fit of the experimental data to the empirical form for the temperature dependence of the stimulated emission threshold (see Eq. 4-1). The characteristic temperature T_0 was estimated to be 162 K in the temperature range of 175-575 K for this sample. The derived value of characteristic temperature is considerably larger than the near room temperature values reported for laser structures based on other III-V and II-VI materials, where the relatively small values of T_0 were a strong limiting factor for high-temperature laser operation. Such a low sensitivity of the stimulated emission threshold to temperature changes in InGaN/GaN MQWs opens up enormous opportunities for high-temperature applications using these materials. Laser diodes with InGaN/GaN lasing mediums can potentially operate at temperatures exceeding room temperature by a few hundred degrees Kelvin.

We found that an increase in temperature leads to a decrease in PL intensity. This indicates the onset of efficient losses and a decrease in the quantum efficiency of the MQWs. At high temperatures, only a small fraction of excitons reach the conduction band minima, and most of them recombine non-radiatively. The modal gain depends only on radiatively recombining excitons. Therefore, the temperature increase efficiently decreases modal gain and leads to an increase in the stimulated emission threshold. To evaluate the number of electrons that recombine radiatively, we studied the integrated photoluminescence intensity as a function of excitation power for different temperatures, as shown in Figure 44. For the temperature range studied, we found that under low

excitation densities, the integrated intensity I_{integ} from the sample almost linearly increases with pump density I_p ($I_{\text{integ}} \propto I_p^\gamma$, where $\gamma = 0.8 - 1.3$), whereas at high excitation densities, this dependence becomes superlinear ($I_{\text{integ}} \propto I_p^\beta$, where $\beta = 2.2 - 3.0$). The excitation pump power at which the slope of I_{integ} changes corresponds to the stimulated emission threshold at a given temperature. Interestingly, the slopes of I_{integ} below and above the stimulated emission threshold do not significantly change over the temperature range involved in this study. This might indicate that the mechanism of stimulated emission in InGaN/GaN MQWs at room temperature remains the same as we raise the temperature to hundreds of degrees above room temperature.

In conclusion, we studied stimulated emission in optically pumped GaN epilayers and InGaN/GaN multi-quantum wells at elevated temperatures. We observed edge-emitted stimulated emission at a record high temperature of 700 K for GaN thin films grown on SiC and sapphire substrates. Stimulated emission at such high temperatures has never been reported for any semiconductor-based system. The energy position of stimulated emission and spontaneous emission peaks were shown to shift linearly with temperature and empirical expressions for the energy positions were given. For InGaN/GaN multi-quantum wells we also examined the integrated emission intensity versus pumping density at different temperatures. We observed that the slopes of the integrated emission intensity below and above the stimulated emission threshold were not sensitive to temperature changes. The effects of doping the GaN barriers with Si on the optical properties of InGaN/GaN multi-quantum wells were discussed. We showed that the low stimulated emission threshold, as well as the weak temperature sensitivity, makes GaN-based structures an attractive material for development of laser diodes that can operate well above room temperatures and creates opportunities for the development of new optoelectronic devices capable of high-temperature operation.

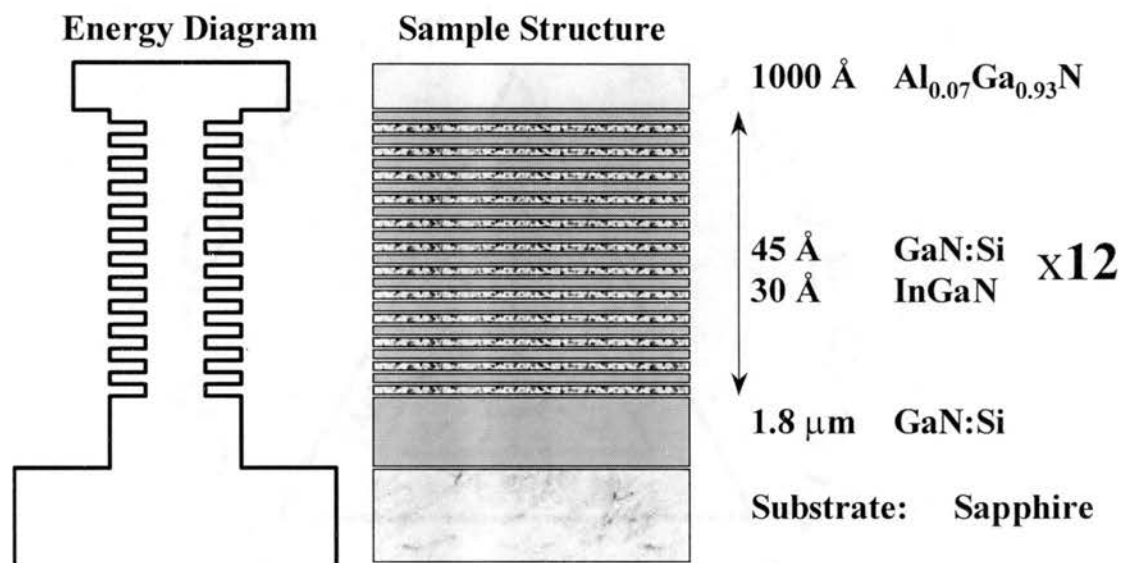


Figure 39. The energy diagram and sample structure of the InGaN/GaN MQWs used in this study. The concentration of Si in the GaN barriers ranged from $<1 \times 10^{17} \text{ cm}^{-3}$ to $3 \times 10^{19} \text{ cm}^{-3}$.

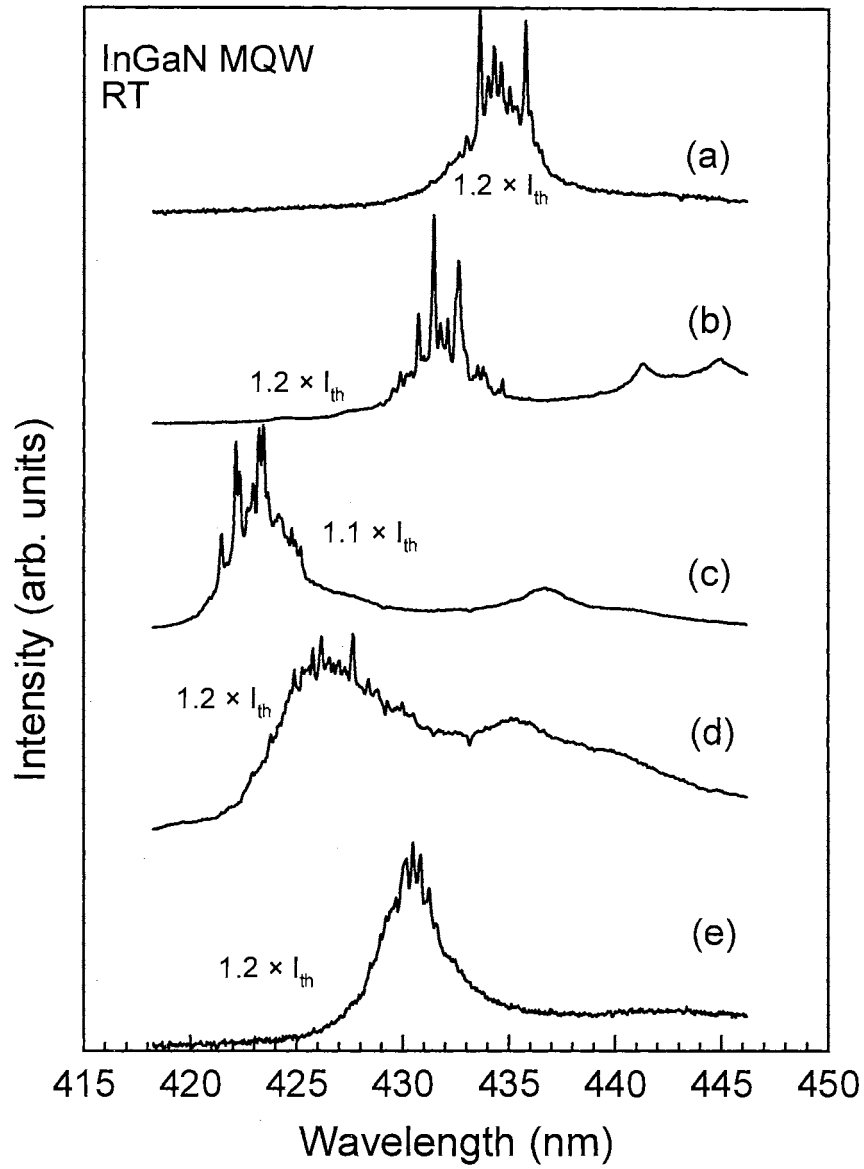


Figure 40. Spectra taken at pump powers slightly above the stimulated emission threshold for samples with GaN barriers doped with silicon at concentration levels of (a) $<1 \times 10^{17} \text{ cm}^{-3}$, (b) $1 \times 10^{18} \text{ cm}^{-3}$, (c) $2 \times 10^{18} \text{ cm}^{-3}$, (d) $1 \times 10^{19} \text{ cm}^{-3}$, and (e) $3 \times 10^{19} \text{ cm}^{-3}$.

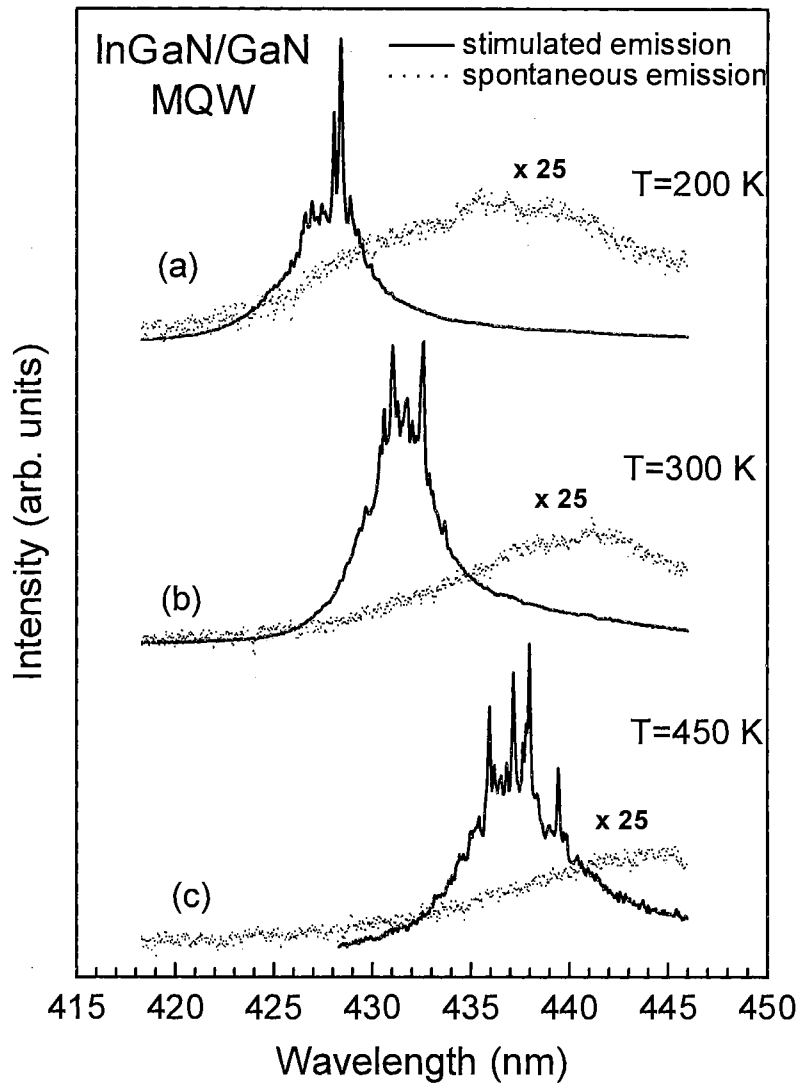


Figure 41. Emission spectra for an InGaN/GaN MQW sample with a Si concentration of $2 \times 10^{18} \text{ cm}^{-3}$ in the barriers at (a) 200 K, (b) 300 K, and (c) 450 K. Spontaneous emission spectra (dotted lines) were taken under an excitation density of $0.5 \cdot I_{th}$ and stimulated emission spectra were obtained for a pump density of $2 \cdot I_{th}$, where I_{th} represents the stimulated emission threshold at the corresponding temperature.

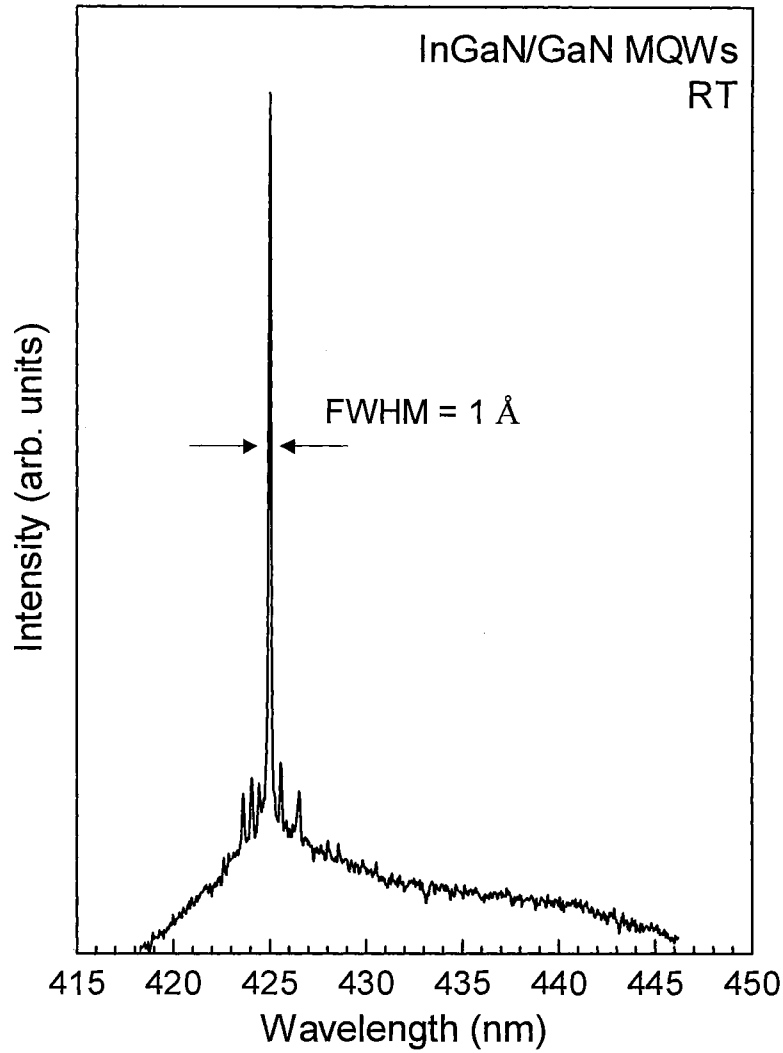


Figure 42. Stimulated emission from a moderately doped (Si concentration of $2 \times 10^{18} \text{ cm}^{-3}$ in the barriers) InGaN/GaN multi-quantum well sample at room temperature. Stimulated emission spectra were strongly dependent on pumping and collecting configuration. Under certain conditions it is possible to generate single-peak stimulated emission even at room temperature.

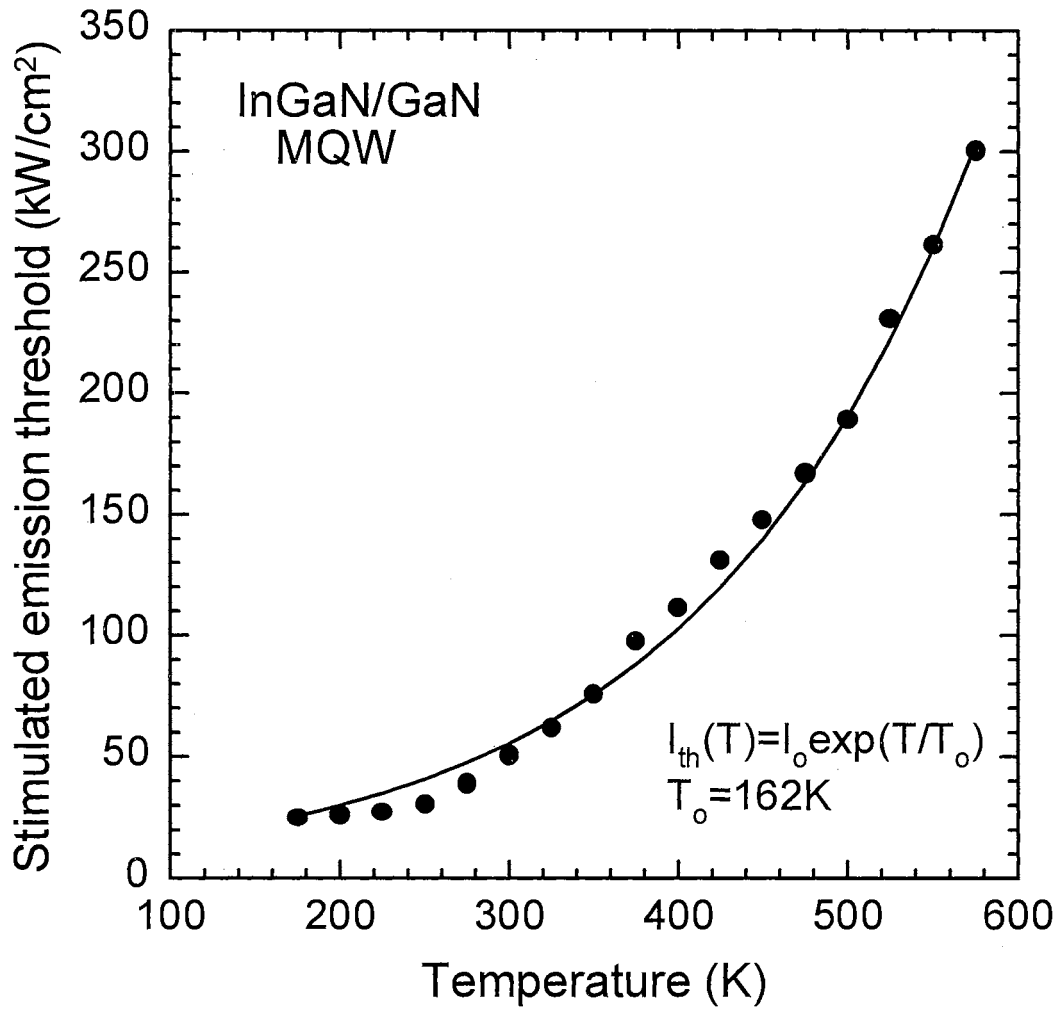


Figure 43. Temperature dependence of the stimulated emission threshold in the temperature range of 175-575 K for the InGaN/GaN MQW sample shown in Figure 41. The solid line represents the best result of a least-squares fit to the experimental data (solid dots). A characteristic temperature of 162 K is derived from the fit.

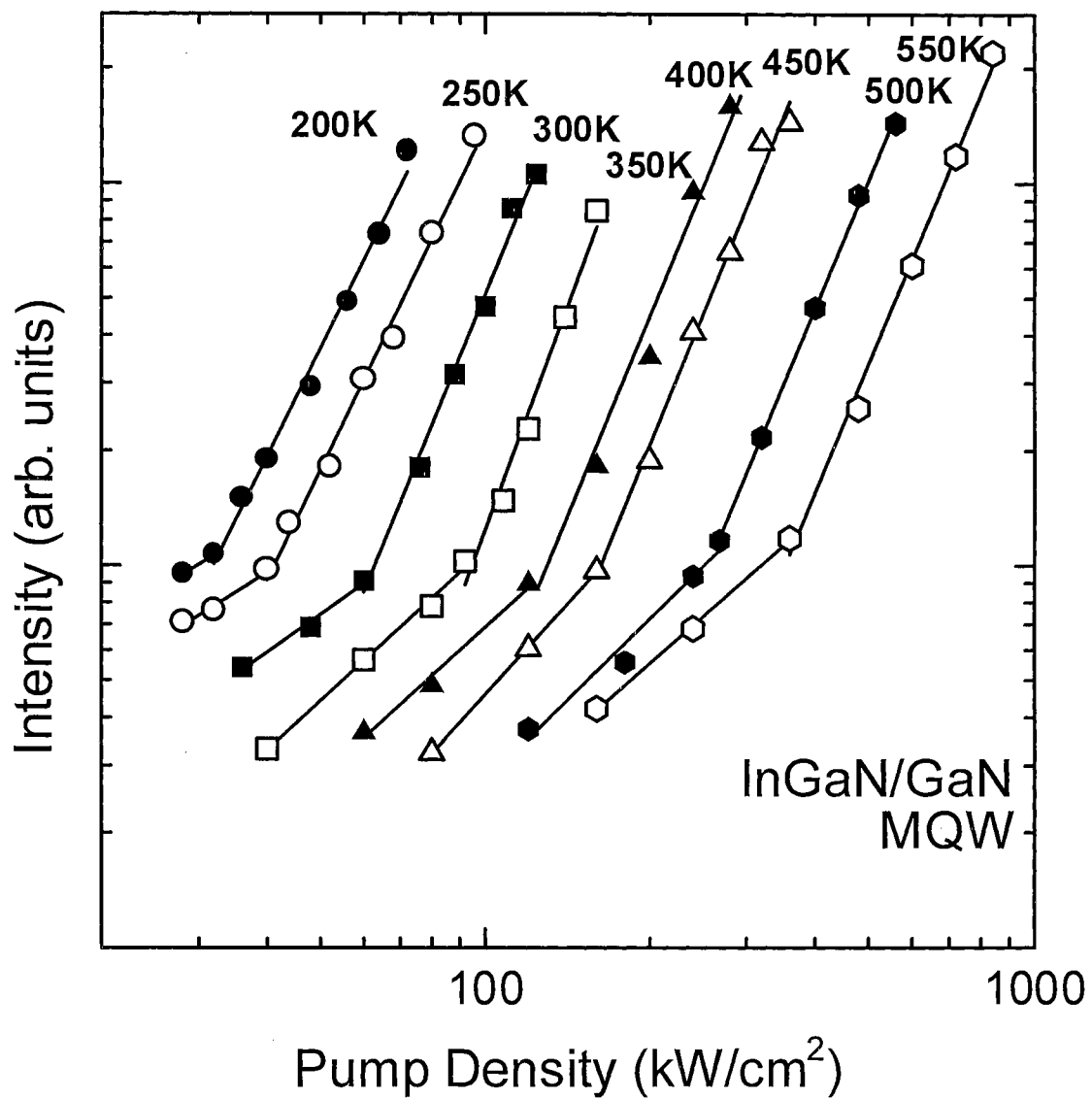


Figure 44. Integrated intensity of InGaN/GaN MQW emission as a function of pump density for different temperatures. The slope change from 0.8-1.3 to 2.2-3.0 indicates the transition from spontaneous emission to stimulated emission.

CHAPTER V

GAIN MECHANISMS IN GaN-BASED LASING STRUCTURES

In order to develop and optimize the lasing characteristics of GaN-based laser diodes it is important to understand the gain mechanisms in this material system. Our research group has performed a large variety of experiments on GaN, InGaN, and AlGaN epilayers as well as InGaN/GaN multiquantum wells and GaN/AlGaN separate confinement heterostructures. We found that the gain mechanisms vary greatly depending on the composition and geometry of the lasing medium. We show that the dominant near-threshold gain mechanism in GaN epilayers is inelastic exciton-exciton scattering for temperatures below ~ 150 K and an electron-hole plasma for temperatures above 150 K, whereas exciton-exciton scattering dominates the lasing spectrum of GaN/AlGaN separate confinement heterostructures from 10 K up to room temperature. Even though excitonic features were observed in AlGaN epilayers at low temperatures, we found that an electron-hole plasma is responsible for stimulated emission over the entire temperature range studied. Finally we investigated the origin of stimulated emission in InGaN epilayers and InGaN/GaN multiquantum wells and concluded that gain originates from the recombination of deeply localized carriers. This chapter describes the experimental results that were used to arrive at these conclusions.

Origin of Stimulated Emission in GaN Epilayers

The first results on stimulated emission (SE) from GaN were reported as early as 1971 by Dingle *et al.* who optically pumped single crystal GaN needles using the 337 nm radiation from a nitrogen laser to achieve SE at cryogenic temperatures.⁹ Since then, SE has been demonstrated in samples grown on different substrates for temperatures as high as 700 K, as was described in Chapter IV. There have been several studies performed in an attempt to explain the origin of SE in GaN films at various temperatures. Amano *et al.* suggested that an electron-hole plasma (EHP) is the most plausible origin of gain in GaN epilayers at room temperature.⁷⁸ Catalano *et al.* suggested exciton-exciton (ex-ex) scattering to be the dominant gain mechanism at 80 K (Ref. [92]). Recently Holst *et al.* performed gain spectroscopy on HVPE-grown GaN films and concluded that biexcitonic decay is responsible for the gain at 1.8 K at low excitation densities, whereas EHP recombination dominates the spectra at higher excitation densities.⁹³ However, the general picture of gain mechanisms in GaN and their implications towards laser diode structures with a GaN active layer was not well understood.

We performed a study of the gain mechanisms in GaN epilayers using nanosecond optical pumping in the temperature range of 20 to 700 K. We observed that for temperatures below 150 K the dominant gain mechanism is inelastic ex-ex scattering characterized by band-filling phenomena and a comparatively low SE threshold. For temperatures in the vicinity of 150 K the SE threshold was found to abruptly increase and the energy position of the SE peak rapidly shifted towards lower energies due to band-gap renormalization. This transition was attributed to a change in the gain mechanism from ex-ex scattering to an EHP. EHP recombination was found to be the dominant recombination mechanism for all temperatures exceeding 150 K (up to 700 K). Based on our results, we discuss possibilities of reducing the room temperature lasing threshold in laser diode structures with a GaN active medium.

The description of GaN samples used in this work was given previously (see page 69). The samples were mounted on a copper heat sink attached to the custom-built wide temperature range heater system (see page 68) used in conjunction with a cryostat cooled by a closed-cycle helium refrigerator. The SE part of this study was performed in an edge emission geometry, as depicted in Figure 32(a). A tunable dye laser pumped by a frequency-doubled, injection-seeded Nd:YAG laser was used as the primary optical pumping source. The deep red output of the dye laser was frequency doubled to achieve a near-UV pumping frequency. The emission was collected from one edge of the sample and coupled into a Spex 1-m spectrometer, then spectrally analyzed with a UV enhanced multi-channel analyzer. Low power cw photoluminescence (PL) studies were also undertaken to measure the spontaneous emission as a function of temperature. A frequency doubled Ar⁺ laser (244 nm, 40 mW) was used as the excitation source. In order to avoid any spectral distortion of the spontaneous emission due to re-absorption, the laser beam was focused on the sample surface and spontaneous emission was collected from a direction near normal to the surface, as shown in Figure 32(b).

Typical power-dependent emission spectra from a GaN epilayer are shown in Figure 45. At low excitation pump densities the sample emission has a full width at half maximum of about 15 nm with the peak positioned at about 366 nm at room temperature. The peak appears to be red-shifted in comparison to low excitation density cw PL due to re-absorption effects. As we increase the excitation pump density, a new peak emerges on the low energy side of the spontaneous emission peak. The full width at half maximum of this new peak is only 2 nm at room temperature. We note that this peak is strongly polarized and its intensity grows superlinearly with excitation power (as shown in the inset of Figure 45). Based on the significant spectral narrowing, superlinear increase with excitation power, high degree of polarization, and directionality of the emission we conclude that the new peak located at ~371 nm at room temperature represents the SE peak.

Recently, Fischer *et al.* convincingly demonstrated the presence of excitonic resonances in GaN epilayers well above room temperature through optical absorption measurements⁴¹ (see page 23 for detailed discussion). Excitons in GaN epilayers cannot be easily ionized due to their relatively large exciton binding energy. However, at near-

SE-threshold (near- I_{th}) pump densities the picture is not straightforward since screening of the Coulomb interaction weakens the binding of the exciton. In general, the existence of excitons depends on the strength of the Coulomb interaction which in turn depends on the density and distribution of carriers among bound and unbound states.⁵² Therefore, the observation of excitons at low excitation powers at room temperature does not assure their presence at SE pump densities.

To determine if the SE threshold density occurs above or below the Mott density (the critical carrier density beyond which no excitons can exist), we studied the temperature behavior of the SE threshold in GaN epilayers grown on SiC, as shown in Figure 46. Note that the SE threshold is plotted on a logarithmic scale. A faster than exponential increase in the SE threshold occurs in the vicinity of 150 K. In order to better understand this phenomenon we extended our study to cover the temperature range from 20 K to 700 K using epilayers grown on different substrates. Figure 47 shows the SE threshold for GaN epilayers grown on SiC (open triangles) and sapphire (solid circles) for temperatures up to 700 K. For temperatures above 200 K, the SE thresholds roughly followed an exponential dependence: $I_{th} = I_0 \exp(T/T_0)$, with $T_0 \cong 170$ K. This exponential behavior of the SE threshold is qualitatively similar to that observed in other material structures.⁹⁴ However, as the temperature decreases to below 200 K, a significant reduction in the SE threshold was observed. We believe that this decrease is due to a change in the dominant gain mechanism indicating a drastic increase in the SE efficiency at low temperatures. It has been predicted theoretically that in a material system with a relatively large exciton binding energy, one can expect inelastic ex-ex scattering to have the lowest SE threshold at low temperatures.⁵² We also confirmed the presence of excitons at pump densities above the SE threshold in reflection spectra,⁹⁵ as shown in Figure 48.

The effects of excitons on SE can be better understood by studying the temperature and power dependence of the SE peak position. We measured the energy position of the SE peak at near- I_{th} pump densities and the position of the spontaneous emission peak using low power cw PL in the temperature range of 20 to 700 K for two samples grown on sapphire and SiC substrates, as shown in Figure 49. The position of the spontaneous and SE peaks in the two GaN epilayers is influenced by residual strain

resulting from thermal-expansion mismatch between the epilayers and the substrates (see page 21 and Ref. [74]). This difference in energy position for the two samples is largest at low temperature and gradually decreases as the temperature is increased.

To avoid strain-related complications we restricted ourselves to an analysis of the relative energy shift between the spontaneous and SE peaks, $\Delta E = E_{spon} - E_{SE}$, as depicted in Figure 50. As we approach low temperatures ($T < 150$ K), ΔE asymptotically approaches the exciton binding energy ($E_x = 21$ meV) measured by photoreflectance.⁴³ However, at temperatures above 150 K, ΔE monotonically increases and reaches values as high as 200 meV at 700 K. The behavior of the energy difference between the spontaneous and SE peaks at low temperatures can be well explained by inelastic ex-ex scattering. In the case of ex-ex scattering the energy difference between the two peaks can be estimated from (see Eq. 3-9 and Ref. [53]):

$$\Delta E = E_{spon} - E_{SE}^{ex-ex} = (E_g - E_x) - (E_g - 2E_x - E_k^{e-h}) = E_x + E_k^{e-h}, \quad (5-1)$$

where E_g is the band-gap energy and E_k^{e-h} is the kinetic energy of the unbound electron-hole pair created during the excitonic collision. At low excitation densities and low temperatures one can consider the bands to be empty. The unbound electron-hole pairs created during this process have a very small kinetic energy ($E_k^{e-h} \approx 0$), thus ΔE approaches E_x as $T \rightarrow 0$ K, as shown in Figure 50.

For high temperatures ($T > 150$ K), the energy difference between spontaneous and SE peaks gradually increases from ~ 35 meV to a few hundred meV. Both the large energy difference and the relatively high SE thresholds in this temperature range (Figure 47) point to EHP recombination. In EHP recombination a large number of excited carriers cause band-gap renormalization effects leading to a large value of ΔE . Under such high excitation conditions, excitons are dissociated by many-body interactions.⁷⁸ As further evidence to support the dominance of the EHP gain mechanism in this temperature range, we point out that excitons have not been clearly observed in GaN at highly elevated temperatures ($T > 450$ K), even under extremely low excitation conditions.⁴¹ We therefore conclude that EHP recombination is responsible for gain in GaN thin films at these elevated temperatures. Since no significant change in the

behavior of the SE threshold or the SE peak position was observed for temperatures between 150 K and 700 K (Figure 47 and Figure 50), we conclude that EHP recombination is the dominant gain mechanism for all temperatures exceeding 150 K.

At temperatures below 150 K, the effect of the kinetic energy E_k^{e-h} on the ex-ex scattering recombination process can be observed in the excitation density dependence of ΔE . As the excitation intensity or temperature is increased, the bottom of the bands become filled. Thus, unbound electron-hole pairs created in the process of ex-ex collision must have higher energies, and the kinetic energy E_k^{e-h} can no longer be neglected. The inset in Figure 51 shows the power dependence of ΔE at three different temperatures near the point when the gain mechanism experiences a transition from inelastic ex-ex scattering to EHP. For temperatures below 150 K, we observed a rapid increase in ΔE at near- I_{th} pump densities, as shown in the inset of Figure 51. This shift is most likely associated with the band-filling effect which causes increased values of E_k^{e-h} . For temperatures above 150 K, such a strong near- I_{th} shift in ΔE is not observed. At these temperatures SE originates from EHP recombination and the gradual increase in ΔE is caused by band-gap renormalization effects. For one-photon pumping and elliptical bands, the band-filling effect associated with ex-ex scattering gives a calculated line shift E_k^{e-h} proportional to $(I - I_{th})^{1/3}$ (see Refs. 53 and 96). The substitution of this expression into Eq. 5-1 yields:

$$\Delta E = E_x + a(I - I_{th})^{1/3}. \quad (5-2)$$

A fit of the experimental data (open circles) taken at 100 K to Eq. 5-2 is shown in Figure 51 by a solid line. From the fit, we obtained an exciton binding energy of $E_x = 28$ meV and an SE threshold of $I_{th} = 100$ kW/cm², which are in a reasonable agreement with experimental results and support the idea of ex-ex scattering being the dominant SE mechanism for temperatures below 150 K.

Since ex-ex scattering has a lower SE threshold than recombination from an EHP (Figure 47), it would be advantageous if SE was dominated by excitonic effects at room temperature and above.⁹⁷ One way this could be achieved is by introducing 2-D spatial confinement.⁹⁸ By tailoring the width of a GaN active layer sandwiched between AlGaIn

confinement layers, one would expect a significant increase in the exciton binding energy. For increased values of exciton binding energy, a strong reduction of the homogeneous broadening due to reduced Fröhlich interactions is expected.⁹⁹ This could potentially extend the ex-ex scattering gain mechanism to room temperature. The SE threshold for such structures would be significantly reduced due to carrier confinement¹⁰⁰ and a shift in the dominant near- I_{th} gain mechanism from EHP to ex-ex scattering.

In conclusion, we have studied the gain mechanisms in GaN epilayers over the temperature range of 20 to 700 K. We observed that for temperatures below 150 K the dominant near-threshold gain mechanism is inelastic exciton-exciton scattering, characterized by a low stimulated emission threshold. For temperatures exceeding 150 K the dominant gain mechanism was shown to be electron-hole plasma recombination, characterized by a relatively high stimulated emission threshold and a large separation between spontaneous and stimulated emission peaks. Based on the results presented here, the increase in binding energy associated with strong confinement (in quantum wells, for example) should result in a significant decrease in the stimulated emission threshold of GaN active layers by extending the range of ex-ex scattering gain to room temperature. This reduction in the gain threshold density will aid in the development of GaN-based near-UV laser diodes.

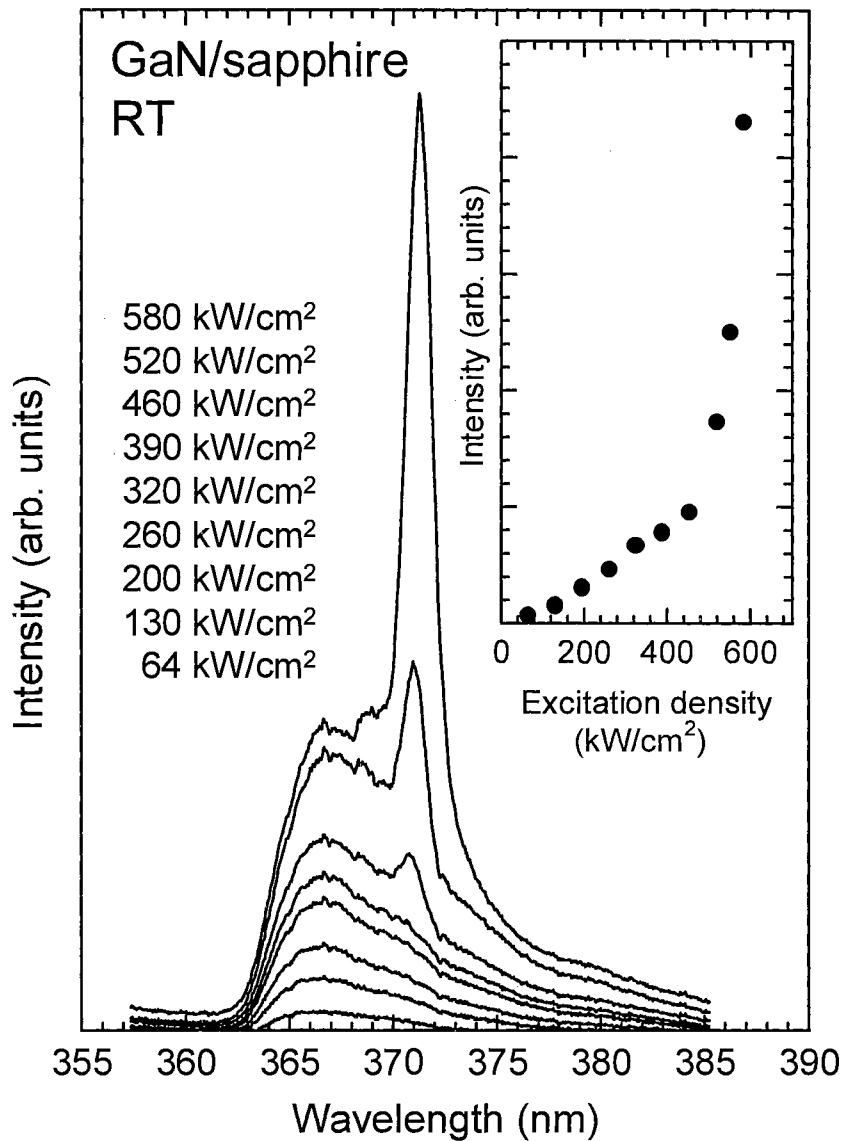


Figure 45. Typical emission spectra from a 4.2- μm -thick GaN epilayer at room temperature for different pumping densities. The inset shows the dependence of the integrated emission intensity on the excitation power. From both spectral narrowing and the superlinear increase in emission intensity we determined the stimulated emission threshold to be 480 kW/cm^2 .

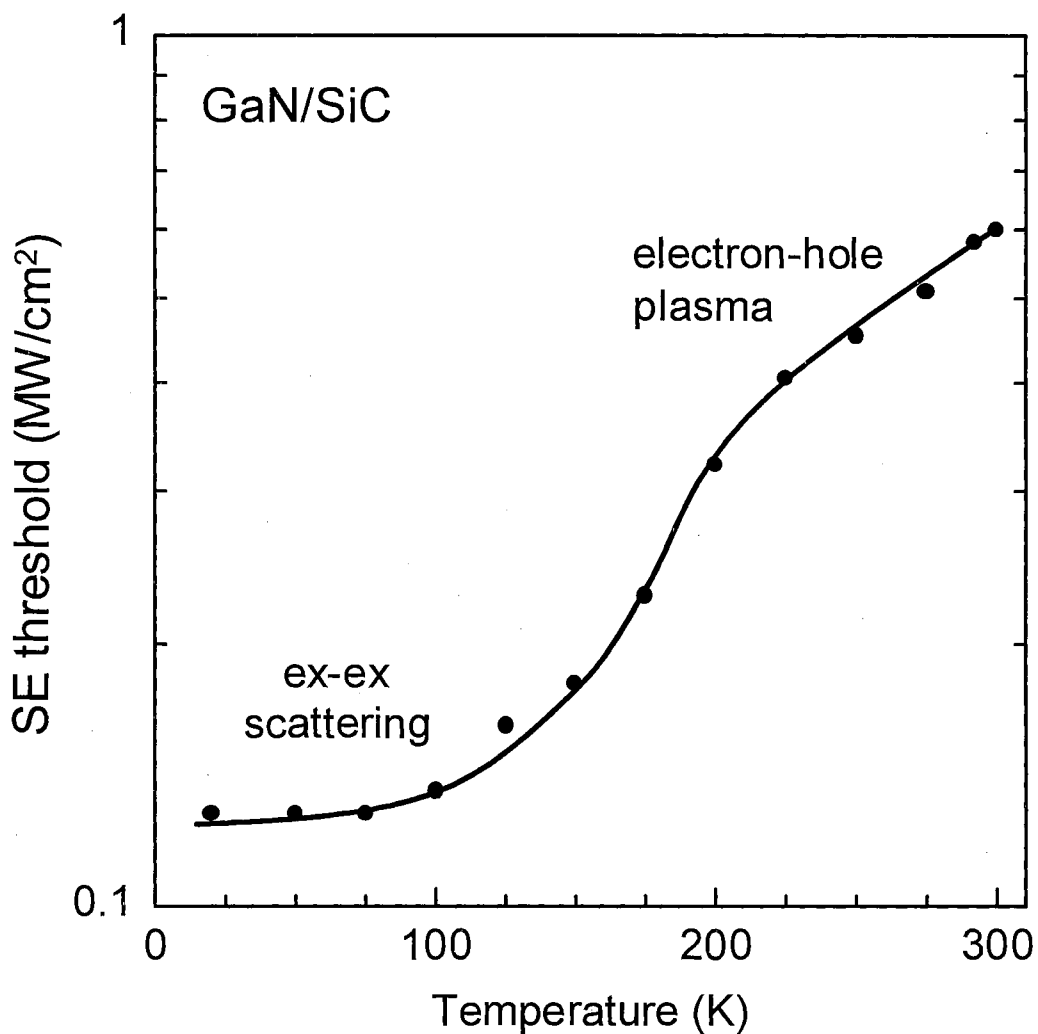


Figure 46. SE threshold as a function of temperature for GaN thin films grown on SiC in the temperature range of 20 to 300 K. The stimulated emission threshold density is plotted on a logarithmic scale. A faster than exponential increase in the stimulated emission threshold can be seen in the vicinity of 150 K.

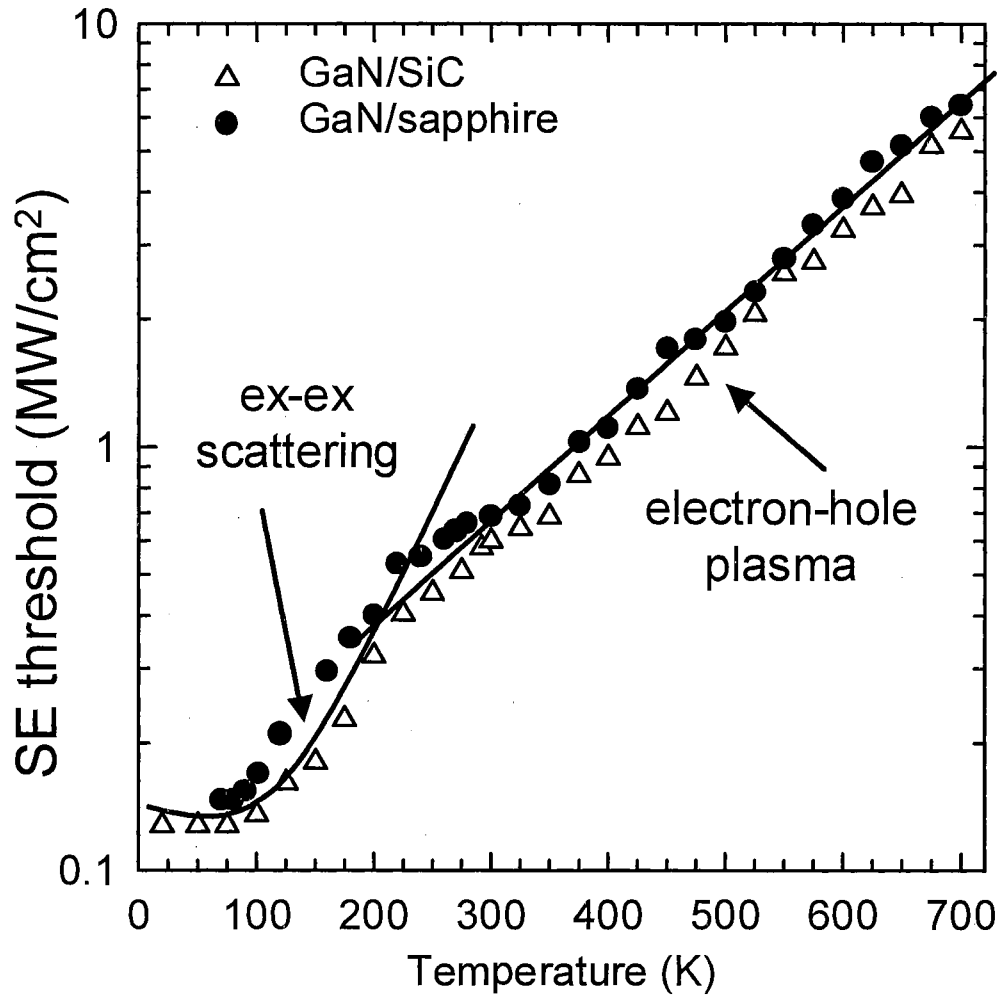


Figure 47. SE threshold as a function of temperature for GaN thin films grown on SiC (open triangles) and sapphire (solid circles) in the temperature range of 20 to 700 K. The SE threshold rises exponentially for temperatures exceeding 200 K, with a characteristic temperature of approximately 170 K. For temperatures below 200 K, the SE threshold is considerably reduced due to excitonic enhancement. The solid lines are given only as guides for the eye.

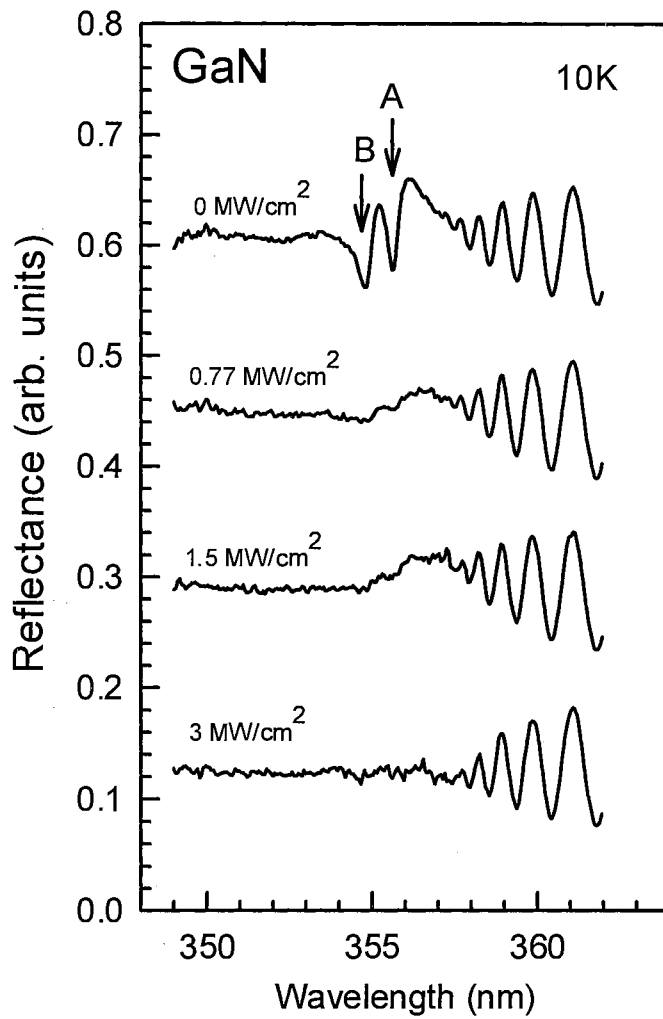


Figure 48. Reflectance spectra at different pump densities at 10 K. Excitonic resonances disappear as the excitation density is increased to values several times higher than the SE threshold. Spectra are offset vertically for clarity. From Ref. [44].

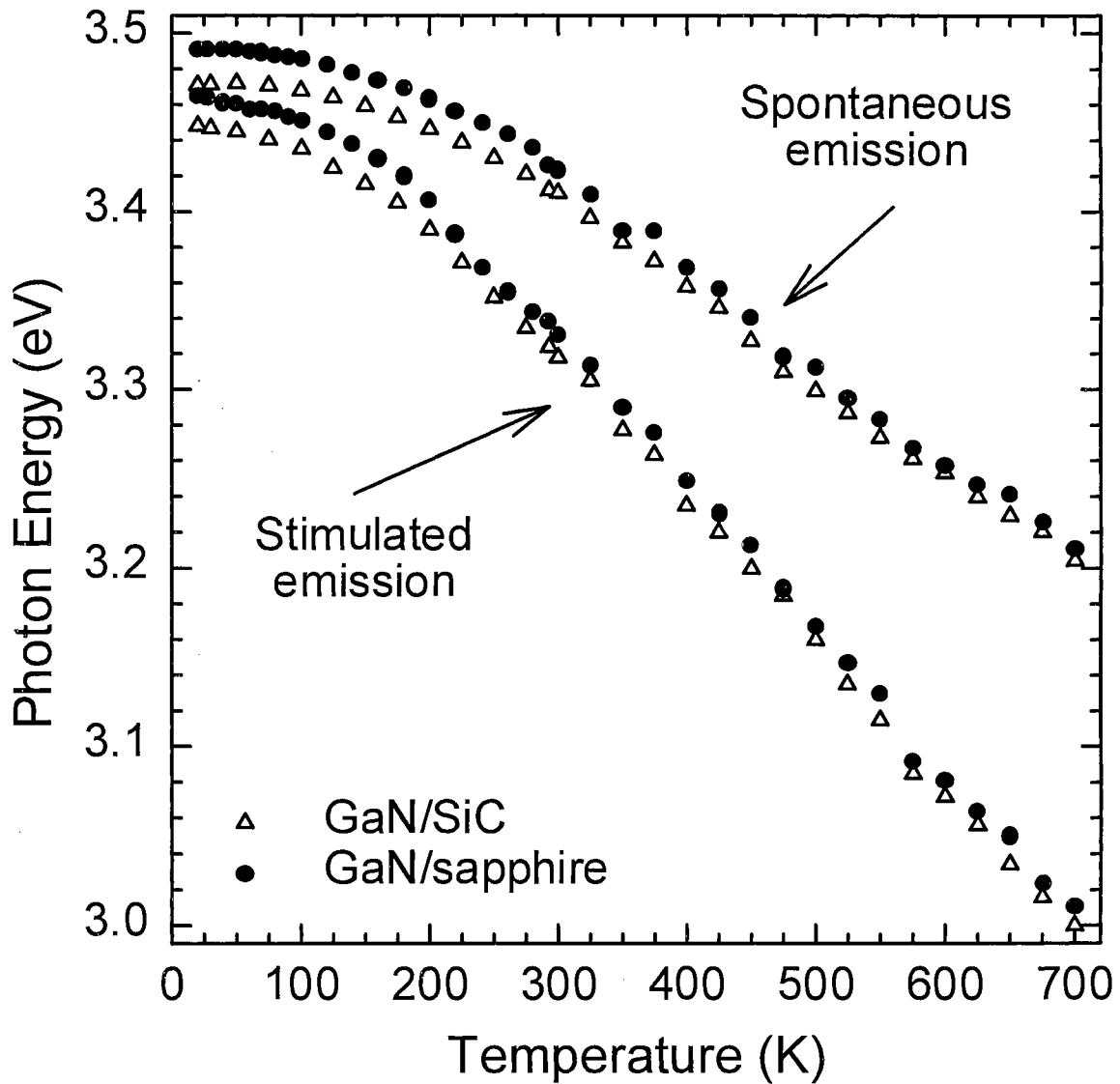


Figure 49. The absolute energy positions of the spontaneous and SE peaks for GaN thin films grown on SiC (open triangles) and sapphire (solid circles). The difference in the energy positions (particularly at low temperature) between the two samples is a result of residual strain between the epilayers and the two different substrates.

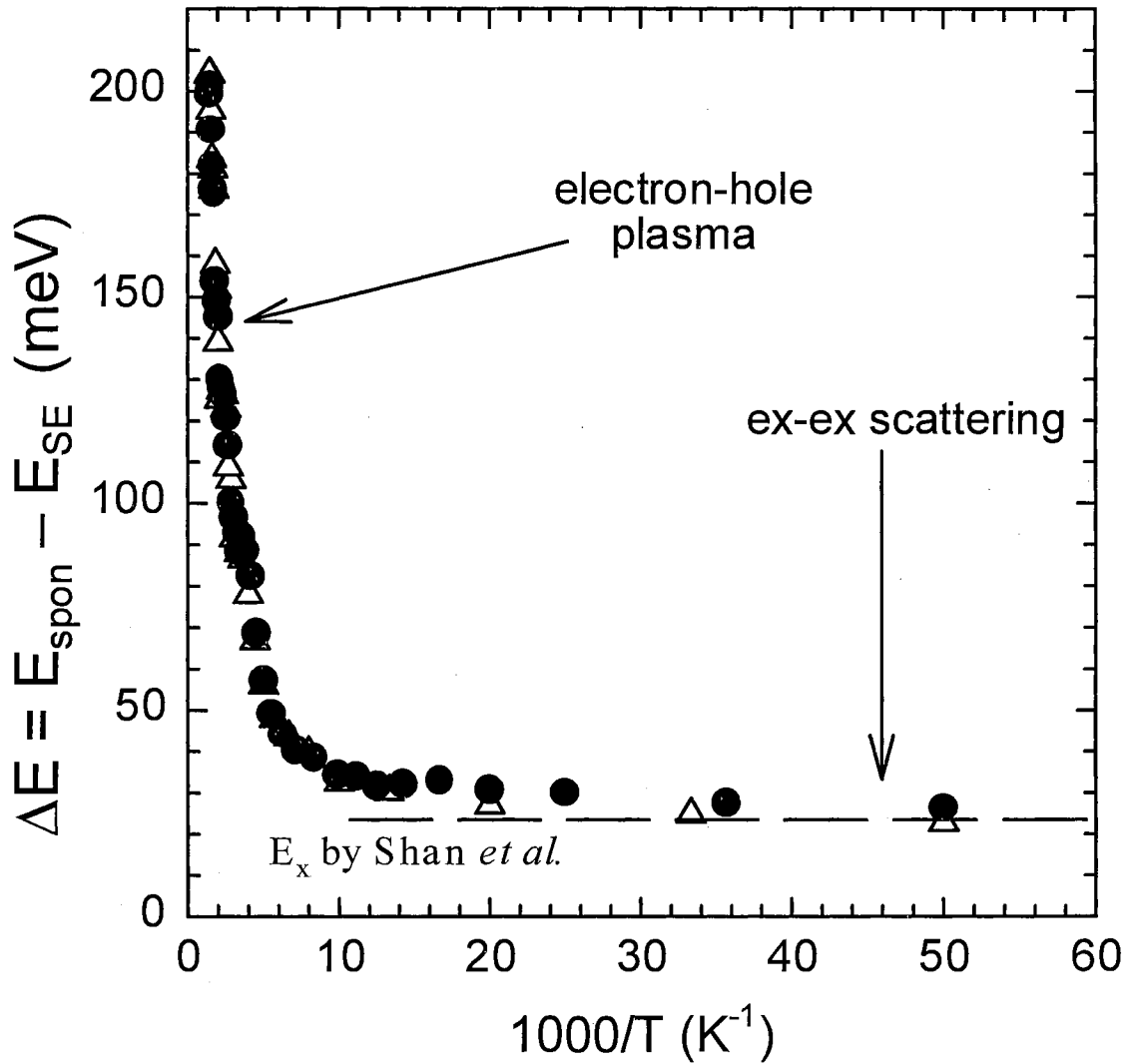


Figure 50. Energy difference (ΔE) between spontaneous and SE peaks as a function of temperature for GaN thin films grown on SiC (open triangles) and sapphire (solid circles). At low temperature ΔE asymptotically approaches the exciton binding energy, indicating that the dominant near- I_{th} gain mechanism is inelastic ex-ex scattering. At elevated temperatures, the large value of ΔE indicates the increased presence of band-gap renormalization effects.

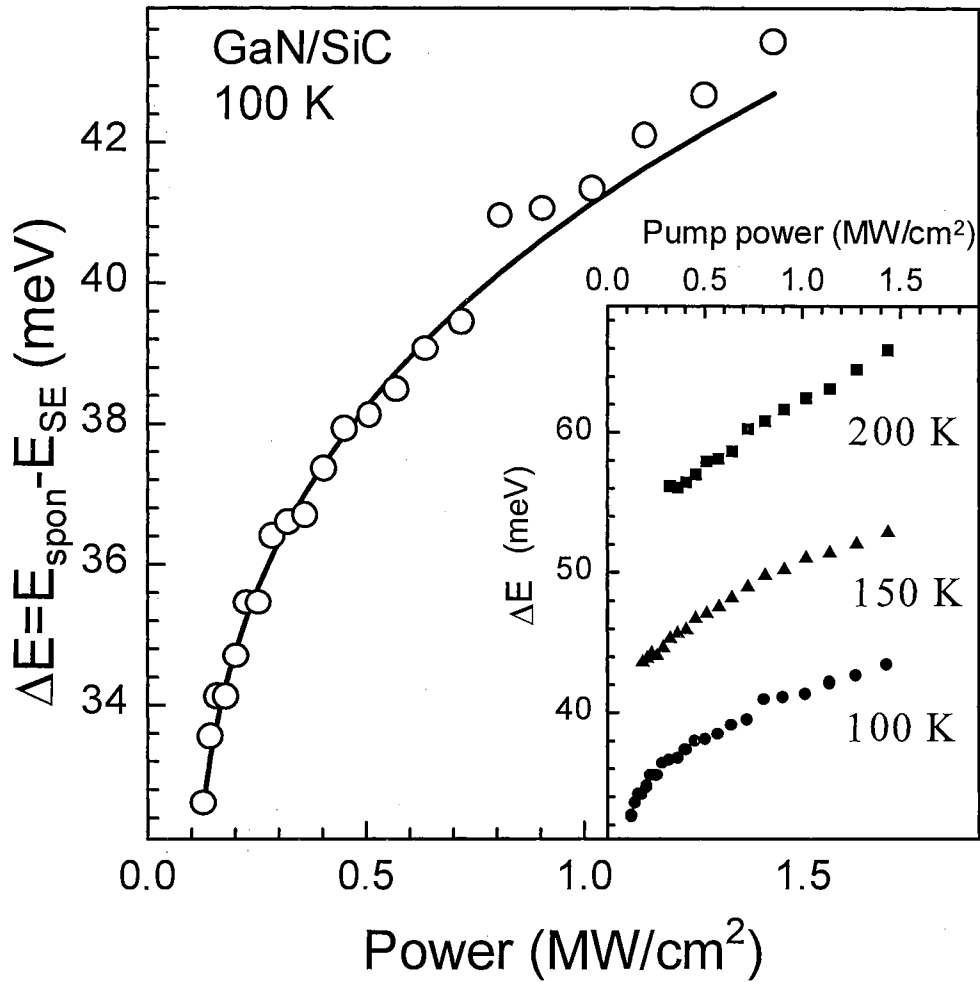


Figure 51. Energy difference (ΔE) between spontaneous and SE peaks as a function of excitation density at 100 K. The solid line represents a theoretical fit of the experimental data (open circles) to Eq. 5-2. The inset shows the change in the behavior of ΔE at different temperatures. An abrupt near- I_{th} shift in ΔE at 100 K is related to band-filling effects associated with increased values of kinetic energy E_k^{e-h} during the ex-ex scattering recombination process. At elevated temperatures and/or high excitation powers, EHP is the dominant gain mechanism.

Mechanism of Efficient Ultraviolet Lasing in GaN/AlGaN Separate Confinement Heterostructures

The successful fabrication of a blue laser diode was largely due to the realization that the incorporation of indium into GaN was concomitant with a dramatic lowering of the lasing threshold,²⁰ an enhancement of the emission intensity,¹⁰¹ and improvements in the temperature characteristics of the material (see Chapter IV and Ref. [8]). The small band-gap of InN (1.9 eV), however, is disadvantageous for the development of near- and deep-UV laser diodes. Lasing structures using a GaN-active medium are required to fabricate LDs with emission wavelengths lying below 370 nm. Our research group observed a reduction of the stimulated emission (SE) threshold in a GaN/AlGaN separate confinement heterostructure (SCH) compared to GaN epilayers.¹⁰⁰ The mechanisms that led to the observation of the SE peak on the high energy side of the spontaneous emission peak and the reduction of the SE threshold merited further research.

In order to better understand the gain mechanisms we optically pumped GaN/AlGaN SCHs over the temperature range of 10 K to 300 K. Through an analysis of the lasing characteristics of these samples, such as the behavior of the temperature-induced shift between spontaneous emission and lasing modes, combined with the temperature dependence of the lasing threshold, we deduced the gain mechanism leading to efficient lasing and developed recommendations for the development of UV LDs with a GaN active medium.

The SCH samples used in this work were grown by metalorganic chemical vapor deposition on 6H-SiC substrates with $\sim 3\text{-}\mu\text{m}$ -thick GaN epilayers deposited prior to the growth of the SCH region. The SCH sample under discussion had a 150-Å-thick GaN active layer surrounded by 1000-Å-thick $\text{Al}_{0.05}\text{Ga}_{0.95}\text{N}$ waveguide layers and 2500-Å-thick $\text{Al}_{0.10}\text{Ga}_{0.90}\text{N}$ cladding layers symmetrically located on each side. For the purpose of comparison, we also studied a 4.2- μm -thick GaN epilayer grown on 6H-SiC. The samples were mounted on a copper heat sink attached to a wide temperature range

cryostat. Conventional photoluminescence (PL) spectra were measured in the back-scattering geometry using a frequency-doubled Ar⁺ laser (244 nm) as the excitation source [see Figure 32(b)]. In order to study the lasing phenomena, a tunable dye laser pumped by a frequency-doubled, injection-seeded Nd:YAG laser was used as the primary optical pumping source (the details of optical pumping configuration are given on page 69). Special precautions were taken to avoid fluctuations in sample position due to the thermal expansion of the mounting system. This allowed us to spatially "pin" the sample and obtain lasing modes from a single microcavity over the entire temperature range studied. Time-resolved photoluminescence measurements were performed using a frequency tunable pulsed laser (2 ps pulse duration, 76 MHz) as an excitation source and a streak camera (2 ps resolution) in conjunction with a ¼-m monochromator as a detection system.

Typical low excitation emission spectra obtained in the surface emission geometry at 30 K [Figure 52(a)] and 300 K [Figure 52(b)] contain three distinct features associated with the active GaN layer, 5% aluminum waveguide layer, and 10% aluminum cladding layer. As seen in the figure, a doublet spectral feature can be seen at both of the AlGaN-related peaks. There are two possible explanations for this phenomenon. First, this feature could arise from a small alloy concentration difference between the two AlGaN cladding and two waveguiding layers (it has been estimated that a 1% fluctuation in aluminum alloy concentration leads to a ~25 meV shift in the observed energy position¹⁰²). The second explanation can be seen by examining the temperature-dependent photoluminescence spectra, shown in Figure 53. Three distinct peaks associated with the 150-Å-thick GaN active region and the two AlGaN confinement layers with different aluminum concentrations persist over the entire temperature range studied, from 10 K to 300 K. We note that the intensity of the 'satellite' peaks (the doublet spectral features) quickly quenches with increasing temperature suggesting that the levels associated with this transition have a low activation energy and could be impurity-related.

At increased excitation powers, a series of equally spaced lasing modes, each with a full width at half maximum of ~3 Å, appears on the low energy side of the GaN-active-region peak, as shown in Figure 52. We note, however, that had the spontaneous emission

been collected from the sample edge and not from the surface, the lasing modes would have appeared on the high energy side of the spontaneous emission peak. This phenomenon is due to strong re-absorption that introduces a shift of several nanometers to the spontaneous emission peak. The lasing modes have a strong superlinear increase in intensity with excitation power. The laser emission has a narrow far-field pattern and is strongly polarized, with TE:TM \geq 300:1 (limited by the signal/noise ratio of our instruments). Cracks were observed on the sample surface along all three cleave planes associated with the hexagonal structure, with the majority running parallel to the length of the bar. The spacing between the lasing modes was correlated to the length of the microcavities formed by the cracks. Consequently, we believe that the observed lasing is of a microcavity origin.¹⁰³ The details on microcavity lasing in this SCH structure are given in Chapter VI. Further refinements to the cleaving process have allowed samples to be cleaved in a manner that resulted in no observable cracking, making them suitable for laser diode development.

A dramatic difference in the lasing threshold of our SCH structure in comparison to a thick GaN epilayer was observed over the entire temperature range studied, as shown in Figure 54. The SCH lasing threshold was estimated to be as low as 15 kW/cm² at 10 K and 105 kW/cm² at room temperature. Note that excitons in the GaN/AlGaIn SCH cannot be easily ionized with temperature due to the relatively large exciton binding energy (see page 26 and Ref. [41]). As was described earlier in this chapter, in order to screen the excitonic Coulomb interaction by free carriers (Mott transition) in GaN epilayers, a pump density of about 250 kW/cm² is required (see Ref. [104]). This pump density corresponds to a carrier density of $\sim 1.1 \times 10^{18}$ cm⁻³, calculated using a carrier lifetime of ~ 35 ps and a penetration depth of 9×10^4 cm⁻¹ (taken from Refs. 39 and 95). This value of the Mott density is almost identical to the one obtained from ultrafast studies (see page 33). At this carrier density, the gain mechanism in GaN epilayers switches from exciton-exciton (ex-ex) scattering to electron-hole plasma (EHP), which is depicted in Figure 54 by a dotted line. Since the lasing threshold density of the SCH sample is considerably below the carrier density corresponding to the Mott transition, excitons are expected to be present at pump densities above the lasing threshold and to make major contributions to the

recombination dynamics. We note that the carrier lifetime of the GaN/AlGaN SCH active layer is not significantly different from that of GaN epilayers.

The consequences of exciton dynamics on lasing in the GaN/AlGaN SCH can be better understood by studying the temperature dependence of the energy position of the emission peaks. However, it was an experimental challenge to obtain the temperature dependence of the lasing modes. Slight variations in the sample position inevitably resulted in different emission spectra. An example of two different sets of lasing modes from two adjacent cavities is depicted in Figure 55. When the cryostat temperature was varied, the length of the rod on which the sample holder was mounted also changed due to a non-zero temperature expansion coefficient. This resulted in the spatial displacement of the sample. To avoid these complications we chose to mount the cryostat horizontally so that the rod expansions occurred in the direction parallel to the direction of the laser beam. This allowed us to obtain lasing from the same microcavity over the entire temperature range. We also used the optical multi-channel analyzer to consistently acquire spectra at $1.3 \times I_{th}$ for each temperature. Figure 56 shows a plot of mode energy position versus temperature. The color pallet corresponds to different emission intensities. As the temperature increases, the gain region broadens and additional modes can be observed.

The energy positions of the spontaneous emission peaks and lasing modes were extracted from Figure 53 and Figure 56. The results of this analysis are summarized in Figure 57. For the purpose of comparison we also plotted the temperature evolution of the spontaneous and SE peaks from a thick GaN epilayer (solid lines), which appears to be distinctly different from that of the SCH sample. The temperature behavior of the energy peak positions did not follow Varshni equation. In fact, we observed a blue shift of the spontaneous emission peaks up to a temperature of 90 K and then a red shift of the emission thereafter. The position of the spontaneous emission from the 150-Å-thick GaN active layer was located 0.15 eV below that of the $\text{Al}_{0.05}\text{Ga}_{0.95}\text{N}$ waveguide layer (open squares) and this difference remains temperature independent.

The behavior of the spontaneous emission and lasing from the two samples can not be directly compared on this graph due to strain-related complications, such as the different thermal expansion coefficients of AlGaN alloys in comparison to GaN. In order

to avoid complications arising from the effects of strain, we restricted ourselves to an analysis of the relative energy difference ΔE between the lasing modes and the GaN-active-region peak, as illustrated in Figure 58 (open circles). We ascertained that the position of the lasing modes is one exciton binding energy below the GaN peak⁴³ and, most interestingly, remains temperature invariant from 10 to 300 K. This behavior is consistent with ex-ex scattering¹⁰⁴ being the dominant gain mechanism in the GaN/AlGaN SCH over the entire temperature range studied. To further corroborate this point, on the same graph we plotted the energy difference (ΔE) between the spontaneous and SE peaks of a thick GaN epilayer (solid line). We showed previously that in GaN epilayers the dominant gain mechanism is ex-ex scattering at temperatures below 150 K. Similar to GaN epilayers, ΔE in the GaN/AlGaN SCH lies one exciton binding energy below the spontaneous emission peak. However, at elevated temperatures ($T > 150$ K) ΔE in GaN epilayers rapidly increases, as opposed to the SCH sample. This was previously attributed to the transition of the gain mechanism from ex-ex scattering to EHP (see pages 97-98 and Ref. [104]). Since this transition was not observed in our SCH sample, we conclude that the ex-ex scattering mechanism remains dominant in our lasing structure even at room temperature.

Note that we neither expected nor observed any enhancement of the exciton binding energy due to 2-D confinement, since the thickness of the active region is a factor of 5 larger than the Bohr radius of the exciton in GaN. We also did not observe carrier recombination from deeply localized states, a situation which has been reported in InGaN/GaN heterostructures (see pages 122-132 and Ref. [105]). In spite of this, very low values of the lasing threshold were measured. In fact, these lasing threshold values are comparable to those of InGaN/GaN multi-quantum well samples published in the literature.⁸ We believe that the low lasing threshold of the GaN/AlGaN SCH is due to improved carrier and optical confinement, as opposed to deeply localized states as in InGaN/GaN heterostructures. Such a low lasing threshold combined with recent improvements in the p-doping of AlGaN alloys indicates that the realization of a GaN-active-medium UV laser diode is imminent.

The carrier dynamics of the GaN/AlGaN SCH was studied through time-resolved photoluminescence and photoluminescence excitation (PLE) experiments. Figure 60

shows time-resolved data obtained at 10 K for the three major peaks depicted in Figure 53. The sample was excited using ~ 50 ps pulses at 302 nm. The mathematical modeling of the intensity decay of the peaks requires fitting with several different exponentials. The short decay time of the GaN active layer peak indicates that the diffusion of carriers from carrier/waveguide regions into this layer is minimal.

This point is further supported by the PLE data depicted in Figure 59. In order to simplify the interpretation we plotted photoluminescence data on the same scale. The scanning of the excitation source from shorter to longer wavelengths is always concomitant with the increase of the detector signal when it is set at the GaN active layer peak. This is consistent with the fact that the diffusion of carriers from outer layers into the GaN active layer is rather weak.

In conclusion, we achieved efficient ultra-violet lasing in optically pumped GaN/AlGaN separate confinement heterostructures over a wide temperature range. Remarkably low values of the lasing threshold were measured. Through an analysis of the relative shift between spontaneous emission and lasing peaks, combined with the temperature dependence of the lasing threshold, we demonstrate that exciton-exciton scattering is the dominant gain mechanism leading to low-threshold ultra-violet lasing over the entire temperature range studied. We show that in GaN/AlGaN heterostructures, carrier and optical confinement play the decisive role in lowering the lasing threshold.

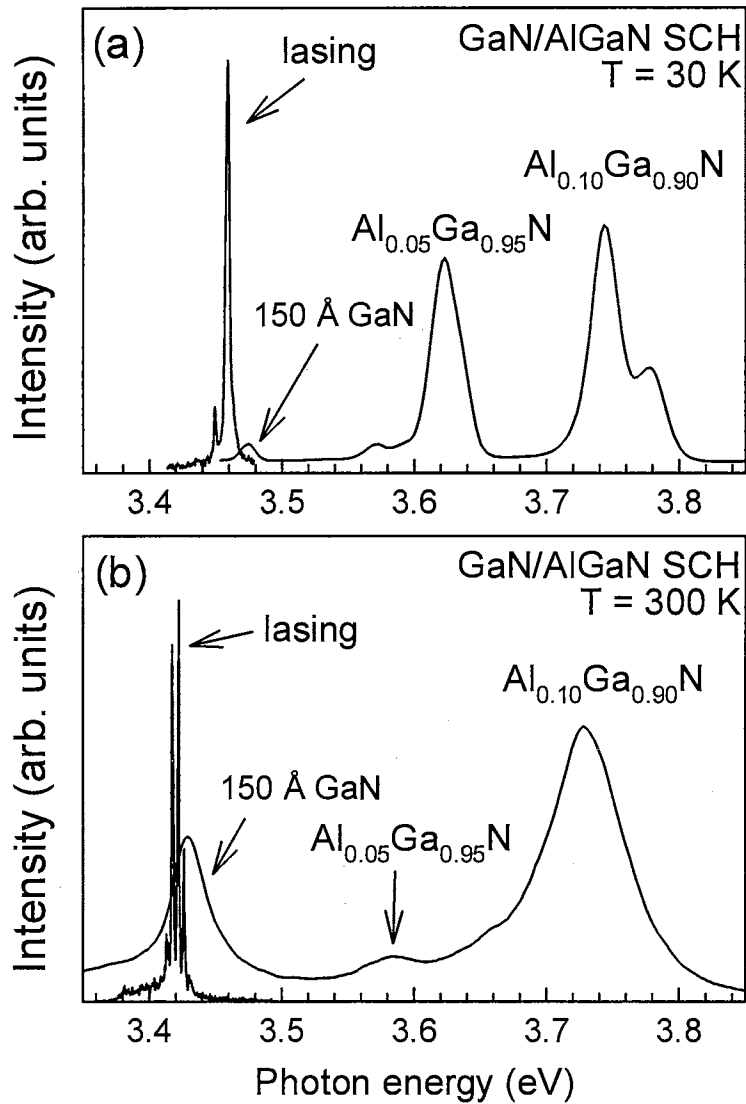


Figure 52. Lasing and low-density PL spectra from a GaN/AlGaN SCH taken at (a) 30 K and (b) 300 K. Lasing spectra were obtained at pump densities of $1.3 \times I_{th}$ for each temperature. The PL spectra have three characteristic peaks, which are associated with the 150-Å-thick GaN active region and the two AlGaN confinement layers with different aluminum concentrations.

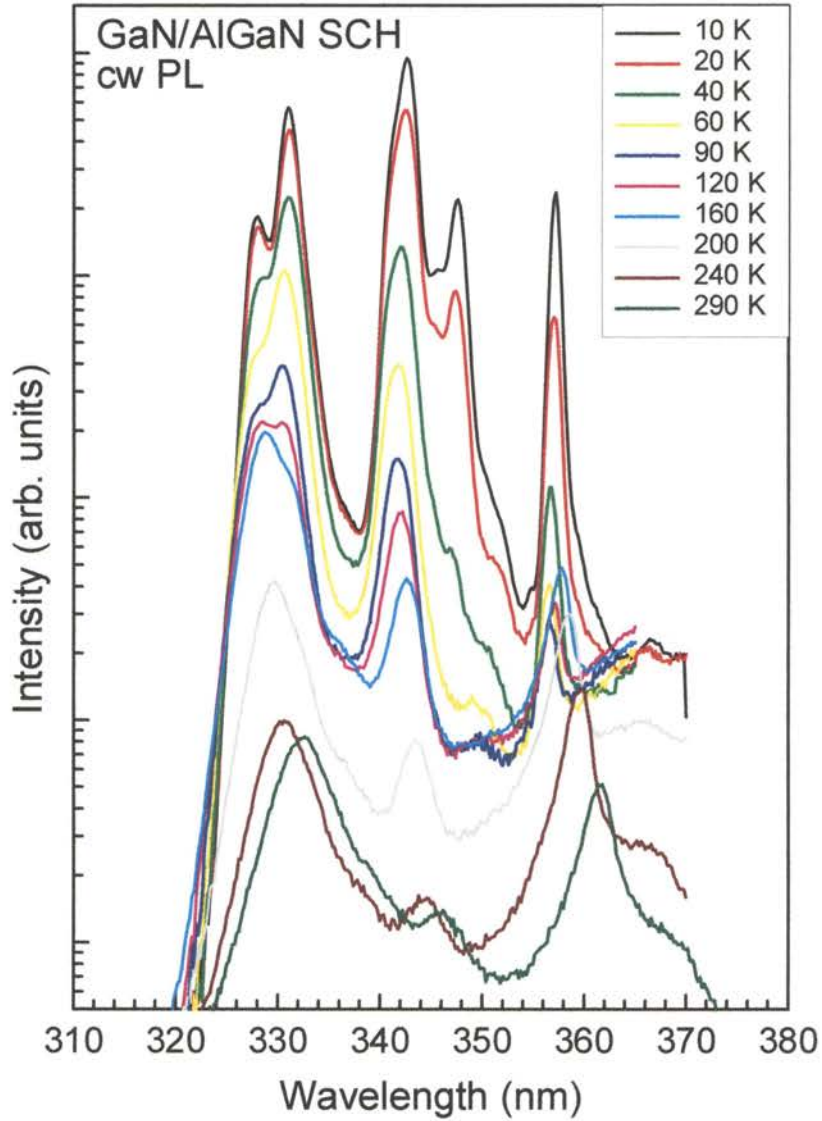


Figure 53. Temperature dependent spontaneous emission spectra. Each spectrum has three distinct peaks which are associated with the 150-Å-thick GaN active region and the two AlGaN confinement layers with different aluminum concentrations.

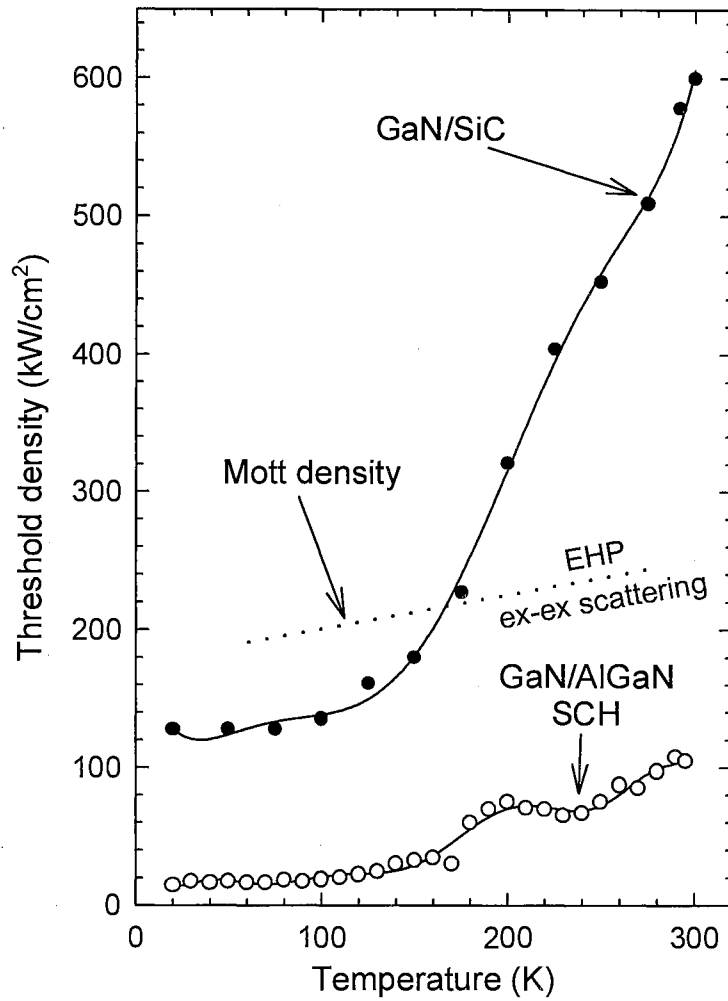


Figure 54. Temperature dependence of threshold pump densities for a 4.2- μm -thick GaN epilayer (solid circles) and GaN/AlGaN SCH (open circles). The lasing threshold of the SCH was measured to be 15 kW/cm^2 at 10 K and 105 kW/cm^2 at room temperature. For the SCH, note that lasing occurs at pump densities much lower than those required for exciton dissociation over the entire temperature range studied. The solid lines are to guide the eye only.

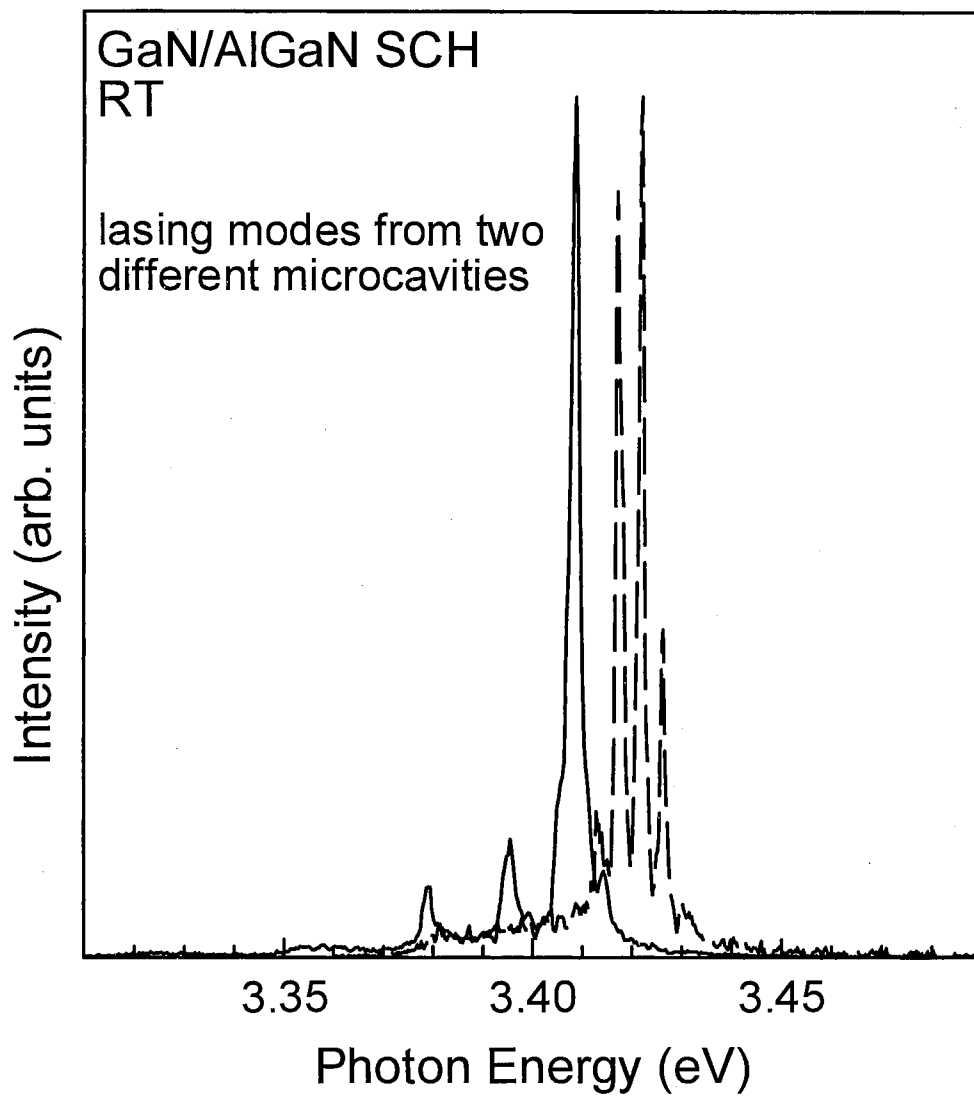


Figure 55. Lasing modes obtained from two different microcavities. When studying the dependence of the energy positions of lasing modes, it is absolutely necessary that the modes are obtained from the same microcavity over the entire temperature range.

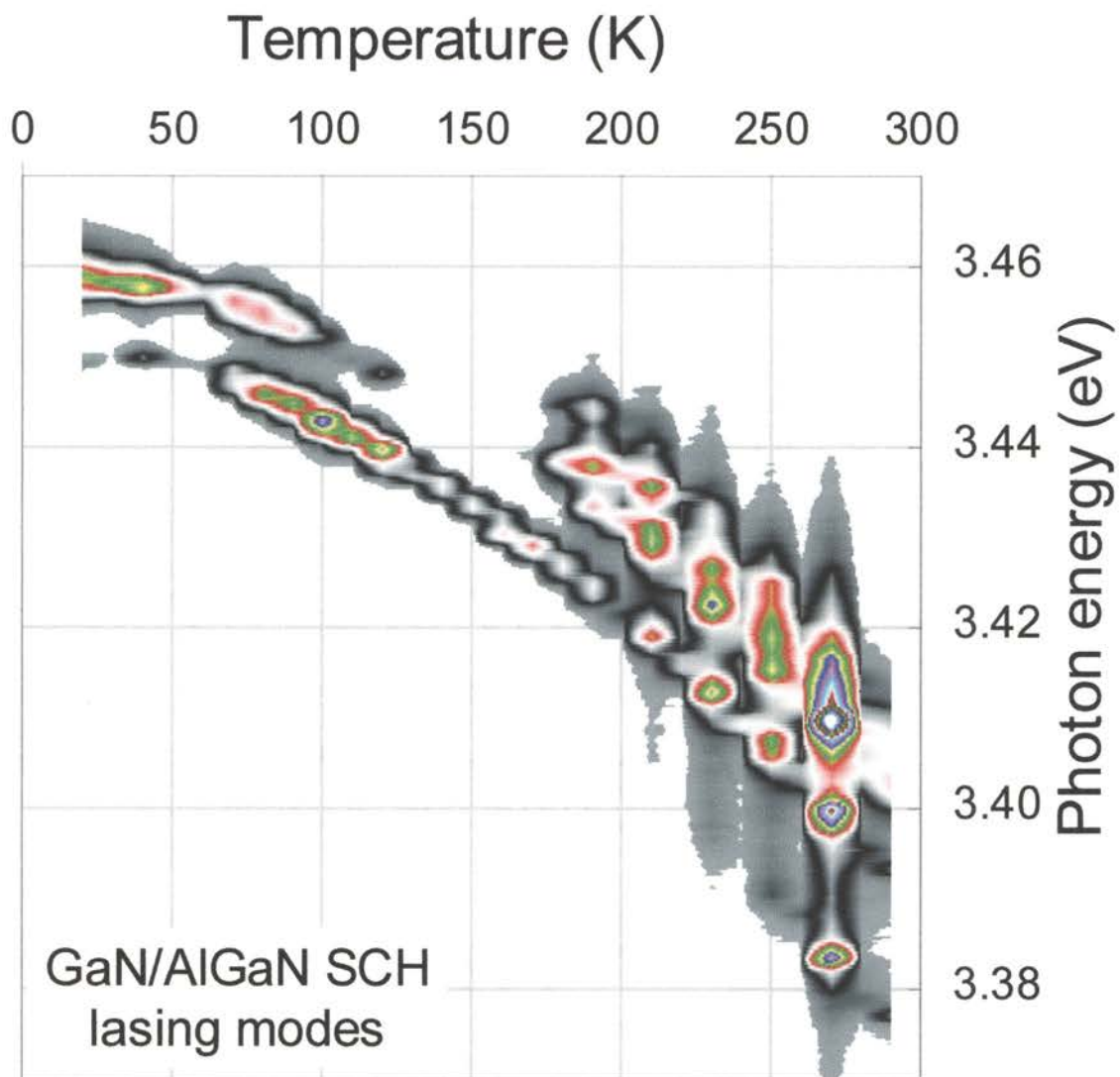


Figure 56. Temperature dependent data obtained for a single microcavity. This image was obtained by consistently taking lasing spectra with an optical multi-channel analyzer at $1.3 \times I_{th}(T)$ while the temperature was gradually varied from 20 K to 295 K.

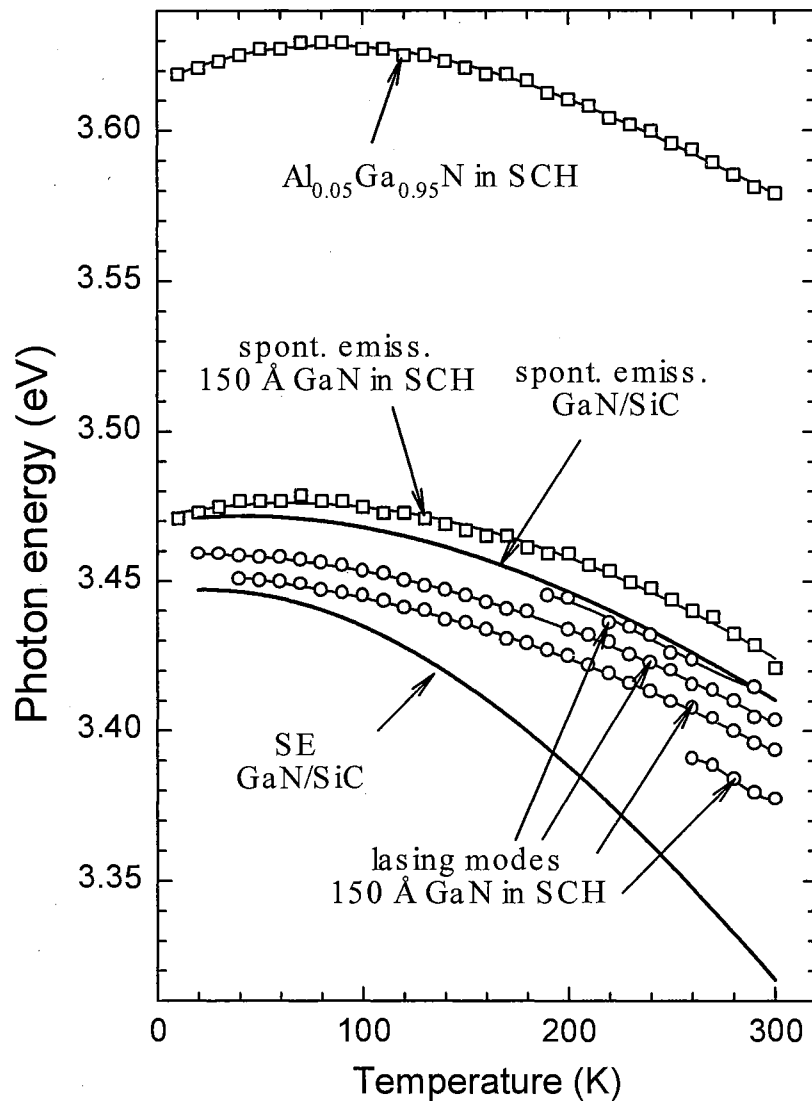


Figure 57. Temperature dependence of low density PL peak positions (open squares) and lasing modes (open circles) in a GaN/AlGaN SCH. For comparison, we also plotted the position of spontaneous and SE peaks from a 4.2- μm -thick GaN epilayer (solid lines). The two samples show distinctly different temperature evolutions associated with the different origins of SE/lasing at elevated temperatures.

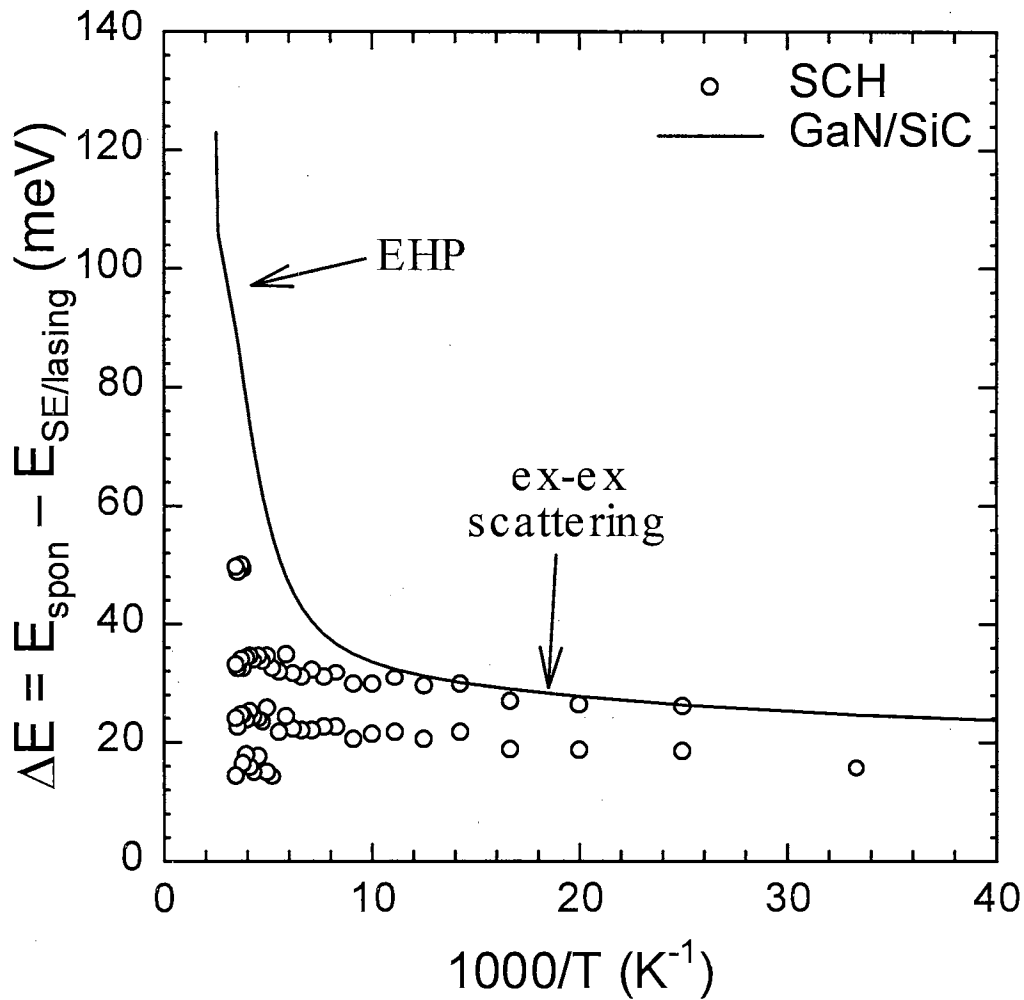


Figure 58. Energy position of lasing modes relative to spontaneous emission from the GaN active region in the SCH (open circles) and the energy difference between spontaneous and SE peaks in a 4.2- μm -thick GaN epilayer (solid line). The lasing modes in the SCH appear one exciton binding energy below the spontaneous emission peak over the entire temperature range studied, indicating that ex-ex scattering is the dominant lasing mechanism. On the contrary, the energy difference between the spontaneous and SE peaks in the GaN epilayer rapidly changes at ~ 150 K due to the gain mechanism transition from ex-ex scattering to EHP.

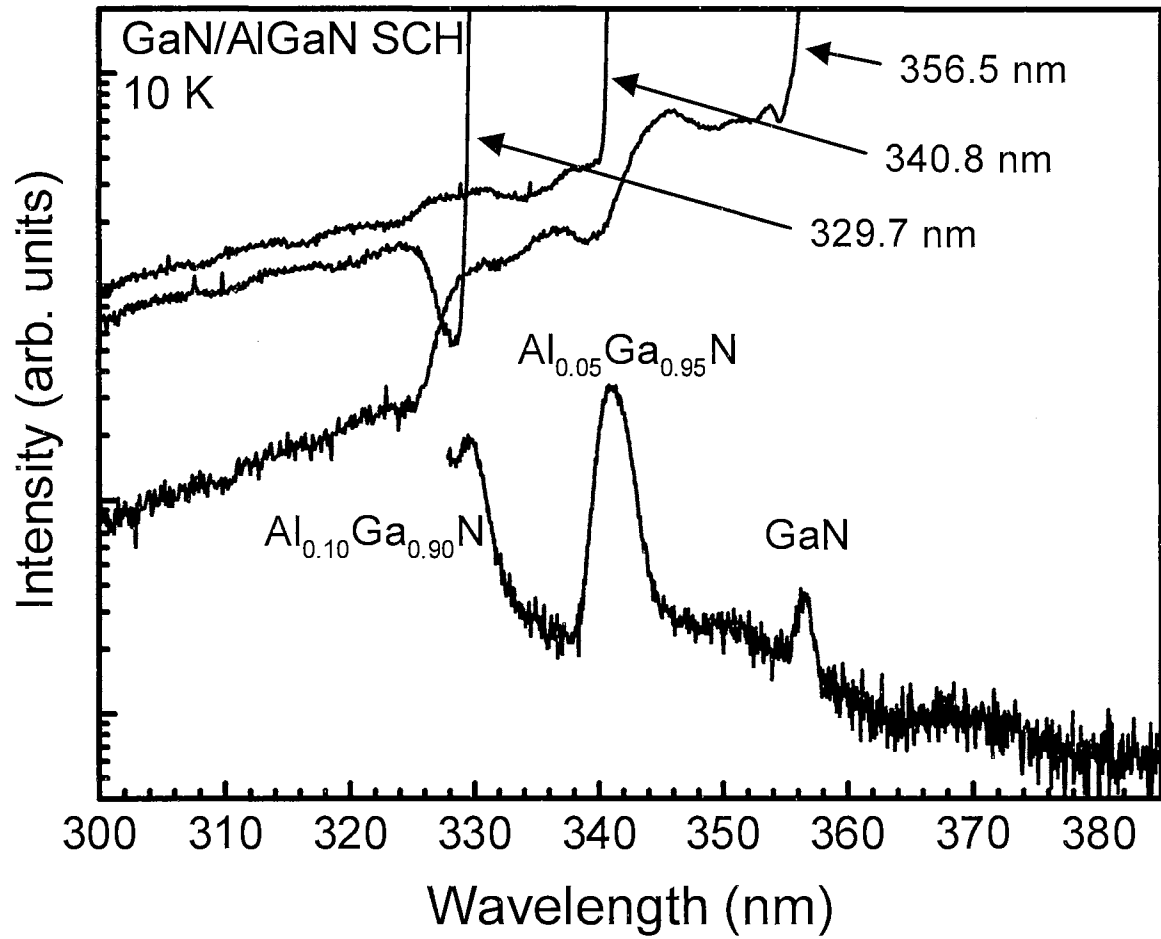


Figure 59. PLE and PL spectra from a GaN/AlGaN SCH taken at 10 K. PLE spectra were obtained at different detection positions: 329.7 nm, 349.8 nm, and 356.5 nm. Adapted from Ref. [106].

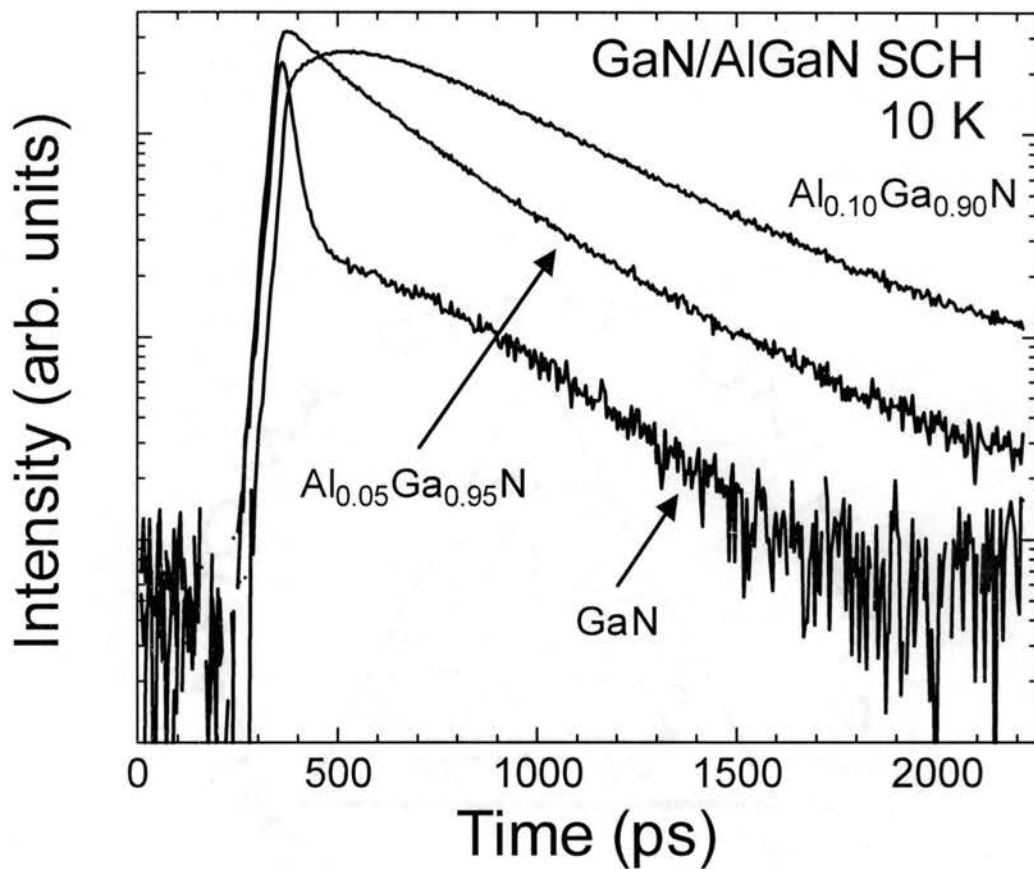


Figure 60. Time-resolved photoluminescence intensity of the three peaks depicted in Figure 53 under picosecond optical excitation at 10 K. The emission from the Al_{0.10}Ga_{0.90}N layer follows a single exponential decay pattern, whereas the emission from the Al_{0.05}Ga_{0.95}N layer has two contributions to its decay presumably due to both direct excitation and the diffusion of carriers from the Al_{0.10}Ga_{0.90}N layer. The GaN active layer has multiple contributions from different layers as well as a direct contribution from the laser excitation. Adapted from Ref. [106].

Critical Issues of Localization in InGaN-Based Lasing Structures

Probably the most controversial issue in blue laser development is the origin of spontaneous and stimulated emission in InGaN-based lasing structures. The nitride researchers can be roughly divided into two groups. The first group believes that spontaneous polarization and/or strain-induced piezoelectric polarization are responsible for carrier recombination in InGaN-based lasing structures (spontaneous polarization is due to charge accumulations at the interface between two constituent materials and piezoelectric polarization is due to lattice-mismatch-induced strain). The second group, to which this author belongs, believes that inhomogeneous potential fluctuations (caused by alloy composition fluctuation, well size irregularity, and other crystal imperfections) result in localized carrier recombination being the dominant spontaneous and stimulated emission mechanism over a wide temperature range. In order to prove this point we have employed various techniques, such as photoluminescence (PL), photoluminescence excitation (PLE), time-resolved photoluminescence (TRPL), optical pumping, variable stripe gain measurements, and nanosecond nondegenerate pump-probe spectroscopy.^{44,107}

The descriptions of the samples used in this study were given in Chapter IV (see pages 122-132). Figure 61 shows typical PL, PLE and TRPL data at 10 K for (a) an InGaN/GaN multi-quantum well and (b) an InGaN epilayer. When the PLE detection energy is set at the InGaN-related emission peak, the contributions from the GaN layers and the AlGaN capping layer are clearly distinguishable, and the energy positions of the absorption edges are well matched to the PL peak positions. A large Stokes shift of the InGaN-related spontaneous emission peak with respect to the absorption edge measured by PLE is observed for both samples. This Stokes shift is seen to be significantly larger in the multi-quantum well than in the epilayer, probably due to the influence of the multi-quantum well interfaces on the overall potential fluctuations. We note that the effective recombination lifetime rises with decreasing emission energy across the PL spectrum, resulting in a redshift of the emission peak energy as time progresses. This gives

evidence that the InGaN-related emission is due to the radiative recombination of carriers localized at potential fluctuations. The difference in recombination lifetimes between the two samples indicates that the potential fluctuations localizing the carriers are significantly smaller in the epilayer than in the multi-quantum wells.

Figure 62 shows the blueshift of the spontaneous emission in InGaN epilayers and InGaN/GaN multi-quantum wells with increasing optical excitation. This blueshift is attributed to band filling of localized states due to the intense optical pump. With increasing excitation pump density, the filling level increases and the PL maximum shifts to higher energies until a sufficient population inversion is achieved and the net optical gain results in the observed stimulated emission. The amount of blueshift further indicates that the potential fluctuations are significantly larger in the multi-quantum wells than in the epilayer.

By utilizing the variable stripe method described in Appendix A we measured the modal gain profiles. Figure 63 shows the relevant gain spectra for (a) the InGaN/GaN multi-quantum wells and (b) the InGaN epilayer plotted together with PL, PLE, and stimulated emission spectra. The stimulated emission peak is situated at the end of the absorption tail for both samples. It is seen to occur on the high energy side of the low power spontaneous emission peak for the multi-quantum well sample and slightly on the low energy side for the epilayer. The stimulated emission peak is situated on the low energy tail of the gain curve measured for small excitation lengths. This can be explained by competition between gain and absorption in the band tail region of this alloy, where gain saturation with longer excitation lengths combined with the background absorption tail leads to a redshift of the stimulated emission peak with increasing excitation length. The modal gain spectrum for the multi-quantum well is seen to be significantly broader than that of the epilayer, although both peaks appear significantly below the onset of the “soft” absorption edge.

The modal gain spectra as a function of above-gap optical excitation density are shown in Figure 64 for the multi-quantum wells and epilayer. A clear blueshift in the gain peak with increasing optical excitation is seen for the multi-quantum wells. This blueshift was observed to cease for $I_{\text{exc}} > 12 \times I_{\text{th}}$. Further increases in I_{exc} resulted only in an increase in the modal gain maximum. The large shift in the gain maximum to higher

energy with increasing I_{exc} is consistent with a band filling of localized states in the InGaN active layers. The blueshift in the gain spectra of the InGaN epilayer is seen to be considerably smaller than that of the multi-quantum wells. It was observed to stop at significantly lower excitation densities.

Figure 65 shows the results of nanosecond non-degenerate optical pump-probe experiments on an InGaN epilayer at (a) 10 K and (b) room temperature. The experimental technique is described in Appendix C. With increasing excitation density of the pump pulse, the absorption coefficient in the band tail region decreases significantly. This bleaching saturated for I_{exc} exceeding $\sim 2 \text{ MW/cm}^2$. We note that the induced transparency associated with the absorption bleaching is quite large, exceeding $3 \times 10^4 \text{ cm}^{-1}$ at both 10 K and room temperature. The spectral region in which stimulated emission is observed is also indicated in Figure 65. Features in the induced absorption bleaching spectra are seen to coincide with these spectral regions and are attributed to net optical amplification (gain) of the probe pulse.

In Figure 66 we give a comparison of nanosecond non-degenerate pump-probe experiments on the (a) InGaN/GaN multi-quantum wells and (b) InGaN epilayer. Absorption bleaching of the band tail states is clearly seen for both structures with increasing excitation density. The bleaching is much broader spectrally for the multi-quantum wells than for the epilayers. The maximum in the absorption bleaching is significantly blueshifted with respect to the luminescence maximum for both samples. This can be explained by the intraband relaxation of photo-generated carriers which are quickly caught in the potential wells of the band tail states. Further intraband relaxation at low temperatures can only occur by phonon-assisted tunneling to deeper potential wells or by further relaxation to lower energy states within the same wells until the potential minima are reached. Thus the radiative recombination mostly occurs from these potential minima. Higher energy states are temporarily occupied by the relaxing carriers and introduce the observed absorption bleaching. All the evidence presented so far strongly supports the idea that spontaneous emission in InGaN epilayers and InGaN/GaN multi-quantum wells originates from localized states.

In order to establish the origin of stimulated emission in the multi-quantum wells, we tuned the excitation wavelength across the absorption edge of the InGaN active

layers. As the excitation wavelength is tuned to longer wavelengths, no noticeable change was observed in the stimulated emission spectrum until a certain value was reached. At this point the stimulated emission spectrum red shifts quickly with decreasing excitation photon energy, as shown in Figure 67. This redshift of the emission for a certain excitation wavelength is consistent with the mobility edge behavior observed for spontaneous emission. The mobility edge measured in these experiments lies ~ 110 meV above the spontaneous emission peak, ~ 62 meV above the stimulated emission peak, and ~ 185 meV below the absorption edge of the InGaN well regions. This further indicates that large potential fluctuations are present in the InGaN active regions, resulting in strong carrier localization. This explains the efficient radiative recombination observed from these structures as well as the low temperature sensitivity of the stimulated emission as was described in Chapter IV.

In summary, we have systematically investigated both the spontaneous and stimulated emission properties of InGaN/GaN multi-quantum well structures and InGaN epilayers. Our findings can be consistently understood in the context of localization of photogenerated carriers associated with strong potential fluctuations in the InGaN active region. We believe that the efficiency of the state-of-the-art blue laser diode and the origin of gain is due to potential fluctuations of indium in the active layers.

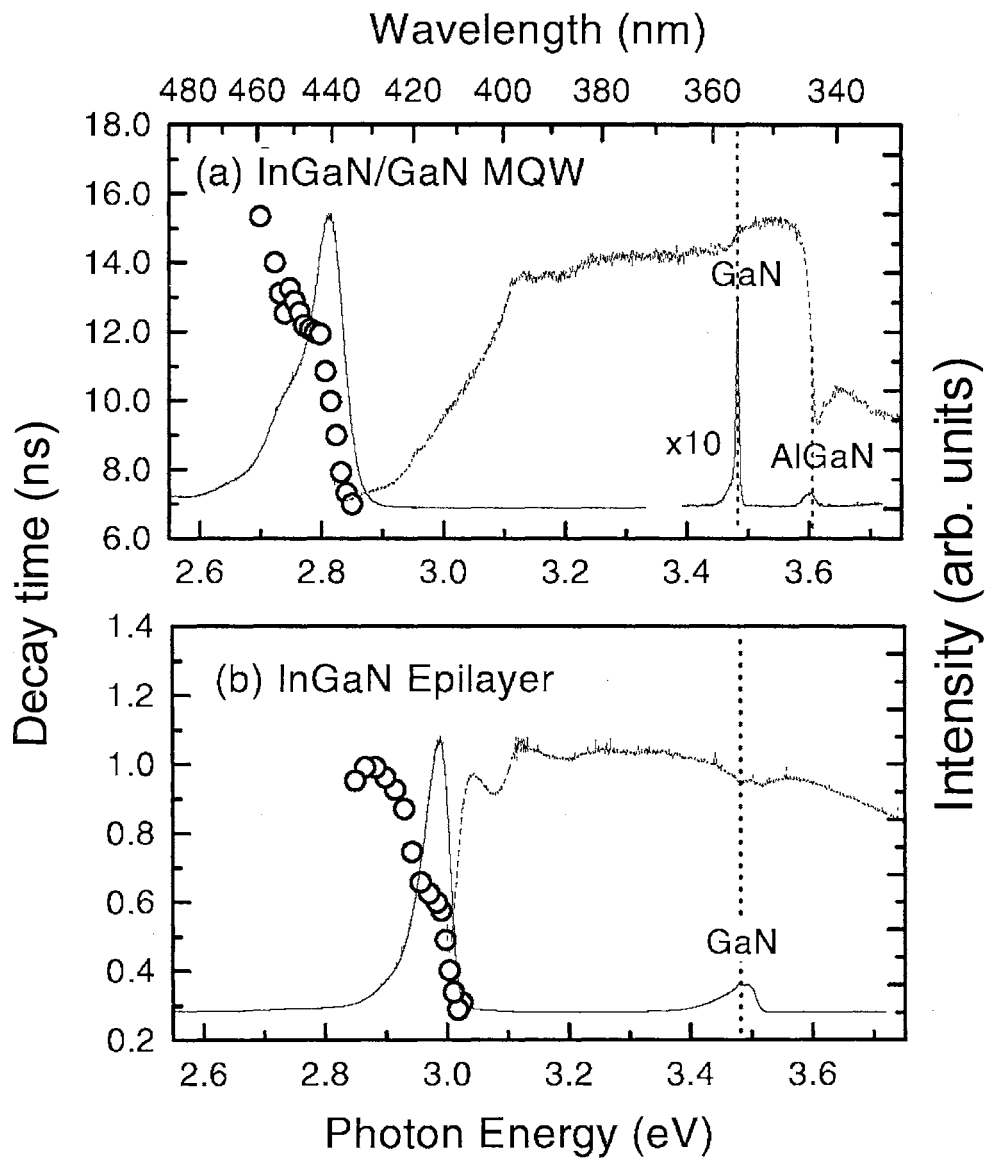


Figure 61. Photoluminescence, photoluminescence excitation, and time-resolved photoluminescence from (a) an InGaN/GaN multi-quantum well and (b) an InGaN epilayer at 10 K. From Ref. [107].

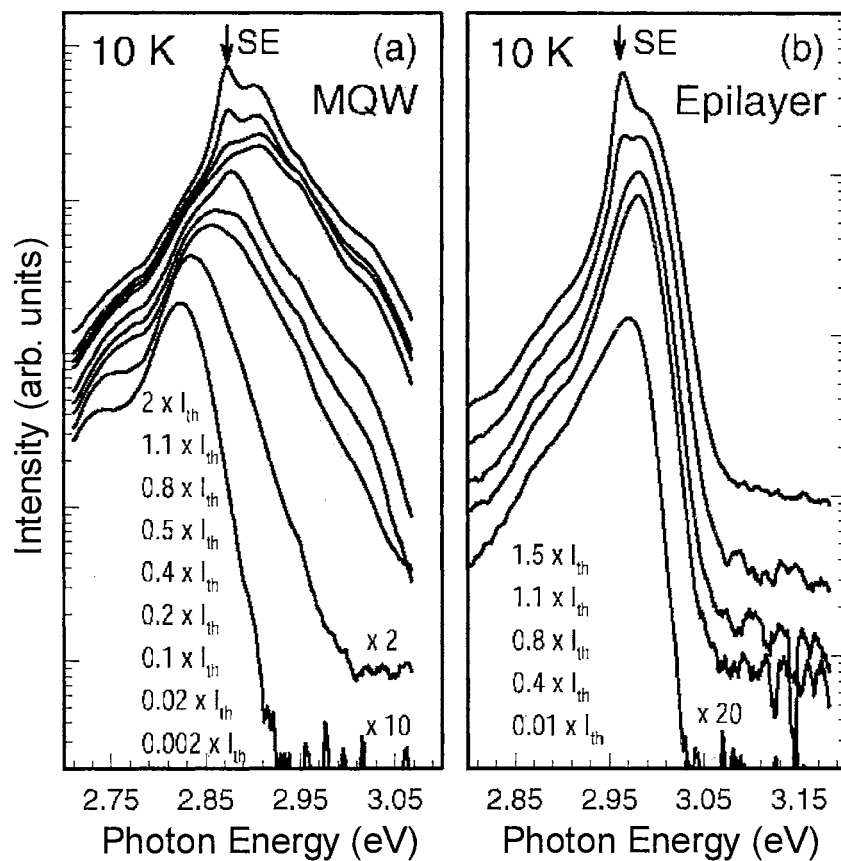


Figure 62. Evolution of emission spectra from below to above the stimulated emission threshold from (a) an InGaN/GaN multi-quantum well ($I_{th} = 170 \text{ kW/cm}^2$) and (b) an InGaN epilayer ($I_{th} = 130 \text{ kW/cm}^2$). From Ref. [107].

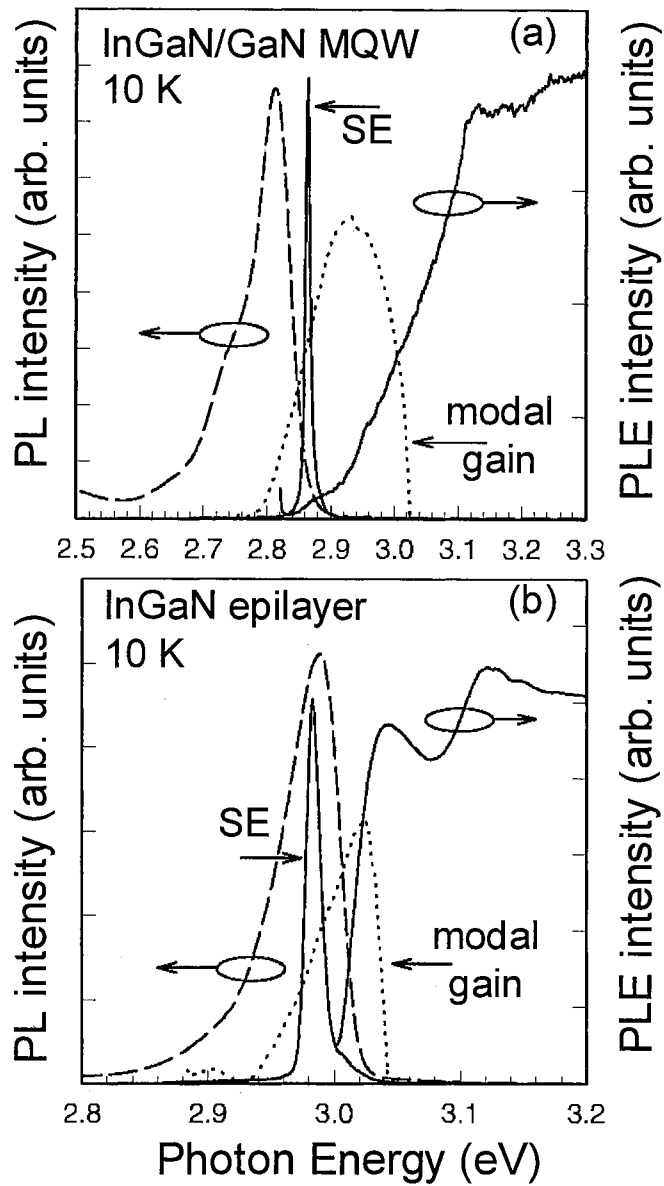


Figure 63. Photoluminescence (dashed lines), stimulated emission (solid lines), PLE (solid lines), and modal gain (dotted lines) spectra taken at 10 K from (a) an InGaN MQW and (b) an InGaN epilayer. From Ref. [44].

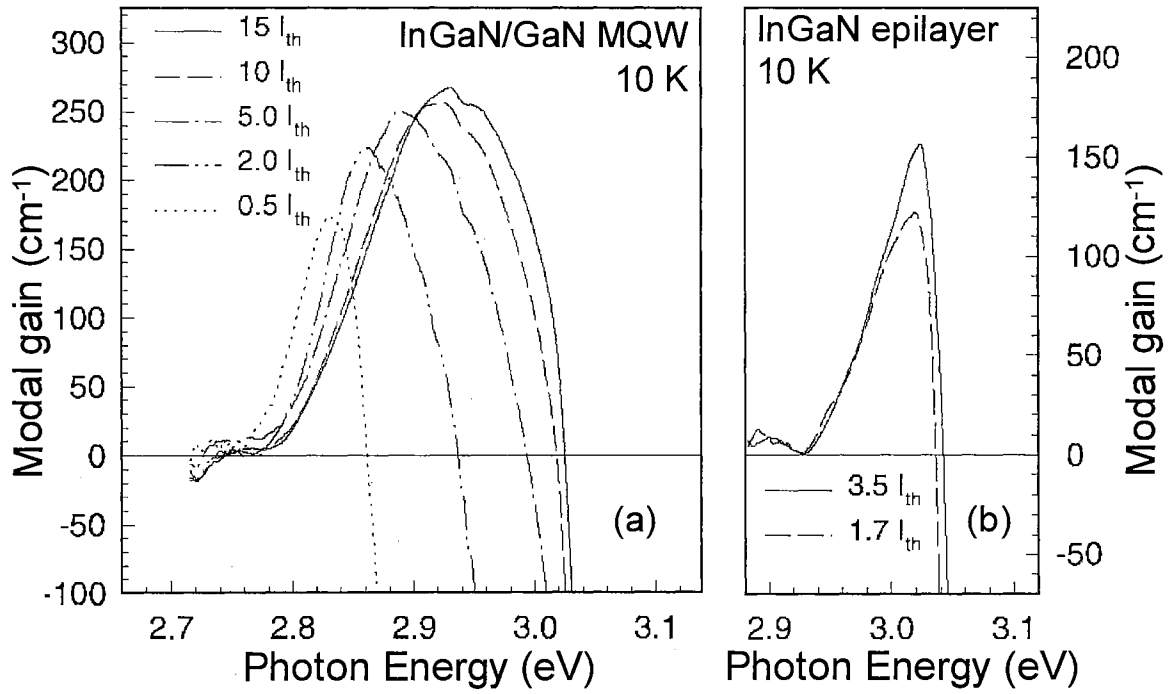


Figure 64. Modal gain spectra of (a) an InGaN/GaN multi-quantum well and (b) an InGaN epilayer as a function of above-gap optical excitation density. The excitation densities are given with respect to the stimulated emission threshold. From Ref. [107].

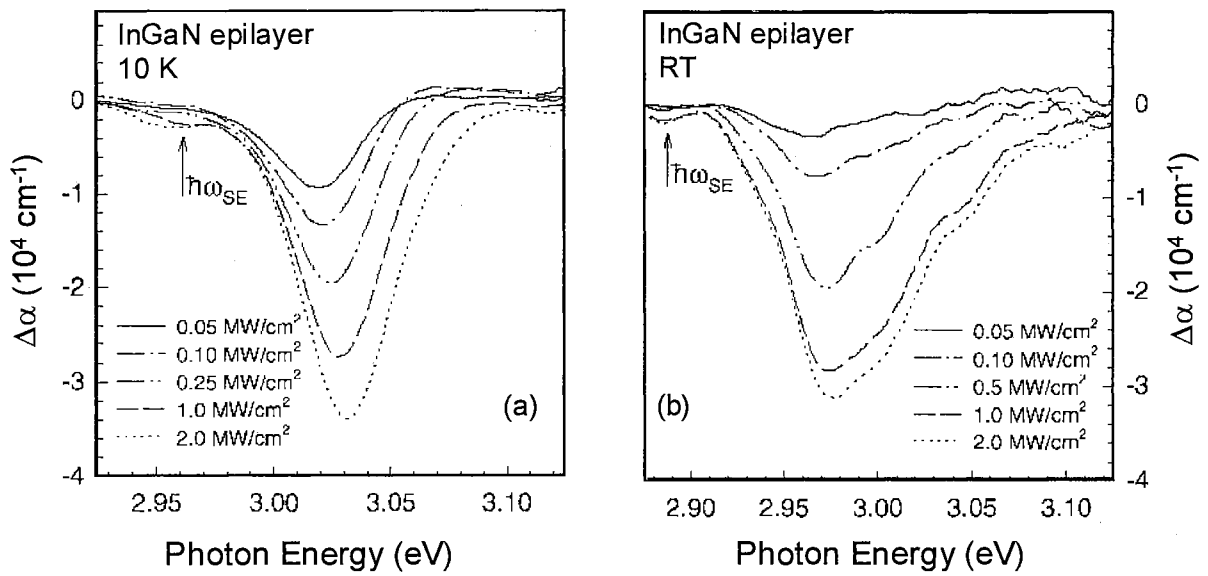


Figure 65. Differential absorption spectra, $\Delta\alpha(I_{\text{exc}}) = \alpha(I_{\text{exc}}) - \alpha(0)$ at (a) 10 K and (b) room temperature as a function of the optical excitation density for the InGaN epilayer. Adapted from Ref. [44].

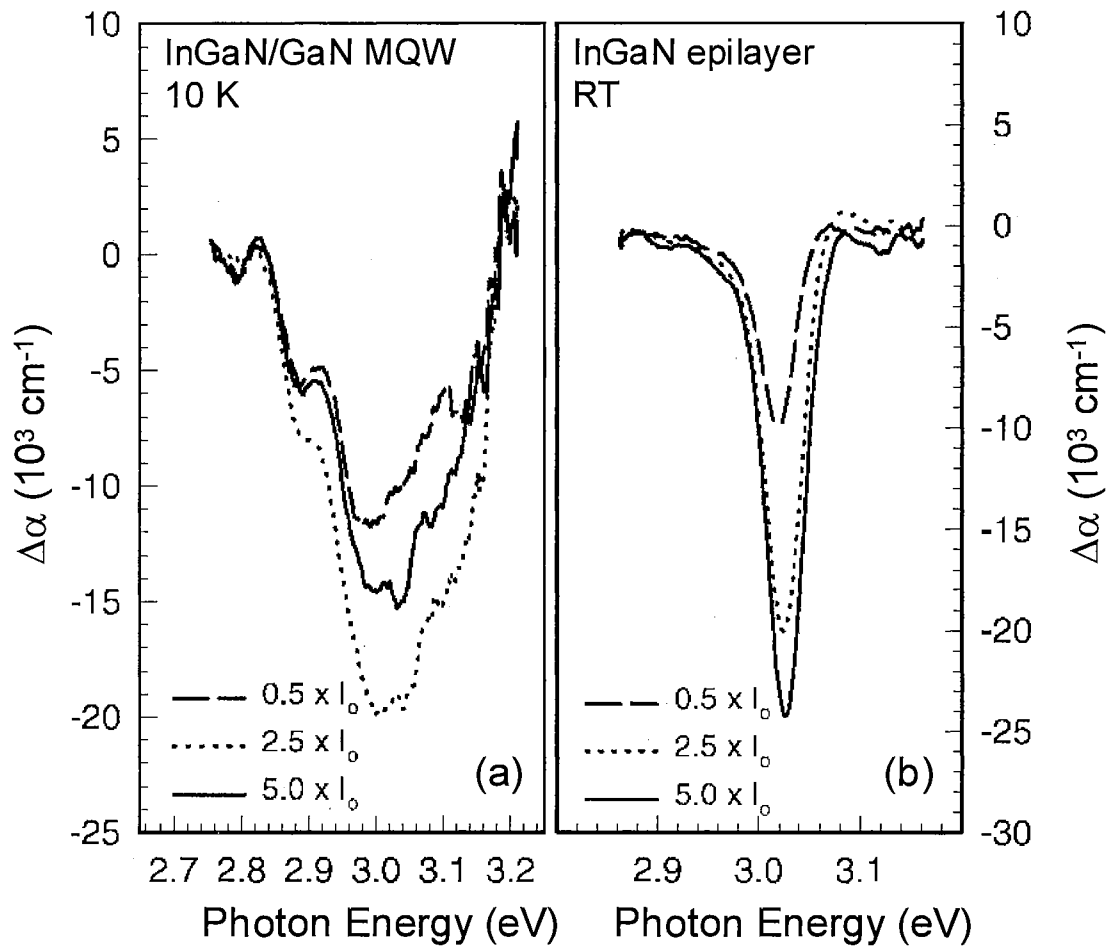


Figure 66. 10 K nanosecond non-degenerate pump-probe experimental results for (a) an InGaN/GaN multi-quantum well and (b) an InGaN epilayer showing absorption bleaching of band tail states with increasing excitation density. From Ref. [107].

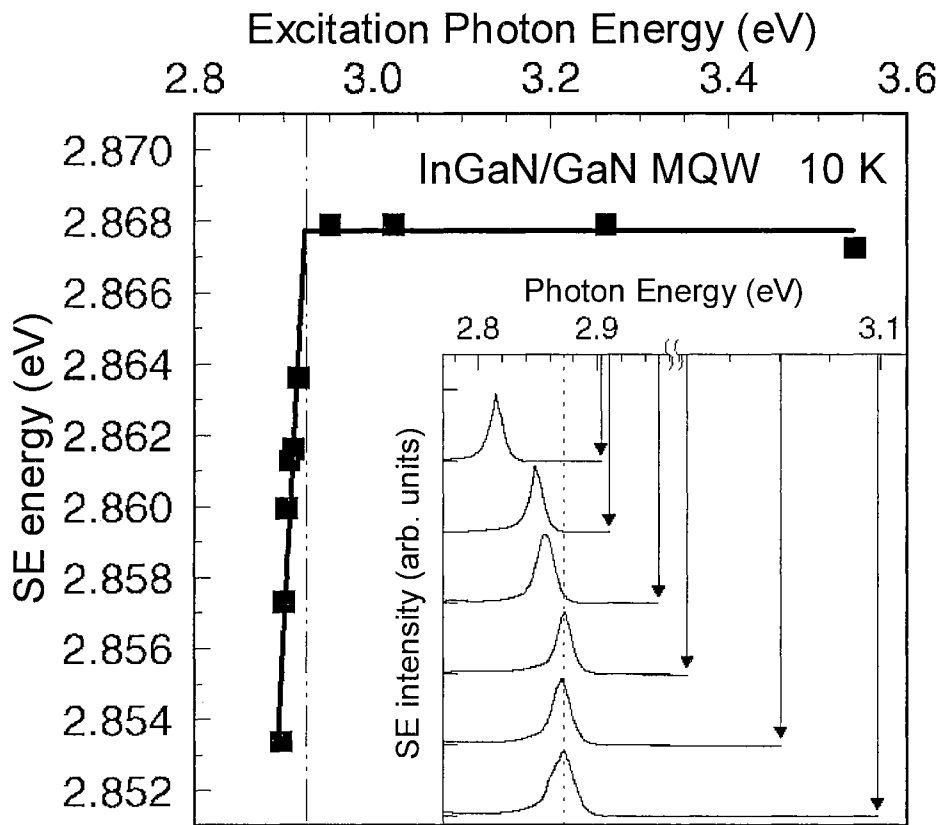


Figure 67. Stimulated emission peak position as a function of excitation photon energy for the InGaN/GaN MQW. “Mobility edge” type behavior is clearly seen in the stimulated emission spectra with decreasing photon energy of the excitation beam. From Ref. [44].

Gain Mechanism in AlGaN Epilayers

The ternary compound AlGaN has the potential for use in light emitting devices and detectors covering the deep-UV region of the spectrum. Room-temperature stimulated emission from AlGaN thin films has been demonstrated by our group at wavelengths as short as 328 nm.¹⁰⁸ We extended our research to perform a study of the temperature-dependent behavior of the spontaneous and stimulated emission characteristics. Based on our research we concluded that the dominant stimulated emission mechanism in the temperature range of 10 K to 300 K is electron-hole plasma recombination.

The $\text{Al}_{0.17}\text{Ga}_{0.83}\text{N}$ layer used in this work was grown by low-pressure metalorganic chemical vapor deposition on (0001) oriented sapphire at a temperature of 1050°C. Prior to the epilayer growth, a thin (~ 50 Å) AlN buffer layer was deposited on the sapphire at a temperature of 625°C. Triethylgallium, triethylaluminum, and ammonia were used as precursors in the growth of the $\text{Al}_{0.17}\text{Ga}_{0.83}\text{N}$ layer, which had a thickness of ~ 0.8 μm . The samples were pumped in the traditional edge emission geometry (see discussion on page 69). The exact position of the spontaneous emission peaks was determined in the surface emission geometry using a frequency-doubled Ar^+ laser (244 nm).

Figure 68 shows photoluminescence spectra as a function of excitation pump density near the stimulated emission threshold for an $\text{Al}_{0.17}\text{Ga}_{0.83}\text{N}$ sample at 30 K. At low excitation powers only a broad spontaneous emission peak is observed at ~ 3.70 eV. As the excitation power is increased above $I_0 = 0.3$ MW/cm^2 , a spectrally narrow peak at approximately 3.64 eV appears on the low energy shoulder of the spontaneous emission. We note that the intensity of this stimulated emission peak increases superlinearly with excitation power. The inset in Figure 68 shows similar spectra taken at room temperature.

The spontaneous and stimulated emission energy peak positions as a function of temperature for the $\text{Al}_{0.17}\text{Ga}_{0.83}\text{N}$ sample are depicted in Figure 69 by open and solid circles, respectively. The behavior of the spontaneous emission peak with temperature cannot be adequately described by the Varshni equation. Currently, several other theories aiming to include the piezoelectric and potential fluctuation contributions to the energy peak position have been invoked, but no definitive explanation has been given. We note that at this time either theory can explain the increased carrier lifetimes in the $\text{Al}_{0.17}\text{Ga}_{0.83}\text{N}$ sample (250 ps at 10 K) in comparison to the carrier lifetime in a typical GaN epilayer (35 ps at 10 K) measured by time-resolved luminescence experiments.

The stimulated emission peak for this sample is located substantially below the spontaneous emission peak. The inset in Figure 69 shows the energy difference between the spontaneous and stimulated emission peaks. This energy difference varies from about 70 meV at 30 K to over a hundred meV at room temperature. Since the exciton binding energy in this sample is expected to be in the range of 20 to 30 meV, we can exclude the participation of excitons in stimulated emission. To further corroborate the point that excitons do not take part in establishing gain in the AlGaN sample studied, we carefully examined the behavior of the stimulated emission threshold with temperature, as shown in Figure 70. The threshold rapidly increases with increasing temperature. The carrier density needed to achieve the stimulated emission threshold at 30 K can be readily evaluated if we take into account the recombination lifetime (250 ps) and the penetration depth ($9 \times 10^4 \text{ cm}^{-1}$). A pump density of 0.3 MW/cm^2 (the threshold value at 30 K) roughly corresponds to a carrier density of $1.2 \times 10^{19} \text{ cm}^{-3}$. This value is one order of magnitude larger than the expected value for the Mott density in GaN samples (see pages 33 and 109). Thus, excitons are likely to be screened out at these pump densities in AlGaN as well, leaving an electron-hole plasma as the only plausible gain mechanism. At elevated temperatures, the stimulated emission threshold requires even higher levels of optical pumping.

In summary, we studied the gain mechanisms in AlGaN alloys in the temperature range from 10 K to room temperature by examining the relative shift between the spontaneous and stimulated emission peaks as well as by evaluating the carrier density required to generate gain in this material system. We concluded that the dominant gain

mechanism in the $\text{Al}_{0.17}\text{Ga}_{0.83}\text{N}$ sample is an electron hole plasma over the entire temperature range studied.

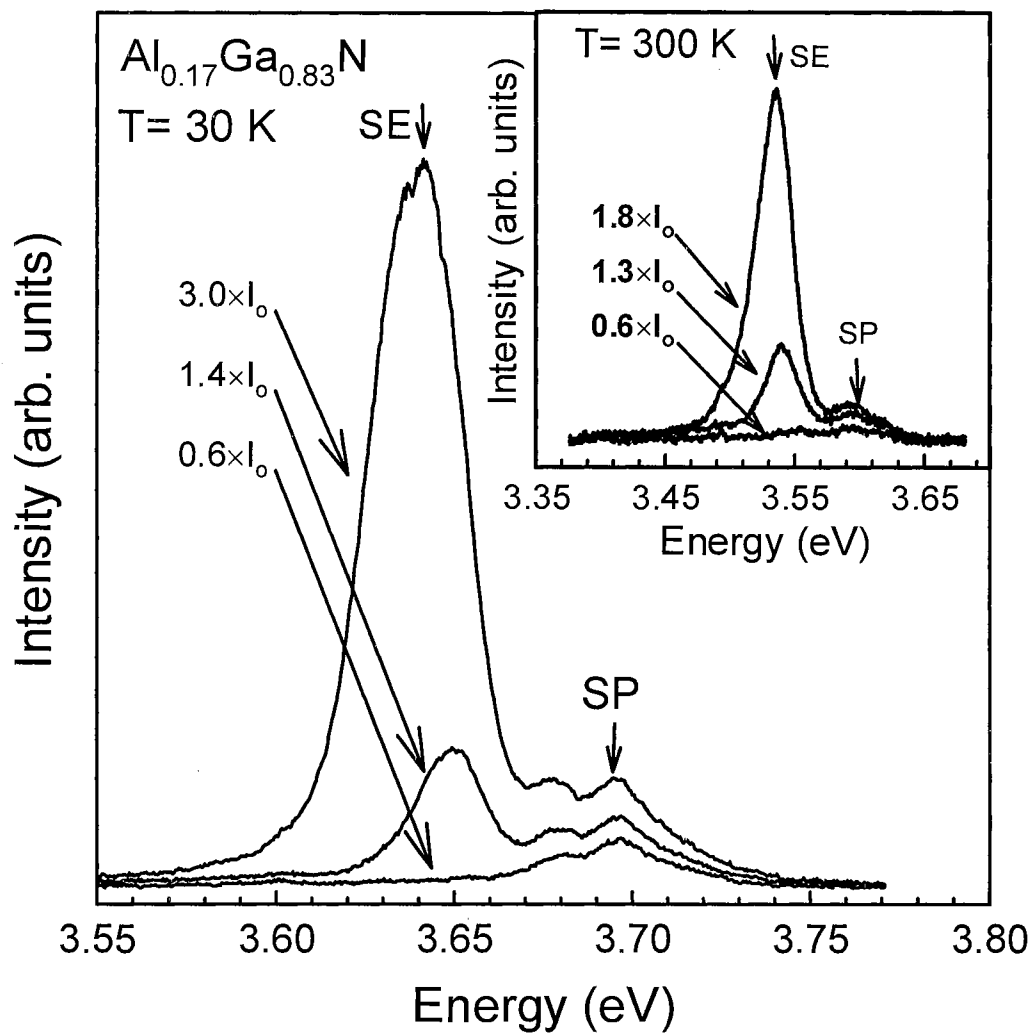


Figure 68. Photoluminescence spectra as a function of excitation pump density near the stimulated emission threshold for the $\text{Al}_{0.17}\text{Ga}_{0.83}\text{N}$ sample at 30 K. The inset shows the same spectra at room temperature. Both spontaneous (SP) and stimulated emission (SE) peaks were clearly observed.

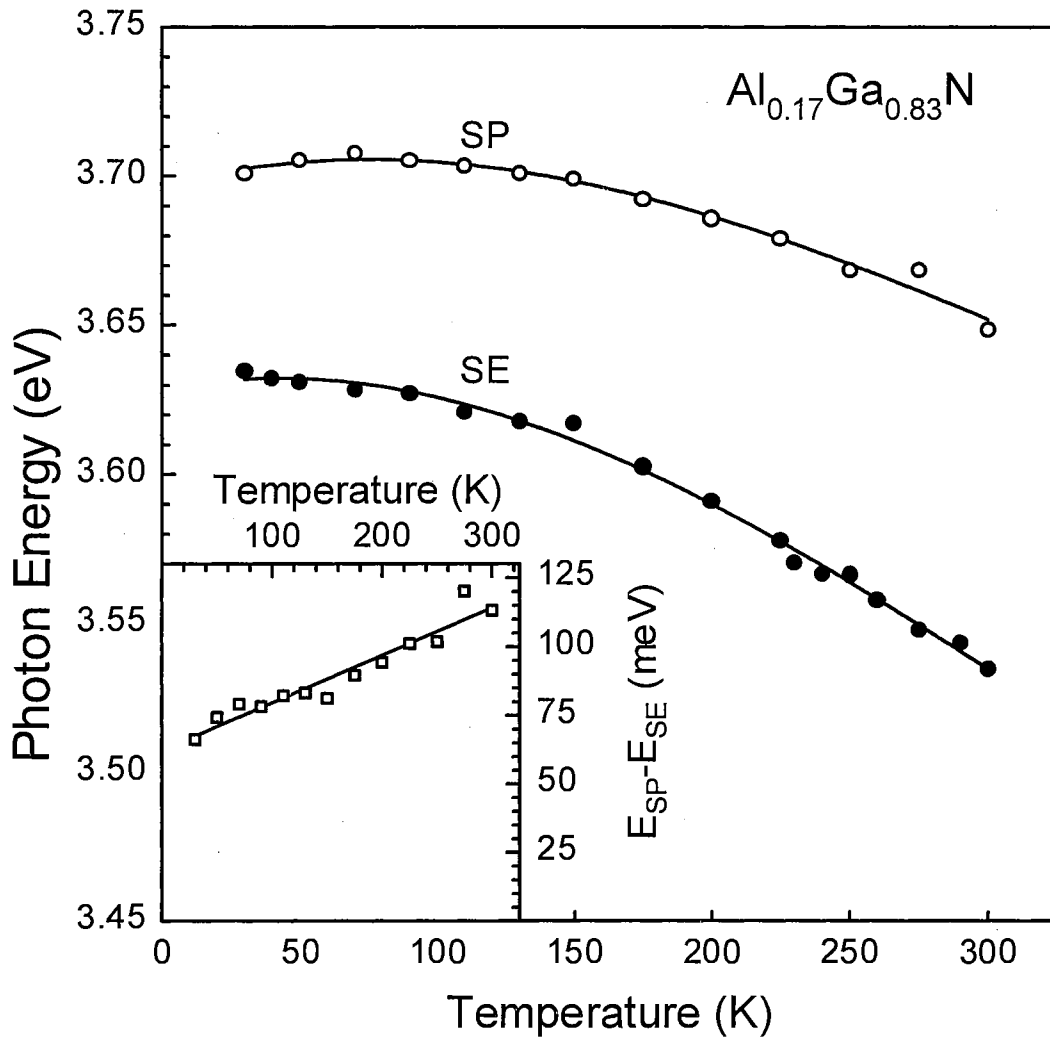


Figure 69. Spontaneous and stimulated emission energy peak positions as functions of temperature for the $\text{Al}_{0.17}\text{Ga}_{0.83}\text{N}$ sample. The inset shows the energy difference between the two peaks. The solid lines are to guide the eye only.

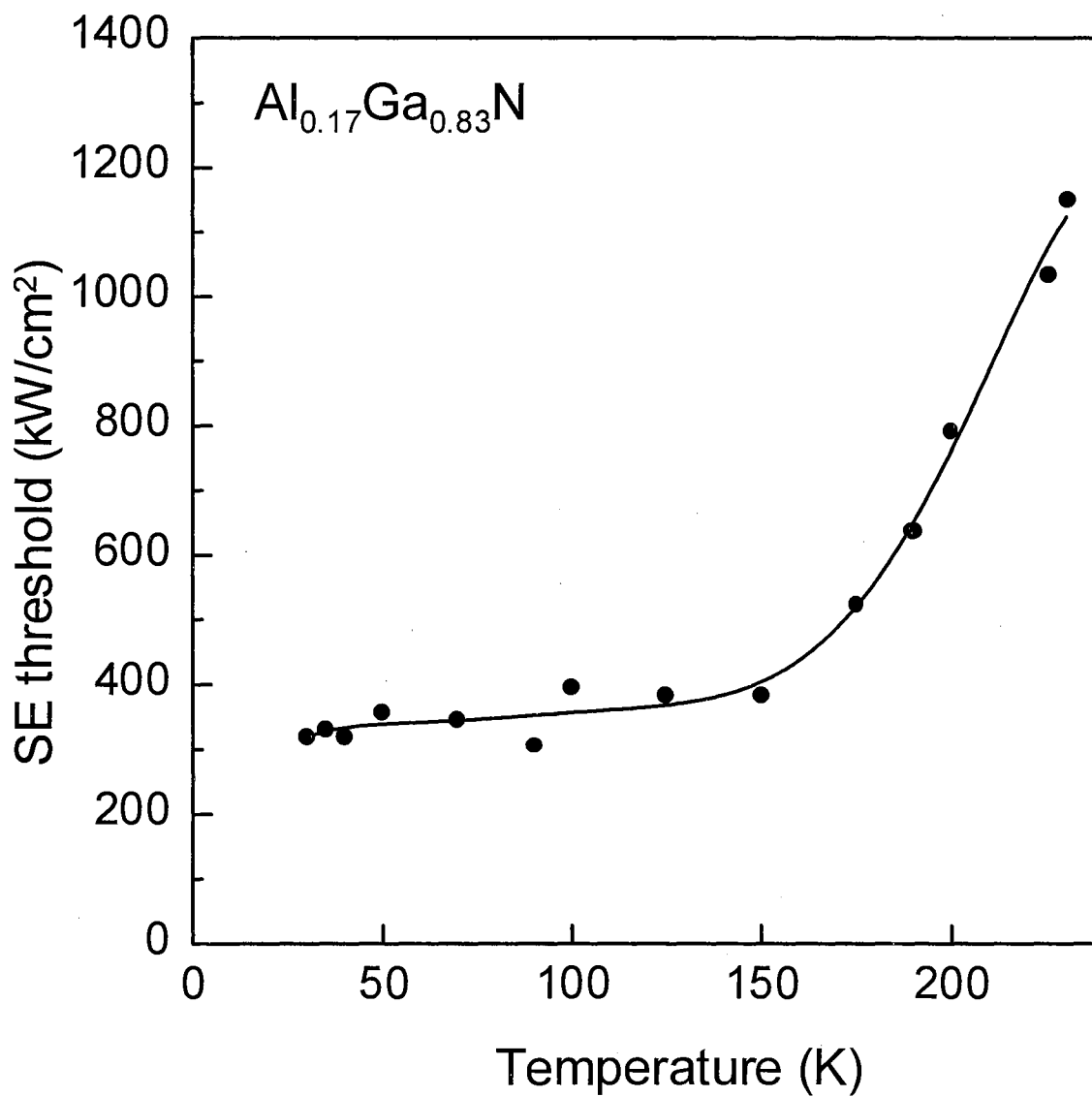


Figure 70. The stimulated emission threshold as a function of temperature for the Al_{0.17}Ga_{0.83}N sample. Solid circles are the experimental data. The solid line is to guide the eye only.

CHAPTER VI

MICROSTRUCTURE LASING

Gallium nitride (and its alloys) is a very intriguing material for optical applications not only because of its large spectral emission range, but also due to the apparent controversy between structural and stimulated emission (lasing) properties. Due to the lack of ideal substrates for the growth of thin film nitrides, a large number of dislocations and cracks are naturally formed in the epitaxial layer to alleviate the lattice mismatch and the strain of postgrowth cooling. However, this does not always negatively affect lasing characteristics, but sometimes introduces interesting lasing properties due to self-formed high-finesse microcavities and efficient scattering centers. A different kind of microcavity can also be formed during lateral overgrowth from a patterned seeding layer. High-finesse lasing cavities resulting from this kind of growth are often of a complex three-dimensional ring-type. This chapter describes research that has been done to study the stimulated emission and lasing properties of GaN in the presence of self- and intentionally-formed microcavities, scattering defects, and dislocations.

Origin of Surface-Emitted Stimulated Emission in GaN Epilayers

Many experimental research groups have reported the observation of surface-emitted stimulated emission in GaN epilayers, but its origin was never fully understood and has led to much conflict of opinion among researchers. Understanding the origin of this surface emitted stimulated emission is important to improve the lasing characteristics

of edge-emitting lasers as well as to develop a vertical cavity laser diode using this material. Vertical cavity stimulated emission from an MOCVD grown GaN layer, as well as for an InGaN/GaN heterostructure, was reported by Khan *et al.*^{109,110} The relatively small cavity lengths (1.5 μm and 4.1 μm) and low mirror reflectivities ($< 30\%$) indicate that stimulated emission within such a cavity requires extremely high gain in the active region. Bagnall and O'Donnell¹¹¹ theoretically estimated the value of the gain under similar conditions to be more than 10^5 cm^{-1} , which is a few orders of magnitude higher than the gain measured by the variable stripe length method reported by many authors.^{112,113} Yung *et al.*¹¹⁴ also reported the observation of surface-emitted stimulated emission from a GaN film grown by ion-assisted molecular beam epitaxy. In contrast, Amano *et al.*^{115,116} studied stimulated emission in an MOVPE-grown GaN epilayer film and AlGaIn/GaN heterostructures and did not observe any surface-emitted stimulated emission for the epilayer film, even though stimulated emission was observed in a side-pumping (edge emission) geometry. Interestingly, the same authors did observe surface emitted stimulated emission from the AlGaIn/GaN heterostructures.

Lester *et al.*⁶⁸ found that GaN-based LEDs were highly efficient in spite of an extremely high density of structural defects ($\sim 10^{10} \text{ cm}^{-2}$). Similar GaAs LEDs have a dislocation density six orders of magnitude lower. This suggests that a high density of structural defects might always be present in GaN-based working devices. Therefore, the effect of defects on lasing in GaN merits further investigation. Wiesmann *et al.*¹¹³ compared the emission spectra from InGaIn and AlGaIn thin films with high quality GaAs thin films and concluded that the observation of a stimulated emission peak in the direction perpendicular to the nitride layer plane was due to scattering of the in-plane stimulated emission. In this chapter the results of a study of spatially resolved surface-emitted stimulated emission in GaN films under conditions of strong optical pumping are reported. We found that stimulated emission can only be observed coming from defects, such as cracks and burned spots, in samples of lesser surface quality. The high quality GaN films used in this work do not exhibit stimulated emission perpendicular to the surface, even under very high excitation powers, as long as the surface is free of defects. We show that imperfections in the sample surface introduce a leak of the photon flux propagating parallel to the sample's surface that can be easily confused with vertical

cavity lasing. Also, we relate our study of surface-emitted stimulated emission to gain measurements in GaN and give a possible explanation for the large discrepancies in reported gain values.^{109,112,113}

The GaN samples used in this work were described previously (see page 69). The samples were mounted on a translation stage driven by a computer-controlled stepper motor. This allowed us to position the sample with a precision of better than 1 μm . A tunable dye laser pumped by a frequency-doubled injection-seeded Nd:YAG laser was used as the primary optical pumping source. The visible output of the dye laser was frequency-doubled to achieve a near-UV pumping frequency. The beam was focused to an ~ 80 μm diameter spot on the sample surface and the emission was collected in the back-scattering geometry, as shown in Figure 71. A $10\times$ magnified image of the sample was projected onto the plane of the slits of a 1-m spectrometer. The signal from the sample was collected by an optical multi-channel analyzer mounted on the spectrometer. This configuration ensured that we pumped and collected the signal normal to the sample's surface. The overall spatial resolution of the system was better than 10 μm . All experiments were performed at room temperature.

The emission spectra were found to vary strongly near defect regions. In Figure 72 we show stimulated emission spectra taken from the 7.2 μm GaN layer at different locations near the vicinity of a defect. The sample was excited with a power density of 1.8 MW/cm^2 (approximately three times the stimulated emission threshold value measured in the side-pumping geometry). The broad emission feature at 363 nm corresponds to band-edge related spontaneous emission from the GaN epilayer. The full width at half maximum of the emission is about 10 nm. The narrow emission feature at 373 nm (with a full width at half maximum of 2 nm) exhibits a superlinear increase with excitation power and therefore represents stimulated emission.⁶⁹ The stimulated emission peak appears as we move the excitation beam close to the defect. In contrast to the stimulated emission collected from the sample's edge facets, the surface-emitted stimulated emission is not strongly polarized. The fact that we observe only spontaneous emission far from the defect and stimulated emission only in close proximity to the defect suggests that the defect acts as a scattering center, *i.e.* the light is amplified inside of the

GaN layer while propagating parallel to the sample surface until it is scattered out of the layer by the defect.

Figure 73 shows the dependence of the integrated stimulated emission intensity on the position on the sample surface for the two samples pumped with an excitation density of 4 MW/cm^2 . Since the widths of the sample bars are different (3 mm and 4 mm), we normalized the x-axis of the scan spectra to line up the sample's edges. A typical scan across the high quality $7.2\text{-}\mu\text{m}$ -thick GaN sample is shown in Figure 73(a). Unpolarized stimulated emission is observed at the sample edges and at a burned spot on the surface. We did not observe any stimulated emission from featureless parts of the sample, even with pump power densities up to the damage point. From Figure 73(b) we observe the $0.8\text{-}\mu\text{m}$ -thick GaN sample to have many more points of origin for surface-emitted stimulated emission. In fact, once we exceeded the damage threshold pumping density, unpolarized stimulated emission coming from the surface could be observed in the backscattering geometry from any GaN sample. Thus we conclude that the observed stimulated emission is not the result of a vertical amplification of light, but is due to a leak of the in-plane photon flux propagating parallel to the surface. We also note that cracks on the sample surface (as depicted in Figure 74) are the most efficient scattering centers for in-plane amplified stimulated emission.

The absorption coefficient of GaN is on the order of 10^5 cm^{-1} (see Figure 12) in the energy region around the fundamental band-gap.^{41,117} This limits the penetration depth of light into the sample, so that even with pump power densities of a few MW/cm^2 , it is only possible to create a population inversion in a layer on the order of $0.5 \mu\text{m}$ in thickness, which constitutes the gain region in the vertical direction. On the other hand, the lateral spot size of the pump beam, even with tight focusing, is orders of magnitude larger. Thus, the gain region in the horizontal direction is considerably larger than that in the vertical direction. With poor optical feedback in the vertical direction, light is preferentially amplified along a direction parallel to the surface rather than perpendicular to it. This light amplified in the horizontal direction can then be scattered by surface imperfections and observed as surface-emitted stimulated emission.

When gain in an epilayer film is measured in the transmission geometry, one usually assumes that the beam undergoing gain, *i.e.* the probe beam, is amplified only in

the direction perpendicular to the surface. When optical feedback is poor, as in the case of a GaN epilayer, the amplification path is then comparable to the thickness of the epilayer (a few microns). If the probe is scattered, though, the derivation of gain can be very complicated. Without making additional assumptions, the calculated gain could be orders of magnitude higher than when the gain is measured by the variable stripe technique, where the excitation length is on the order of a hundred microns and loss due to scattering is unaccounted for. Therefore, in GaN epitaxial layers with high levels of defects, caution is needed in using traditional techniques for measuring gain.

To summarize, we have performed a spatially resolved study on surface-emitted stimulated emission in GaN epilayer films. The intensity of surface-emitted stimulated emission was found to be dependent on the location of its origin on the sample's surface. For high quality GaN films with nearly perfect surfaces, stimulated emission was not observed in backscattering geometry, even under excitation power densities close to the damage threshold. In parts of the samples with poorer surface quality, surface-emitted stimulated emission was observed and was shown to come from cracks, burned spots, and other imperfections. Based on these experimental observations, we conclude that the surface-emitted stimulated emission reported by several authors is due to a scattering of the photon flux propagating parallel to the surface by defects, rather than vertically amplified emission. These results show that the influence of imperfections in GaN epilayers can not be ignored when determining gain values from experiment, and may be one of the reasons there are large discrepancies in gain values measured in different experimental geometries.

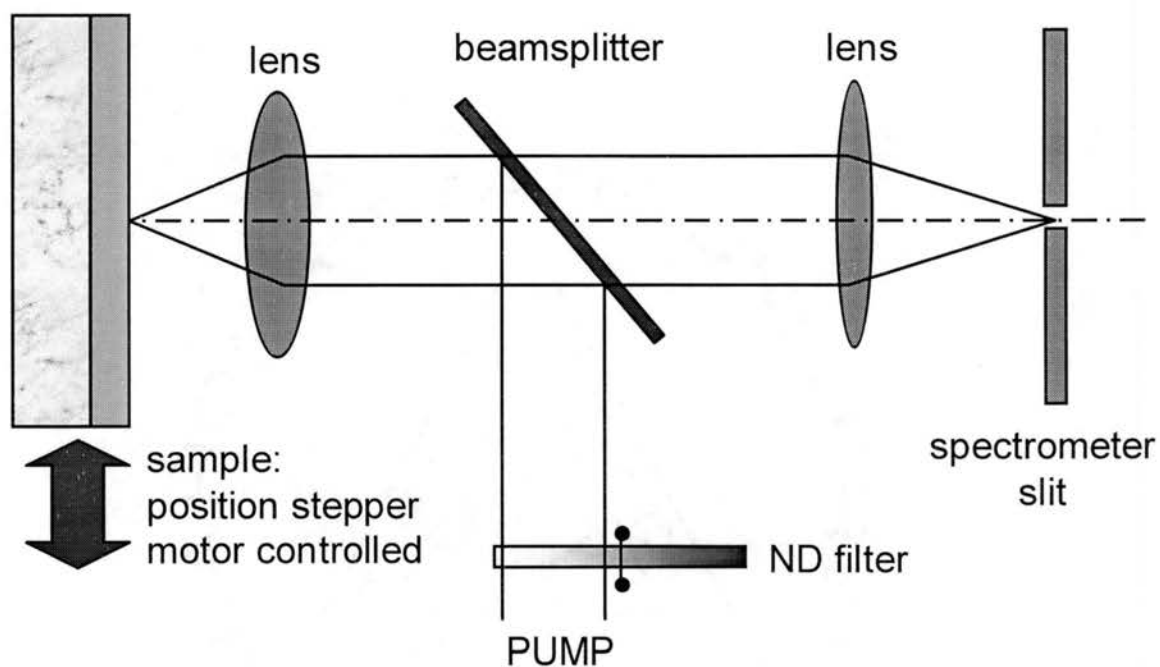


Figure 71. Schematic diagram of the backscattering geometry experimental setup. The sample is mounted on a translation stage driven by a stepper motor. A magnified image of the sample is projected onto the plane of the spectrometer slit.

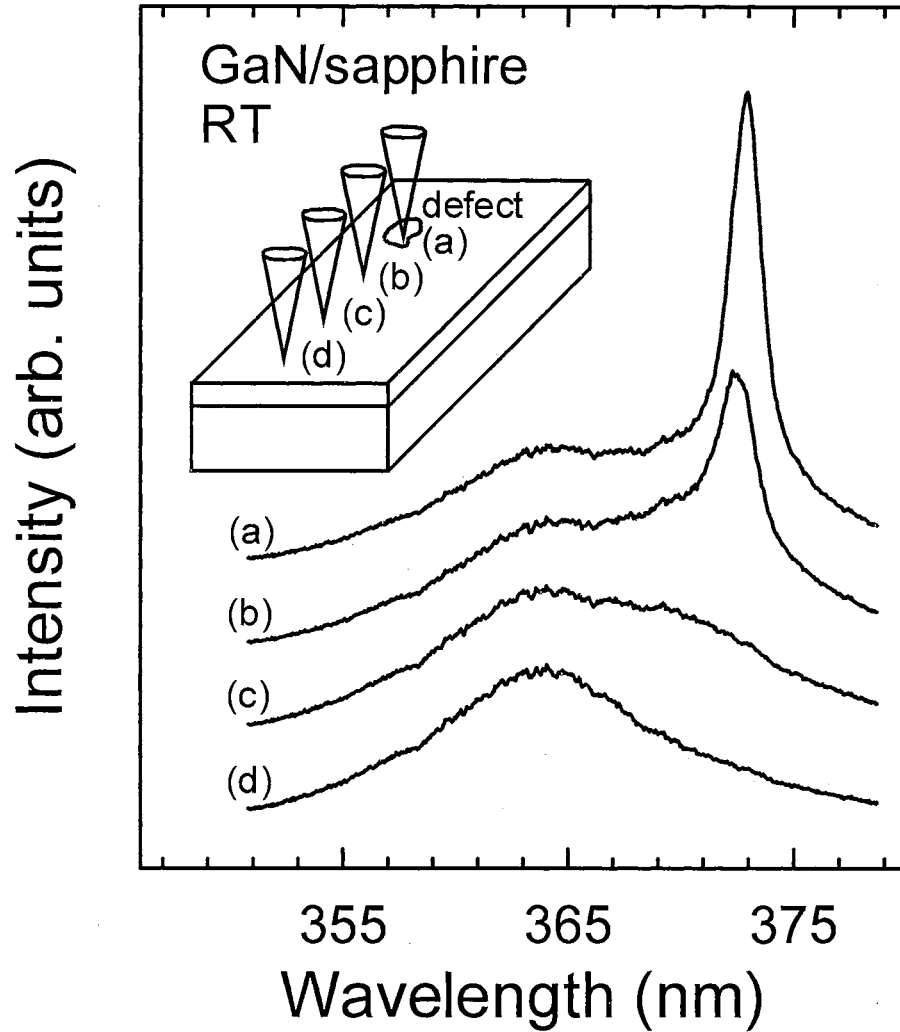


Figure 72. Emission spectra in the backscattering geometry from a 7.2- μm -thick GaN epilayer as a function of the distance from a defect. The four spectra were taken at 50 μm intervals; spectrum (a) was taken at the defect, whereas spectrum (d) was taken 150 μm away from the defect. The picture shows the locations (relative to the defect) where the spectra were taken.

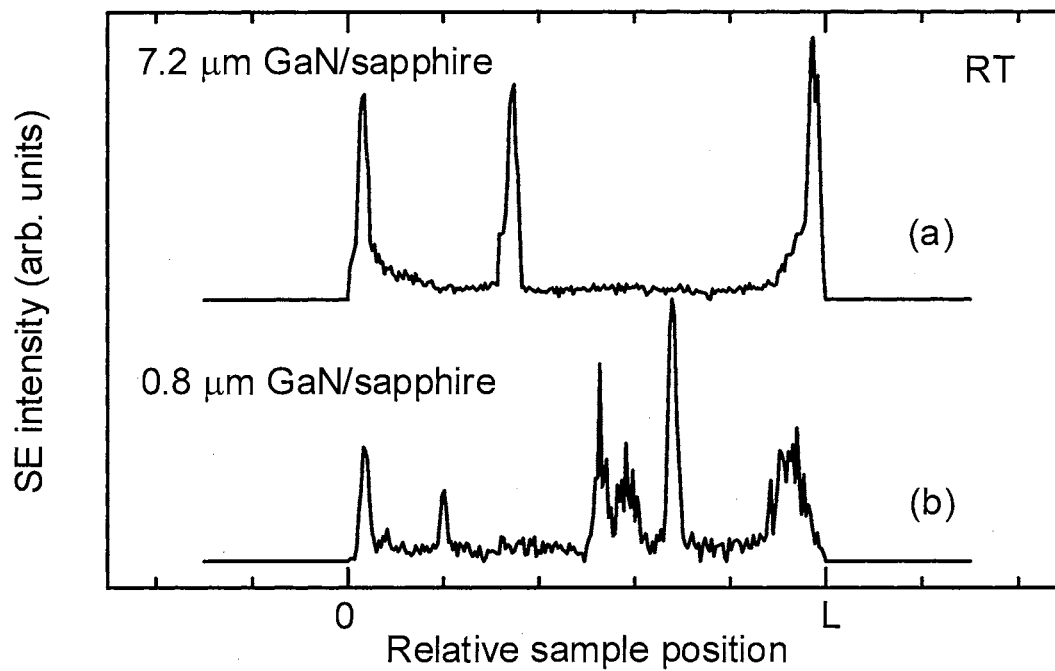


Figure 73. Stimulated emission intensity versus position relative to the sample edges for GaN samples of thickness (a) 7.2 μm and (b) 0.8 μm . Stimulated emission appears to originate from the sample edges as well as from burned spots, cracks, and other imperfections. The widths of the samples on the graphs were normalized to line up the edges.

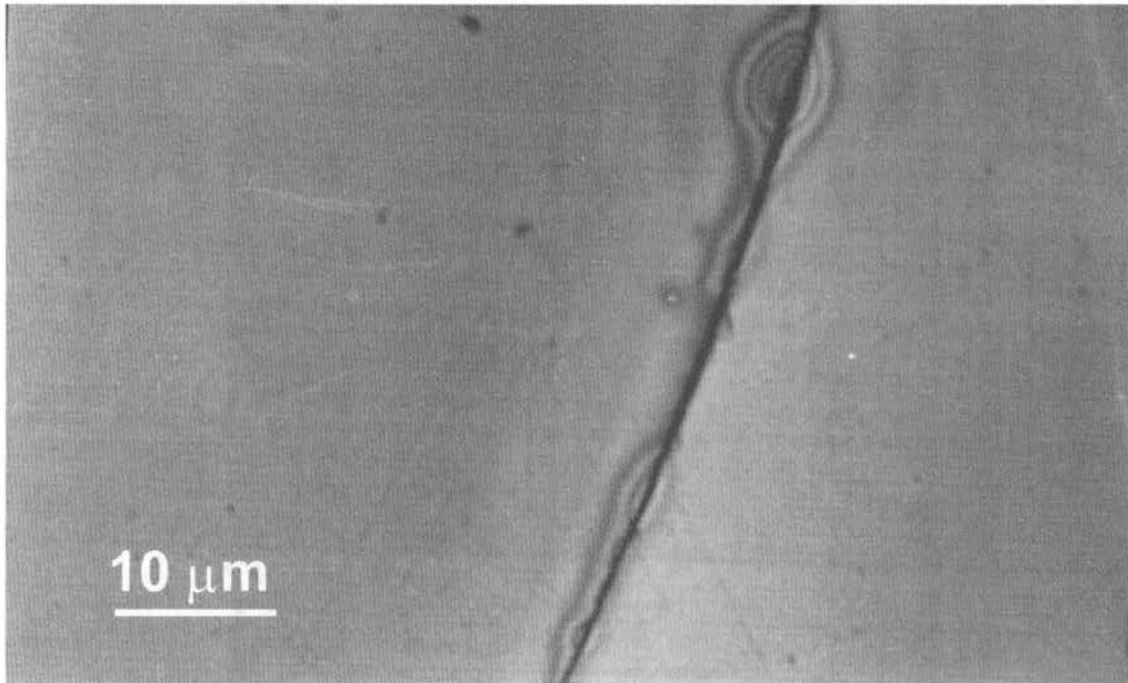


Figure 74. Crack on the surface of a 4.2- μm -thick GaN epilayer grown on sapphire. Cracks are effective scattering centers for in-plane amplified emission.

Effects of Microcracks on the Lasing Characteristics of GaN-Based Structures

Microcracks in GaN-based structures can appear either as a result of cleaving or the natural relaxation of strain between the epilayer and substrate during postgrowth cooling. Cracks formed in this manner have been found to introduce interesting effects on the emission properties of nitrides under high levels of optical excitation, such as high-finesse cavity modes.

Stimulated emission with Fabry-Pérot cavity modes in GaN grown on SiC was first observed by Zubrilov *et al.*⁷⁰ and is shown in Figure 75. The full width at half maximum of the Fabry-Pérot modes was measured to be 0.2-0.5 nm and the distance between fringes was ~ 0.7 nm at room temperature. The cavity length was estimated to be 20 μm , which is much smaller than the sample size. Optical microscopy revealed that the sample had microcracks produced by cleaving. The authors believed that the cracks served as cavity mirrors and generated the Fabry-Pérot modes.

We extended this lasing work to systematically cover GaN/AlGaN separate confinement heterostructures. The sample description was given previously (see page 107). In order to evaluate the effects of cracks, we cleaved our samples into submillimeter-wide bars (note that when GaN is grown on SiC, it can be easily cleaved along the $(11\bar{2}0)$ direction¹¹⁸). Before cleaving, the samples did not exhibit any noticeable defects on the surface. After the cleaving process, however, cracks were observed along all three cleave planes associated with a hexagonal crystal structure, with the majority running parallel to the length of the bar, as shown in Figure 76.

Samples were excited in the edge-emission geometry (342 nm, 6 ns) with an excitation spot in a shape of a line as shown in Figure 32(a). An order of magnitude reduction in the lasing threshold was found in comparison to bulk-like GaN epilayers. In fact, the lasing threshold was measured to be as low as 65 kW/cm² at room temperature for one of the samples.¹⁰³ We believe that such a low lasing threshold of the GaN/AlGaN

separate confinement heterostructure is due to improved carrier and optical confinement as well as increased optical feedback introduced by cracks (see page 111 and Ref. [119]).

When the sample was excited above the lasing threshold, high-finesse cavity modes were observed. Typical emission spectra from a separate confinement heterostructure are shown in Figure 77. We were able to correlate the spacing between the modes to the distance between the cracks depicted in Figure 76. Assuming that the unity round-trip condition is satisfied and there is no loss due to absorption in the GaN layer, the threshold gain can be estimated from:¹¹¹

$$g_{th} > \frac{\ln(R^{-2})}{2L}, \quad (6-1)$$

where R is the mirror reflectivity (20% for a GaN-air interface) and L is the distance between the cracks. We obtained a gain value on the order of 500 cm^{-1} , which is consistent with gain measured by the variable stripe technique.

It was found that by pumping different areas along the length of the bar, the emission exhibited varying degrees of cavity finesse. This is presumably due to the presence of cavities of varying quality formed by parallel cracks running through the active layer. Areas exhibiting high finesse consistently had a narrower far-field pattern than those exhibiting low finesse.

We further note that the high finesse emission exits the sample at an angle of $\phi \sim 18^\circ$, as shown in Figure 78. In order to understand this phenomenon, the samples were examined in cross section using a scanning electron microscope. A large number of cracks were noticed lying at small angles ($\sim 7^\circ$) to the c axis. Taking into account the refractive index of GaN, we were able to correlate the geometry of the cracks to the emission angle through Snell's law.

Thus, the existence of microcracks in GaN-based structures (particularly those grown on SiC) results in many new features when the emission is collected from the sample edge. It significantly affects the directionality, spectral appearance, and lasing threshold. Consequently, one has to take into account the effects of these microstructures to correctly interpret experimental data.

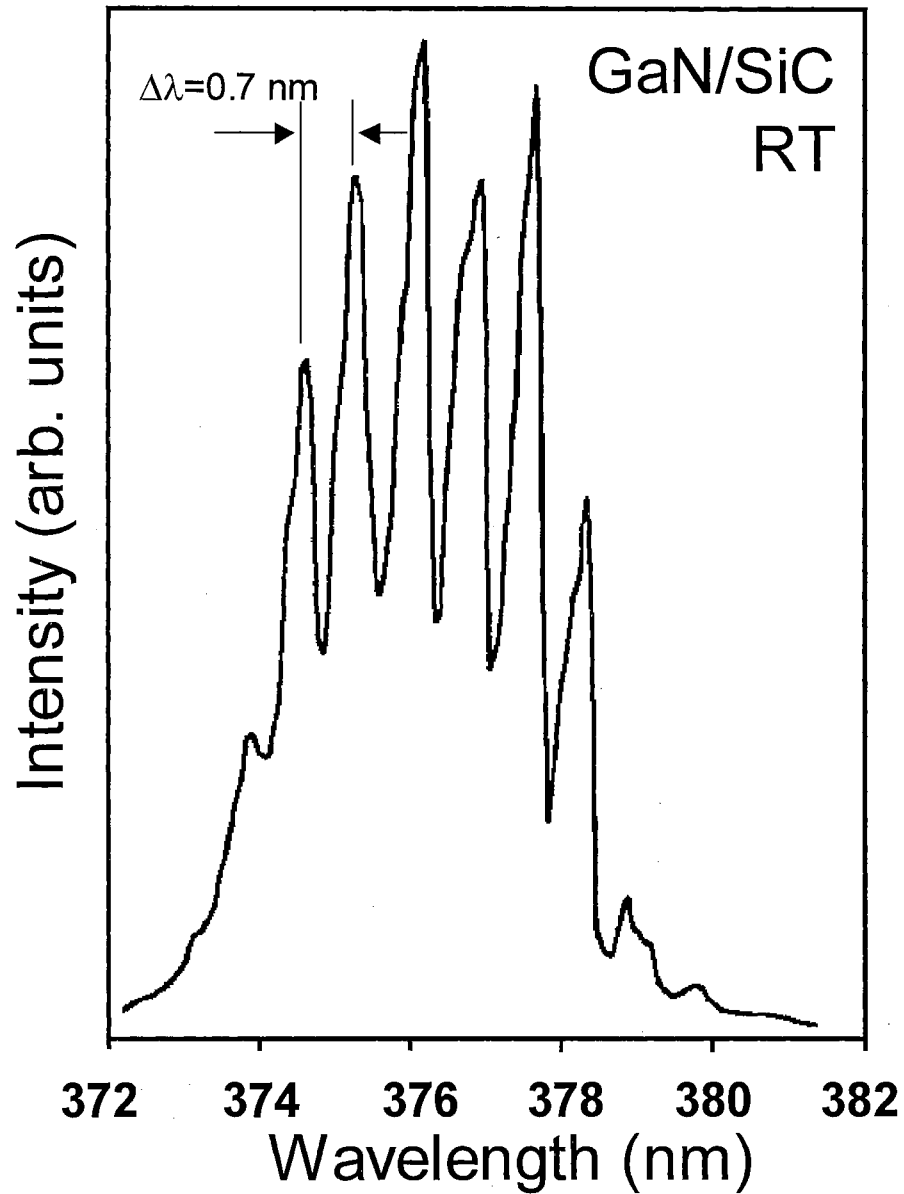


Figure 75. Stimulated emission from a GaN sample grown on SiC at room temperature. Fabry-Pérot modes were clearly resolved. The spectrum corresponds to an excitation pump power density of 5 MW/cm². Adapted from Ref. [70].

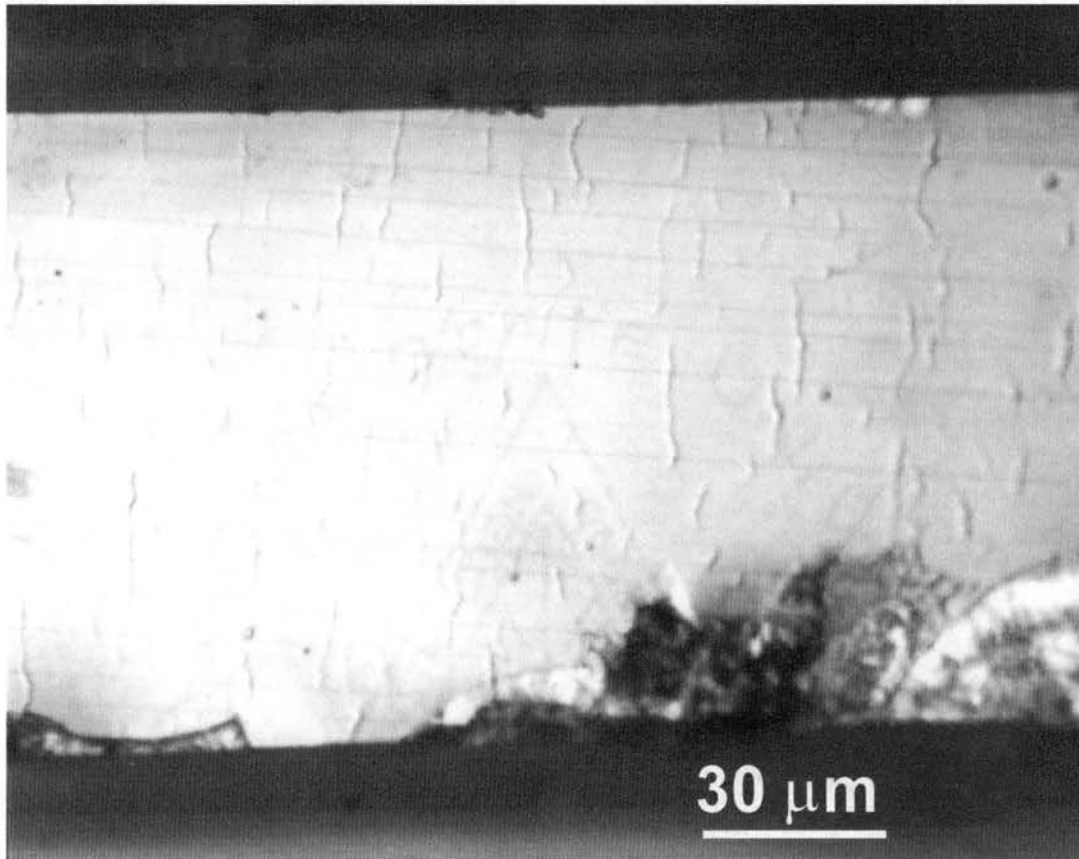


Figure 76. A picture of the sample surface of the GaN/AlGaN separate confinement heterostructure after cleaving. Before cleaving, the sample exhibited no noticeable defects on the surface. After the cleaving process, however, cracks can be seen running parallel to the length of the bar.

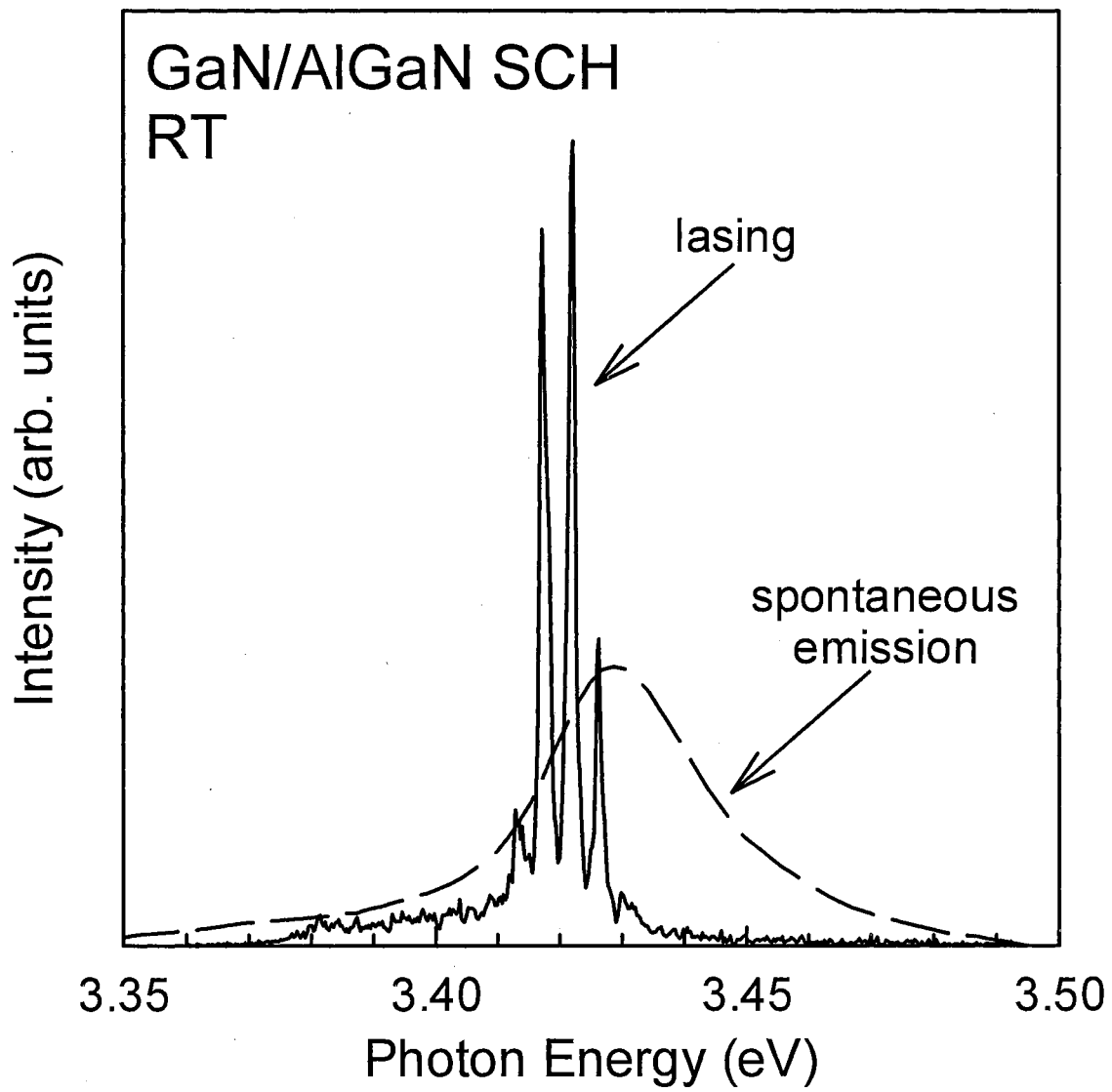


Figure 77. Lasing and spontaneous emission in the GaN/AlGaN separate confinement heterostructure at room temperature. Lasing is believed to be of microcavity origin.

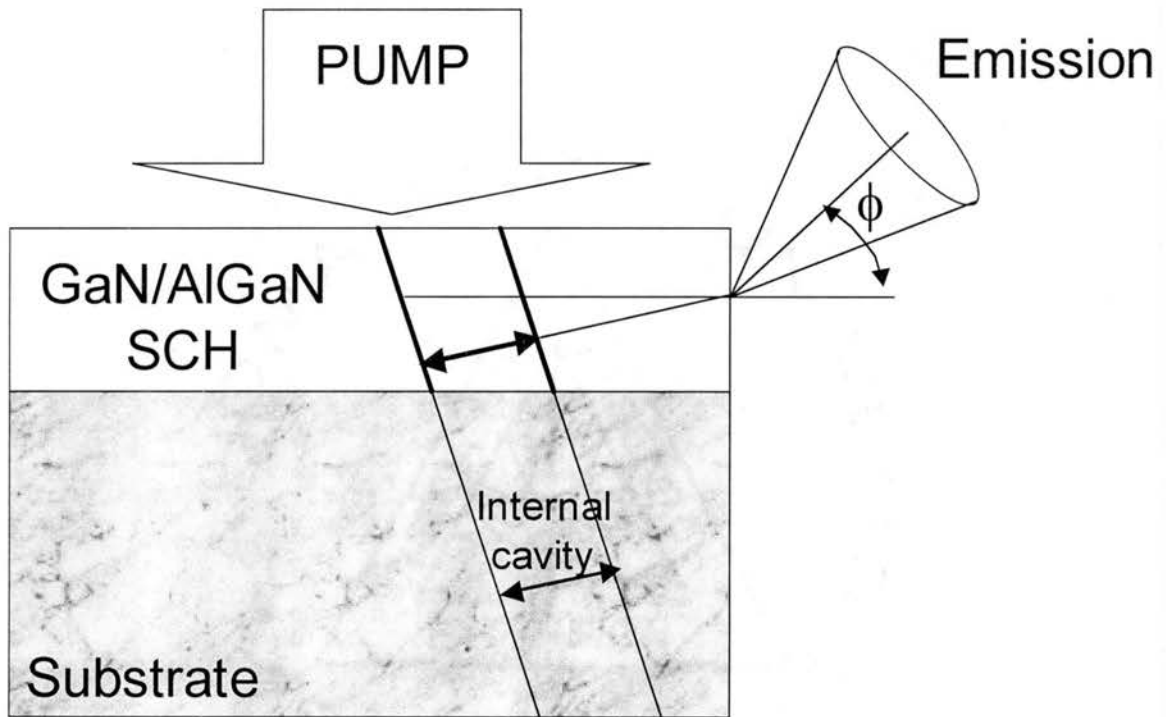


Figure 78. Optical pumping geometry. The high finesse emission exits the sample at a large angle ($\phi \sim 18^\circ$). The cracks in the surface parallel to the cleaved edges ran through the active layer at an inclination consistent with the emission angle observed. Adapted from Ref. [103].

Ring-Cavity Lasing in Laterally Overgrown GaN Pyramids

Microcavity lasers, in addition to vertical cavity surface emitting lasers, offer many benefits resulting from optical confinement, which include an enhanced quantum efficiency and a greatly reduced lasing threshold. Modern growth techniques allow the formation of microcavities with a variety of different geometries. These microcavities can also be arranged to form arrays. These arrays are a natural choice for applications involving optical displays, imaging, scanning, optical parallel interconnects, and ultra-parallel optoelectronics. Furthermore, success in the fabrication of long lifetime cw InGaN edge-emitting laser diodes is largely due to a significant reduction in defects attained by using lateral overgrowth on sapphire substrates.¹²⁰ The selective area growth of wide-band-gap semiconductors is believed to be one of the most important methods to realize high performance laser diodes in the short wavelength region.^{121,122} Because of the large physical dimensions of their resonator cavities (several hundred microns), traditional edge-emitting lasers may only be used for constructing one-dimensional arrays. On the other hand, surface-emitting or microstructure-based lasers¹⁰³ (with a typical cavity of a few microns) could potentially be used for the development of two-dimensional laser arrays.

Our research group was the first to observe single and multi-mode room temperature laser action in GaN pyramids under strong optical pumping. We proposed that the laser cavity in a pyramid is of a ring type, formed by total internal reflections of light off the pyramid surfaces. The mode spacing of the laser emission was correlated to the size of pyramids. The effects of pyramid geometry and pulse excitation on the nature of laser oscillations inside of the pyramids was explained. Finally, we suggested practical applications for the development of light-emitting pixels and laser arrays.

The samples used in this study were grown by low-pressure metal-organic chemical vapor deposition (MOCVD). First, a 0.10- μm -thick AlN buffer layer was deposited on a (111) Si wafer. A GaN layer was subsequently grown, resulting in a

thickness of about 0.15 μm . To prepare samples for selective growth, a 0.1- μm -thick Si_3N_4 masking layer was deposited on the wafer by plasma-enhanced chemical vapor deposition. Arrays of openings were created in this mask by photolithography and reactive ion etching. The openings were arranged in a hexagonal pattern with a spacing of 20 μm , and the average diameter of the openings ranged from 2 to 5 μm depending on the size of pyramids to be grown. GaN regrowth was then performed in the MOCVD reactor with the ammonia flow set at 1.8 slm and the triethylgallium (TEG) flow varying from 1.9 to 5.3 $\mu\text{mol}/\text{min}$ over the course of 3 hours at a temperature of 1050°C. The smaller TEG flow for the initial growth was used to avoid nucleation on the mask. The growth conditions are described elsewhere¹²³ in more detail. The result of the selective lateral overgrowth was a two-dimensional array of GaN pyramids. A scanning electron microscope (SEM) image of one of the samples is shown in Figure 79. The base diameter of the pyramids was estimated to be about 5 and 15 μm for the two different arrays of pyramids, which is considerably larger than the corresponding 2 and 5 μm openings in the mask, indicating substantial lateral growth of the pyramids. Transmission electron microscope pictures revealed a drastic reduction in defect densities.

The samples were mounted on a translation stage that allowed for a 3-D positioning of the sample with ~ 1 micron resolution. The third harmonic of an injection-seeded Q-switched Nd:YAG laser was used as the pumping source. The pulse width of the laser was varied from 5 to 25 ns by adjusting the Q-switch delay. The laser beam was focused to a spot with a diameter of 4 μm through a microscope objective. The laser light intensity was continuously attenuated using a variable neutral density filter. This study was performed in a surface emitting geometry where emission from the sample was collected through the same microscope objective in the direction normal to the sample surface, as shown in Figure 80. Two cross-polarized Glan-laser prisms were used to avoid a leak of the pump beam into the detection system. A 30 \times magnified image of the sample was projected onto the slits of a Spex 1-m spectrometer and the emission spectra were recorded by an optical multi-channel analyzer. The overall spatial resolution of the system was better than 5 μm . This allowed us to pump, image, and spectrally analyze emission from separate pyramids.

Figure 81 shows the room temperature emission spectra for a 15- μm -wide GaN pyramid at several different pump densities near the lasing threshold. Note that these spectra correspond to the emission from a single pyramid. At excitation densities below the lasing threshold, only a spontaneous emission peak with a full width at half maximum (FWHM) of approximately 14 nm is present, as shown in Figure 81(a). The energy position and spectral width of the peak are very similar to that observed from high-quality single-crystal GaN epilayers.⁶⁹ As the pump density is increased to values slightly above the lasing threshold, several equally spaced narrow peaks with FWHMs of less than 0.3 nm appear, as illustrated in Figure 81(b). The position of the peaks remains the same as we further raise the excitation density. Due to the pump density dependence of the effective gain profile, the maximum intensity mode tends to hop to modes with lower energies, as shown in Figure 81(c).

The intensity dependence of the spontaneous and lasing peaks was studied as a function of excitation power. We observed that the intensity of the spontaneous emission peak increases almost linearly with pump density ($I_{\text{spon}} = I_{\text{pump}}^{0.93}$), as illustrated in Figure 82 (open squares) for a 15- μm -wide GaN pyramid. On the other hand, the intensity of the lasing peaks experiences a strong superlinear increase ($I_{\text{lasing}} = I_{\text{pump}}^{2.8}$) with excitation power (open circles). The lasing threshold corresponds to an incident pump density of approximately 25 MW/cm². Such a high value of pump density does not accurately represent the real lasing threshold since most of the pump beam scatters off the surface of the pyramid. In order to estimate the coupling coefficient of the pump beam one has to consider the surface roughness and geometry of each specific pyramid.

Note that the spontaneous emission in Figure 81(a) does not exhibit a mode structure, indicating that it does not come from a laser cavity inside of the pyramid, but rather from the surface. On the other hand, the lasing peaks [as shown in Figure 81(b) and Figure 81(c)] appear to be modes from a high-finesse cavity. The perimeter of either a ring or standing-wave cavity giving rise to these modes, taking into account the dispersion of the refractive index with wavelength, can be evaluated as:¹²⁴

$$p = \frac{\lambda^2}{\left(n - \lambda \frac{dn}{d\lambda}\right) \Delta\lambda} = \frac{\lambda^2}{\bar{n} \Delta\lambda} = 58\mu\text{m}, \quad (6-2)$$

where we have used $\lambda = 370$ nm for the center lasing wavelength, $\Delta\lambda = 0.89$ nm for the mode spacing, and $\bar{n} = n - \lambda \frac{dn}{d\lambda} = 2.65$ for the effective refractive index of GaN at 370 nm (taken from Ref. [125]). The high finesse lasing modes (open circles) were fitted with the assumption of a Gaussian profile. The result of the fit is shown Figure 83 with a solid line. The perimeter of the cavity appears to be several times larger than the diameter of the pyramid base. This result suggests that the photon flux propagating in the cavity undergoes several ($N \geq 4$) reflections inside of the pyramid prior to completing one round-trip.

For a semiconductor laser, the typical turn-on delay time is on the order of nanoseconds.¹²⁶ In addition, the electron and photon populations undergo oscillations before attaining their steady-state values. In practice these oscillations might require additional time (up to 15 ns) to become sufficiently dampened before mode intensities reach their steady-state values.¹²⁷ These initial transients are on the same order as our 6 ns excitation pulse. During the course of the electron and photon population oscillations, a considerable number of lasing modes experience temporary amplification. It is plausible that the observed multi-mode laser action in the GaN pyramids [as shown in Figure 81(c)] is due to the transient conditions associated with short-pulse excitation. To further corroborate this point we note that a large inhomogeneous broadening of the gain region is not expected due to the high structural quality of GaN pyramids.

When the excitation pulse length was increased to ~ 20 ns, along with multimode laser action in the GaN pyramids we could also observe single-mode operation, as shown in Figure 84 for a 15- μm -wide GaN pyramid. As the pump density is increased to values slightly above the lasing threshold, a very narrow peak with a FWHM of less than 0.3 nm appears on the low energy side of the spontaneous emission peak. Note that the FWHM of the stimulated emission peak in high-quality GaN epilayers is typically 2 nm at room temperature. As in the case of multimode operation, the intensity of the peak shown in Figure 84 increases superlinearly with excitation power.

A similar set of experiments was performed on the smaller pyramids. For 5- μm -wide pyramid [Figure 85(b)] the mode spacing increased to approximately 2.2 nm which corresponds to a 23 μm cavity perimeter. The difference in mode spacing for the two pyramids of different sizes is inversely proportional to their physical dimensions [Figure 85(a) and Figure 85(b)].

To understand the geometry of the cavity formed inside of the pyramids we have to consider the limited penetration depth of the pump. We expect that the gain region can only lie in the vicinity of the surface rather than deep in the body of the pyramid. The existence of the highly modulated lasing spectra shown in Figure 83 with such a short gain region suggests that the losses associated with cavity mirror reflectivity and absorption at the lasing wavelength are very small. For multiple reflections, only highly reflective mirrors could provide a reasonable optical feedback. Under normal incidence, a GaN-air interface reflects back approximately $R = 0.2$ of the incident signal. Having N near-normal reflections will result only in $R^N \leq 10^{-3}$ (for $N \geq 4$) of the transmitted signal after one round trip in the cavity, which would require unrealistically high gain in a standing wave cavity with normally oriented end mirrors. Therefore, the cavity inside of the pyramid is most likely of a ring type formed by total internal reflections off the pyramid surfaces. This cavity could potentially lead to a large build-up of the electric field in the pyramid. The collected emission from the sample is believed to be only a scattered fraction of this field, as in the case of the scattered stimulated emission observed in GaN epilayers (see page 141 and 128).

Picosecond time-resolved photoluminescence spectroscopy has been used by other experimental groups to further investigate the optical properties of GaN pyramids.¹²⁹ It was found that (i) the release of the biaxial compressive strain in overgrown GaN pyramids on GaN/AlN/sapphire led to a 7 meV redshift of the spectral peak position with respect to a strained GaN epilayer grown under identical conditions; (ii) in the GaN pyramids on GaN/AlN/sapphire, strong band-edge transitions with much narrower linewidths than those in the GaN epilayer were observed, indicating the improved crystalline quality of the overgrown pyramids; (iii) PL spectra taken from different parts of the pyramids revealed that the top of the pyramid had the highest crystalline quality; and (iv) the presence of strong band-to-impurity transitions in the

pyramids was primarily due to the incorporation of oxygen and silicon impurities from the SiO₂ mask. Studies of the optical modes in a ring-type three-dimensional microcavity formed inside of the pyramids were also reported in the literature.¹³⁰

We further note that the pyramids used in this work are of a much smaller size than conventional edge-emitting LD cavities. Even though efficient carrier injection and coupling of the emission are yet to be developed, these GaN microstructures could potentially be used as pixel elements and as high density two-dimensional laser arrays.^{131,132} The Si substrate used to grow the pyramids might facilitate the integration of GaN microstructures into Si-based electronics.

In summary, we have observed single-mode and multi-mode laser action in GaN pyramids under strong optical pumping at room temperature. The pyramids were individually pumped, imaged, and spectrally analyzed through a high magnification optical system using a high density pulsed excitation source. We suggest that the cavity formed in a pyramid is of a ring type, formed by total internal reflections of light off the pyramid surfaces. The mode spacing of the laser emission was found to be correlated to the size of the pyramids. This study suggests that GaN microstructures could potentially be used as pixel elements and high density two-dimensional laser arrays.

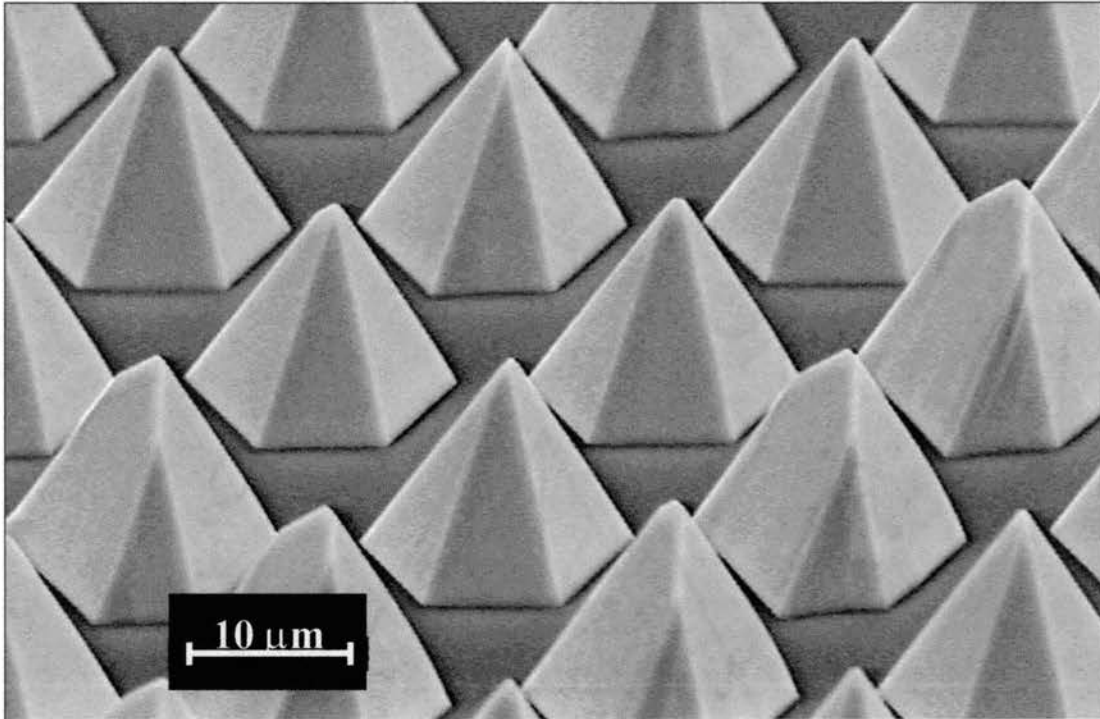


Figure 79. SEM image of GaN pyramids with a 15- μm -wide hexagonal base, grown on a (111) Si substrate by selective lateral overgrowth.

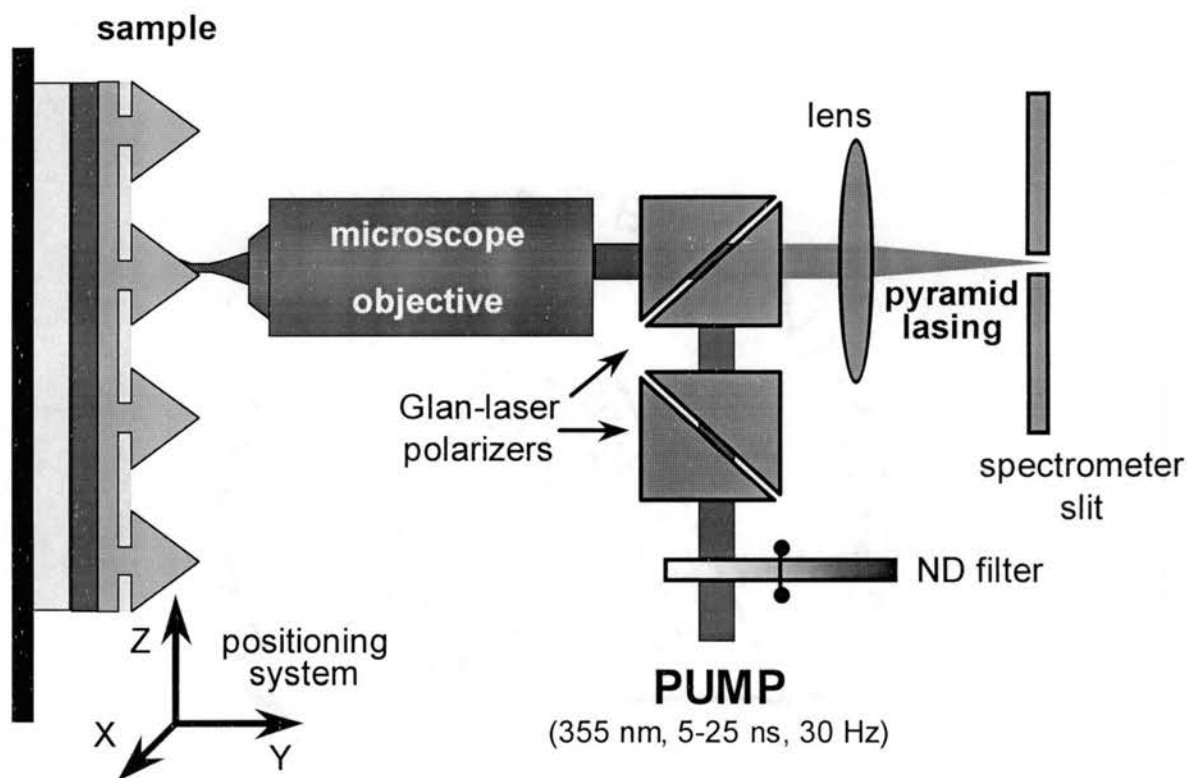


Figure 80. Experimental geometry. The pyramids were individually pumped, imaged, and spectrally analyzed through a high-magnification telescope system. Two cross-polarized Glan-laser prisms were used to avoid a leak of the pump beam into the detection system.

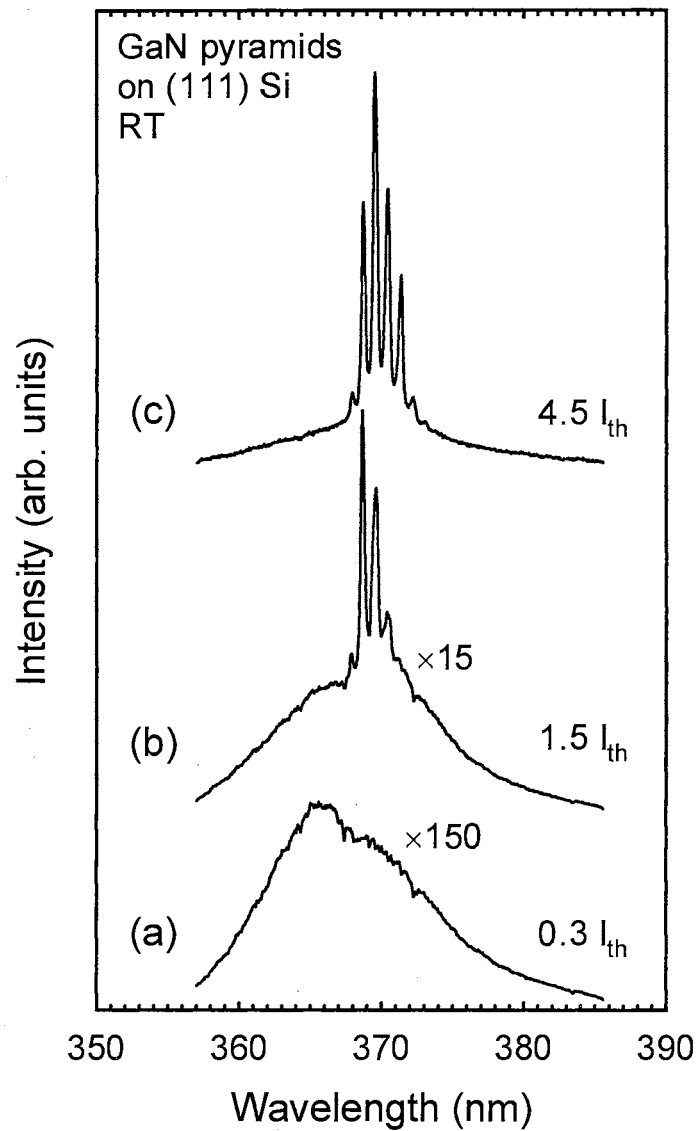


Figure 81. Emission spectra of a 15- μm -wide GaN pyramid under different levels of optical pumping above and below the lasing threshold at room temperature. At pump densities below the lasing threshold only a 14-nm-wide spontaneous emission peak is present, whereas at excitation levels above the lasing threshold multimode laser action is observed.

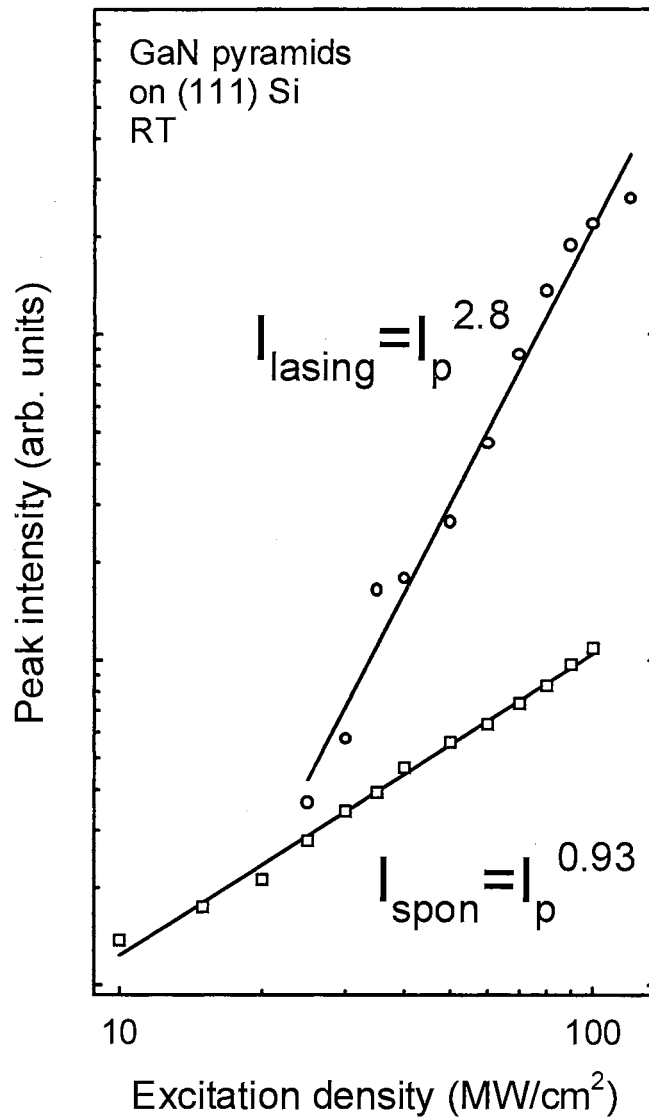


Figure 82. Peak intensity as a function of excitation density. The intensity of the spontaneous emission peak (open squares) increases almost linearly with excitation power. The lasing peak intensity (open circles) exhibits a strong superlinear increase as the pump density is raised. The solid lines represent linear fits to the experimental data.

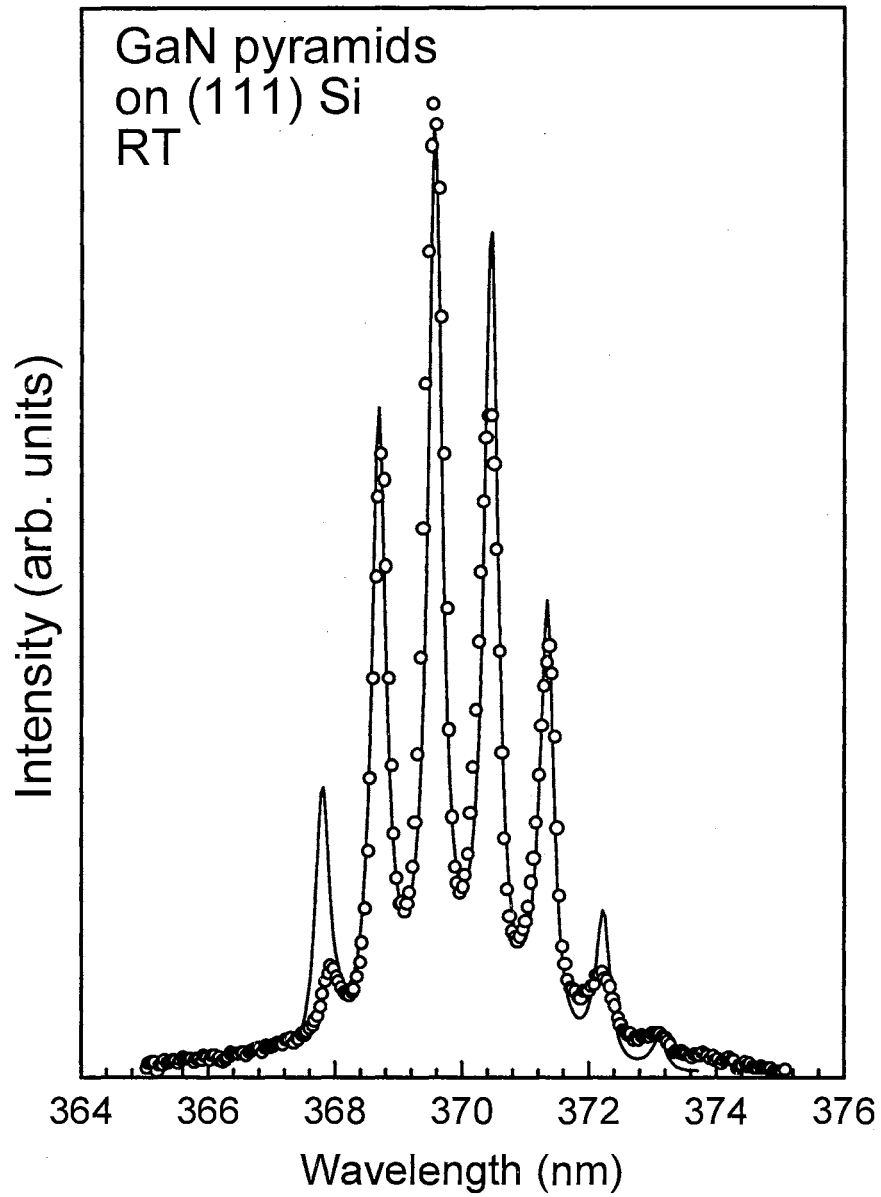


Figure 83. Lasing modes in a 15- μm -wide GaN pyramid. High finesse modes (open circles) were observed when the sample was excited above the lasing threshold. The solid line represents a fit to the experimental data with the assumption of a Gaussian gain profile. The perimeter of the cavity was estimated to be 58 μm .

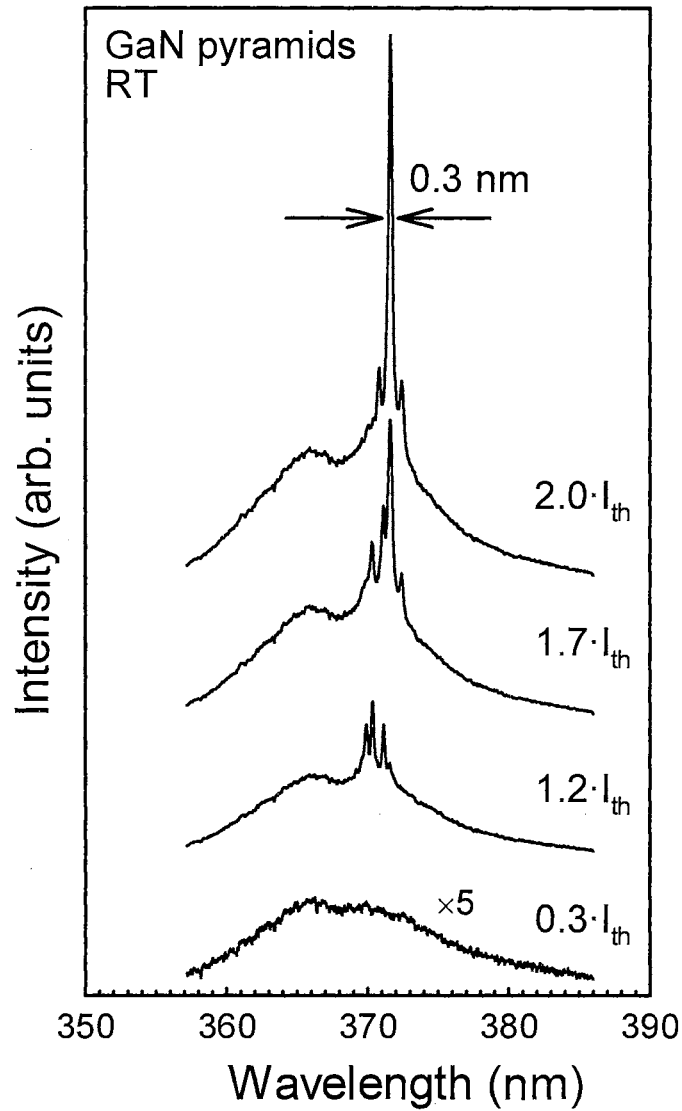


Figure 84. Emission spectra of a 15- μm -wide GaN pyramid under different levels of optical pumping above and below the lasing threshold at room temperature (excitation pulse width is 25 ns). A single-mode laser peak of less than 0.3 nm FWHM was observed when the sample was pumped above the lasing threshold.

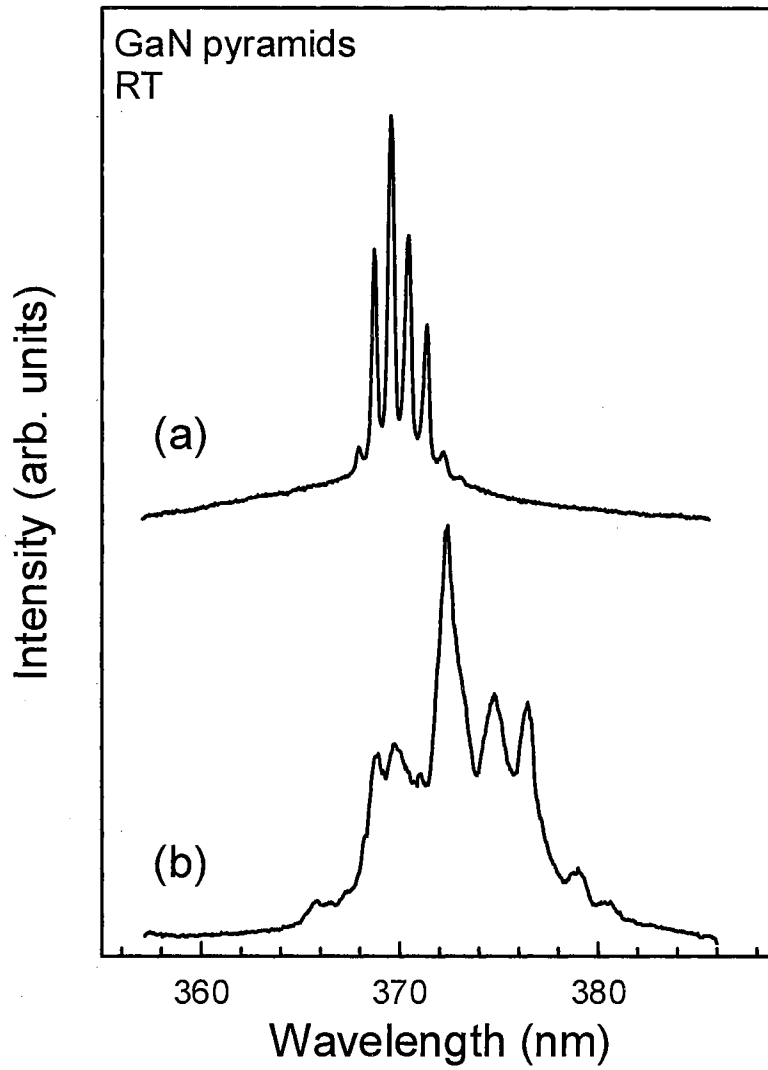


Figure 85. Multi-mode laser action in (a) 15- μm -wide and (b) 5- μm -wide pyramids. The mode spacings correspond to cavities of 58 and 23 μm , respectively.

CHAPTER VII

IMAGING TECHNIQUES FOR WIDE-BAND-GAP SEMICONDUCTORS

In a laser diode it is desirable to have a well-designed laser cavity producing a narrow zero-order transverse mode pattern with smooth transverse amplitude, even phase profiles, and low diffraction losses. It is equally desirable to obtain a laser with the lowest lasing threshold possible. To achieve these objectives the geometry of the laser cavity should be optimized, paying special attention to the waveguiding properties of the confinement layers. This chapter deals with issues related to near- and far-field stimulated emission patterns of GaN-based lasing structures and describes a novel experimental technique for evaluating optical confinement in wide-band-gap semiconductors.

Transverse Lasing Modes in GaN-Based Lasing Structures

The beam properties of a laser diode become critical when it is necessary to couple the laser output into another optical element. For example, a smaller beam divergence can increase the coupling efficiency of a laser diode to an optical fiber. In the DVD optical storage system (and even more so in DVD/HD), it is also necessary to reduce the perpendicular divergence angle to below 25° (see Ref. [133]). However, in the conventional separate confinement heterostructure laser, the tight optical confinement normally results in a large beam divergence in the direction perpendicular to the junction. Such a large transverse beam divergence will lead to a low coupling efficiency and a

highly asymmetric elliptical far-field pattern. To overcome this problem, different structures have been used to expand the size of the transverse electrical field in the optical cavities. This leads to improvements in both the near-field (Fresnel) and far-field (Fraunhofer) regions. However, the decrease of the far-field angle will normally result in a higher threshold current. This higher current can cause power dissipation and heat generation problems which would jeopardize the realization of the much longer lifetime that is essential for commercial applications of laser diodes. Only very limited attention has been paid to strict lateral carrier and photon confinement in InGaN-based laser diodes, since no reliable technique for measuring optical confinement existed.

Current state-of-the-art InGaN/GaN multi-quantum well laser diodes have many problems associated with poor optical confinement. Figure 86 shows the near-field pattern of a laser diode at output powers of 70 and 100 mW taken by a charge-coupled device camera through an optical microscope.¹³⁴ The fundamental transverse mode was observed at output powers below 80 mW, as shown in Figure 86(a). When the output power was increased above 80 mW, the first-order transverse mode appeared, as shown in Figure 86(b). In order to suppress this change, one must force the transverse mode to be the fundamental mode over the entire range of operating currents by further narrowing the ridge width and improving optical confinement.

We performed an intensity analysis of the near- and far-field patterns from InGaN/GaN multi-quantum well structures. The samples were pumped using the 3rd harmonic of an Nd:YAG laser (355 nm, 6 ns). The emission from the sample edge was projected onto a Spiricon CCD camera using a 100× microscope objective with NA=0.9. The signal was averaged over 500 laser pulses and converted into a two-dimensional array of numbers for intensity analysis using a custom-programmed digital filter.

Typical emission intensity profiles when the sample was excited above the stimulated emission threshold are shown in Figure 87. The near-field pattern [Figure 87(a)] resembles a line that lies along the sample surface. However, the far-field pattern bears the signature of a TEM₀₁ mode, consisting of two distinct bright spots. An example of such a pattern taken at a distance of 20 μm from the sample edge is shown in Figure 87(b). We estimated the divergence of the beam in the direction perpendicular to the surface to be ~35°.

In order to confirm our observations, we performed computer simulations. Higher order transverse modes are usually of a Hermite-Gaussian type in rectangular coordinates or Laguerre-Gaussian in cylindrical coordinates.¹³⁵ The preliminary analysis of the far-field pattern depicted in Figure 87(b) suggested that it did not represent the fundamental mode, but rather a higher order TEM mode.

The free-space Hermite-Gaussian TEM_{nm} solutions can be written in the following form:

$$\bar{u}_n(x, z) = \left(\frac{2}{\pi}\right)^{1/4} \left(\frac{\exp[j(2n+1)\psi(z)]}{2^n n! \omega(z)}\right)^{1/2} \times H_n\left(\frac{\sqrt{2}x}{\omega(z)}\right) \exp\left[-jkz - j\frac{kx^2}{2R(z)} - \frac{x^2}{w^2(z)}\right], \quad (7.1)$$

where $\omega(z)$ is the spot size, $\psi(z)$ is the Guoy phase shift, and $R(z)$ is the radius of curvature. The first two (unnormalized) Hermite polynomials are given by:

$$H_0 = 1 \text{ and } H_1(x) = 2x. \quad (7.2)$$

We can use the information given in Eqs. 7-1 and 7-2 to perform a computer simulation of the TEM₀₁ mode. The result of such a modeling is depicted in Figure 88. Note that the computer simulation depicted in Figure 88 closely resembles (at least qualitatively) the far-field pattern shown in Figure 87(b).

Since the far-field pattern observed from the InGaN/GaN multi-quantum well sample is not in the shape of a single Gaussian, we conclude that the fundamental mode (TEM₀₀) could not be observed due to poor optical confinement of the sample emission at excitation densities above the stimulated emission threshold. Thus, further improvement in waveguiding characteristics is needed. Unfortunately, the intensity profiles do not contain information about the depth of the optically confined region, and the “leak” of stimulated emission into the buffer/substrate region is rather difficult to estimate from this technique.

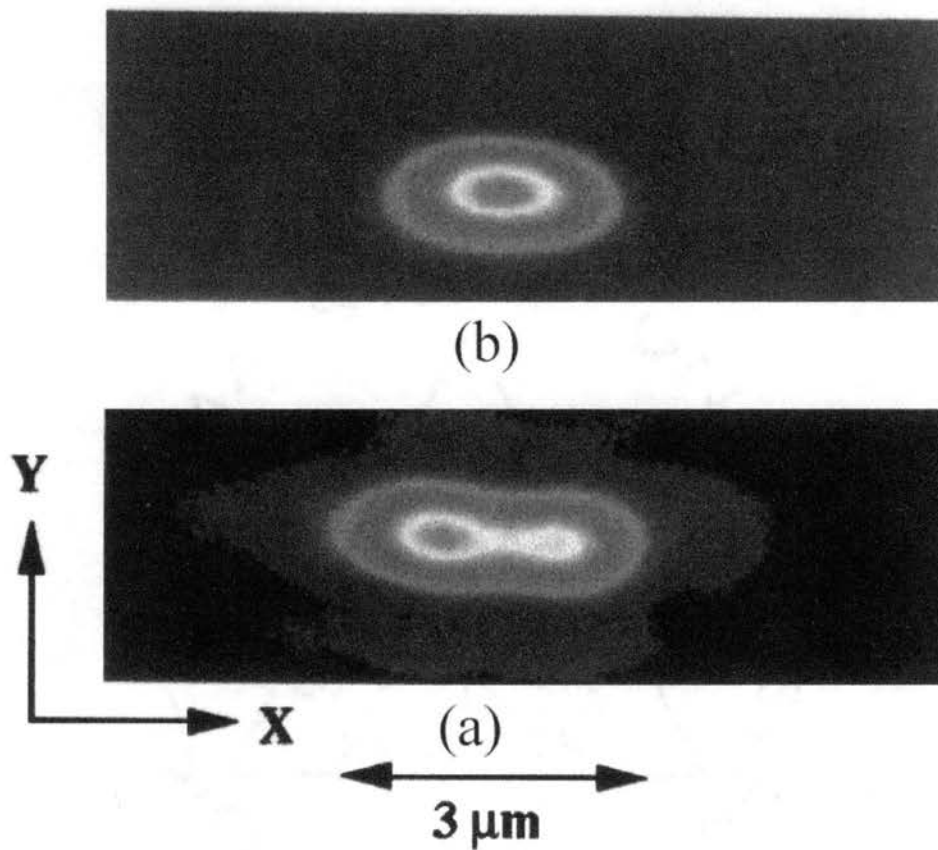


Figure 86. Near-field pattern of InGaN MQW laser diodes at output powers of (a) 70 mW and (b) 100 mW under room temperature cw operation. The X and Y directions are parallel and perpendicular to the junction of the laser diode, respectively. From Ref. [134].

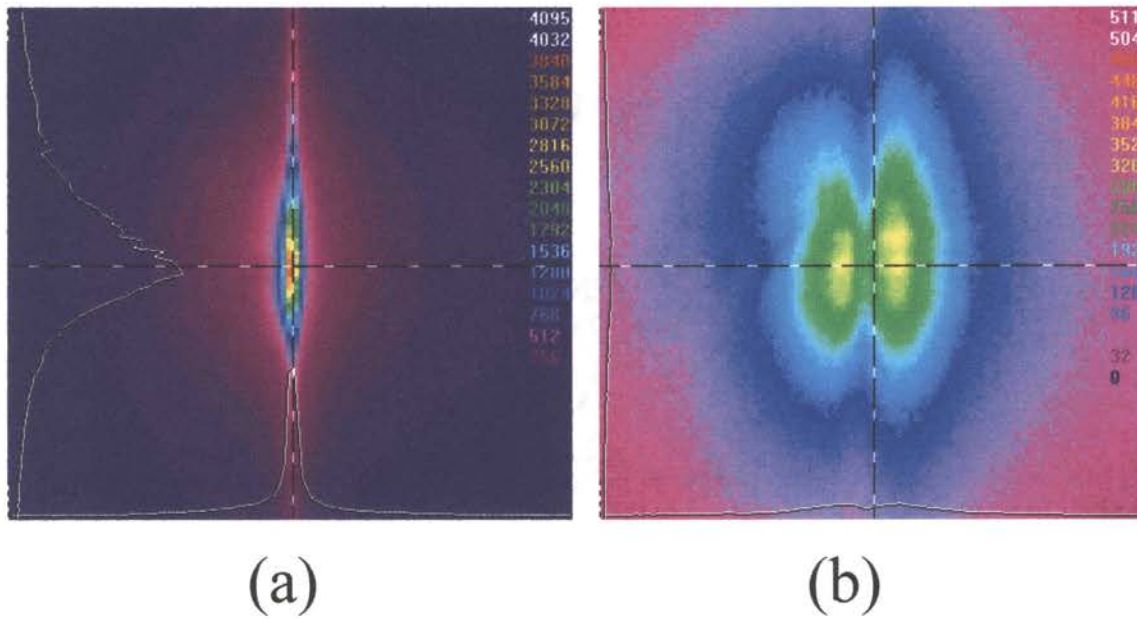


Figure 87. Images of the beam propagation from (a) near-field to (b) 20 μm from the sample taken from an InGaN/GaN MQW sample at room temperature under pulsed excitation. Improvements in optical confinement are necessary to improve the far-field pattern of the laser emission.

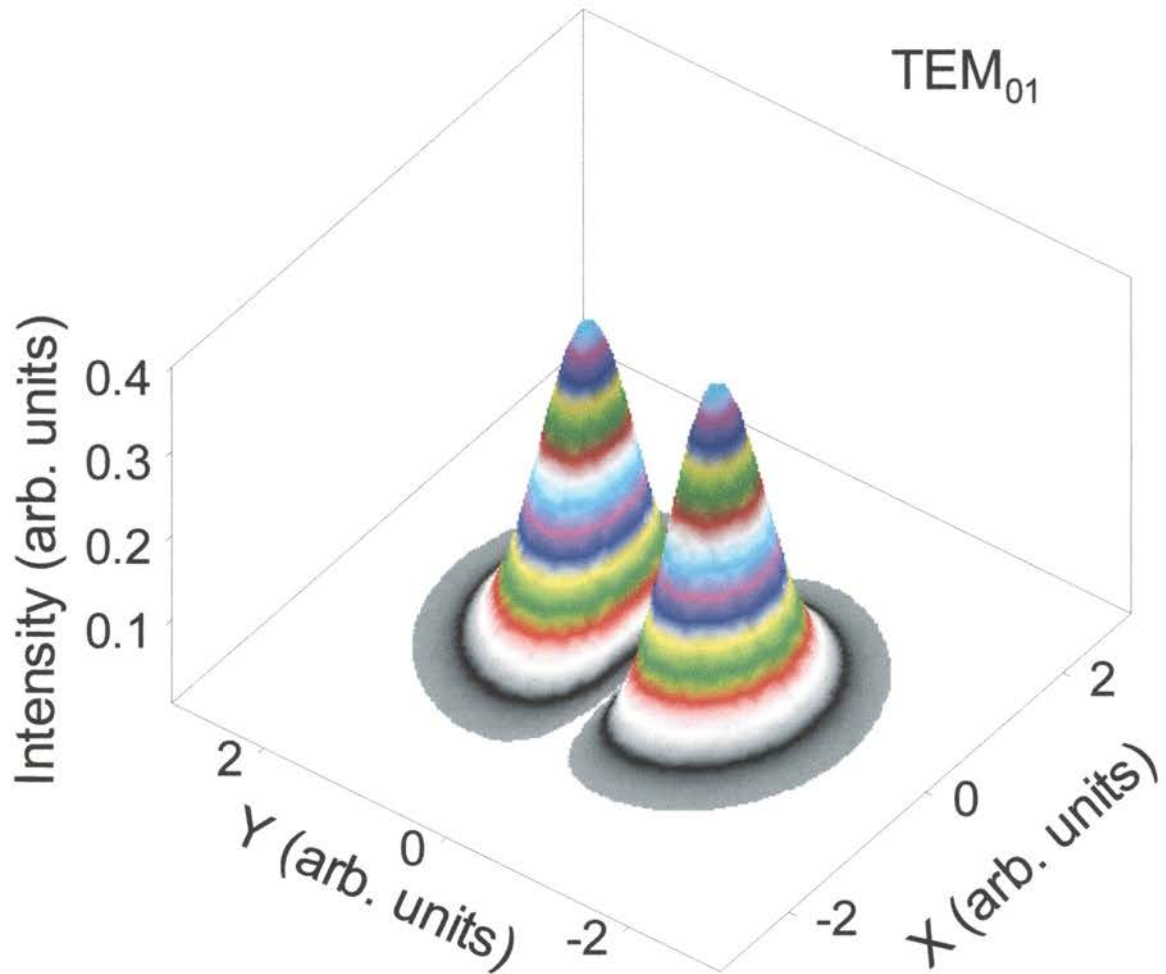


Figure 88. Computer simulation of the TEM₀₁ mode using the Hermite-Gaussian solutions given by Eq. 7-1.

Novel Technique for Evaluating Optical Confinement in GaN-Based Lasing Structures

In December of 1999, the success in the fabrication of room temperature cw violet laser diodes was marked by Nichia's announcement of "engineering sample shipments." However, the realization of longer lifetime and higher power laser diodes for commercial applications was still contingent upon further qualitative improvements to the design of UV and blue laser diodes. Current state-of-the-art LDs cannot efficiently confine the optical field of the fundamental mode at high output powers due to the penetration of the laser radiation from the waveguide region into the GaN substrate region.¹³⁴ In particular, the beam property of an LD is a critical parameter in coupling the output of the laser to other optical elements since it can severely affect the coupling efficiency.¹³⁶

While numerous theoretical models for the evaluation of optical confinement have been given in the literature,¹³⁷ experimental techniques have been limited mostly to measuring the beam divergence and extrapolating to obtain the thickness of the confinement layer under the assumption of Gaussian fields, as was described previously. The limitations of this technique prompted our research group to develop an advanced measurement technique that can resolve the laser emission not only spatially but also spectrally. We successfully achieved this objective by combining positioning and dispersion instruments in a single high-resolution experimental setup. We performed an evaluation of the optical confinement in GaN-based lasing structures by spectrally resolving the near-field pattern observed on the facets of the laser structures. We demonstrated that the confinement layers introduce a unique signature onto the near-band-edge emission spectra that can be used to deduce the optical confinement characteristics. Information extracted through this technique can be applied towards lowering the internal optical losses and improving the transverse beam profile by eliminating optical leakage and the presence of higher order modes.

The experimental configuration of our experimental setup is shown in Figure 89. A tunable dye laser pumped by a frequency-doubled injection-seeded Nd:YAG laser was

used as the primary optical pumping source. The visible output of the dye laser was frequency doubled using a nonlinear crystal to achieve a near-UV pumping frequency. The laser beam was focused with a cylindrical lens into a line on the sample surface (see page 69). The near-field pattern of the emission from the edge of the sample was imaged and spectrally resolved using a high-magnification optical assembly (NA=0.9) in conjunction with a 1-m spectrometer and an optical multi-channel analyzer. The optical assembly was mounted on a translation stage driven by a computer-controlled stepper motor which allowed the microscope objective to be positioned with sub-micron resolution relative to the sample. The spectral resolution of the system was better than 0.1 nm.

The samples used in this study were MOCVD-grown GaN films with thicknesses ranging from 1.7 to 7.2 μm as well as a GaN/AlGaN separate confinement heterostructure (SCH). The details of the sample growth have been described previously (see pages 69 and 107). Experiments were performed at room temperature with excitation power densities of two times the stimulated emission (SE)/lasing thresholds for each sample studied. We note that the SCH exhibited low-threshold lasing at room temperature due to microcavity effects as described in Chapter VI.

We observed drastic changes in the emission spectra for different positions of the sample relative to the microscope objective while exciting samples above the SE/lasing threshold. A 3-D plot of the spectrally and spatially resolved emission from a 7.2- μm -thick GaN epilayer is shown in Figure 90. The horizontal axes represent the emission energy and the position of the microscope objective relative to the active layer. The scanning of the near-field pattern under optical pumping was performed in the growth direction (normal to the sample active layer). The vertical axis indicates the intensity of the sample emission on a logarithmic scale. Utilizing this scanning technique, we could resolve fine spectral features that would otherwise be averaged out in spatially unresolved experiments. 3-D plots obtained in this way contain a substantial amount of information about the optical confinement characteristics of the structure under investigation.

Several different cross sections of the 3-D plot from Figure 90 are shown in Figure 91. When the emission is collected at a significant distance above the surface of

the epilayer [Figure 91(a)], we observe only non-reabsorbed surface-scattered spontaneous emission. As we move the microscope objective closer to the sample surface, a weak stimulated emission peak appears on the low energy side of the spontaneous emission peak [Figure 91(b)]. In this case, the stimulated emission is amplified in-plane and scattered off the sample edge (see page 141 and Ref. [128]). When the optical axis of the objective is aligned with the GaN epilayer, only a strong stimulated emission peak is observed [Figure 91(c)], since spontaneous emission is entirely reabsorbed in the direction parallel to the surface.

The sample emission becomes strongly modulated when it is collected from the sapphire substrate just below the GaN epilayer, as shown in Figure 91(d). This interference pattern results from multiple reflections within the active layer very close to the critical angle for total internal reflection between the epilayer and substrate interface, and the beams emerge at a grazing angle.

In order to understand this phenomenon we have to consider the different refractive indices for the GaN epilayer, sapphire substrate, and air. For simplicity, let's assume the refractive index of GaN to be $n \approx 2.4$. In general, however, we should account for the dispersion of the refractive index with wavelength, since stimulated emission is by its very nature close to the GaN band-gap. The photon flux propagating inside the GaN epilayer will be totally internally reflected off the GaN-air interface for angles larger than 25° . For the GaN-sapphire interface the incident angle has to be as steep as 49° in order for the beam to be totally reflected (assuming the refractive index of sapphire to be $n \approx 1.8$). Thus, for angles slightly below 49° , the photon flux is totally reflected off the air-GaN interface and is almost totally reflected off the sapphire-GaN interface, as shown in Figure 92. Some of this light will be scattered off the sapphire-GaN interface and emerges at a grazing angle. This is the signal that is picked up by our apparatus and depicted in Figure 91(d).

Therefore, this spatially resolved emission bears a spectral signature that can be used to deduce optical confinement characteristics. Combined with the near-band-edge dispersion of the GaN refractive index,¹³⁸ this interference pattern can be used to obtain the thickness of the layer to which the emission is confined. In the simplest case (a GaN epilayer), the fit of the experimental data into a tilted cavity Fabry-Pérot equation¹³⁹

yields the thickness of the epilayer. This has been confirmed to a high degree of accuracy in a variety of GaN samples, as illustrated in Figure 93.

We further extended our work to cover GaN/AlGaN SCH samples, as shown in Figure 94. Besides a strong lasing peak at 3.42 eV, weak modulated emission was observed in the low-energy spectral region of 3.31-3.40 eV. The observed mode spacing suggests that the modulated emission is due to the photon flux leaking from the waveguide region into the GaN buffer region, as depicted in Figure 95.

A qualitative analysis of optical confinement can be given by further analyzing the data obtained by means of the technique described in this chapter. Since the edge emission is spectrally resolved, we can separately calculate the spectrally integrated intensity of the emission leaking into the buffer or substrate layers (I_{leak}) and the spectrally integrated intensity of SE/lasing ($I_{\text{SE/lasing}}$) for each position z of the microscope objective relative to the sample edge. We can extend the analysis by spatially integrating the SE/lasing and leak intensities and evaluating the ratio of the integrals:

$$\Omega = \frac{\int I_{\text{SE/lasing}}(z) dz}{\int I_{\text{leak}}(z) dz} \quad (7-3)$$

In general, Ω will depend not only on the degree of optical confinement but also on excitation power. Thus, it is necessary to maintain the power at the same level relative to the SE/lasing threshold for each of the samples. For the two spectra shown in Figure 90 and Figure 94, the ratios were found to be $\Omega = 4$ and 10 for a GaN epilayer and a GaN/AlGaN SCH sample, respectively. The higher ratio corresponds to a higher degree of optical confinement.

Optical confinement has a significant effect on the lasing threshold and transverse beam profile of laser diodes. The technique described in this work introduces a way to directly compare the quality of optical confinement in GaN-based lasing structures through the analysis of both spectrally and spatially resolved emission. By comparing the mode spacing as well as the intensity ratio of the emissions, one gains insight into both the amount of emission leak and the layer thicknesses.

To summarize, in this chapter we have introduced a novel technique for evaluating the optical confinement in GaN-based lasing structures by studying their

spectrally resolved near-field pattern under high optical excitation. The emission spectra vary greatly with the position of the collection optics relative to the active layer when the sample is excited above the lasing threshold. The spatially resolved spectra contain a modulation signature that can be used to evaluate the optical confinement characteristics. This technique can provide valuable data that will help improve the transverse beam profile of GaN-based lasing structures.

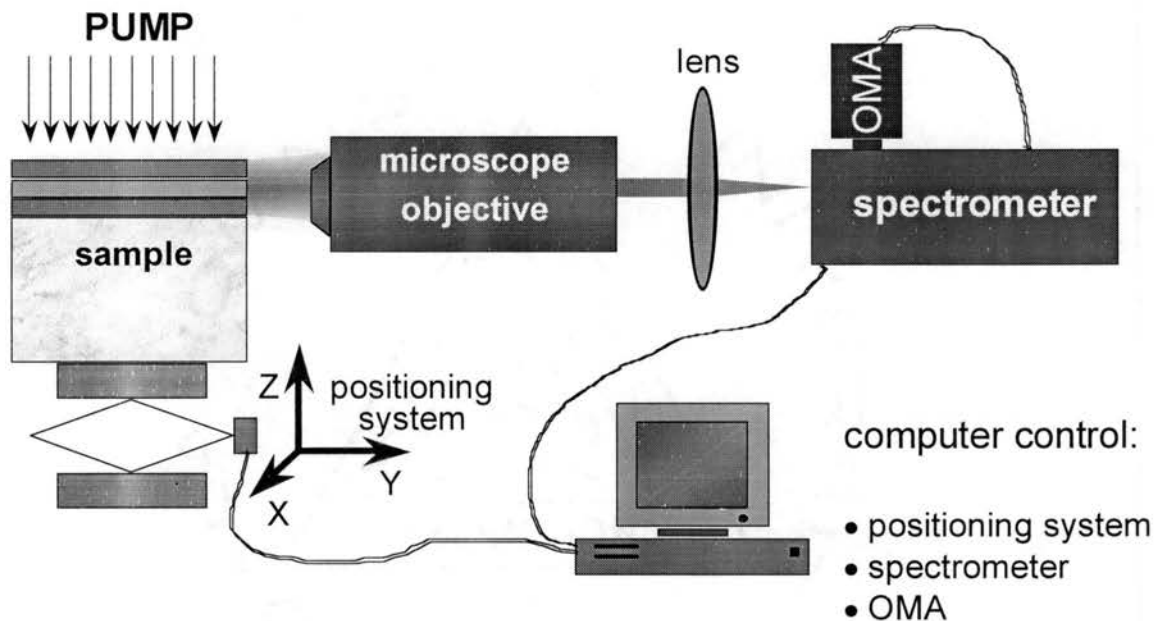


Figure 89. Experimental configuration. A microscope assembly (NA=0.9) was used to project the image of the sample onto the spectrometer slits. The microscope assembly was mounted on a translation stage with submicron resolution for scanning the sample perpendicular to the active layer.

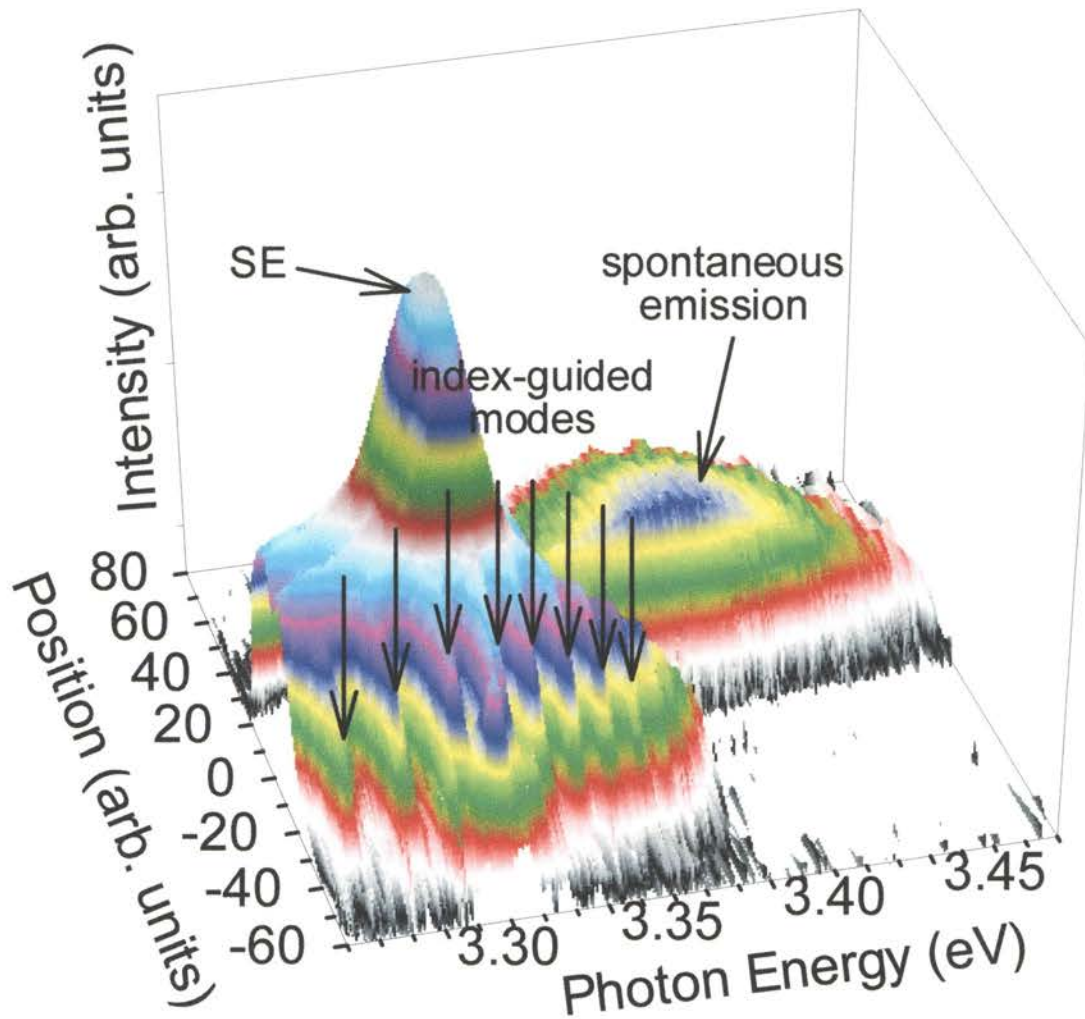


Figure 90. Spatially resolved emission spectra from a 7.2-μm-thick GaN epilayer at excitation densities above the SE threshold. The horizontal axes indicate the emission photon energy and position of the microscope objective relative to the sample active layer. The vertical axis is the emission intensity plotted on a logarithmic scale.

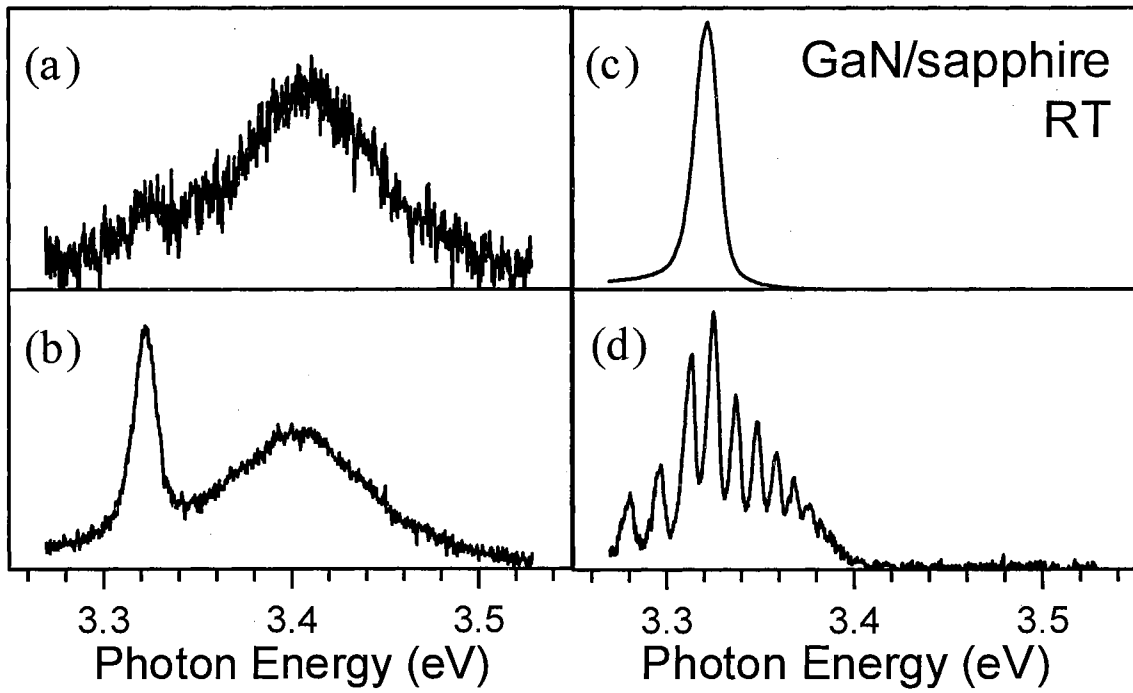


Figure 91. Cross sections of the 3-D plot shown in Figure 90 taken at (a) substantially above the GaN epilayer, (b) slightly above the epilayer, (c) in line with the epilayer, and (d) slightly below the epilayer.

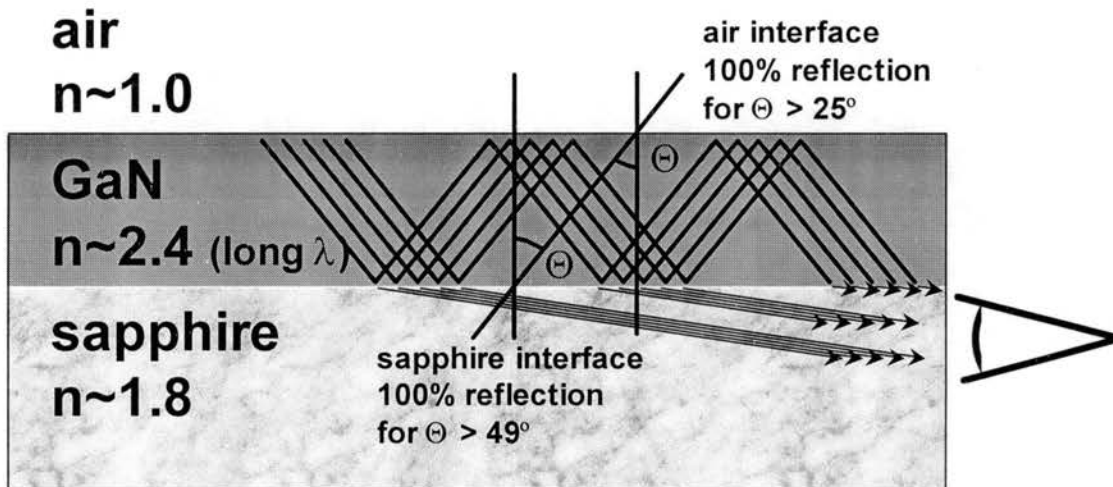


Figure 92. Formation of an interference pattern in a GaN epilayer. The difference in refractive indices for air, sapphire, and GaN creates a tilted Fabry-Pérot cavity.

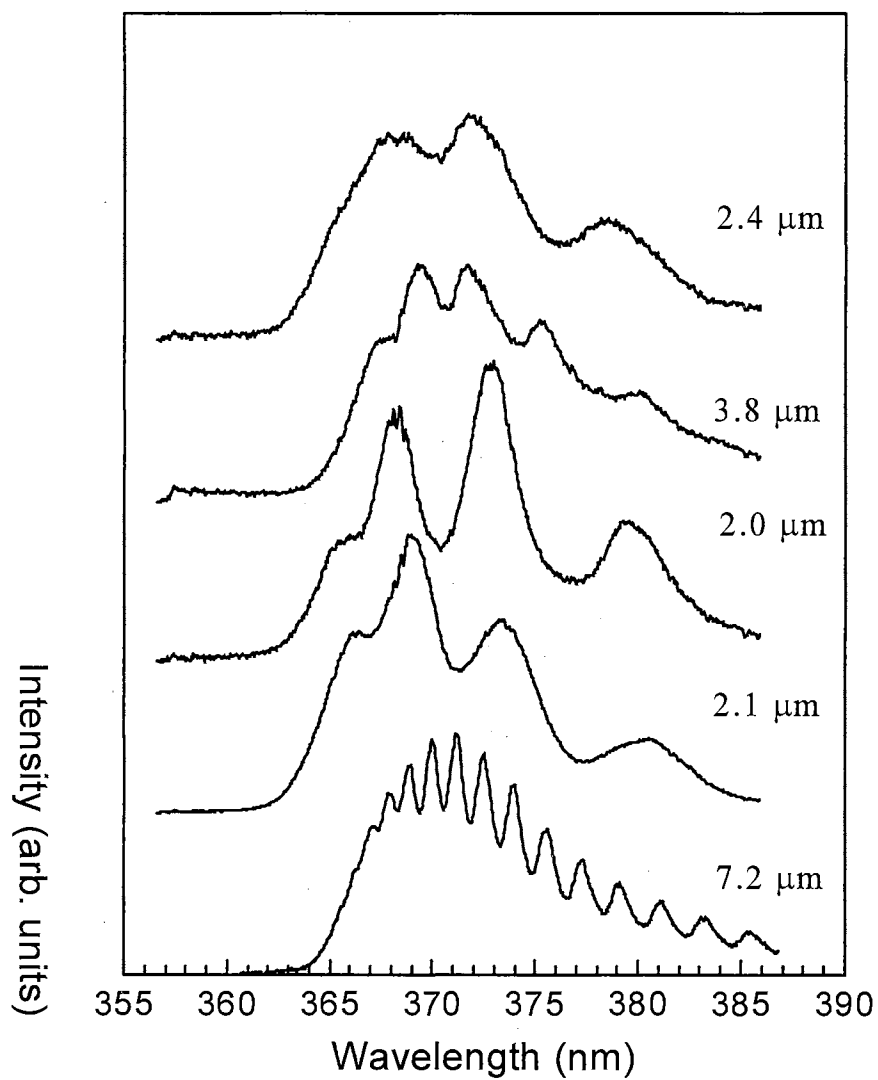


Figure 93. Edge emission from GaN epilayers with different thicknesses. Emission was taken with a microscope objective positioned slightly below the GaN epilayer. The spatially and spectrally resolved measurement technique gives precise information on the thicknesses of the epilayers.

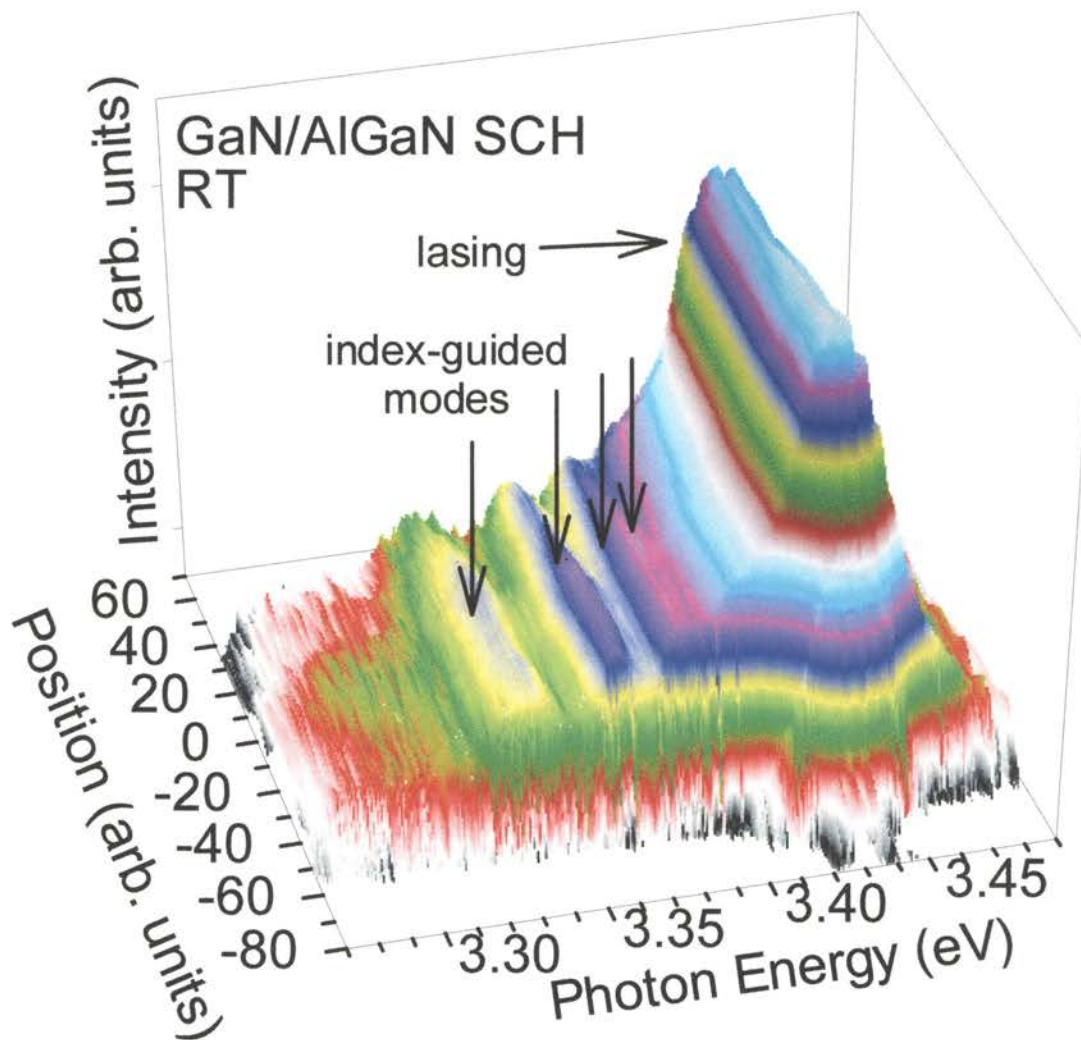


Figure 94. Spatially resolved emission spectra from a GaN/AlGaN SCH at excitation densities above the lasing threshold. Index guided modes appearing on the lower energy side of the lasing peak indicate a leak of emission from the waveguide region to the GaN substrate region.

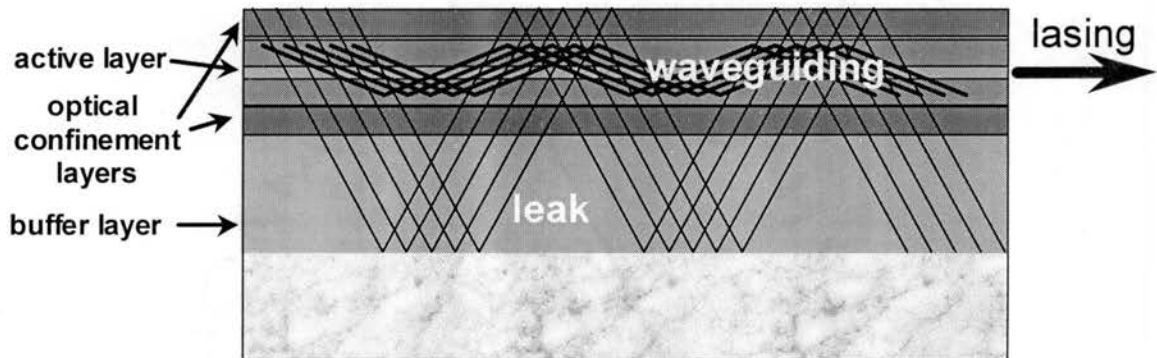


Figure 95. Mechanism of optical confinement and leak in a GaN/AlGaN separate confinement heterostructure. The observed mode spacing in Figure 94 suggests that the modulated emission is due to the photon flux leaking from the waveguide region into the GaN buffer region.

CHAPTER VIII

SUMMARY

Many aspects of the group-III nitrides have not been thoroughly explored yet. This thesis has hopefully answered many issues related to gain mechanisms, microstructure lasing, imaging, and high-temperature optical properties of this material system, as well as provided some background information on the general properties of group-III nitrides.

In this monograph the observation of stimulated emission in GaN at temperatures as high as 700 K was reported and issues pertinent to sample degradation were addressed. Stimulated emission at such high temperatures has never been observed in any semiconductor system. By raising the temperature from 300 K to 700 K we achieved a “tuning” of the stimulated emission peak in GaN from the near-UV spectral region to blue (a range of more than 40 nm). This unique property of stimulated emission might result in new types of optoelectronic devices utilizing this temperature tuning. We also studied stimulated emission in InGaN/GaN multi-quantum wells at elevated temperatures. The low sensitivity of the stimulated emission threshold was clearly demonstrated. This creates opportunities for the development of light-emitting devices capable of high-temperature operation.

In this monograph we reported the gain mechanisms in GaN epilayers over the temperature range of 20 to 700 K. We observed that for temperatures below 150 K the dominant near-threshold gain mechanism is inelastic exciton-exciton scattering, characterized by a low stimulated emission threshold. For temperatures exceeding 150 K the dominant gain mechanism was shown to be electron-hole plasma recombination,

characterized by a relatively high stimulated emission threshold and a large separation between spontaneous and stimulated emission peaks.

We also achieved efficient lasing in optically pumped GaN/AlGaN separate confinement heterostructures with the shortest emission wavelength reported to date. Remarkably low values of the lasing threshold were measured over a wide temperature range. Through an analysis of the relative shift between spontaneous and lasing peaks, combined with the temperature dependence of the lasing threshold, we demonstrated that exciton-exciton scattering is the dominant gain mechanism leading to low-threshold ultraviolet lasing over the entire temperature range studied.

We have systematically investigated both the spontaneous and stimulated emission properties of InGaN/GaN multi-quantum well structures and InGaN epilayers. Our findings were explained in the context of localization of photogenerated carriers associated with strong potential fluctuations in the InGaN active region. We believe that the efficiency of the state-of-the-art blue laser diode and the origin of gain is due to potential fluctuations of indium in the active layers.

Gain mechanisms in AlGaN alloys were also studied in the temperature range of 10 K to 300 K. Through a careful analysis of the carrier densities we concluded that stimulated emission occurs at densities significantly above the Mott density, and consequently, the origin of gain was attributed to an electron-hole plasma recombination.

By studying the origin of surface-emitted stimulated emission in GaN epilayer films we have resolved a long lasting controversy in GaN research. Based on our experimental observations, we clearly demonstrated that the surface-emitted stimulated emission reported by several groups is not vertically amplified emission, but rather is due to a scattering of the photon flux propagating parallel to the surface by defects. These results show that the influence of imperfections in GaN epilayers cannot be ignored when determining gain values from experiment, and may be one of the reasons that there are large discrepancies in the gain values measured in different experimental geometries. The existence of microcracks in GaN-based structures (particularly those grown on SiC) affects the directionality, spectral appearance, and the threshold of lasing. Consequently, one has to take into account the effects of these microstructures to correctly interpret experimental data.

For the first time, we reported the observation of single-mode and multi-mode laser action in GaN pyramids under strong optical pumping at room temperature. We suggested that the cavity formed in a pyramid is of a three-dimensional ring type, introduced by total internal reflections of light off the pyramid surfaces. This study suggested that GaN microstructures could potentially be used as pixel elements and high density two-dimensional laser arrays.

Finally, we described the intensity profiles for far-field emission from InGaN/GaN multi-quantum well samples. We showed that good carrier and optical confinement are critical in order to maintain the fundamental Gaussian mode. We have introduced a novel technique for evaluating the optical confinement in GaN-based lasing structures by studying their spectrally resolved near-field pattern under high optical excitation. This new technique could provide help in improving the transverse beam profile of GaN-based lasing structures.

Much of the research on group-III nitrides is still in progress. This thesis gives only an up-to-date summary of research projects undertaken by the author. The results reported in this monograph are directed towards future applications and aimed at explaining high-density carrier phenomena observed in this material system.

BIBLIOGRAPHY

1. J. Y. Duboz, Oral presentation at 3rd Int. Conf. Nitride Semicond., **Mo_01**, Montpellier, France (1999).
2. S. Bidnyk, B. D. Little, Y. H. Cho, J. Krasinski, J. J. Song, W. Yang, and S. A. McPherson, *Appl. Phys. Lett.* **73**, 2242 (1998).
3. S. Nakamura and G. Fasol, "*The Blue Laser Diode*," (Springer, New York, 1997), pp. 7-9.
4. A. J. Steckl and J. M. Zavada, *MRS bulletin* **24** (9), 33 (1999).
5. Z. Huang, D. B. Mott, and P. K. Shu, *Tech Briefs* **23** (10), 50 (1999).
6. W. Yang, T. Nohava, S. Krishnankutty, R. Torreano, S. McPherson, and H. Marsh, *Appl. Phys. Lett.* **73**, 978 (1998).
7. S. Bidnyk, B. D. Little, T. J. Schmidt, Y. H. Cho, J. Krasinski, J. J. Song, B. Goldenberg, W. G. Perry, M. D. Bremser, and R. F. Davis, *J. Appl. Phys.* **85** (3), 1792 (1999).
8. S. Bidnyk, T. J. Schmidt, Y. H. Cho, G. H. Gainer, J. J. Song, S. Keller, U. K. Mishra, and S. P. DenBaars, *Appl. Phys. Lett.* **72** (13), 1623 (1998).
9. R. Dingle, K. L. Shaklee, R. F. Leheny, and R. B. Zetterstrom, *Appl. Phys. Lett.* **19**, 5 (1971).
10. I. Akasaki, H. Amano, S. Sota, H. Sakai, T. Tanaka, and M. Koike, *Jpn. J. Appl. Phys.* **34**, L1517 (1995).
11. H. Amano, M. Kito, K. Hiramatsu, and I. Akasaki, *Jpn. J. Appl. Phys.* **28**, L2112 (1989).
12. S. Nakamura, M. Senoh, S. Nagahama, N. Iwasa, T. Yamada, T. Matsushita, H. Kiyoku, and Y. Sugimoto, *Jpn. J. Appl. Phys.* **35**, L74 (1996).

13. S. Nakamura, M. Senoh, S. Nagahama, N. Iwasa, T. Yamada, T. Matsushita, H. Kiyoku, and Y. Sugimoto, *Jpn. J. Appl. Phys.* **35** L217 (1996).
14. S. Nakamura, M. Senoh, S. Nagahama, N. Iwasa, T. Yamada, T. Matsushita, H. Kiyoku, and Y. Sugimoto, *Appl. Phys. Lett.* **68**, 2105 (1996).
15. S. Nakamura, M. Senoh, S. Nagahama, N. Iwasa, T. Yamada, T. Matsushita, H. Kiyoku, and Y. Sugimoto, *Appl. Phys. Lett.* **68**, 3269 (1996).
16. S. Nakamura, M. Senoh, S. Nagahama, N. Iwasa, T. Yamada, T. Matsushita, Y. Sugimoto, and H. Kiyoku, *Appl. Phys. Lett.* **69**, 1568 (1996).
17. I. Akasaki, S. Sota, H. Sakai, T. Tanaka, M. Koike, and H. Amano, *Electron. Lett.* **32**, 1105 (1996).
18. S. Nakamura, M. Senoh, S. Nagahama, N. Iwasa, T. Yamada, T. Matsushita, Y. Sugimoto, and H. Kiyoku, *Appl. Phys. Lett.* **69**, 3034 (1996).
19. K. Itaya, M. Onomura, J. Hishio, L. Sugiura, S. Saito, M. Suzuki, J. Rennie, S. Nunoue, M. Yamamoto, H. Fujimoto, Y. Kokubun, Y. Ohba, G. Hatakoshi, and M. Ishikawa, *Jpn. J. Appl. Phys.* **35**, L1315 (1996).
20. S. Nakamura, M. Senoh, S. Nagahama, N. Iwasa, T. Yamada, T. Matsushita, Y. Sugimoto, and H. Kiyoku, *Appl. Phys. Lett.* **69**, 4056 (1996).
21. S. Nakamura, M. Senoh, S. Nagahama, N. Iwasa, T. Yamada, T. Matsushita, Y. Sugimoto, and H. Kiyoku, *Appl. Phys. Lett.* **70**, 868 (1997).
22. S. Nakamura, M. Senoh, S. Nagahama, N. Iwasa, T. Yamada, T. Matsushita, Y. Sugimoto, and H. Kiyoku, *Appl. Phys. Lett.* **70**, 1417 (1997).
23. S. Nakamura, M. Senoh, S. Nagahama, N. Iwasa, T. Yamada, T. Matsushita, Y. Sugimoto, and H. Kiyoku, *Appl. Phys. Lett.* **70**, 2753 (1997).
24. S. Nakamura, *MRS Internet J. Nitride Semiconductor Res.* **2**, Article 5 (1997).
25. G. E. Bulman, K. Doverspike, S. T. Sheppard, T. W. Weeks, H. S. Kong, H. M. Dieringer, J. A. Edmond, J. D. Brown, J. T. Swindell, and J. F. Schetzina, *Electron. Lett.* **33**, 1556 (1997).
26. Cree Inc, Press release from PR Newswire on July 29 (1997).

27. S. Nakamura, M. Senoh, S. Nagahama, N. Iwasa, T. Yamada, T. Matsushita, H. Kiyoku, Y. Sugimoto, T. Kozaki, H. Umemoto, M. Sano, and K. Chocho, *Appl. Phys. Lett.* **72**, 211 (1998).
28. M. P. Mack, A. Abare, M. Aizcorbe, P. Kozodoy, S. Keller, U. K. Mishra, L. Coldren, and S. DenBaars, *MRS Internet J. Nitride Semiconductor Res.* **2**, Article 41 (1997).
29. A. Kuramata, K. Domen, and T. Tanahashi, *Appl. Phys. Lett.* **72**, 1359 (1998); oral presentation at ICNS, Tokushima, Japan (1997).
30. F. Nakamura, oral presentation at ICNS, Tokushima, Japan (1997).
31. S. Nakamura, oral presentation at MRS Fall Meeting, Boston, USA (1997).
32. L. Sugiura, Toshiba, oral presentation at MRS Fall Meeting, Boston, USA (1997).
33. M. P. Mack, oral presentation at MRS Fall Meeting, Boston, USA (1997).
34. M. Kneissl, D. P. Bour, N. M. Johnson, L. T. Romano, B. S. Krusor, R. Donaldson, J. Walker, and C. Dunnrowicz, *Appl. Phys. Lett.* **72**, 1539 (1998); Oral presentation at ICNS, Tokushima, Japan (1997).
35. SDL Inc, Press release from PR Newswire on February 13 (1998).
36. S. Nakamura, M. Senoh, S. Nagahama, N. Iwasa, T. Yamada, T. Matsushita, H. Kiyoku, Y. Sugimoto, T. Kozaki, H. Umemoto, M. Sano, and K. Chocho, *Appl. Phys. Lett.* **72**, 2014 (1998).
37. T. Nishida and N. Kobayashi, *Proc. 3rd Int. Conf. Nitride Semicond.* 90, Montpellier (1999).
38. K. P. O'Donnell, "*Group III Nitride semiconductor compounds: physics and applications*," edited by B. Gil, (Clarendon Press, Oxford, 1998), pp. 1-18.
39. J. J. Song and W. Shan, "*Group III Nitride semiconductor compounds: physics and applications*," edited by B. Gil, (Clarendon Press, Oxford, 1998), pp. 182-241.
40. M. Tchouankeu, O. Briot, B. Gil, J. P. Alexis, and R. L. Aulombard, *J. Appl. Phys.* **80**, 5352 (1996).
41. A. J. Fischer, W. Shan, J. J. Song, Y. C. Chang, R. Horning, and B. Goldenberg, *Appl. Phys. Lett.* **71**, 1981 (1997).
42. J. B. Lam, S. Bidnyk, and J. J. Song, unpublished.

43. W. Shan, B. D. Little, A. J. Fischer, J. J. Song, B. Goldenberg, W. G. Perry, M. D. Bremser, and R. F. Davis, *Phys. Rev. B* **54**, 16369.
44. T. J. Schmidt, Ph. D. Thesis, Oklahoma State University (1998).
45. T. J. Schmidt, Y. C. Chang, and J. J. Song, *Proc. SPIE* **3419**, 61 (1998).
46. S. D. Hersee, J. C. Ramer, and K. J. Malloy, *Mater. Res. Bull.* **22**, 45 (1997).
47. T. J. Schmidt, J. J. Song, S. Keller, U. K. Mishra, and S. P. DenBaars, *Mat. Res. Symp. Proc.* **572**, 351(1999).
48. T. J. Schmidt, Y. H. Cho, S. Bidnyk, J. J. Song, S. Keller, U. K. Mishra, and S. P. DenBaars, *Proc. SPIE* **3625**, 57 (1999).
49. J. J. Song, S. Bidnyk, and T. J. Schmidt, (invited), *SPIE Conf. Proc.* **3896** (1999).
50. A. J. Fischer, unpublished.
51. L. A. Rivlin, A. T. Semenov, and C. D. Yakubovich, "*Dynamics and Spectral Emission of Semiconductor Lasers*," (Radio i Svyaz, Moscow, 1983).
52. I. Galbraith and S. W. Koch, *J. Crystal Growth* **159**, 667 (1996).
53. R. Levy and J. B. Grun, *Phys. Stat. Sol. (a)* **22**, 11 (1974).
54. Benoit à la Guillaume, J. M. Debever, and F. Salvan, *Phys. Rev.* **177**, 567 (1969).
55. K. Leo and J. H. Collet, *Phys. Rev. B* **44**, 5535 (1991).
56. H. Kuroda, S. Shionoya, H. Saito, and E. Hanamura, *Sol. State Comm.* **12**, 533 (1973).
57. D. G. Thomas and J. J. Hopfield, *J. Appl. Phys.* **33**, 3243 (1962).
58. H. Haug, *J. Appl. Phys.* **19**, 4687 (1968).
59. J. R. Packard, D. A. Campbell, and W. C. Tait, *J. Appl. Phys.* **38**, 5255 (1967).
60. E. F. Gross, S. A. Permogorov, and B. S. Razbirin, *Sov. Phys. Sol. State* **8**, 1180 (1966).
61. J. M. Hvam and E. Ejder, *J. of Lumin.* **12/13**, 611 (1976).
62. C. Klingshirn, *Phys. Stat. Sol. (b)* **71**, 547 (1975).
63. H. Haug and S. Koch, *Phys. Stat. Sol. (b)* **82**, 531 (1977).
64. S. W. Koch, H. Haug, G. Schmieder, W. Bohnert, and C. Klingshirn, *Phys. Stat. Sol. (b)* **89**, 431 (1978).

65. J. Bille, T. Fischer, H. Liebing, and W. Ruppel, Proc XI. Int. Conf. Phys. Semicond. **I**, 193, Warsaw (1972).
66. O. Hildebrand, B. O. Faltermeier, and M. H. Pilkuhn, Sol. State Comm. **19**, 841 (1976).
67. O. Hildebrand, E. O. Goebel, K. M. Romanek, H. Weber, and G. Mahler, Phys. Rev. **B 17**, 4775 (1978).
68. S. D. Lester, F. A. Ponce, M. G. Craford, and D. A. Steigerwald, Appl. Phys. Lett. **66**, 1249 (1995).
69. X. H. Yang, T. J. Schmidt, W. Shan, J. J. Song, and B. Goldenberg, Appl. Phys. Lett. **66**, 1 (1995).
70. A. S. Zubrilov, V. I. Nikolaev, D. V. Tsvetkov, V. A. Dmitriev, K. G. Irvine, J. A. Edmond, and C. H. Carter, Jr., Appl. Phys. Lett. **67**, 533 (1995).
71. W. Fang and S. L. Chuang, Appl. Phys. Lett. **67**, 751 (1995).
72. B. Goldenberg, J. D. Zook, and R. J. Ulmer, Appl. Phys. Lett. **62**, 381 (1993).
73. T. W. Weeks, Jr., M. D. Bremser, K. S. Ailey, E. Carlson, W. G. Perry, and R. F. Davis, Appl. Phys. Lett. **67**, 401 (1995).
74. W. Shan, A. J. Fischer, S. J. Hwang, B. D. Little, R. J. Hauenstein, X. C. Xie, J. J. Song, D. S. Kim, B. Goldenberg, R. Horning, S. Krishnankutty, W. G. Perry, M. D. Bremser, and R. F. Davis, J. Appl. Phys. **83**, 455 (1998).
75. H. Shoji, Y. Nakata, K. Mukai, Y. Sugiyama, M. Sugawara, N. Yokoyama, and H. Ishikawa, Appl. Phys. Lett. **71**, 193 (1997).
76. H. Jeon, J. Ding, A. V. Nurmikko, W. Xie, D. C. Grillo, M. Kobayashi, R. L. Gunshor, G. C. Hua, and N. Otsuka, Appl. Phys. Lett. **60**, 2045 (1992).
77. W. W. Chow, A. Knorr, and S. W. Koch, Appl. Phys. Lett. **67**, 754 (1995).
78. H. Amano and I. Akasaki, Proc. Topical Workshop on III-V Nitrides, 193, Nagoya, Japan (1995).
79. S. Bidnyk, B. D. Little, T. J. Schmidt, J. Krasinski, and J. J. Song, Proc. SPIE **3419**, 35, Taipei, Taiwan (1998).

80. C. Kirchner, V. Schwegler, F. Eberhard, M. Kamp, K. J. Ebeling, K. Kornitzer, T. Ebner, K. Thonke, R. Sauer, P. Prystawko, M. Leszczynski, I. Grzegory, and S. Porowski, *Appl. Phys. Lett.* **75**, 1098 (1999).
81. B. D. Little, M.S. report, OSU (1997).
82. S. Nakamura, M. Senoh, S. Nagahama, N. Iwasa, T. Yamada, T. Matsushita, Y. Sugimoto, and H. Kiyoku, *Appl. Phys. Lett.* **69**, 1477 (1996).
83. B. P. Keller, S. Keller, D. Kapolnek, W. N. Jiang, Y. F. Wu, H. Masui, X. H. Wu, B. Heying, J. S. Speck, U. K. Mishra, and S. P. DenBaars, *J. Electron. Mater.* **24**, 1707 (1995).
84. S. Keller, B. P. Keller, D. Kapolnek, A. C. Abare, H. Masui, L. A. Coldren, U. K. Mishra, and S. P. DenBaars, *Appl. Phys. Lett.* **68**, 3147 (1996).
85. S. Keller, A. C. Abare, M. S. Minsky, X. H. Wu, M. P. Mack, J. S. Speck, E. Hu, L. A. Coldren, U. K. Mishra, and S. P. DenBaars, *Proc. Int. Conf. Silicon Carbide, III-Nitrides and Related Materials*, Stockholm, Sweden (1997).
86. S. Ruvimov, Z. Liliental-Weber, T. Suski, J. W. Ager III, J. Washburn, J. Krueger, C. Kisielowski, E. R. Weber, H. Amano, and I. Akasaki, *Appl. Phys. Lett.* **69**, 990 (1996).
87. E. F. Schubert, I. D. Goepfert, W. Grieshaber, and J. M. Redwing, *Appl. Phys. Lett.* **71**, 921 (1997).
88. P. A. Grudowski, C. J. Eiting, J. Park, B. S. Shelton, D. J. H. Lambert, and R. D. Dupuis, *Appl. Phys. Lett.* **71**, 1537 (1997).
89. K. C. Zeng, J. Y. Lin, H. X. Jiang, A. Salvador, G. Popovici, H. Tang, W. Kim, and H. Morkoç, *Appl. Phys. Lett.* **71**, 1368 (1997).
90. S. Chichibu, T. Azuhata, T. Sota, and S. Nakamura, *Appl. Phys. Lett.* **69**, 4188 (1996).
91. Y. Narukawa, Y. Kawakami, S. Fujita, S. Fugita, and S. Nakamura, *Phys. Rev. B* **55**, R1938 (1997).
92. I. M. Catalano, A. Cingolani, M. Ferrara, M. Lugarà and A. Minafra, *Sol. State Comm.* **25**, 349 (1978).

93. J. Holst, L. Eckey, A. Hoffman, I. Broser, B. Schöttker, D. J. As, D. Schikora, and K. Lischka, *Appl. Phys. Lett.* **72**, 1439 (1998).
94. See, for example, D. Wood, "*Optoelectronic Semiconductor Devices*," (Prentice Hall, New York, 1994), pp. 136-138.
95. T. J. Schmidt, J. J. Song, Y. C. Chang, R. Horning, and B. Goldenberg, *Appl. Phys. Lett.* **72**, 1504 (1998).
96. X. H. Yang, J. M. Hays, W. Shan, J. J. Song, and E. Cantwell, *Appl. Phys. Lett.* **62**, 1071 (1992).
97. T. Uenoyama, *Phys. Rev. B* **51**, 10228 (1995).
98. R. Dingle, "*Semiconductors and Semimetals*," Vol. **24** (Academic Press, Inc., New York, 1987), pp. 18-23.
99. H. Jeon, J. Ding, A. V. Nurmikko, H. Luo, N. Samarth, and J. K. Furdyna, *Appl. Phys. Lett.* **57**, 2413 (1990).
100. T. J. Schmidt, X. H. Yang, W. Shan, J. J. Song, A. Salvador, W. Kim, Ö. Aktas, A. Botchkarev, and H. Morkoç, *Appl. Phys. Lett.* **68**, 1820 (1996).
101. S. Nakamura, M. Senoh, S. Nagahama, N. Iwasa, T. Matushita, and T. Mukai, *MRS Internet J. Nitride Semicond. Res.* **4S1**, G1.1 (1999).
102. W. Shan, A. J. Fischer, J. J. Song, G. E. Bulman, H. S. Kog, M. T. Leonard, W. G. Perry, M. D. Bremser, and R. F. Davis, *Appl. Phys. Lett.* **69**, 740 (1996).
103. J. J. Song, A. J. Fischer, T. J. Schmidt, S. Bidnyk, and W. Shan, *Nonlinear Optics* **18**, 269 (1997).
104. S. Bidnyk, T. J. Schmidt, B. D. Little, and J. J. Song, *Appl. Phys. Lett.* **74**, 1 (1999).
105. T. J. Schmidt, S. Bidnyk, Y. H. Cho, A. J. Fischer, J. J. Song, S. Keller, U. K. Mishra, and S. P. DenBaars, *Appl. Phys. Lett.* **73**, 3689 (1998).
106. G. H. Gainer, S. Bidnyk, Y. H. Kwon, and J. J. Song, unpublished.
107. Y. H. Cho, T. J. Schmidt, S. Bidnyk, G. H. Gainer, J. J. Song, S. Keller, U. K. Mishra, and S. P. DenBaars, unpublished.
108. T. J. Schmidt, Y. H. Cho, J. J. Song, and W. Yang, *Appl. Phys. Lett.* **74**, 245 (1999).
109. M. A. Khan, D. T. Olson, J. M. Van Hove, and J. N. Kuznia, *Appl. Phys. Lett.* **58**, 1515 (1991).

110. M. A. Khan, S. Krishnankutty, R. A. Skogman, J. N. Kuznia, D. T. Olson, and T. George, *Appl. Phys. Lett.* **65**, 520 (1994).
111. D. M. Bagnall and K. P. O'Donnell, *Appl. Phys. Lett.* **68**, 3197 (1996).
112. G. Frankowsky, F. Steuber, V. Hä rle, F. Scholz, and A. Hangleiter, *Appl. Phys. Lett.* **68**, 3746 (1996).
113. D. Wiesmann, I. Brener, L. Pheiffer, M. A. Khan, and C. J. Sun, *Appl. Phys. Lett.* **69**, 3384 (1996).
114. K. Yung, J. Yee, J. Koo, M. Rubin, N. Newman, and J. Ross, *App. Phys. Lett.* **64**, 1135 (1994).
115. H. Amano, T. Asahi, M. Kito, and I. Akasaki, *J. Lumin.* **48 & 49**, 889 (1991).
116. H. Amano, N. Watanabe, N. Koide, and I. Akasaki, *Jpn. J. Appl. Phys.* **32**, L1000 (1993).
117. M. O. Manasreh, *Phys. Rev. B* **53**, 16425 (1996).
118. B. D. Cullity, "*Elements of X-ray diffraction*," 2nd edition (Addison-Wesley Publishing company, Reading, Massachusetts, 1978), 502.
119. S. Strite and H. Morkoç, *J. Vac. Sci. Technol.* **B10**, 1237 (1992).
120. S. Nakamura, M Senoh, S Nagahama, N Iwasa, T Yamada, T Matsushita, H Kiyoku, Y Sugimoto, T Kozaki, H Umemoto, M. Sano, and K Chocho, *Jpn. J. Appl. Phys.* **37**, L309 (1998).
121. Y. Kato, S. Kitamura, K. Hiramatsu, and N. Sawaki, *J. Crystal Growth* **144**, 133 (1994).
122. S. Kitamura, K. Hiramatsu, and N. Sawaki, *Jpn. J. Appl. Phys.* **34**, L1184 (1995).
123. W. Yang, S. A. McPherson, Z. Mao, S. McKernan, and C. B. Carter, (unpublished); T. S. Zheleva, O. H. Nam, M. D. Bremser, and R. F. Davis, *Appl. Phys. Lett.* **71**, 2472 (1997).
124. J. J. Song and W. C. Wang, *J. Appl. Phys.* **55**, 660 (1984).
125. E. Ejder, *Phys. Status Sol. (a)* **6**, 445 (1971).
126. D. Marcuse and T. P. Lee, *IEEE J. Quantum Electron.* **QE-19**, 1397 (1983).
127. G. H. B. Thompson, *Physics of Semiconductor Laser Devices* (Wiley, New York, 1980), pp. 402-474.

128. S. Bidnyk, T. J. Schmidt, G. H. Park, and J. J. Song, Appl. Phys. Lett. **71**, 729 (1997).
129. K. C. Zeng, J. Y. Lin, H. X. Jiang, and W. Yang, Appl. Phys. Lett. **74**, 1227 (1999).
130. H. X. Jiang, J. Y. Lin, K. C. Zeng, and W. Yang, Appl. Phys. Lett. **75**, 763 (1999).
131. K. Iga, S. Kinoshita, and F. Koyama, Electron. Lett. **23**, 134 (1987).
132. F. Koyama, K. Tomomatsu, and K. Iga, Appl. Phys. Lett. **52**, 528 (1988).
133. W. D. Herzog, M. S. Ünlü, B. B. Goldberg, G. H. Rhodes, and C. Harder, Appl. Phys. Lett. **70**, 688 (1997).
134. S. Nakamura, M. Senoh, S. Nagahama, N. Iwasa, T. Yamada, T. Matsushita, H. Kiyoku, Y. Sugimoto, T. Kozaki, H. Umemoto, M. Sano, and K. Chocho, Appl. Phys. Lett. **73**, 832 (1998).
135. A. E. Siegman, "*Lasers*," (University Science Books, Mill Valley, California, 1986), pp. 642-648.
136. W. L. Li, Y. K. Su, S. J. Chang, and C. Y. Tsai, Appl. Phys. Lett. **71**, 2245 (1997).
137. *see, for example*, G. H. B. Thompson, "*Physics of Semiconductor Laser Devices*," (John Wiley & Sons, New York, 1980), pp. 132-162.
138. M. D. Bremser, T. W. Weeks, Jr., R. S. Kern, R. F. Davis, and D. E. Aspnes, Appl. Phys. Lett. **69**, 2065 (1996).
139. *see, for example*, A. E. Siegman, "*Lasers*," (University Science Books, Mill Valley, 1986), pp. 398-447.

APPENDICES

APPENDIX A

DETERMINATION OF GAIN THROUGH THE VARIABLE STRIPE METHOD

The direct determination of optical gain in semiconductor crystals by the variable stripe method was first suggested by Shaklee and Leheny^{*} in 1971. This method is a modification of a method used on pulsed metal vapor lasers by Silfvast and Deech.[†] Cross and Oldham[‡] presented a detailed theoretical analysis of the variable stripe measurement technique that explicitly investigated gain saturation and the effects of a nonzero collection aperture on the interpretation of experimental data. The advantage of this technique is that the crystal need not be fabricated into an optical cavity in order to determine its suitability for producing semiconductor lasers. With the advent of this technique, it became possible to evaluate crystals in their early stages of technological development.

The variable stripe method has been extensively used to study the gain dynamics of GaN-based lasing mediums. This measurement technique involves the detection of single-pass amplified light emitted along the length of an optically excited crystal. A rectangular beam of uniform intensity was focused into a line. Spontaneous emission was amplified (via stimulated emission) as it passed through the excited volume towards the edge of the crystal as shown in Figure A-1. The pumped region was a narrow stripe of length l translated a distance d from the sample edge with the output $I(l, d)$ collected along the stripe axis. The length of the stripe was varied by a computer-controlled stepper

^{*} K. L. Shaklee and R. F. Leheny, Appl. Phys. Lett. **18**, 475 (1971).

[†] W. T. Silfvast and J. S. Deech, Appl. Phys. Lett. **11**, 97 (1967).

[‡] P. S. Cross and W. G. Oldham, IEEE J. Quantum Electronics, **QE-11**, 190 (1975)

motor. The acquisition setup used a set of apertures to assure that it only collected the light that passed through the edge of the crystal and not through the side.

Let us define the net gain as

$$g = g' - \alpha, \quad (\text{A-1})$$

where g' is the gain due to stimulated emission and α is the optical loss. The ideal dependence of $I(l, d)$ is

$$I(l, d) = \left(\frac{I_s A}{g} \right) [\exp(gl) - 1] \exp(-\alpha d), \quad (\text{A-2})$$

where I_s is the spontaneous emission rate per unit volume and A is the cross-sectional area of the excited volume. Figure A-2 shows the ideal output-intensity characteristics for different values of d . When l is sufficiently large and the excitation region starts from the edge of the sample ($d = 0$), the exponential factor in Eq. A-2 dominates and one can obtain the gain from the slope of the curve plotted on a logarithmic scale.

Figure A-3 shows how the emission intensity from a 1.9- μm -thick GaN sample varies as a function of excitation length. By utilizing an optical multi-channel analyzer and a stepper motor, we collected a series of spectra for different values of excitation length. The two emission peaks at 367 and 372 nm represent spontaneous and stimulated emission, respectively. With increasing excitation length, the intensity of the spontaneous emission peak (seen due to a non-zero collection aperture) linearly increases, whereas the intensity of the stimulated emission peak exhibits an exponential increase, as was predicted by Eq. A-2. Typical values of gain for GaN epilayers obtained by utilizing the variable stripe technique are on the order of several hundred cm^{-1} .

Let's define $\Phi(E)dE$ to be the flux of photons with energy between E and $E + dE$, R_{nr} to be the nonradiative transition rate, R_{spn} to be the total spontaneous-emission rate per unit volume, and R_{stim} to be the total stimulated-emission rate per unit volume. Under steady-state excitation, the total downward-transition rate must equal the pumping rate R as expressed by

$$R = R_{spn} + R_{stim} + R_{nr}, \quad (\text{A-3})$$

or

$$R = \int r_{spont}(E) dE + \int \Phi(E) dE + R_{nr}. \quad (\text{A-4})$$

R_{spont} can be characterized by a lifetime τ_{spont} :

$$R_{spont} = \frac{n}{\tau_{spont}}, \quad (\text{A-5})$$

where n is the density of the excited species. Similarly, the nonradiative transition rate is given by:

$$R_{nr} = \frac{n}{\tau_{nr}}, \quad (\text{A-6})$$

where τ_{nr} is the nonradiative lifetime. Now we can rewrite Eq. A-3 as:

$$R = R_{stim} + R_{spont} \left(1 + \frac{\tau_{spont}}{\tau_{nr}} \right). \quad (\text{A-7})$$

In general it is difficult to establish a relation between R_{stim} and R_{spont} without some assumptions. In order to reduce the computational complexity, the photon-energy dependence is eliminated by approximating the emission characteristics with a rectangular spectra of width ΔE . Thus the transition probabilities (both spontaneous and stimulated) become independent of photon energy within the bandwidth ΔE , which requires short energy-relaxation times. Results based on the rectangular approximation give an upper bound to the degree of saturation. Carrying out the integral for R_{stim} in Eq. A-4 we get:

$$R_{stim} = \Phi \cdot g \cdot \Delta E = \frac{I \cdot g}{E}, \quad (\text{A-8})$$

where I is the integrated radiation intensity. The general approach of Einstein was to assign rate constants to spontaneous and stimulated emission with the assumption that both of them are proportional to the carrier density. Einstein stated that the rate of stimulated emission is also proportional to the radiation intensity. To find the proportionality constant relating R_{stim} to R_{spont} for the case of rectangular spectra, let us define I_{sat} as the radiation intensity at which the gain has dropped to one half its low-intensity value. Thus when $I = I_{sat}$, from Eq. A-7 and Eq. A-8 we get:

$$\frac{R_{sp,0}}{2} \left(1 + \frac{\tau_{sp}}{\tau_{nr}} \right) = \frac{I_{sat} \cdot g_0}{2E} = \frac{R}{2}. \quad (\text{A-9})$$

We can rearrange Eq. A-9 to give:

$$g = \frac{E \cdot R_{sp}}{I_{sat}} \left(1 + \frac{\tau_{sp}}{\tau_{nr}} \right). \quad (\text{A-10})$$

Now we can combine Eqs. A-7, A-8, and A-10 to obtain:

$$R = \frac{g \cdot I}{E} + \frac{g \cdot I_{sat}}{E}, \quad (\text{A-11})$$

and substituting for R from Eq. A-9 we arrive at:

$$g = \frac{g_0}{1 + \frac{I}{I_{sat}}}. \quad (\text{A-12})$$

Therefore, we expect gain to decrease as the radiation intensity increases, which is in good agreement with experiment.

The measured value of gain can also be diminished by the effect of a nonzero collection aperture. The fraction of photons emitted by a volume element that is collected by external optics is the fraction within a certain cone originating from the volume element. A significant fraction of the rays within the cone pass out of the active region before reaching the edge of the sample and some of them are amplified over the entire distance from the emitting volume to the sample edge. Due to limited detector sensitivity and a lack of total control over the excited region, the conditions necessary for the ideal amplified stimulated emission experiment cannot be met. We note, however, that all of these effects tend to reduce the measured value of gain, making our measured value a lower limit.

The variable stripe gain method is a rather simple and effective technique for measuring optical gain in semiconductors. Unlike other methods involving transmission of light through the sample, it works equally well if the band-gap of the substrate is lower than the band-gap of the epilayer, *e.g.* GaN on SiC.

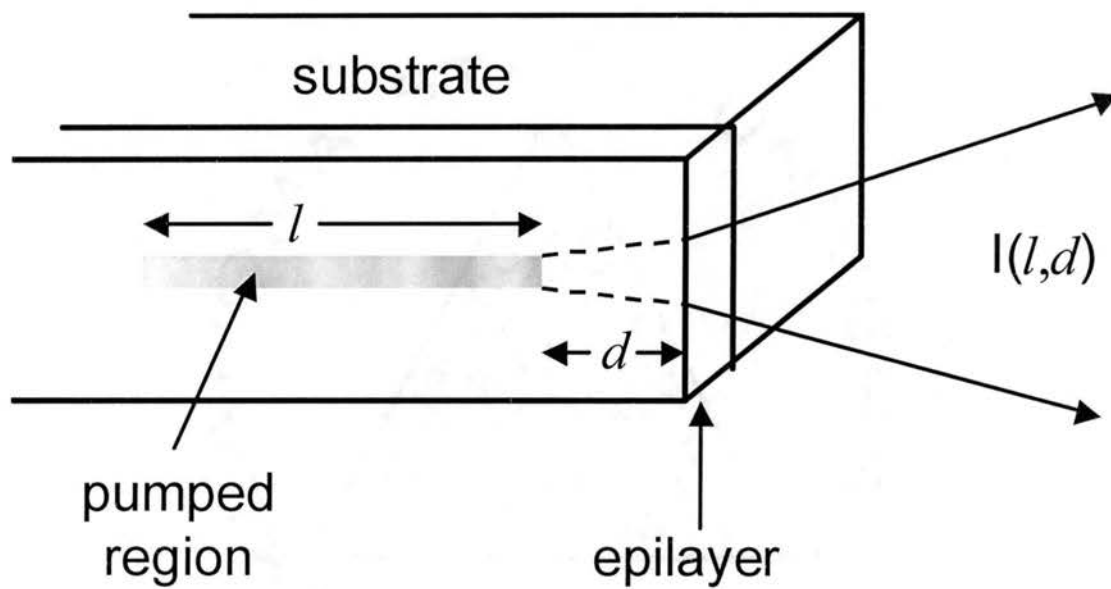


Figure A-1. Pumping configuration for the variable stripe gain experiment.

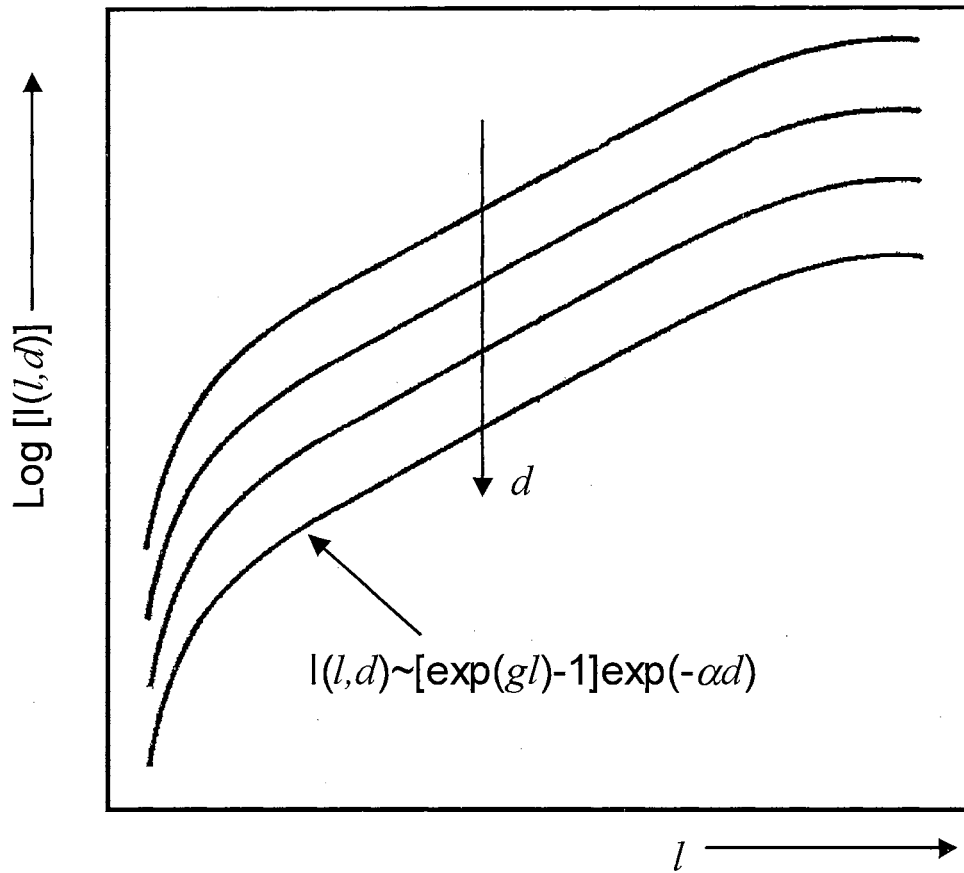


Figure A-2. Ideal output intensity characteristics for different values of d in the variable stripe experiment.

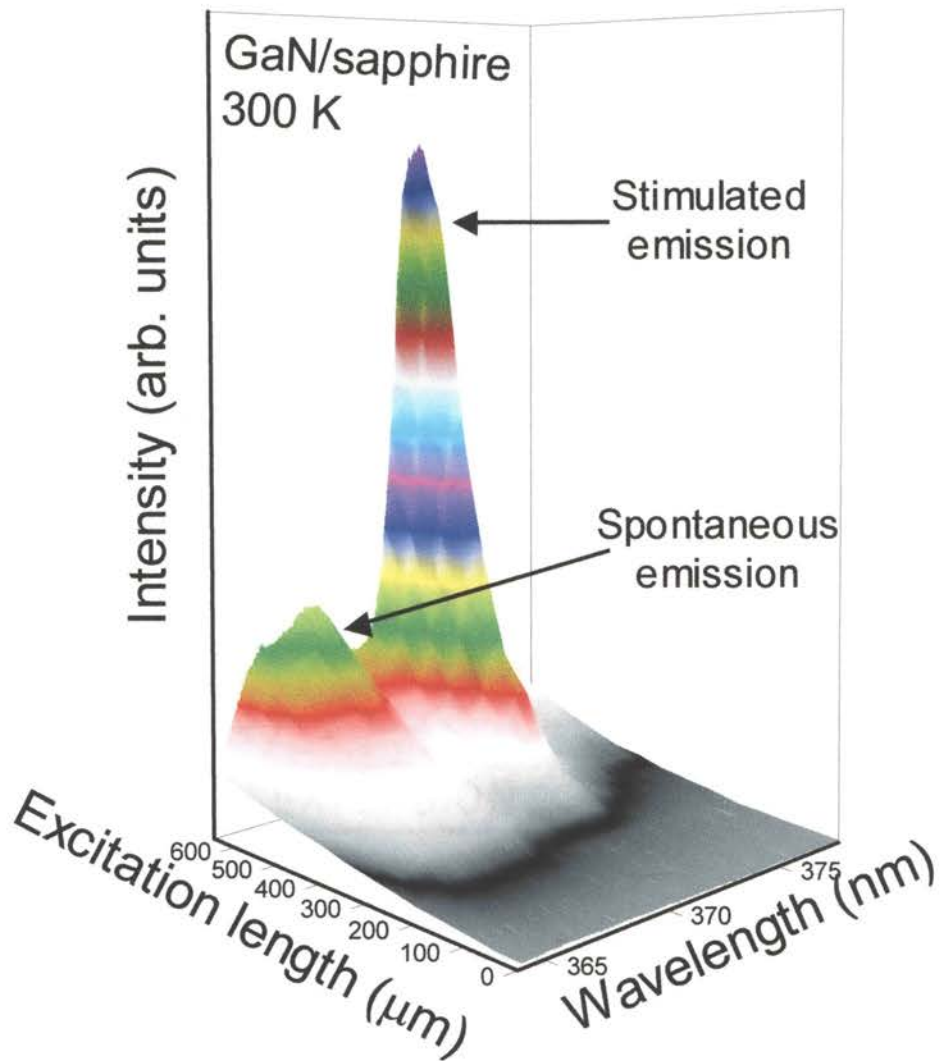


Figure A-3. Dependence of emission intensity on excitation length for a 1.9- μm -thick GaN epilayer grown on α -sapphire ($1.5 \cdot I_{th}$, 349 nm, 4 ns, 30 Hz). The intensity of the spontaneous emission peak increases almost linearly with excitation length. An exponential increase in the emission intensity of the stimulated emission peak can be seen.

APPENDIX B

EXTRACTION OF GAIN FROM SPONTANEOUS EMISSION SPECTRA

There have been many attempts to deduce gain spectra from an analysis of measured spontaneous emission spectra. Bernard and Duraffourg^{*} considered the case of stimulated emission in semiconductors for transitions between the conduction band and the valence band, or between one of these bands and an impurity level. They derived relations for spontaneous emission, stimulated emission, and optical absorption. Bebb and Williams[†] derived the same relations for many different transitions. Finally, Henry *et al.*[‡] presented a new method for obtaining absorption and gain spectra of lasers which made no assumption on the nature of the optical transition. The method for extraction of optical gain described here is based on their publication as well as Landau and Lifshitz's[§] work and applied to GaN epilayers grown on sapphire.

Einstein postulated that the rates of absorption, spontaneous emission, and stimulated emission are governed by three coefficients, but these three processes are not independent. By demanding that the emission and absorption processes lead to the same equilibrium values for the radiation density and level populations it is possible to derive two relations between the three coefficients. This argument can be made for any material, including a semiconductor.

^{*} M. G. A. Bernard and G. Duraffourg, *Phys. Status Sol.* **1**, 699 (1961).

[†] H. B. Bebb and E. W. Williams, "*Semiconductors and Semimetals*," (Academic Press, New York, 1972).

[‡] C. H. Henry, R. A. Logan, and F. R. Merritt, *J. Appl. Phys.* **51**, 3042 (1980).

[§] L. D. Landau and E. M. Lifshitz, "*Statistical Physics*," 2nd edition, (Academic Press, New York, 1972).

Consider a thin layer of semiconductor with light propagating along a path length t through the layer. A beam of photons with an occupation of $n_{h\nu}$ per mode is passing through the layer. The change in $n_{h\nu}$ can be written as:

$$\Delta n_{h\nu} = -\alpha t n_{h\nu} + A + B n_{h\nu}, \quad (\text{B-1})$$

where $-\alpha t n_{h\nu}$ is the decrease in mode occupation number due to absorption, and the coefficients A and B describe the increases in occupation number due to spontaneous and stimulated emission, respectively. A steady-state equilibrium for some value $n_{h\nu} = \bar{n}_{h\nu}$ can be reached if B is greater than αt . At equilibrium, the rates of emission and absorption are equal and $\Delta n_{h\nu} = 0$. Eq. B-1 becomes:

$$0 = -\alpha t \bar{n}_{h\nu} + A + B \bar{n}_{h\nu}, \quad (\text{B-2})$$

or, solving for $\bar{n}_{h\nu}$:

$$\bar{n}_{h\nu} = \frac{A/B}{\frac{\alpha \cdot t}{B} - 1}. \quad (\text{B-3})$$

We can consider the interaction of photons with the semiconductor as a non-equilibrium Bose gas. Landau and Lifshitz derived a formula for the entropy of such a gas:

$$\Delta S = k \sum_i \ln \left(\frac{\bar{n}_i + 1}{\bar{n}_i} \right) \Delta n_i, \quad (\text{B-4})$$

where the index i represents different states. When a photon of energy $h\nu$ is added to the gas, only modes with the same occupation number $\bar{n}_{h\nu}$ will change, hence:

$$\Delta S_{h\nu} = k \sum_i \ln \left(\frac{\bar{n}_{h\nu} + 1}{\bar{n}_{h\nu}} \right) \Delta n_i = k \ln \left(\frac{\bar{n}_{h\nu} + 1}{\bar{n}_{h\nu}} \right) \sum_i \Delta n_i. \quad (\text{B-5})$$

For a single photon, $\sum_i \Delta n_i = 1$ and Eq. B-5 can be written as:

$$\Delta S_{h\nu} = k \ln \left(\frac{\bar{n}_{h\nu} + 1}{\bar{n}_{h\nu}} \right). \quad (\text{B-6})$$

In order for a photon to be emitted, an electron has to drop from the conduction band to the valence band. The free energy ΔF of the semiconductor changes by $-\Delta E_F$,

where ΔE_F is the separation between the quasi-Fermi levels of the two bands. At the same time the energy ΔE of the semiconductor changes by $-h\nu$. At constant temperature we can write the equation for the change in entropy as:

$$\Delta S = \frac{\Delta E - \Delta F}{T} = -\frac{h\nu - \Delta E_F}{T}. \quad (\text{B-7})$$

From the point of view of statistical mechanics and thermodynamics, the entropy of the combined system of the semiconductor and the radiation at equilibrium will be a maximum. In other words, there will be no net increase in entropy when a photon is emitted or absorbed. Therefore, the sum of Eq. B-6 and Eq. B-7 should be equal to 0:

$$\Delta S_{h\nu} + \Delta S = k \ln\left(\frac{\bar{n}_{h\nu} + 1}{\bar{n}_{h\nu}}\right) - \frac{h\nu - \Delta E_F}{T} = 0. \quad (\text{B-8})$$

From Eq. B-8 we can obtain the equilibrium occupation number:

$$\bar{n}_{h\nu} = \frac{1}{\exp\left(\frac{h\nu - \Delta E_F}{kT}\right)}. \quad (\text{B-9})$$

If radiative equilibrium is to lead to a state of maximum entropy, Eq. B-3 and Eq. B-9 should be identical, since they define the same quantity $\bar{n}_{h\nu}$. This is satisfied only if:

$$A = B = \alpha(h\nu, \Delta E_F) t \exp\left(\frac{h\nu - \Delta E_F}{kT}\right). \quad (\text{B-10})$$

Optical gain was defined in Eq. 3-3, but in the current notation it looks somewhat different:

$$g(h\nu, \Delta E_F) = \frac{\Delta n_{h\nu}}{n_{h\nu}} t. \quad (\text{B-11})$$

If we neglect the spontaneous emission in Eq. B-1 we get:

$$g(h\nu, \Delta E_F) = \alpha(h\nu, \Delta E_F) \left[\exp\left(\frac{\Delta E_F - h\nu}{kT}\right) - 1 \right]. \quad (\text{B-12})$$

The rate of spontaneous emission into a single mode is given by:

$$\frac{dn_{h\nu}}{dt} = \frac{dx}{dt} \frac{dn_{h\nu}}{dx} = \frac{c}{n} \frac{dn_{h\nu}}{dx} = v_g \frac{dn_{h\nu}}{dx} = \alpha(h\nu, \Delta E_F) v_g \exp\left(\frac{\Delta E_F - h\nu}{kT}\right), \quad (\text{B-13})$$

where n is the index of refraction and $v_g = d\omega/dk$ is the group velocity of light in the semiconductor. The number of modes per unit solid angle per unit energy per unit volume is:

$$\frac{dN}{dh\nu d\Omega} = \frac{2k^2 dk}{(2\pi)^3 dh\nu} = \frac{n^2 (h\nu)^2}{\pi h^3 c^2 v_g}, \quad (\text{B-14})$$

where $k = 2\pi n\nu/c$ is the wavevector. The detected spontaneous emission intensity is a function of the photon energy and pumping power (quasi-Fermi level separation). It is proportional to the theoretically calculated value, given in Eq. B-13, with the aperture consideration given in Eq. B-14, and the relative quantum efficiency of the detection system $F_s(h\nu)$, *i.e.*:

$$L(h\nu, \Delta E_F) \propto \left(\frac{dn_{h\nu}}{dt} \right) \left(\frac{dN}{dh\nu d\Omega} \right) F_s(h\nu). \quad (\text{B-15})$$

The substitution of Eq. B-13 and Eq. B-14 into Eq. B-15 yields:

$$L(h\nu, \Delta E_F) \propto F_s(h\nu) (h\nu)^2 \alpha(h\nu, \Delta E_F) \exp\left(\frac{\Delta E_F - h\nu}{kT}\right). \quad (\text{B-16})$$

The absorption coefficient $\alpha(h\nu, \Delta E_F)$ can be obtained from Eq. B-12:

$$\alpha(h\nu, \Delta E_F) = \frac{g(h\nu, \Delta E_F)}{\exp\left(\frac{\Delta E_F - h\nu}{kT}\right) - 1}. \quad (\text{B-17})$$

Let's insert Eq. B-17 into Eq. B-16:

$$L(h\nu, \Delta E_F) \propto F_s(h\nu) (h\nu)^2 \frac{g(h\nu, \Delta E_F)}{\exp\left(\frac{\Delta E_F - h\nu}{kT}\right) - 1} \exp\left(\frac{\Delta E_F - h\nu}{kT}\right). \quad (\text{B-18})$$

Finally, we can deduce gain from Eq. B-18:

$$g(h\nu, \Delta E_F) \propto \frac{L(h\nu, \Delta E_F)}{F_s(h\nu) (h\nu)^2} \left[1 - \exp\left(\frac{h\nu - \Delta E_F}{kT}\right) \right]. \quad (\text{B-19})$$

To summarize, if one has to extract the shape of the gain curve from spontaneous emission spectra, one must perform the following steps:

- Experimentally obtain spontaneous emission spectra $L(h\nu, \Delta E_F)$ and the position of the laser line $h\nu_L$ (stimulated emission peak).

- Substitute $L(h\nu, \Delta E_F)$ into Eq. B-19 in order to obtain the gain spectra as a function of only one parameter (ΔE_F).
- Numerically adjust ΔE_F in the equation so that the peak of the gain curve will coincide with the laser line $h\nu_L$.

We applied the above recipe to calculate gain from a 1.9- μm -thick GaN epilayer grown on *a*-sapphire. The room temperature spontaneous emission spectrum $L(h\nu, \Delta E_F)$ is shown in Figure B-1(a). The spectrum was taken at pump densities slightly below the stimulated emission threshold. The position of the stimulated emission is marked by $h\nu_L$. We substituted $L(h\nu, \Delta E_F)$ into Eq. B-19 and numerically adjusted the parameter ΔE_F so that the gain curve depicted in Figure B-1(b) coincided with the stimulated emission peak $h\nu_L$.

It is also possible to determine the value of ΔE_F for each current or pumping intensity without a fit, as well as to calculate the absolute values of gain — not just the shape. ΔE_F can be determined by the ratios of the luminescence intensities. Let's define ΔE_F^L to be the bias energy at laser threshold. Then from Eq. B-16:

$$\frac{L(h\nu, \Delta E_F)}{L(h\nu, \Delta E_F^L)} = \frac{\alpha(h\nu, \Delta E_F)}{\alpha(h\nu, \Delta E_F^L)} \exp\left(\frac{\Delta E_F - \Delta E_F^L}{kT}\right). \quad (\text{B-20})$$

Usually, the carrier injection or pumping intensity modifies the absorption edge (through band-gap renormalization, exciton screening, etc.), but for photon energies sufficiently far above the absorption edge ($h\nu > h\nu_1$), the absorption coefficient is independent of ΔE_F . Eq. B-20 simplifies to:

$$\frac{L(h\nu, \Delta E_F)}{L(h\nu, \Delta E_F^L)} = \exp\left(\frac{\Delta E_F - \Delta E_F^L}{kT}\right). \quad (\text{B-21})$$

Eq. B-21 determines ΔE_F relative to the threshold value ΔE_F^L . The absolute value of ΔE_F^L can be determined from the requirement that at the lasing threshold $\Delta E_F = \Delta E_F^L$, the gain spectrum is a maximum at $h\nu = h\nu_L$. The maximum of the gain spectrum can be found by setting the derivative of B-19 to zero:

$$\left. \frac{d g(h\nu, \Delta E_F^L)}{d h\nu} \right|_{h\nu=h\nu_L} = 0 \quad (\text{B-22})$$

This yields:

$$\exp\left(\frac{\Delta E_F^L - h\nu_L}{kT}\right) = 1 + \frac{1}{kT \left(\frac{L}{L'} - \frac{F'_s}{F_s} - \frac{2}{h\nu_L} \right)}, \quad (\text{B-23})$$

where the prime denotes the derivative with respect to $h\nu$ evaluated at $h\nu_L$.

Eq. B-21 and Eq. B-23 completely determine the value of ΔE_F^L for each pumping intensity.

We can determine the gain relative to its threshold value directly from Eq. B-19:

$$g(h\nu, \Delta E_F) = g_L \frac{L(h\nu, \Delta E_F) F_s(h\nu_L)}{L(h\nu, \Delta E_F^L) F_s(h\nu)} \left(\frac{h\nu_L}{h\nu} \right)^2 \frac{1 - \exp\left(\frac{h\nu - \Delta E_F}{kT}\right)}{1 - \exp\left(\frac{h\nu - \Delta E_F^L}{kT}\right)}, \quad (\text{B-24})$$

where $g_L = g(h\nu_L, \Delta E_F^L)$ is the gain at threshold at the position of the laser line. It is equal to the sum of the mirror facet losses α_m and other waveguide losses α_g :

$$g_L = \alpha_m + \alpha_g. \quad (\text{B-25})$$

Eqs. B-24 and B-25, together with Eq. B-21 and Eq. B-23 can be used to completely determine the gain $g(h\nu, \Delta E_F)$ from spontaneous emission spectra.

The described technique is the easiest from an experimental point of view since it requires only spontaneous emission spectra and the position of the stimulated emission (or lasing) peak. However, in group-III nitrides, photoluminescence is a strong function of the pumping/collecting geometry. This introduces some ambiguity into the derivation of gain profiles.

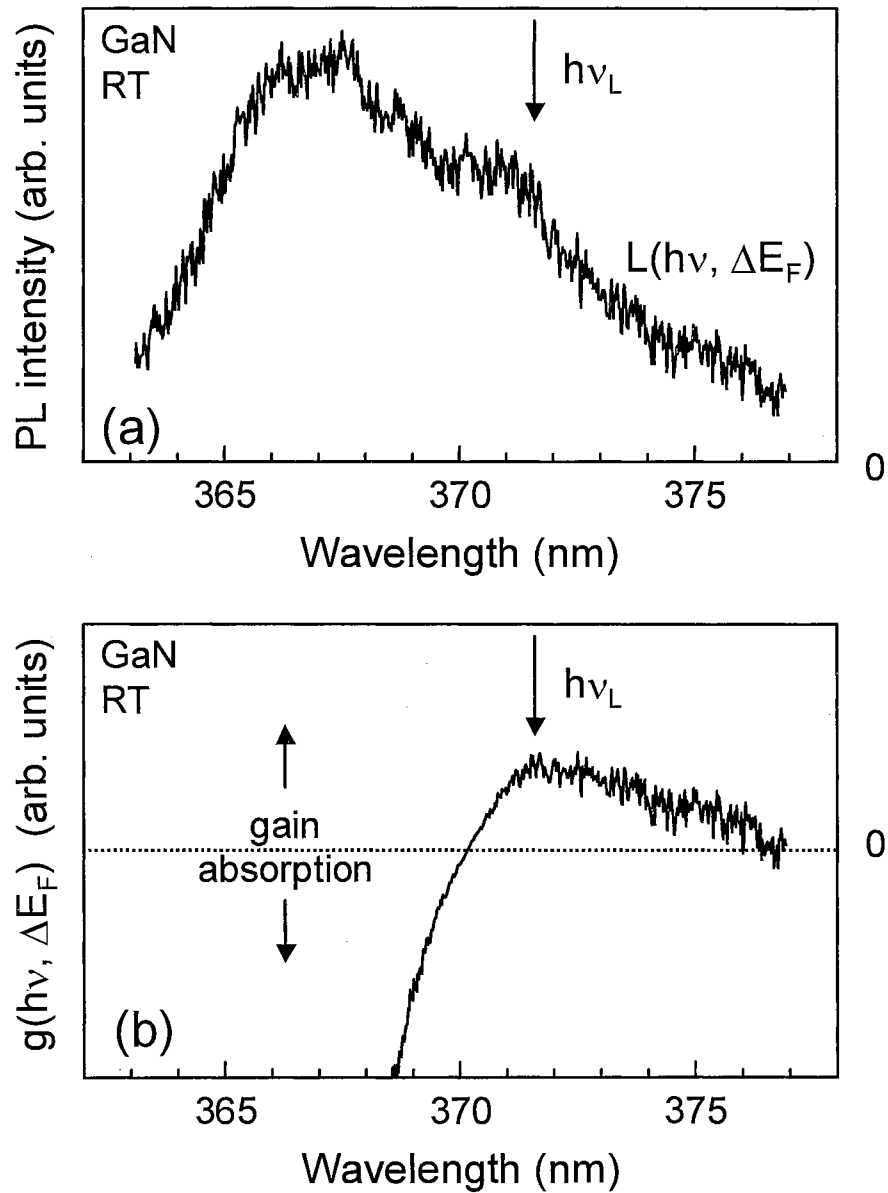


Figure B-1. (a) Spontaneous emission $L(h\nu, \Delta E_F)$ from a 1.9- μm -thick GaN epilayer grown on *a*-sapphire taken at an excitation power slightly below the stimulated emission threshold. (b) Gain spectra $g(h\nu, \Delta E_F)$ calculated from the spontaneous emission using the technique described in Appendix B. The position of the stimulated emission peak is indicated by $h\nu_L$.

APPENDIX C

PUMP-PROBE EXPERIMENTAL CONFIGURATIONS

The pump-probe technique is a frequently used method for extracting information about optical phenomena associated with high carrier concentrations, such as stimulated emission and gain. A discussion of results obtained with this technique was presented in Chapters I and V; here we will concentrate mostly on technical issues related to pump-probe experiments in nitrides. In describing the pump-probe technique we will use suggestions and equation derivations given by Klingshirn *et al.*,^{*} Yamada *et al.*,[†] and Bohnert *et al.*[‡]

In pump-probe experiments, the sample is first excited with an intense and spectrally narrow laser beam. The changes in absorption or transmission are then probed with a weak and spectrally wide beam as shown in Figure C-1(a). An alternative technique uses a weak and spectrally narrow probe beam which is scanned in frequency, as illustrated in Figure C-1(b).

Usually, two spectra are required to extract information from pump-probe experiments. The first spectrum is taken in the presence of the pump beam while the second spectrum is taken without the pump. The difference between the two spectra gives information about the changes caused by the pump beam. There are two requirements for the intensity of the probe beam: (1) it should be low enough so it does not introduce any changes to the optical properties of the sample, and (2) it should be high enough to give a

^{*} C. Klingshirn and H. Haug, "*Optical properties of highly excited direct gap semiconductors*," (North-Holland Publishing Company, Amsterdam, 1981).

[†] Y. Yamada, Y. Masumoto, J. T. Mullins, and T. Taguchi, *Appl. Phys. Lett.* **61**, 2190 (1992).

[‡] K. Bohnert, G. Schmieder, and C. Klingshirn, *Phys. Stat. Sol. (b)* **98**, 175 (1980).

good signal-to-noise ratio. As a rule of thumb, the intensity of the probe beam should be five times stronger than the luminescence arising from the pump.

The pump-probe technique can be used in both the continuous wave and pulsed regimes. However it is crucially important to satisfy the following conditions, which minimize lateral and longitudinal diffusion of the excited species:

1. The probe beam should be temporally narrower than the pump. It should begin after the pump pulse starts and end before the pump pulse ends.
2. The probe beam should be spatially smaller than the pump and it should probe only the central part of the pump.

In the case of pulsed pump-probe experiments, the pump pulse repetition rate should be low enough not to considerably increase the lattice temperature of the sample. One of the most difficult aspects of pump-probe experiments is the inhomogeneity of the excitation beam. In GaN, the pump beam is in the region of strong absorption and the penetration depth is around 0.5 μm . It is important to select samples with a thickness equal to or smaller than the penetration depth. If the sample is thicker than the penetration depth, one has to consider a many layer model where each layer is excited with different intensity. Alternatively, to uniformly excite a thick sample one can use two-photon excitation. In our studies we chose to use samples with thicknesses not exceeding 0.4 μm .

The experimental setup for reflection and gain spectroscopy using the pump-probe technique is shown in Figure C-2. The output of the 3rd (or 4th) harmonic of an Nd:YAG laser was split into two parts, one to excite the crystal and the other to pump a broad-band dye, which acted as the probe beam. The two laser beams were focused on a pinhole to assure spatial coincidence. This pinhole was imaged on the sample mounted in a closed-cycle helium cryostat. Temporal coincidence resulted from the equal optical path length for the two beams and the fact that the temporal width of the dye emission is 4 ns as compared to the Nd:YAG emission of 6-8 ns. The transmitted (or reflected) light was dispersed by a 1-m spectrometer and detected by a CCD camera.

For the determination of absorption or gain spectra, we measure $I_T^0(\hbar\omega)$, $I_T(\hbar\omega)$, and $I_T^*(\hbar\omega)$, which are spectra transmitted without the sample, through the unexcited sample, and through the excited sample, respectively. For the reflection spectra, we

measure $I_R^0(\hbar\omega)$, $I_R(\hbar\omega)$, and $I_R^*(\hbar\omega)$, which are the broad-band spectra of the dye, the signal from the unexcited sample, and the signal from the excited sample, respectively. In the band-gap region the absorption coefficient is sufficiently high to neglect reflection from the backside of the sample. The reflection spectrum $r(\hbar\omega)$ is given by $I_R(\hbar\omega)/I_R^0(\hbar\omega)$ or $I_R^*(\hbar\omega)/I_R^0(\hbar\omega)$.

The absorption coefficient α of the unexcited crystal is calculated with the following formula:

$$\alpha = -\frac{1}{d} \ln \left(\frac{I_T}{I_T^0(1 - I_R/I_R^0)} \right) - \frac{1}{d} \ln F, \quad (\text{C-1})$$

where F is a function which allows to correct for multiple reflections. The formula for the determination of the gain spectrum $g(\hbar\omega)$ in the excited volume reads:

$$g = -\frac{1}{d} \ln \left(\frac{I_T}{I_T^0(1 - I_R/I_R^0)} \right) + \frac{1}{\delta} \ln \frac{I_T^*}{I_T} - \frac{1}{d} \ln F, \quad (\text{C-2})$$

where δ is the excited thickness of the sample.

We note that by keeping aperture sizes small (Figure C-2), the contribution of the luminescence to $I_T(\hbar\omega)$ or $I_R(\hbar\omega)$ is generally negligible. If this is not sufficient, the luminescence is subtracted.

Due to the large number of dislocations in group-III nitrides (see Chapter VI), one has to pay extra attention to scattering effects from interfaces and surface imperfections. One of the most challenging experiments is to observe absolute gain in the transmission geometry. Due to the substantial size (several tens of micron) of the pump and probe beams, it is common to observe scattered in-plane amplified emission in transmission spectra (see page 141).

We observed that AlGaIn samples used in pump-probe experiments have additional limitations with regard to the sample thickness. In particular, if the sample is too thick, excitonic features can not be observed due to the limited signal-to-noise ratio of our instrumentation. However, if the sample is too thin, excitonic features are absent due to the inferior quality of the AlGaIn epilayer close to the interface. We experimentally determined that the best values for the thickness of AlGaIn epilayers for the transmission pump-probe experiments are in the range of 0.3-0.4 μm .

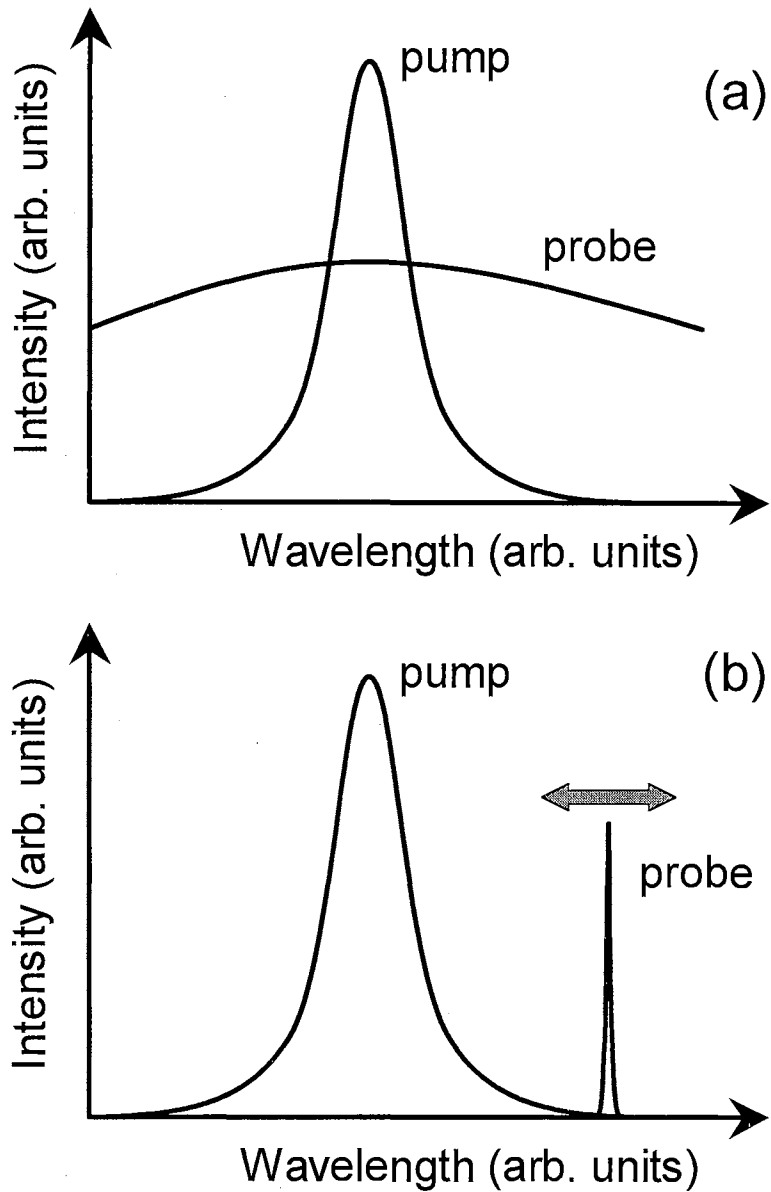


Figure C-1. Relative spectral width of the beams in pump-probe experiments. The sample is excited with an intense and spectrally narrow laser beam and (a) probed with a weak and spectrally wide beam or (b) probed with a weak and spectrally narrow probe beam which is scanned in frequency.

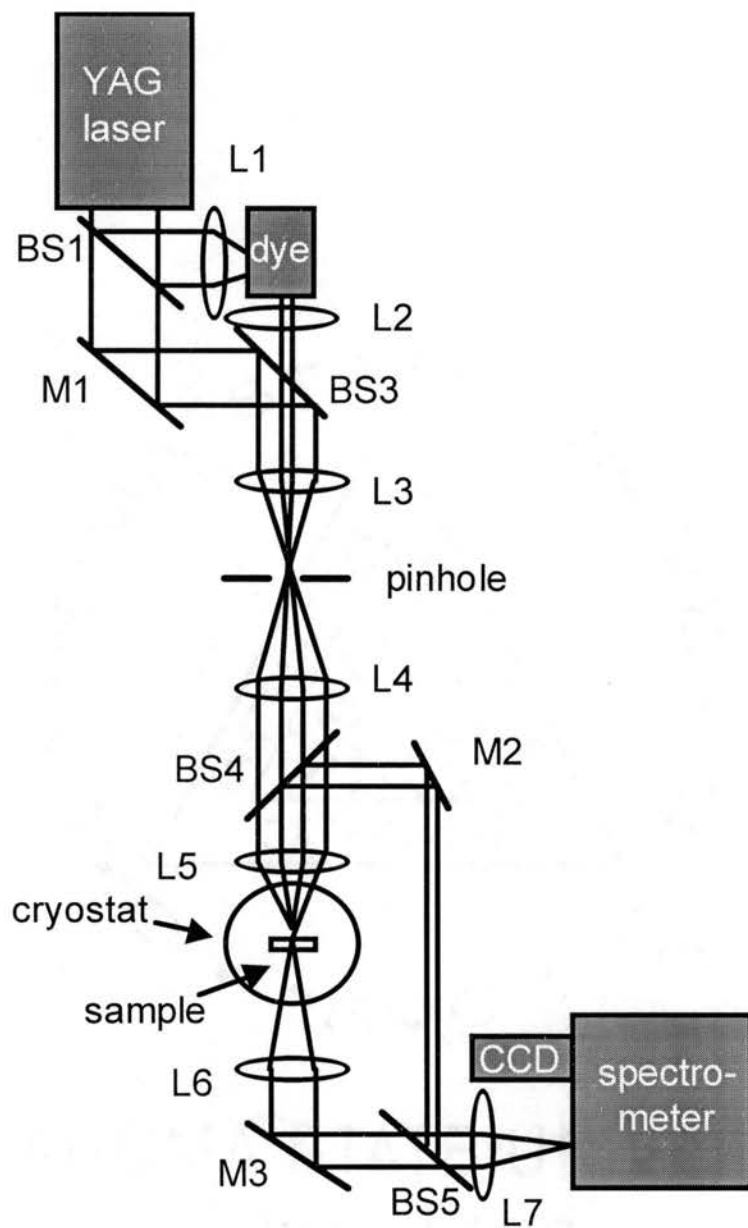


Figure C-2. Experimental set-up for the two-beam transmission and reflection spectroscopy.

VITA

Sergiy Bidnyk

Candidate for the Degree of

Doctor of Philosophy

Thesis: GAIN MECHANISMS, MICROSTRUCTURE LASING, AND IMAGING OF GaN-BASED LASING STRUCTURES

Major Field: Physics

Biographical:

Personal Data: Born in Ivano-Frankivsk, Ukraine, on February 6, 1972, the son of Dmytro and Galyna Bidnyk.

Education: Graduated (Silver Medal recipient) from Ivano-Frankivsk High School #16, Ivano-Frankivsk, Ukraine in June 1989; received Honor Diploma in Engineering Physics from Lviv National University, Lviv, Ukraine, June 1994; obtained a Master of Science Degree in Photonics from Oklahoma State University, Stillwater, Oklahoma in December 1997. Completed the requirements for the Doctor of Philosophy Degree with a major in Physics at Oklahoma State University in December 1999.

Professional Experience: Employed by Oklahoma State University, Department of Physics as a graduate teaching assistant, August 1994 to December 1995. Employed by Oklahoma State University, Center for Laser and Photonics Research and Department of Physics as a graduate research assistant, August 1995 to December 1999.

Professional Memberships: American Physical Society, Optical Society of America, Materials Research Society.